

# Evaluating Fluorine's Impact on Amyloid Formation – a Systematic Study Using a Coiled-Coil Based Model Peptide



Dissertation zur Erlangung des akademischen Grades des  
Doktors der Naturwissenschaften (Dr. rer. nat.)

eingereicht im Fachbereich Biologie, Chemie, Pharmazie  
der Freien Universität Berlin

vorgelegt von

Ulla I. M. Gerling

aus Prenzlau (Brandenburg), Deutschland

Oktober 2013



1. Gutachterin: Prof. Dr. Beate Kokschi (Freie Universität Berlin)  
2. Gutachter: Prof. Dr. Rainer Haag (Freie Universität Berlin)  
Disputation am: 12.12.2013





## ERKLÄRUNG

Die vorliegende Arbeit wurde auf Anregung und unter Anleitung von Prof. Dr. Beate Kokschi in der Zeit von Mai 2009 bis Oktober 2013 am Institut für Chemie und Biochemie des Fachbereiches Biologie, Chemie, Pharmazie der Freien Universität Berlin angefertigt.

Hiermit versichere ich, die vorliegende Arbeit mit dem Titel „*Evaluating Fluorine's Impact on Amyloid Formation – a Systematic Study Using a Coiled-Coil Based Model Peptide*“ ohne Benutzung anderer als der zugelassenen Hilfsmittel selbständig angefertigt zu haben. Alle angeführten Zitate sind als solche kenntlich gemacht. Die vorliegende Arbeit wurde in keinem früheren Promotionsverfahren angenommen oder als ungenügend beurteilt.

Berlin, Oktober 2013

Ulla Gerling

Die Dissertation wurde in englischer Sprache verfasst.

Aus dieser Dissertation gingen bisher folgende Veröffentlichungen hervor:

- **U.I.M. Gerling**, M. Salwiczek, C. D. Cadicamo, H. Erdbrink, C. Czekelius, S. L. Grage, P. Wadhvani, A. S. Ulrich, M. Behrends, G. Haufe, B. Kokschi; Fluorinated amino acids in amyloid formation: a symphony of size, hydrophobicity, and  $\alpha$ -helix propensity; *Chem. Sci.* **2014**, *5*, 819-830.
- J. Maity, **U.I.M. Gerling**, S. Vukelić, A. Schäfer, B. Kokschi; Proline-glutamate chimera's side chain conformation directs the type of  $\beta$ -hairpin structure; *Amino Acids* **2014**, *46*, 177-186.
- H. Erdbrink, E. K. Nyakatura, S. Huhmann, **U.I.M. Gerling**, D. Lentz, B. Kokschi Constantin Czekelius; A synthesis of enantiomerically pure (2S,3S)-5,5,5-trifluoroisoleucine and (2R,3S)-5,5,5-trifluoro-allo-isoleucine; *Beilstein J. Org. Chem.* **2013**, *9*, 2009-2014.
- H. Erdbrink, I. Peuser, **U.I.M. Gerling**, D. Lentz, B. Kokschi, C. Czekelius; Conjugate hydrotrifluoromethylation of  $\alpha$ ,  $\beta$  -unsaturated acyl-oxazolidinones: synthesis of chiral fluorinated amino acids; *Org. Biomol. Chem.* **2012**, *10*, 8583-8586.
- M. Salwiczek, E. K. Nyakatura, **U.I.M. Gerling**, S. Ye, B. Kokschi; Fluorinated Amino Acids: Compatibility with native protein structures and effects on protein-protein interactions; *Chem. Soc Rev.* **2012**, *41*, 2135-2171.



For data security reasons the curriculum vitae has been omitted from the published version.

For data security reasons the curriculum vitae has been omitted from the published version.

For data security reasons the curriculum vitae has been omitted from the published version.

## **PUBLICATIONS, ORAL PRESENTATIONS, POSTER PRESENTATIONS**

---

### **PUBLICATIONS:**

12. **U.I.M. Gerling**, M. Salwiczek, C. D. Cadicamo, H. Erdbrink, C. Czekelius, S. L. Grage, P. Wadhvani, A. S. Ulrich, M. Behrends, G. Haufe, B. Kokschi; Fluorinated amino acids in amyloid formation: a symphony of size, hydrophobicity, and  $\alpha$ -helix propensity; *Chem. Sci.* **2014**, *5*, 819-830.
11. J. Maity, **U.I.M. Gerling**, S. Vukelić, A. Schäfer, B. Kokschi; Proline-glutamate chimera's side chain conformation directs the type of  $\beta$ -hairpin structure; *Amino Acids* **2014**, *46*, 177-186.
10. H. Erdbrink, E. K. Nyakatura, S. Huhmann, **U.I.M. Gerling**, D. Lentz, B. Kokschi; A synthesis of enantiomerically pure (2*S*,3*S*)-5,5,5-trifluoroisoleucine and (2*R*,3*S*)-5,5,5-trifluoro-*allo*-isoleucine; *Beilstein J. Org. Chem.* **2013**, *9*, 2009-2014.
9. P. D. Rakowska, H. Jiang, S. Ray, A. Pyne, B. Lamarre, M. Carr, P. J. Judge, J. Ravi, **U.I.M. Gerling**, B. Kokschi, G. J. Martyna, B. W. Hoogenboom, A. Watts, J. Crain, C. R. M. Grovenor, M. G. Ryadnov; Nanoscale imaging reveals laterally expanding antimicrobial pores in lipid bilayers; *Proc. Natl. Acad. Sci. U.S.A* **2013**, *110*, 8918-8923.
8. H. Erdbrink, I. Peuser, **U.I.M. Gerling**, D. Lentz, B. Kokschi, C. Czekelius; Conjugate hydrotrifluoromethylation of  $\alpha$ ,  $\beta$ -unsaturated acyl-oxazolidinones: synthesis of chiral fluorinated amino acids; *Org. Biomol. Chem.* **2012**, *10*, 8583-8586.
7. J. Maity, P. Saha, **U.I.M. Gerling**, D. Lentz, B. Kokschi; An approach for simultaneous synthesis of *cis*- and *trans*-3-substituted proline-glutamic acid chimeras. *Synthesis*; **2012**, *44*, 3063-3070.
6. M. Salwiczek, E. K. Nyakatura, **U.I.M. Gerling**, S. Ye, B. Kokschi; Fluorinated Amino Acids: Compatibility with native protein structures and effects on protein-protein interactions; *Chem. Soc Rev.* **2012**, *41*, 2135-2171.

5. R. Rezaei Araghi, C. Baldauf, **U.I.M. Gerling**, C. D. Cadicamo, B. Kokschi; A systematic study of fundamentals in  $\alpha$ -helical coiled coil mimicry by alternating sequences of  $\beta$ - und  $\gamma$ -amino acids; *Amino Acids* **2011**, *41*, 733-742.
4. E. Brandenburg, H. v. Berlepsch, **U.I.M. Gerling**, C. Böttcher, B. Kokschi; Inhibition of Amyloid Aggregation by Formation of Helical Assemblies; *Chem. Eur. J.* **2011**, *17(38)*, 10651-10661.
3. **U.I.M. Gerling**, E. Brandenburg, H.v. Berlepsch, K. Pagel, B. Kokschi; Structure Analysis of an Amyloid-Forming Model Peptide by a Systematic Glycine and Proline Scan; *Biomacromolecules*. **2011**, *12(8)*, 2988-96.
2. A.Botev, L.M. Munter, R. Wenzel, L. Richter, V. Althoff, J. Ismer, **U. Gerling**, C. Weise, B. Kokschi, P.W. Hildebrand, R. Bittl, G. Multhaupt; The Amyloid Precursor Protein C-Terminal Fragment C100 Occurs in Monomeric and Dimeric Stable Conformations and Binds  $\gamma$ -Secretase Modulators; *Biochemistry*, **2011**, *50*, 828-825.
1. J.A. Falenski, **U. Gerling**, B. Kokschi; Multiple glycosylation of *de novo* designed  $\alpha$ -helical coiled coil peptides; *Bioorg. Med. Chem.* **2010**, *18*, 3703-3706.

#### ORAL PRESENTATIONS AT CONFERENCES AND WORKSHOPS:

13. "Evaluating Fluorine's Impact on Amyloid Formation - a Systematic Study Using a Coiled-Coil Based Model Peptide"; *workshop "Biomolecules and synthetic nanostructures in cells and model systems: experimental and theoretical studies"*, funded by Alexander von Humboldt Foundation, Kiev / Ukraine, 17.11.**2013**.
12. "Investigation of the Structure of Amyloid forming model peptides"; *The Role of Sugar Moieties in Folding and Assembly of Amyloids – Novel Targets for Treating Neurodegenerative Diseases*, Workshop of Freie Universität Berlin – Tel Aviv University, Berlin / Germany, 07.11.**2013**.
11. "The Influence of Fluorine on Amyloid forming Model Peptides"; *Summer School 2013 of the Helmholtz Graduate School for "Macromolecular Bioscience"*, Berlin / Germany, 23.09.**2013**.

10. "Der Einfluss fluorierter Aminosäuren auf Amyloid-bildende Modellpeptide"; *Defence for the second period of funding for the Graduate School # 1582 "Fluorine as a Key Element"*, Berlin / Germany, 17.09.**2013**.
9. "Forschungspraktikum: Peptide, Struktur und ihre Funktion"; *Ideenwerkstatt zur Forschungsorientierten Lehre in interdisziplinären Verbundprojekten*, Berlin / Deutschland, 04.07.**2013**.
8. "The Influence of Fluorine on Amyloid forming Model Peptides"; *1<sup>st</sup> PhD workshop of the Helmholtz Graduate School for "Macromolecular Bioscience"*, Teltow / Germany, 29.04.**2013**.
7. "The Influence of Fluorine on Amyloid forming Model Peptides"; *Seminar of the Graduate School # 1582 "Fluorine as a Key Element"*, Berlin / Germany, 08.02.**2013**.
6. "The Influence of Fluorine on Amyloid forming Model Peptides"; *21<sup>st</sup> Winter Fluorine Conference*, St. Pete Beach (FL) / USA, 17.01.**2013**.
5. "The Influence of Fluorine on Amyloid forming Model Peptides"; *3<sup>rd</sup> PhD workshop of the Graduate School # 1582 "Fluorine as a Key Element"*, Burg / Germany, 23.10.**2012**.
4. "The Influence of Fluorine on Amyloid forming Model Peptides"; *6<sup>th</sup> Peptide Engineering Meeting*, Atlanta (GA) / USA, 03.10.**2012**.
3. "The Influence of Fluorine on Amyloid forming Model Peptides"; *Seminar of the Graduate School # 1582 "Fluorine as a Key Element"*, Berlin / Germany, 27.01.**2012**.
2. "The Influence of Fluorine on Amyloid forming Model Peptides"; *1<sup>st</sup> PhD workshop of the Graduate School # 1582 "Fluorine as a Key Element"*, Rheinsberg / Germany, 08.10.**2010**.
1. "The Influence of Fluorine on Amyloid forming Model Peptides"; *14. Deutscher Fluortag*, Schmitten / Germany, 27.09.**2010**.

## POSTERS:

4. "Der Einfluss fluorierter Aminosäuren auf Amyloid-bildende Modellpeptide"; *Defence for the second period of funding for Graduate School # 1582 "Fluorine as a Key Element"*, Berlin / Germany, 17.09.**2013**.
3. "The Influence of Fluorine on Amyloid forming Model Peptides"; *243<sup>th</sup> ACS National Meeting*, San Diego (CA) / USA, 25.03.-29.03.**2012**.
2. "The Influence of Fluorine on Amyloid forming Model Peptides"; *10<sup>th</sup> German Peptide Symposium*, Berlin / Germany, 07.03.-10.03.**2011**.
1. "The Influence of Fluorine on Amyloid forming Model Peptides"; *Perugia Fluorine Days*, Perugia / Italy 11.07.-15.07.**2010**.



## DANKSAGUNG

Ich danke Frau Prof. Dr. Beate Koksch für die Überlassung dieses vielseitigen Themas. Besonders dankbar bin ich für den mir stets gewährten Freiraum eigene Ideen zu verfolgen und umzusetzen. Darüber hinaus danke ich Ihr für die Förderung meiner Arbeit durch die Teilnahme an zahlreichen nationalen und internationalen Konferenzen, die es mir ermöglichten in Kontakt mit vielen Wissenschaftlern zu treten.

Herrn Prof. Dr. Rainer Haag danke ich für die Übernahme des Zweitgutachtens meiner Dissertation.

Ich bedanke mich herzlich bei Frau Dr. Allison Ann Berger für die zügige und gründliche Korrektur dieser Dissertation sowie zahlreicher englischsprachiger Manuskripte. Den ehemaligen Arbeitsgruppenmitgliedern Herrn Dr. Mario Salwiczek und Herrn Dr. Cosimo Cadicamo danke ich für die stete Bereitschaft Fragestellungen zu meinem Projekt zu diskutieren, sowie für die Bereitstellung der fluorierten Aminosäure *(S)*-2-amino-4,4-difluorobutansäure. Herrn Dr. Kevin Pagel danke ich für das Design des hier verwendeten Modellpeptids. Frau Dr. Elizabeth Nyakatura danke ich für die geduldige Einführung in die Methodik der SEC/SLS Messungen. Den Mitgliedern der Arbeitsgruppe danke ich für das angenehme Arbeitsklima. Desweiteren danke ich den Studenten, die mir im Rahmen Ihrer Praktika, Bachelor- oder Masterarbeiten bei der Synthese einiger Peptide hilfreich waren.

Herrn Prof. Dr. Czekelius danke ich für die Bereitstellung der fluorierten Aminosäuren *(2S,3R)*-2-(*tert*-butoxycarbonylamino)-4,4,4-trifluoro-3-methylbutansäure, *(2S,3R)*-2-amino-4,4,4-trifluoro-3-methylbutansäure, *(2S,3S)*-2-amino-4,4,4-trifluoro-3-methylbutansäure und *(2S,3R)*-2-amino-3-trifluoromethylpentansäure. Ich danke Holger Erdbrink herzlich für die Synthese dieser Verbindungen sowie für die geduldige Bereitschaft Fragen zur Synthese, und dem gemeinsamen Projekt zu diskutieren.

Desweiteren danke ich Herrn Prof. Dr. Günter Haufe und Herrn Dr. Malte Behrends (Universität Münster) für die Bereitstellung der Aminosäure *(S)*-2-amino-4-fluoraminobutansäure, die diese Arbeit komplettiert hat.

Großer Dank gebührt Frau Prof. Dr. Anne Ulrich, Herrn Dr. Stephan Grage und Herrn Dr. Parvesh Wadhvani (Karlsruher Institut für Technologie) für die Festphasen NMR-Messungen an den monofluorierten Fibrillen, die das Projekt entscheidend bereichert haben.

Herrn Dr. Maity danke ich für die Synthese der beiden Prolin-Glutaminsäure-chimera, die er im Rahmen seines Postdocs synthetisiert hat. Ich bedanke mich bei Herrn Dr. Schäfer für 2D-NMR-Messungen an den daraus entstandenen Peptiden sowie den Mitarbeitern der NMR-Abteilung für die zuverlässigen Messungen aller meiner Verbindungen.

Ich danke Herrn Dr. H. von Berlepsch für die Anfertigung der TEM-Aufnahmen.

Mein besonderer Dank gilt meinem Partner und meiner Familie für deren Rückhalt, Unterstützung und Verständnis während dieser Arbeit und meines gesamten Studiums. Das in mich gesetzte Vertrauen und der stete Zuspruch haben mich immer angetrieben und mir Motivation und Kraft gegeben.



## KURZZUSAMMENFASSUNG

Ein gemeinsames Merkmal vieler neurodegenerativer Erkrankungen ist die strukturelle Umfaltung von Peptiden aus einer nativen, funktionalen Konformation in unlösliche Amyloid-Ablagerungen. Amyloidbildung tritt aber nicht nur im Zusammenhang mit Krankheiten auf, sondern ist eine generelle Eigenschaft von Peptiden. Durch ihre besondere Stabilität und ihre regelmäßigen Strukturen sind Amyloide mittlerweile auch interessante Materialien für Bio- oder Nanotechnologische Anwendungen geworden. In dieser Hinsicht wurde der Einbau nicht natürlicher Bausteine, insbesondere fluorierter Aminosäuren, eine Standardstrategie um solche Strukturen zu modifizieren. Durch seine besonderen stereoelektronischen Eigenschaften kann Fluor die Struktur, die Funktion und die Stabilität von Peptiden und Proteinen drastisch beeinflussen. Frühere Ansätze, die Eigenschaften fluorierter Aminosäuren zu untersuchen, haben sich hauptsächlich auf helikale Systeme beschränkt. In Amyloiden wurde Fluor bisher hauptsächlich als diagnostisches Label eingebaut. Inwieweit Fluorierungen den Prozess der Amyloidbildung beeinflussen wurde bisher nicht systematisch untersucht.

Die vorliegende Arbeit untersucht den Einfluss von Fluor auf die Amyloidbildung anhand eines Modellpeptids, das in der Arbeitsgruppe von Frau Prof. Dr. B. Kokschi entwickelt wurde. Das Modell wurde so generiert, dass es unter kontrollierten Bedingungen aus einer anfänglich helikalen Struktur in  $\beta$ -faltblattreiche Amyloidstrukturen umfalten kann. Frühere Arbeiten lieferten fundierte Erkenntnisse hinsichtlich der anfänglichen *coiled coil*-Struktur und des internen Faltungsmotivs der Fibrille. Diese stellten die Grundlage für die aktuellen Untersuchungen dar. Im Rahmen dieser Arbeit wurden zwei benachbarte Valine, die eine Schlüsselfunktion für den Umfaltungsprozess darstellen durch verschiedene fluoridierte Aminosäuren ersetzt. Diese Aminosäuren unterschieden sich hinsichtlich ihres Fluorgehaltes und ihrer intrinsischen Eigenschaften, wie Größe, Hydrophobie und  $\alpha$ -Helixpropensität. Mithilfe des systematischen Ansatzes wurden diese Eigenschaften fluorierter Aminosäuren hinsichtlich ihres Einflusses auf den Prozess der Amyloidbildung untersucht. Die Peptide, welche mit einer Reihe von Methoden untersucht wurden, zeigten ein unerwartetes Faltungsverhalten als Folge der variierten stereoelektronischen Eigenschaften, die wiederum direkt auf den Einbau der jeweiligen Aminosäure zurückgeführt werden konnten. Anhand von Berechnung der kritischen Größe des Nukleus, einem Intermediat das als Templat für die Aggregation fungiert, konnte ein möglicher Mechanismus für den Faltungsprozess vorgeschlagen werden. Die Ergebnisse dieser Arbeit werden dazu beitragen den Prozess der Amyloidbildung und dessen Modulation durch fluoridierte Aminosäuren besser zu verstehen.



## ABSTRACT

A common hallmark of many neurodegenerative diseases is the conformational transition of peptides from a native, functional form into insoluble amyloid deposits. Amyloid formation, however, is not a specific feature of disease-related proteins, but instead appears to be a general property of peptides and proteins. The outstanding mechanical stability and remarkably regular fibrous architecture have made amyloids also attractive materials for bio- or nano-technological applications. In this regard nonnatural building blocks and fluorinated amino acids in particular, have become standard tools for modulating such structures. Due to its unique stereoelectronic properties fluorine can have dramatic effects on structure, function, and stability of peptides and proteins. Previous approaches to assessing the properties of fluorinated amino acids have mainly focused on helical systems. In terms of amyloid forming peptides, fluorine has mainly been used as diagnostic reporter group. As to what extent fluorination influences the process of amyloid formation has not been investigated systematically so far.

The present thesis evaluates the impact of fluorine on amyloid formation with the help of a model peptide that was developed in the group of Prof. Dr. Beate Kokschi. The model was designed to provide an  $\alpha$ -helical starting structure that can fold into  $\beta$ -sheet rich amyloids under controlled conditions. Previous studies revealed solid structural information about the initial coiled coil structure and the final fibril architecture, which serve as a basis for the present investigations. In the course of this work two neighboring valine residues that play a key role in the structural transition were replaced by several fluorinated amino acids that contain different fluorine content in their side chains. These amino acids vary with regard to their intrinsic properties, such as size, hydrophobicity, and secondary structure propensities. By means of this systematic approach the properties of fluorinated amino acids have been investigated for their impact on the amyloid formation process. The resulting peptides, which have been analyzed by a battery of high and low resolution techniques, show unexpected folding behaviors as a consequence of the interplay between stereoelectronic effects that can be directly attributed to the particular incorporated amino acid. By determining the critical size of the nucleus, an intermediate species that serves as template for peptide aggregation, a potential pathway for the structural transition has been suggested. The results of this thesis will contribute to an understanding of amyloid formation and how this process can be modulated by fluorinated amino acids.



## ABBREVIATIONS

<b>Å</b>	Angstrom (1 Angstrom = $1.0 \times 10^{-10}$ m)
<b>AA</b>	Amino acid
<b>A<math>\beta</math></b>	Amyloid $\beta$
<b>ACN</b>	Acetonitrile
<b>AD</b>	Alzheimer's disease
<b>AFM</b>	Atomic force microscopy
<b>AMP</b>	Antimicrobial peptides
<b>APP</b>	Amyloid Precursor Protein
<b>AU</b>	Analytical ultracentrifugation
<b>Boc</b>	tert-Butyloxycarbonyl
<b>CAT</b>	Chloramphenicol acetyltransferase
<b>cAMP</b>	cyclic adenosine monophosphate
<b>CD</b>	Circular dichroism
<b>COSY</b>	Correlation spectroscopy
<b>CR</b>	Congo red
<b>Da</b>	Dalton
<b>DBU</b>	1,8-diazabicyclo[5.4.0]undec-7-ene
<b>DCM</b>	Dichloromethane
<b>DIC</b>	Diisopropylcarbodiimide
<b>DIPEA</b>	N,N-diisopropyl ethylamine
<b>DMF</b>	Dimethylformamide
<b>DMSO</b>	Dimethylsulfoxide
<b>DNA</b>	Desoxyribonucleic acid
<b>E. coli</b>	Escherichia coli
<b>eq.</b>	equivalent
<b>ESI</b>	Electrospray ionization
<b>Fmoc</b>	9-fluorenylmethyloxycarbonyl
<b>GdnHCl</b>	Guanidine hydrochloride
<b>GFP</b>	Green fluorescent protein
<b>HOAt</b>	1-hydroxy-7-azabenzotriazole
<b>HOBt</b>	1-hydroxybenzotriazole
<b>HPLC</b>	High performance liquid chromatography
<b>IAPP</b>	Islet amyloid polypeptide
<b>IR</b>	Infrared
<b>MD</b>	Molecular dynamics
<b>MW</b>	Molecular weight
<b>NMP</b>	N-Methyl-2-pyrrolidinone
<b>NMR</b>	Nuclear magnetic resonance
<b>NOE</b>	Nuclear Overhauser effect
<b>NOESY</b>	Nuclear Overhauser effect spectroscopy
<b>P<sup>cis-E</sup></b>	cis-proline glutamate chimera

<b>PET</b>	Positron emission tomography
<b>Pip</b>	Piperidine
<b>P<sup>trans-E</sup></b>	trans-proline glutamate chimera
<b>ROESY</b>	Rotating frame nuclear Overhauser effect spectroscopy
<b>RP</b>	Reversed phase
<b>SEC</b>	Size exclusion chromatography
<b>SLS</b>	Static light scattering
<b>SPPS</b>	Solid phase peptide synthesis
<b>TBTU</b>	O-(benzotriazol-1-yl)-N,N,N',N'-tetramethyluronium tetrafluoroborate
<b>TEM</b>	Transmission electron microscopy
<b>tert</b>	tertiary
<b>TFA</b>	Trifluoroacetic acid
<b>TFE</b>	Trifluoroethanol
<b>ThT</b>	Thioflavin T
<b>TIS</b>	Triisopropylsilane
<b>TOCSY</b>	Total correlation spectroscopy
<b>ToF</b>	Time of flight
<b>UV</b>	Ultraviolet
<b>VdW</b>	van der Waals
<b>Vis</b>	visible

Abbreviations of the 20 canonical amino acids are consistent with the biochemical nomenclature proposed by the IUPAC-IUB commission (*Eur. J. Biochem.* **1984**, *138*, 9-37).

Abbreviations of non-coded amino acids relevant to the present thesis are given below. If not stated otherwise, the abbreviations correspond to the L-amino acids.

<b>4'-Tfl</b>	4',4',4'-trifluoroisoleucine; (2S,3R)-2-amino-3-(trifluoromethyl)pentanoic acid
<b>5-Tfl</b>	5,5,5-trifluoroisoleucine; (S)-2-amino-5,5,5-trifluoropentanoic acid
<b>Abz</b>	ortho-aminobenzoic acid
<b>Abu</b>	aminobutyric acid; (S)-2-aminobutyric acid
<b>DfeGly</b>	difluoroethylglycine; (S)-2-amino-4,4-difluorobutanoic acid
<b>DfpGly</b>	difluoropropylglycine; (S)-2-amino-4,4-difluoropentanoic acid
<b>HfL</b>	5,5,5,5',5',5'-hexafluoroleucine
<b>HfV</b>	4,4,4,4',4',4'-hexafluorovaline
<b>MfeGly</b>	monofluoroethylglycine; (S)-2-amino-4-fluorobutanoic acid
<b>TfeGly</b>	trifluoroethylglycine; (S)-2-amino-4,4,4-trifluorobutanoic acid
<b>TfV</b>	4,4,4-trifluorovaline; (S)-2-amino-3-(trifluoromethyl)butanoic acid



## CONTENTS

<b>1</b>	<b>Introduction</b> .....	<b>1</b>
<b>2</b>	<b>Properties of fluorinated amino acids</b> .....	<b>3</b>
2.1	Fluorination of aliphatic amino acids .....	3
2.2	Fluorination of aromatic amino acids .....	6
2.3	Fluorination of polar or charged amino acids .....	7
2.4	Fluorination of proline .....	8
<b>3</b>	<b>Amyloids: regarding pathogenicity and potential biomaterials</b> .....	<b>11</b>
3.1	The phenomenon of aggregation and common structural characteristics of amyloids .....	11
3.2	Amyloidogenic structures found in diseases .....	14
3.3	Amyloid structures as scaffolds and templates for biomaterials .....	17
<b>4</b>	<b>Aliphatic fluorinated amino acids in peptides and proteins</b> .....	<b>21</b>
4.1	Fluorinated amino acids in helical peptides .....	21
4.1.1	Proteolytic stability of fluorinated peptides .....	22
4.1.2	Hydrophobicity, packing, or the “fluorous effect” .....	23
4.1.3	Altered activity and function of fluorinated peptides .....	27
4.2	Fluorinated amino acids in $\beta$ -sheet forming peptides .....	28
4.3	Fluorinated amino acids in amyloid forming peptides .....	32
4.3.1	Fluorinated amino acids as $^{19}\text{F}$ -NMR-labels in amyloid structures .....	33
4.3.2	Fluorinated amino acids as tools to modulate amyloid fibrils .....	36
<b>5</b>	<b>Aim of the work</b> .....	<b>39</b>
<b>6</b>	<b>Applied Methods</b> .....	<b>41</b>
6.1	Circular dichroism spectroscopy .....	41
6.2	Dye Binding studies .....	44
6.3	Size exclusion / static light scattering .....	45
6.4	Solid state $^{19}\text{F}$ -NMR .....	48
6.4.1	The CODEX experiment .....	50
<b>7</b>	<b>Results and discussion</b> .....	<b>53</b>
7.1	The coiled coil as a model to study amyloid formation .....	53
7.2	The internal fibril architecture of VW18 .....	57
7.3	The impact of proline ring puckering on turn conformations .....	62
7.3.1	The different turn motifs of $\beta$ -hairpins and amyloids .....	62
7.3.2	The effect of a glutamate side chain on proline’s ring conformation .....	64
7.4	The role of oligomeric intermediates in the amyloid formation process of VW18 .....	72
7.5	Altering the amyloid formation process by fluorinated amino acids .....	79
7.5.1	The fluorinated building blocks .....	80
7.5.2	Hydrophobicity and spatial demand of fluorinated amino acids .....	81
7.5.3	The $\alpha$ -helix propensity of fluorinated amino acids .....	82
7.5.4	Amyloid formation rates of fluorinated VW18 variants .....	86
7.5.5	Analysis of the overall VW18 fibril structure by solid state $^{19}\text{F}$ -NMR .....	91
7.5.6	The importance of the initial structure on amyloid formation rates .....	95

<b>8</b>	<b>Summary</b> .....	<b>101</b>
<b>9</b>	<b>Outlook</b> .....	<b>105</b>
<b>10</b>	<b>Experimental Section</b> .....	<b>109</b>
10.1	General Methods.....	109
10.2	Synthesis of fluorinated amino acids.....	109
10.2.1	Synthesis of (S)-2-amino-4,4,4-trifluorobutanoic acid (TfeGly) (3) <sup>433,237</sup> .....	110
10.2.2	Synthesis of (S)-2-amino-4-fluorobutanoic acid (MfeGly) (1) .....	113
10.2.3	Synthesis of Fmoc protected TfV and Tfl.....	114
10.3	Peptide synthesis, purification and characterization.....	117
10.3.1	Automated peptide synthesis .....	117
10.3.2	Manual peptide synthesis.....	118
10.3.3	Capping .....	119
10.3.4	Cleavage from the resin .....	119
10.3.5	Preparative HPLC .....	119
10.3.6	Analytical HPLC .....	120
10.3.7	Characterization by ESI-ToF .....	121
10.4	Synthesized peptides.....	121
10.5	Folding studies.....	122
10.5.1	Sample preparation and concentration determination .....	122
10.5.2	pH adjustment.....	124
10.5.3	CD spectroscopy.....	124
10.5.4	$\alpha$ -helix propensity measurements.....	125
10.5.5	HPLC assay to estimate the hydrophobicity and side chain volume of the Fmoc-amino acids .....	125
10.5.6	Size exclusion / static light scattering .....	126
10.5.7	Thioflavin T fluorescence staining assay .....	127
10.5.8	Transmission electron microscopy .....	127
10.5.9	Solution <sup>1</sup> H-NMR spectroscopy of P1_P variants.....	128
10.5.10	Solid-state <sup>19</sup> F-NMR of VW18 variants containing MfeGly .....	128
<b>11</b>	<b>Literature</b> .....	<b>131</b>

## 1 Introduction

More than one hundred years ago the neurodegenerative disorder, later known as Alzheimer's disease (AD), was discovered by Aloys Alzheimer, who detected neurofibrillary tangles and deposits corresponding to senile plaques in the brain of a woman suffering from progressive memory impairment, hallucinations, delusions, paranoid ideas, apraxia, and several behavioral disorders.<sup>1</sup> Over the years many other degenerative diseases, such as Huntington's, Parkinson's, Creutzfeldt-Jakob, and other prion related diseases, have been attributed to deposits consisting of non-covalently bound peptides.<sup>2</sup> These insoluble fibrillar peptide aggregates, commonly called amyloids, share microscopic and macroscopic features such as a characteristic cross- $\beta$  core structure, although their primary peptide sequences can be strikingly different.<sup>3</sup> However, amyloid formation was later declared as a generic, inherent property of polypeptide chains, since such a behavior was also found for peptides and proteins that are non-disease related.<sup>4-7</sup>

The late-onset form of Alzheimer's occurs with ever-increasing frequency due to the greater life expectancy of people in industrial countries worldwide. The risk for developing AD between the ages of 65 and 100 is 33% for men and 45% for women, with an annual increase of 1-2% in the seventh decade of life and more than 4% in the eighth decade of life.<sup>1</sup> The annual world-wide cost for the treatment and informal care for approximately 29 million dementia patients was estimated at 315 billion USD for the year 2009.<sup>8</sup> Since the number of aging people is expected to double within the next 15 years, AD and other dementia disorders will become an even greater public, social, and economic problem.

Interestingly, recent studies indicate that AD and type 2 diabetes mellitus (T2DM) share several molecular processes that underlie the respective degenerative developments.<sup>9,10</sup> This was attributed to impaired insulin signaling and insulin resistance associated with T2DM which mediate cognitive impairment and AD.<sup>9,11-13</sup> Also, tau gene expression and phosphorylation are regulated through insulin and insulin-like growth factor (IGF) signaling cascades.<sup>14,15</sup> Abnormally phosphorylated tau plays a major role in the pathology of AD as these species form the intracellular neurofibrillary tangles that cause neurodegeneration.<sup>16</sup> Increased risk of developing mild cognitive impairment (MCI), dementia, or AD have been found for individuals suffering from T2DM.<sup>17,18</sup> Also, obesity increases the risk three fold for subsequently developing AD.<sup>9</sup> Although treatments are still limited, improvements in diagnostic methods allow for an early diagnosis,<sup>19-21</sup> at stages where symptoms can be more effectively reduced. Advances in molecular neurobiology, as well as emerging

imaging technologies, promise to provide surrogate markers to detect and monitor progression during the early clinical asymptomatic stages.

Since amyloid formation was discovered to be a general property of also non-disease related proteins, many natural occurring and also *de novo* designed peptides were studied with regard to their structure-environment relationship. Several environmental triggers, such as oxidative stress, pH extremes, ionic strength, the presence of metal ions or membranes, and the local peptide concentration have been found to influence the amyloid formation process.<sup>22-25</sup> The structural features of amyloids that are responsible for their devastating pathogenic effects have also made these structures interesting for materials scientists. Their outstanding mechanical stability and remarkably regular fibrous architecture give them the potential to be used as ideal scaffolds for a variety of bio- and nano-technological applications.<sup>26-28</sup> In this context, also unnatural amino acids are likely to be of special interest as they have been found to, in many cases, beneficially alter the chemical and biophysical properties of peptides and proteins. In this regard, especially fluorination of amino acid side chains has become a powerful tool for peptide and protein modification.<sup>29</sup> The small size of fluorine, paired with the strongest inductive effect among all elements, can be accompanied by profound and unexpected changes in biological activity. Fluorinated peptides have become a paradigm for fashioning materials with unusual and useful properties.<sup>30</sup> Moreover, fluorination of organic compounds was established as a successful strategy for drug development. Such materials often show higher bioavailability,<sup>31</sup> and, in terms of peptidic materials, also higher proteolytic resistance, in some cases allowing for oral administration. More than 20% of current pharmaceuticals contain at least one fluorine atom.<sup>32</sup>

In terms of amyloids, however, fluorinated amino acids have rarely been investigated. They were efficiently used as reporter groups for analytical methods, such as nuclear magnetic resonance (NMR)<sup>33,34</sup> or positron emission tomography (PET),<sup>35</sup> to elucidate the structure of amyloid fibrils, detect fibrillar deposits *in vivo*, or to follow the structural transition of functional peptides to insoluble amyloid aggregates. Their effect on the amyloid formation process itself has been less studied to date.

Since future developments of amyloid structures as biomaterials could profit by fluorination in terms of either a diagnostic or a functional perspective, it is of fundamental interest to study the impact of fluorinated amino acids on amyloid formation. Understanding the mechanism of protein aggregation, and the factors that influence it, is a key step in controlling such processes, in identifying effective therapeutic strategies for protein aggregation disorders, and in developing new self-assembling materials with improved properties.

## 2 Properties of fluorinated amino acids

Fluorine, in form of minerals, is one of the most abundant elements in the earth's crust.<sup>36</sup> However, naturally occurring organo-fluorine compounds are rarely found, especially in terms of biological molecules.<sup>37,38</sup> None of the 20 naturally occurring amino acids encoded in the universal genetic code contains fluorine substituents. The incorporation of fluorine into biomolecules turned out to be very successful for the development of pharmaceuticals, since such molecules have been found to gain an increase in bioavailability<sup>39</sup> as well as biological activity.<sup>40,41</sup> Fluorinated amino acids have also become a powerful tool to modulate the properties of peptides and proteins. The unique stereoelectronic properties that arise from an unprecedented combination of small size, very low polarizability and the strongest inductive effect found among chemical elements, allow altering biophysical and chemical properties of peptides and proteins in terms of hydrophobicity, acidity/basicity, reactivity and conformation. The incorporation of fluorine substituents into natural amino acids has led to often desirable yet unpredictable results. In the following sections, a few prominent examples are given that illustrate what can be expected from the fluorination of amino acids.

### 2.1 Fluorination of aliphatic amino acids

Interestingly, most studies published in recent years deal with fluorinated analogues of aliphatic or aromatic hydrophobic amino acids as well as fluorinated methionines and prolines, although synthesis of other fluorinated amino acids have been described as well.<sup>42,43</sup> Hydrogen-to-fluorine substitutions are often discussed to be conservative in terms of size.<sup>32</sup> However, a careful distinction between single or multiple fluorination of alkyl chains is necessary. Although hydrogen and fluorine are often discussed to be almost isosteric, this can not be simply extrapolated to a higher amount of fluorine substituents per alkyl chain.<sup>44</sup> In fact the  $\text{CF}_3$  group is approximately twice the van der Waals volume of a  $\text{CH}_3$  group and the steric effects of the  $\text{CF}_3$  are more similar to that of an isopropyl group,<sup>45</sup> or even larger substituents, such as cyclohexyl and sec-butyl groups.<sup>46</sup>

Size and shape of a side chain determine its ability to participate in packing interactions with other side chains and size and hydrophobicity closely correlate for aliphatic amino acids.<sup>47</sup> The electronegativity of the fluorine atom explains one major distinction between the C-H and the C-F bond. The C-F bond exhibits a considerable dipole moment, which is reversed in its orientation compared to the relatively small C-H dipole. Thus, single

fluorination of aliphatic side chains actually reduce rather than increase the hydrophobicity.<sup>48</sup> A certain number of fluorine atoms per alkyl chain is necessary to achieve an increase in hydrophobicity for the particular amino acid, likewise the replacement of one or two CH<sub>3</sub> groups with CF<sub>3</sub> groups.<sup>49</sup>

The common way to quantify hydrophobicity is to measure the distribution coefficient between two immiscible liquid phases, such as water and octanol or heptanol.<sup>47</sup> In addition, some HPLC-based methods have been developed to measure the hydrophobicity of nonfluorinated molecules.<sup>50,51</sup> These methods were based on the assumption that the nonpolar stationary phase mimics a biological membrane.<sup>52</sup> However, due to different scaling the absolute hydrophobicity values of the amino acids that were investigated show disparities.

Kovacs *et al.* used a 10-residue peptide sequence, Ac-XGAKGAGVGL-amide, in which X was replaced by all natural amino acids, to study the impact of pH and buffer conditions on the intrinsic hydrophilicity/hydrophobicity of amino acid side chains in peptides.<sup>47</sup> The authors found a dependency of the intrinsic hydrophilicity/hydrophobicity on pH and buffer conditions, including the type of salt or ion-pairing reagent (only for partially charged side chains, such as Lys, His, Arg, Asp, and Glu).

Another RP-HPLC-based approach using the Fmoc protected form of aliphatic amino acids and fluorinated analogues of  $\alpha$ -aminobutyric acid (Abu) was accomplished by Samsonov *et al.* in the group of Prof. B. Kokschi (*Figure 2.1*).<sup>49</sup>

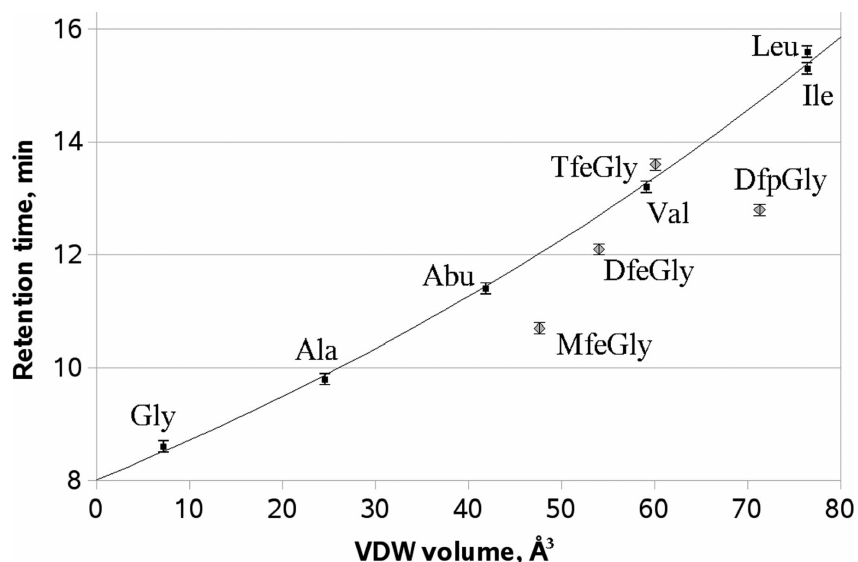


**Figure 2.1:** Retention times of the Fmoc-amino acids plotted against the van der Waals volume of the side chains. Nonfluorinated amino acids are represented by black squares, the correlation between them is shown with a black line, and fluorinated amino acids are represented by gray diamonds (reproduced with permission from Samsonov *et al.*, Copyright © American Chemical Society).<sup>49</sup>

They showed that the retention time of aliphatic amino acids increases non linearly with increasing side chain volume, and explained this by a decreasing polarizing effect of the  $\alpha$ -amide and the carboxyl group on the alkyl chain with elongated chains length.<sup>47</sup>

For the partially fluorinated analogues of Abu (MfeGly, DfeGly, TfeGly, and DfpGly) the retention times do not fit into the correlation shown for the pure hydrocarbon derivatives. Here, hydrophobicity increases more progressively with increasing fluorine content than it does with size. The single fluorinated analogue of Abu (MfeGly) is less hydrophobic than Abu although it is larger in size. Also, DfpGly that is close to leucine in size, is much less hydrophobic than one might expect from only considering its side chain volume. Only TfeGly was found to be similar to valine with regard to both properties, namely size and hydrophobicity. The results are consistent with the finding that partial aliphatic fluorination decreases hydrophobicity, whereas perfluorination results in a progressive increase in hydrophobicity.<sup>48</sup> However, since only a few fluorinated analogues have been investigated so far, a complete hydrophobicity scale of fluorinated amino acids is still missing at this time. Moreover, the RP-HPLC-based method only gives reasonable results for non-ionizable side chains. Charged residues cause uncertainties due to dependency on pH and the presence of ions, as shown by Kovacs *et al.*<sup>47</sup>

The very low polarizability paired with the high electronegativity that comes along with fluorine could offer an explanation for the high hydrophobicity of highly fluorinated aliphatic hydrocarbons. These molecules tend to segregate from hydrophilic as well as from lipophilic environments. The strong electron withdrawing effect of fluorine on its surrounding results in less favorable interactions with water. The molecule is thus more hydrophobic. Just as increased hydrophobicity can not be generalized for fluorinated compounds, same holds true for increased lipophilicity. While fluorination of aromatic compounds in general leads to an increase in lipophilicity, the situation is more complex for partially fluorinated aliphatic carbonyl compounds. Their apparent lipophilicity depends on the choice of partitioning solvent.<sup>53</sup> The effect of fluorination on acidity and hydrogen bonding becomes more important in this context. Fluorinated components show a preference for the organic phase. The partitioning coefficient, however, is a measure of relative solubility in water and thus represents the hydrophobicity of a molecule rather than its lipophilicity. Especially highly fluorinated aliphatic compounds can form a third phase, the fluorous phase,<sup>54,55</sup> in addition to the aqueous and the organic phase. Also less favorable dispersion interactions between fluorinated and hydrocarbon compounds have been found.<sup>48</sup> Thus aliphatic fluorinations can also decrease lipophilicity and generalization for all fluorinated compounds would be misleading.

The strong inductive effect of fluorine can also influence the  $pK_a$  values of neighboring functional groups.<sup>56,57</sup> In general, the presence of fluorine increases the acidity of adjacent

groups and the effect is stronger on the  $\alpha$ -amino function than on the carbonyl group (*Figure 2.2*). These alterations affect the strength of hydrogen bonds that are crucial for secondary structure formation. Although the C-F bond exhibits a strong dipole moment, it is not generally accepted that it acts as a hydrogen bond acceptor. Nevertheless, some orthogonal polar interaction with carbonyl groups have been found in co-crystals of proteins with small molecules.<sup>44</sup> Still the individual impacts of properties like hydrogen bond strength,  $pK_a$ , and hydrophobicity on structure and stability of a molecule is context dependent and can not be easily predicted.

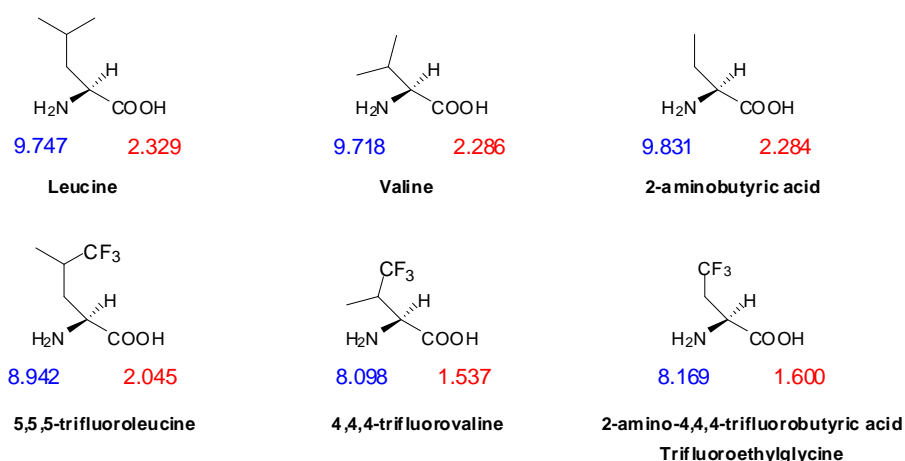


**Figure 2.2:** Comparison of the  $pK(NH_2)$  (blue) and the  $pK(COOH)$  (red) of natural amino acids with their corresponding fluorinated analogue.

## 2.2 Fluorination of aromatic amino acids

A hydrogen-to-fluorine substitution of an aromatic ring leads to a rearrangement of the electrostatic potential (*Figure 2.3*).<sup>58</sup> The hydrophobicity of the aryl side chain is usually increased. Single fluorination cause only little perturbation,<sup>59</sup> but the replacement of all five hydrogen atoms by fluorine leads to a notable increase in size, which can result in destabilization of proteins due to steric effects.<sup>60</sup> The molecular volume of  $C_6F_5$  (141Å<sup>3</sup>) is significantly higher than that of the nonfluorinated analogue  $C_6H_6$  (106Å<sup>3</sup>).<sup>60</sup> The quadrupole moment of aromatic rings arises from the partial positive charge of the sigma framework between two regions of  $\pi$ -electron density on the faces of the ring.<sup>61</sup> Usually the electrostatic potential of aromatic compounds is negative inside the aromatic ring and the hydrogen atoms at the outside of the ring are partially positively charged. This results in repulsive face-to-face interactions, whereas edge-to-face stacking is favored (*Figure 2.3 C*).<sup>62,63</sup> Due to inversed polarity of fully fluorinated aryl side chains attractive interactions between nonfluorinated and fluorinated phenyl side chains can be enhanced, thus face-to-face stacking is favored for this scenario.<sup>58,64</sup>



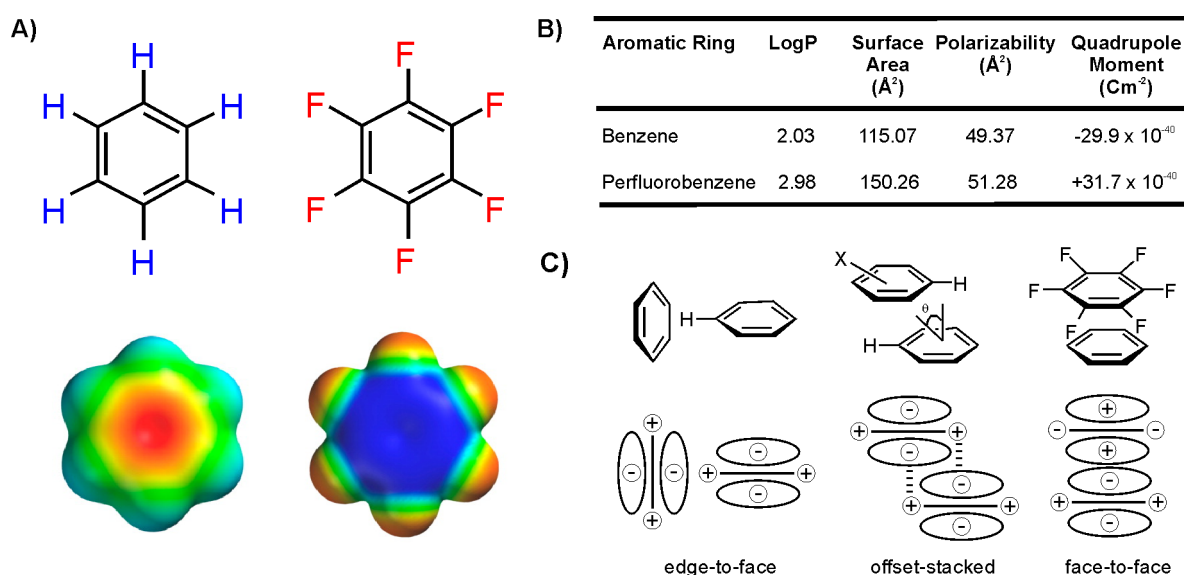


**Figure 2.3:** Influence of fluorine substitution on the aromatic ring. **A)** Electrostatic potential maps showing reversed electron distribution of perfluorobenzene in comparison to benzene. **B)** Comparison of the physical properties of benzene and perfluorobenzene (modified with permission according to Pace et al., Copyright © American Chemical Society).<sup>58</sup> **C)** Preferred  $\pi$ - $\pi$  stacking of hydrocarbon and halogenated aryl rings (redrawn from Waters et al.).<sup>62</sup>

The position of single fluorination on the aryl ring determines the direction of the dipole moment. The phenyl derivatives carrying a single fluorine substituent in position 2F, 3F, or 4F have the same size and overall polarity, but differ in their shape and dipole direction. Hence, they can be used to study the positional effect of fluorine substitution on aryl side chains.<sup>65</sup>

Similar effects regarding polarity and dipole moment can be found for fluorination of the other aromatic amino acids tyrosine and tryptophan. However, these examples are not further discussed here, since during the work of this thesis, only aliphatic fluorinated amino acids have been investigated. An overview of all fluorinated derivatives of natural amino acids that have been incorporated into peptides or proteins has been published by our group recently.<sup>66</sup>

## 2.3 Fluorination of polar or charged amino acids

Fluorine brings to bear a strong electronic effect on the properties of charged or polar functional groups.<sup>57</sup> Fluorination causes a decrease in the  $pK_a$  value of nearby carboxyl side chains. This causes a stabilization of the negatively charged residues for amino acids like Asp or Glu, and a destabilization of the positive charge in the side chain of Lys (protonated ammonium), His (imidazolium), and Arg (guanidinium).

Polar amino acids, like Ser, Thr, Asn, and Gln often participate in hydrogen bonding that stabilize secondary structures or plays a role in enzymatic reactions. Also,

posttranslational modifications, such as phosphorylation or glycosylation, usually take place on these functional side chains. The inductive effect of fluorine could strongly affect these interactions. However, fluorinated analogues of charged or polar amino acids have rarely been investigated in peptides and proteins. This might result from the difficulties that are inherent to the synthesis of these molecules. Often, either the final unprotected products or some precursors are found to be unstable.<sup>67</sup>

## 2.4 Fluorination of proline

Peptide bonds including a proline residue are clearly distinguishable from those formed by other amino acids. The  $N_\alpha$  and  $C_\alpha$  are both incorporated in the cyclic side chain of proline. The rigid side chain conformation induces a kink in the backbone of a peptide chain; therefore Pro is often found in turn or bend positions of polypeptides, instead of adopting  $\alpha$ -helical or  $\beta$ -sheet structures.<sup>68,69</sup>

The property of proline that is mainly affected upon fluorination is the conformation of the pyrrolidine ring. Native proline exists in an equilibrium of two common ring conformations, the  $C^Y$ -endo vs. the  $C^Y$ -exo conformation (Figure 2.4 A). Introduction of electronegative substituents like fluorine or carboxyl groups at the carbon atoms of the pyrrolidine alters the ring conformation, creating a preference for a *gauche* over an *anti* orientation.<sup>44</sup> This effect is especially enhanced when the substituent of the adjacent C atom is an amide (Figure 2.4 B).<sup>70</sup> Therefore, fluorination at C3 or C4 of the pyrrolidine ring leads to a strong *gauche* effect. Depending on the stereochemistry of the substituted carbon, the fluorination influences the equilibrium of  $C^Y$ -endo vs. the  $C^Y$ -exo conformation towards the conformation that enables a *gauche* orientation of the amide and the fluorine substituent.

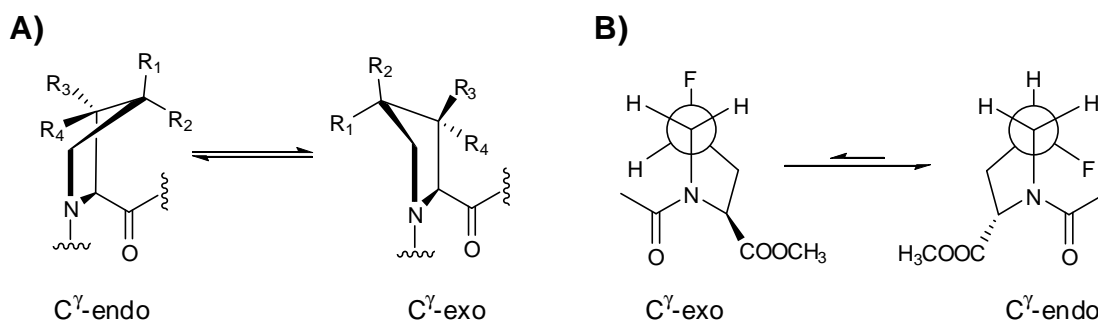


**Figure 2.4:** **A)** Equilibrium between the two most abundant ring conformations of the pyrrolidine ring. **B)** Newman projection of the C4-C5 single bond of C4 fluorinated Ac-Pro-OMe showing the preference for the *gauche* conformation in which the pyrrolidine ring adopts the  $C^Y$ -endo puckering.

---

Furthermore, the conformation of the ring directly affects the main-chain torsional angles ( $\psi$ ,  $\omega$ ,  $\phi$ ) that dictate the orientation of the peptide bond. The *cis/trans* equilibrium depends on the C $^{\gamma}$ -puckering,<sup>71</sup> and can thus be shifted upon fluorination as a consequence of a changed ring conformation. Usually peptides prefer the *trans*-peptide bond, but when a proline is involved the probability for a *cis*-peptide bond is much higher.<sup>72</sup> *Cis*-peptide bonds are often found with a C $^{\gamma}$ -endo pucker whereas *trans*-peptide bonds do not show such a preference.<sup>73</sup> Fluorine substituents that induce the C $^{\gamma}$ -exo pucker of the ring have a higher preference for a *trans* form, which is reflected by a higher value for  $K_{trans/cis}$  relative to the unsubstituted proline ring, while those with a C $^{\gamma}$ -endo pucker show a stabilization of the *cis* form.<sup>74-76</sup> This effect was also found for other electron withdrawing substituents that have been introduced into the pyrrolidine ring of proline.<sup>77</sup>



### 3 Amyloids: regarding pathogenicity and potential biomaterials

The self-assembly of misfolded proteins to large fibrillar aggregates is a common pathological feature of a number of human disorders, including several neurodegenerative diseases. Today it is known that almost every peptide sequence can be converted to amyloids under appropriate conditions, since the potential to form amyloids is an intrinsic characteristic of peptide and proteins.<sup>4-7</sup> Recently, amyloid fibrils have become more attractive in terms of nanotechnological application. These materials are characterized by great mechanical stability and a high degree of regularity in their structures, which makes them ideal starting points for functional and responsive biomaterials. Examples for both amyloid-related fields are briefly presented in the following section.

#### 3.1 The phenomenon of aggregation and common structural characteristics of amyloids

The term “amyloid” originally means starch-like and refers to protein deposits that are similar to those found for starch.<sup>78</sup> Today it generalizes all peptide and protein fibrils that contain the so called cross- $\beta$  structure,<sup>79-82</sup> short  $\beta$ -sheets that are parallel to each other, but aligned perpendicular to the direction of the stretched aggregate. The common X-ray diffraction signature of the cross- $\beta$ -structure includes two major bands at around 4.7 Å and 10 Å.<sup>79,82</sup> The strong meridional band around 4.7 Å corresponds to the spacing between the individual  $\beta$ -strands. This spacing occurs along the fibril axis and reflects the length of the hydrogen bonds connecting the respective  $\beta$ -sheets. The weaker equatorial band around 10 Å corresponds to spacing perpendicular to the fibril axis, and results from side chain packing within the individual  $\beta$ -strands of a particular  $\beta$ -sheet (*Figure 3.1 A*). This cross- $\beta$  pattern has become a hallmark of amyloid structures. Amyloids are typically long, unbranched, fibrous structures that can consist of hundreds or thousands of monomeric peptide strands. Amyloids show general similarities in the appearance of the fibril structure, although slight differences in morphology can be found, depending on the peptide sequence. The fibrils are usually 5-15 nm in width and up to several micrometers long. Another common property they share is a fluorescence birefringence upon binding to dyes like Congo Red or Thioflavin T (see also *section 6.2*).<sup>83</sup>

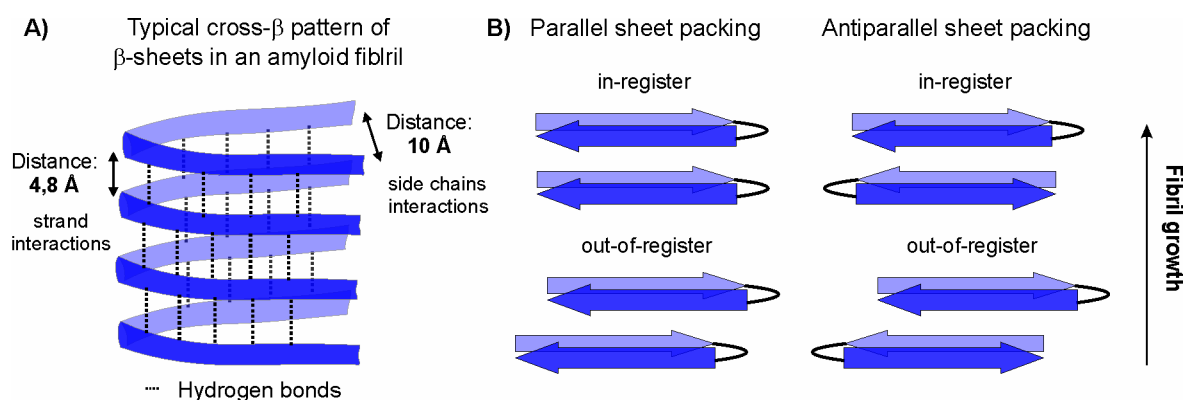


**Figure 3.1:** **A)** Cartoon illustrating the assembly of several  $\beta$ -strands into an amyloid fibril with typical cross- $\beta$  structure. The side chains interact intramolecularly while intermolecular H-bonds connect the individual  $\beta$ -strands. **B)** The individual  $\beta$ -sheets can align in a parallel or antiparallel fashion along the axis of fibril growth.

Amyloid fibrils usually consist of several subunits, so called protofilaments, that twist around each other with a regular periodicity giving a helix-like supercoil.<sup>5,84</sup> The helical morphology results from the preferred right-handed twist of  $\beta$ -sheets.<sup>81</sup> The individual  $\beta$ -sheets can be aligned in a parallel or anti-parallel fashion (Figure 3.1 B), whereby the parallel orientation is most commonly found among amyloid fibrils.<sup>85</sup> For both packing scenarios an in-register or out-of-register alignment of the  $\beta$ -sheets is possible. In-register means that within one  $\beta$ -sheet each  $\beta$ -strand is composed of identical residues that are aligned in register with respect to one another. Although most amyloids appear in parallel in-register form, some examples have been found with parallel pseudo-in register,<sup>86,87</sup> or antiparallel structures.<sup>88-90</sup>

Apart from overall morphology, little was known about the structural details of amyloid fibrils until recently. This lack of information on an atomic level was a result of the noncrystalline character of amyloids that complicates, for example, crystal analysis. Recent advancements in the field of solid state NMR-analysis have revealed new insights into the internal arrangement and interactions of the respective  $\beta$ -strands within amyloid fibrils.<sup>91-93</sup> Tycko *et al.* suggested a folding motif for the amyloid- $\beta$  protein (Figure 3.2) based on findings from solid state NMR-measurements and electron microscopy.<sup>94-96</sup>

Further insights into how the  $\beta$ -strands interact to form fibrils were made possible by means of naturally occurring short amyloid sequences containing only 4-10 residues that can form microcrystals.<sup>97-101</sup> These studies revealed that amyloids have two interfaces, a dry one and a wet one. The dry interface is located at the inside of the fibril where primarily hydrophobic side chains interlock like the teeth of a zipper to ensure optimal packing with the exclusion of water. The authors described this interaction as a 'steric zipper'.<sup>101</sup> Polar side chains that are located at the dry interface do not form hydrogen bonds, but are stabilized via van der Waals interactions. The outside of the fibril is described as a wet interface because charged and polar residues oriented toward this

side of the  $\beta$ -strand are hydrated by water molecules. Also, the lateral packing of several  $\beta$ -sheets within a fibril involves polar and electrostatic interactions of the wet interface.

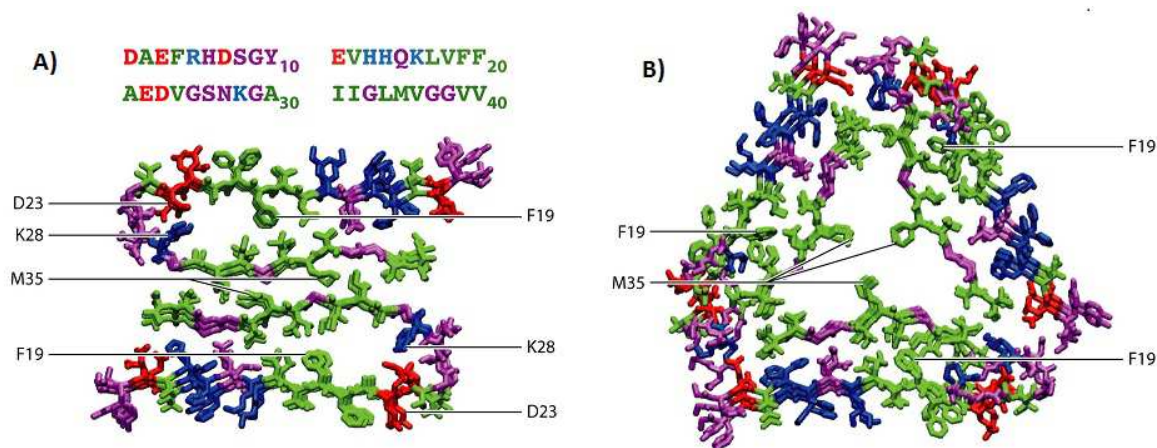


**Figure 3.2:** Structural models for  $A\beta$ 1-40 fibrils derived from solid state NMR measurements with constraints from electron microscopy. **A)** striated-ribbon model and **B)** twisted-pair model with hydrophobic residues highlighted in green, negatively charged in red, positively charged (including His) in blue, and polar (including Gly) in purple (modified according to Tycko et al. copyright © Annual Reviews).<sup>93</sup>

The realization that even very short sequences consisting of only a few amino acids are able to form amyloids led to the hypothesis that short aggregation prone regions in the primary sequence of peptide and proteins could be a driving force for amyloid formation.<sup>102</sup> This so called ‘amyloid stretch hypothesis’<sup>103,104</sup> results from extensive investigations of many amyloid forming proteins that mapped such amyloid prone regions, usually consisting of hydrophobic residues with a high tendency to form  $\beta$ -sheet structures. So called ‘amyloid stretches’ were found in many disease related amyloid forming proteins.<sup>102,105-108</sup> The short  $A\beta$  segment consisting of the residues 16-20 (KLVFF) is perhaps the most prominent example.<sup>109</sup> Incorporation of short amyloid stretches into the sequence of  $\alpha$ -SH3, which normally does not show a tendency to form amyloids, induced fibril formation in this protein.<sup>108</sup> This clearly indicates that short hydrophobic  $\beta$ -sheet inducing segments located in an arbitrary primary sequence have the potential to promote amyloid formation. However, aggregation of proteins also depends on many other factors. Specific side chain contributions and electrostatic interactions also play a major role in amyloid formation.<sup>110</sup> In addition, several environmental conditions that trigger the amyloid formation process have been identified over time. Among the most important are pH-sensitivity,<sup>23</sup> increased temperature,<sup>111</sup> mutations in the primary sequence,<sup>112</sup> proteolysis,<sup>113</sup> and the presence of certain metal ions.<sup>114-117</sup> Also the presence of membranes,<sup>25,33</sup> certain salts,<sup>24</sup> or solvents<sup>118,119</sup> can induce structural changes toward misfolded or partially unfolded species which are thought to represent an early step in the amyloid formation process.<sup>6,120</sup>

### 3.2 Amyloidogenic structures found in diseases

The structural transition from a native functional protein into the pathological form of amyloid fibrils that deposit as plaques is a common feature of more than 20 degenerative diseases affecting either the central nervous system or a variety of peripheral tissues.<sup>5</sup> A selection of such diseases with their corresponding symptom causing misfolded proteins is summarized in *Table 3.1*. Although the primary sequences and their initial conformations can be strikingly different,<sup>121</sup> they show a notable similarity in the morphology of their fibril structure. Also, the mechanisms leading to the structural transition and aggregation follow the same principles.

**Table 3.1:** Selection of amyloid related diseases and the particular aggregation protein.

Disease	Aggregation protein
Alzheimer's disease	Amyloid- $\beta$ , Tau
Parkinson's disease	$\alpha$ -synuclein (wt or mutated)
Diabetes type II	Amylin fragment (islet amyloid polypeptide (IAPP))
Atrial amyloidosis	Atrial natriuretic factor
Haemodialysis-related amyloidosis	$\beta$ -myoglobin
Huntington's disease	Huntingtin
Injection-localised amyloidosis	Insulin
Spongiform encephalopathies	Prion (whole or fragments)
Secondary systemic amyloidosis	Serum amyloid A (whole or 76-residue fragment)
Familial amyloid polyneuropathy III	Apolipoprotein AI (fragments)

Three possible scenarios of amyloid formation are distinguished on the basis of whether the protein is natively unfolded or folded in a defined secondary structure, the latter of which comprises two cases.<sup>82,122</sup> The case in which an initial conformation reorganizes completely towards a  $\beta$ -sheet fold serving as template for accumulation of further peptide strands is described by the 'refolding' model. This mechanism is assumed for insulin, myoglobin, and the SH3-domain, for instance.<sup>122</sup> A scenario in which only a part of the peptide chain becomes unfolded and thereby accessible for interactions with other parts of the peptide chain is the 'gain-of-interaction' model. If amyloid formation occurs starting from an initially unfolded structure, as is the case for many natural proteins like A $\beta$  and prion-HET-s, the process is described by the 'native disordered' model.<sup>101,123,124</sup>

The mechanism of amyloid formation as well as the diversity of the resulting fibril structures is presumably best studied for the Alzheimer's disease (AD). AD is the most



common form of dementia and has become a rising problem in industrial countries with increasing average age of the human population. Two types of aggregates are usually found upon autopsy of the brains of AD patients. Intracellular neurofibrillary tangles that are composed of abnormally hyperphosphorylated tau protein and extracellular plaques containing aggregates of amyloid- $\beta$  protein ( $A\beta$ ).<sup>125,126</sup> The trans membrane protein *amyloid precursor protein* (APP) is proteolytically cleaved by the enzymes  $\alpha$ -,  $\beta$ -, and  $\gamma$ -secretases. Cleavage by the  $\beta$ - and  $\gamma$ -secretases generates 39-42 residue fragments of  $A\beta$ .<sup>127</sup>  $A\beta$  1-42 is the predominant component of the plaques, and is the most toxic and aggregation prone isoform.<sup>128-133</sup> It follows a nucleation polymerization mechanism with a sigmoidal increase in the concentration of amyloid aggregates (*Figure 3.3*).<sup>109</sup> The familial related early-onset form of AD is caused by mutations in the genes encoding APP and the secretase enzymes.<sup>134</sup> This mutation results in the increased production of  $A\beta$  1-42.

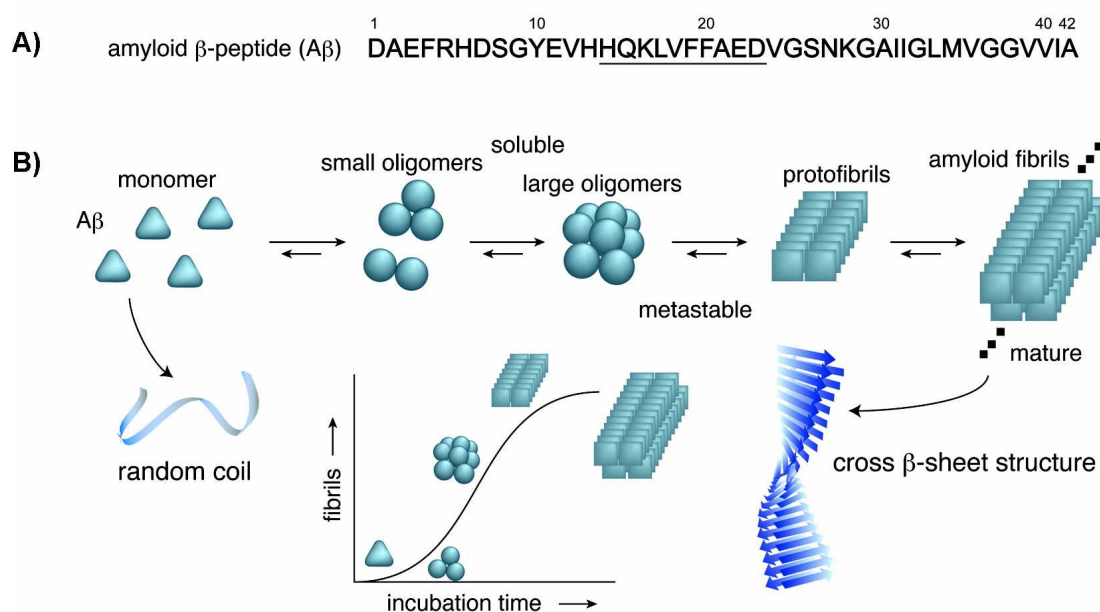


**Figure 3.3:** **A)** Amino acid sequence of  $A\beta$  1–42 peptide with underlined aggregation prone region. **B)** schematic mechanism of amyloid formation for  $A\beta$  (1–42) indicates the transition from a monomeric unfolded state into mature fibrils via the formation of several oligomeric intermediate species (reproduced with permission from Takahashi et al. copyright © American Chemical Society).<sup>109</sup>

The process of amyloid formation of  $A\beta$  and other proteins includes intermediate oligomers of different sizes and conformations.<sup>131,135-137</sup> These pre-fibrillar precursors are suspected to be the actual neuronal toxic species.<sup>138-141</sup> The toxicity of these early aggregates appears to result from an ability to impair cellular processes.<sup>5</sup> Their interaction with the cellular membrane can cause oxidative stress and increase concentrations of free  $Ca^{2+}$  that eventually lead to neuronal cell death. The observation that the protofilaments are more toxic than the mature fibrils seems to also hold true for the tau protein,

implicated in AD as well.<sup>142</sup> The ability of the intermediate species to damage cells is, however, a subject of intense debate.

Strategies for a therapeutic approach apply to different stages of the process.<sup>143</sup> One possibility is the inhibition of the  $\beta$ - or  $\gamma$ -secretases that cleave the APP, thereby reducing the production of the  $A\beta$  (1-42) segment.<sup>144,145</sup> Promising results were found for the inhibition of  $\beta$ -secretase, where only marginal side effects were found in a mouse model.<sup>146-148</sup> The  $\gamma$ -secretase, in contrast, plays a role in many other physiological functions, which makes its inhibition complicate because it can result in a toxic mode of action.<sup>149,150</sup> The third protease,  $\alpha$ -secretase, cleaves APP within the  $A\beta$  domain. If this cleavage step occurs first, the so called non-amyloidogenic pathway is activated (*Figure 3.4*) in which the formation of the aggregation prone fragment  $A\beta$  (1-42) is precluded.<sup>151</sup> Along this pathway a secreted form of APP,  $APP_{s\alpha}$ , is generated, which has neurotrophic and neuroprotective properties.<sup>152-154</sup> The additional cleavage product produced by the  $\alpha$ -secretase, C83, gives rise to the p3 peptide after further cleavage by  $\gamma$ -secretase. P3 is a form of  $A\beta$  that lacks the 16 N-terminal amino acids, and is thus unable to form insoluble fibrils found for  $A\beta$  (1-42). Hence, the therapeutic approach here is activation of the  $\alpha$ -secretase to increase the production of the non-toxic and neuroprotective cleavage products of APP via the non-amyloidogenic pathway; this may mitigate the effects of the pathological  $A\beta$  fragments produced by  $\beta$ - and  $\gamma$ -secretases.<sup>151</sup>

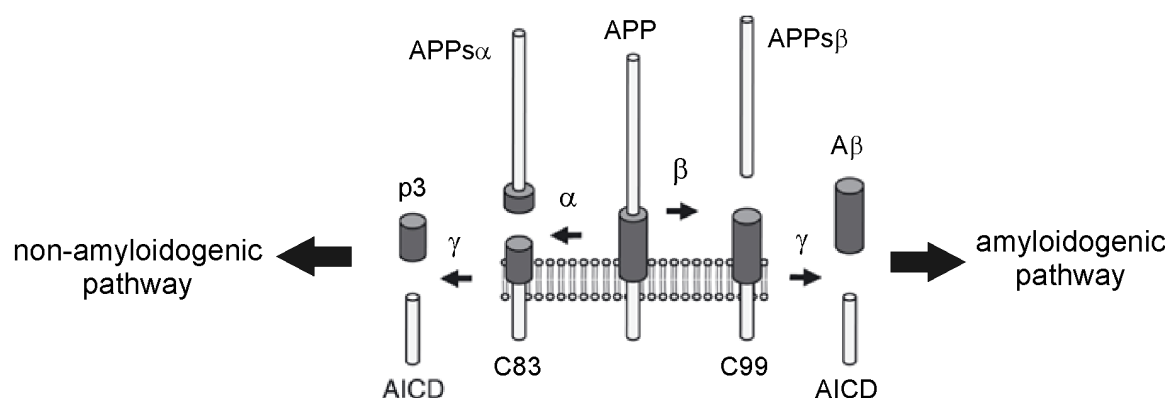


**Figure 3.4:** Proteolytic cleavage of APP by  $\alpha$ -,  $\beta$ -, and  $\gamma$ -secretase leading to two competing pathways (reproduced with permission from Lichtenthaler copyright © John Wiley & Sons).<sup>151</sup>

Aside from their role in disease states, it must also be emphasized that amyloid structures are a normal occurrence in healthy individuals,<sup>155</sup> and that in the case of a balanced equilibrium between the generation and degradation of  $A\beta$  no AD symptoms arise.<sup>156,157</sup> In older individuals the protective functions of the body become weaker, explaining the observation that dementia and AD develop later in life. Therefore, another therapeutic approach is to increase the rate of degradation of amyloid plaques. For example,

immunizations with A $\beta$  at stages before the symptoms of AD develop have been shown in animal trials to prevent the development of the pathological A $\beta$  1-42.<sup>158,159</sup> Also, stimulation of the body's own antibodies by intravenous immunoglobulin treatment is considered as a potential AD therapy.<sup>160,161</sup> Other strategies involve the activation of enzymes that degrade A $\beta$ .<sup>162-166</sup> Although many potential and promising therapy concepts exist already, the cure for AD remains elusive. Understanding the amyloid formation process and all the potential influencing factors in a detailed manner is a crucial prerequisite for success in this field.

### 3.3 Amyloid structures as scaffolds and templates for biomaterials

The mechanical properties of amyloid fibrils, such as their highly stable and insoluble character as well as the regular organization of subunits within the fibril structure, have a great potential for the *de novo* design of self-assembling materials that have biomedical or scaffold-based applications.<sup>26</sup> The similarity of properties that amyloid proteins share with synthetic polymers or plastics make them attractive natural building blocks for the design of nanostructures and nanomaterials.<sup>167</sup> Both materials evolve their assembly properties under specific conditions and show isomorphism by containing different monomeric units. In both cases, subunits are linked via non-covalent interactions to form a condensed state. The main difference, however, is that amyloid peptides consist of specific and complex sequences that allow the utilization or insertion of additional functionalities such as binding sites and catalytic features. Variation of the building blocks can be accomplished by simple protein-engineering techniques.

Despite their association with pathological agents in neurodegenerative diseases, certain amyloids fibrils also have a functional role in nature. Hydrophobins and chaplins are proteins found in filamentous fungi<sup>168</sup> and bacteria<sup>169,170</sup> that modulate the surface tension of the fluid environment inhabited by the organism. These proteins self-assemble into amphipathic rod-like structures at the air-water interface.<sup>171</sup> Another class of natural amyloids are the 'curli'-fibrils produced by some enterobacteria as an extra-cellular matrix that facilitates the formation of biofilms.<sup>172-174</sup> Beside their protective effect, these fibrils exhibit other functional properties like binding to abiotic or biotic surfaces or cell internalization.<sup>169,170</sup> These properties are very attractive with regard to biotechnological applications. The amphipathic character can be used to change the physical properties of surfaces (hydrophilic to hydrophobic and vice versa). Also, they can potentially improve the biocompatibility of surfaces or serve as templates for cell culture and tissue engineering.

Pmel17 is a glycoprotein that supports the biosynthesis of melanin. Proteolytic cleavage releases a luminal fragment of Pmel17 that rapidly self-assembles into amyloid fibrils which serve as a template for the polymerization of melanin precursors.<sup>175,176</sup> The fact that this protein remains soluble until an external trigger (the protease) initiates self assembly, and displays function only upon fibril formation is highly desirable for potential bionanomaterial fabrication. Also, for example, spider silk shares some structural characteristics with amyloids.<sup>177,178</sup> This includes an irreversible transition from a partially or largely unstructured state into  $\beta$ -sheet rich fibrils, a similar morphology to amyloids, similar binding to dyes like Congo Red and Thioflavin T, hydrogen bonded sheet packing, and a comparable cross- $\beta$ -pattern as observed with X-ray diffraction. Thus amyloids and silk might represent related subclasses of materials with common structural features.

Since nature has made use of the remarkable physical properties of amyloids, technical applications of amyloid fibrils are likely to continue to emerge. A series of molecular nanobiomaterials based on amyloid fibrils (e.g wires, layers, gels, scaffolds, templates, and liquid crystals) have been demonstrated in the last few years.<sup>26</sup> The structural compatibility and efficient assembly of small subunits into well-defined ultrastructures can lower the cost and effort of production.

The use of amyloid fibrils as templates or scaffolds is presumably the most popular application so far. Some interesting examples are highlighted briefly in this section.

The amyloidogenic NMSup35, derived from yeast prion Sup35, is characterized by thermal, chemical, and proteolytic stability in the fibrillar form. It was modified in such a way that cysteine residues are displayed on the surface upon fibril formation. The covalent linkage of colloidal gold particles to the cysteines results in conductive nanowires.<sup>179</sup> The fabrication of nanowires from amyloids was demonstrated on the short sequence KLVFFAE that forms tubular structures under certain conditions.<sup>180</sup> These tubes can also be formed by a simple dipeptide, diphenylalanine (FF).<sup>181-183</sup>

Amyloid fibrils have great potential as biofunctional materials because their sequences tolerate chemical elaboration, making possible the conjugation of functional groups or proteins to the fibril. On this basis Kodama *et al.* displayed biotin on the surface of matured fibrils that allow the incorporation of a functional group to the amyloid fibril via biotin-streptavidin binding (*Figure 3.5 A*).<sup>184</sup> In further studies, complete functional proteins were successfully attached to fibrils. Baxa *et al.* showed the binding of GFP to amyloid fibrils of the prion peptide 'Ure2p' under retention of fluorescence properties.<sup>185</sup> The group of Dobson efficiently attached functional cytochrome b to amyloid fibrils formed by SH3 and demonstrated incorporation of heme molecules at very high densities on the surface of the fibril (*Figure 3.5 B*).<sup>186</sup>

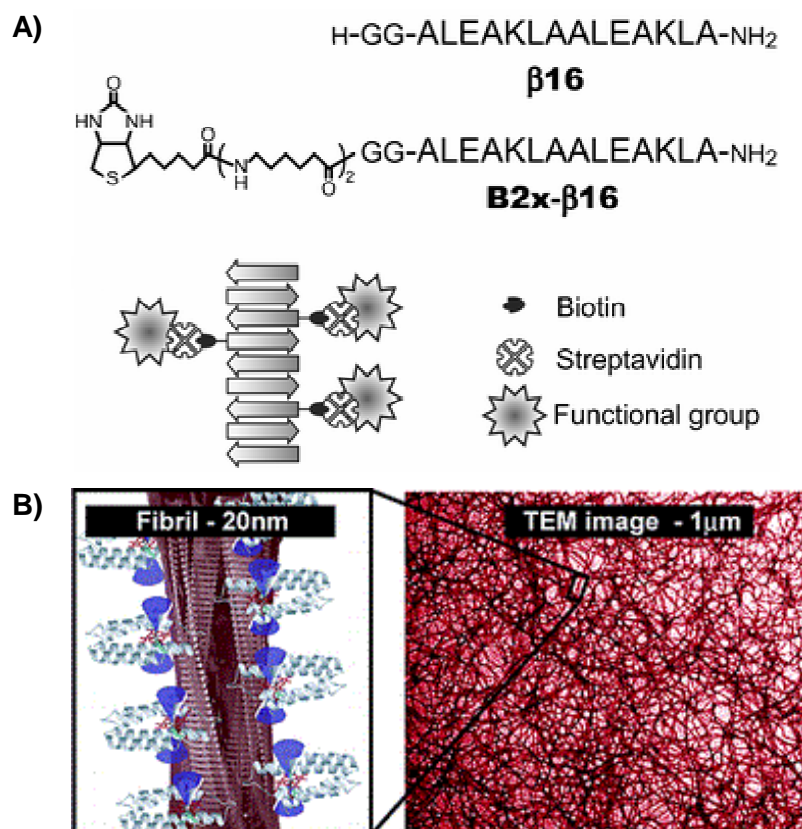


**Figure 3.5:** **A)** Illustration of the assembly of two types of fibrils allowing the introduction of a functional group via a biotin – streptavidin interaction (According to Kodama et al. copyright © Royal Society of Chemistry).<sup>184</sup> **B)** Attachment of cytochrome *b* in its functional form to SH3 fibrils (reproduced with permission from Baldwin et al. copyright © American Chemical Society).<sup>186</sup>

Amyloids have also shown gelation properties under certain conditions making them potential candidates for hydrogel applications. Lysβ-21, the 41-61 fragment of the hen lysozyme protein, could be converted from a gel into a Newtonian fluid at high pH values.<sup>187,188</sup> This pH response was further investigated as a trigger for β-sheet self assembly into ribbons, fibrils or fibers.<sup>188</sup> Such a trigger is useful for the design of materials with controlled mechanical properties. Attractive is also the fact that these materials are biocompatible and biodegradable.<sup>189,190</sup> An Fmoc derivative of the diphenylalanine motif forms a rigid hydrogel composed of a fibrous network.<sup>191,192</sup> This hydrogel showed notable stability at a broad range of temperatures, pH values, and in the presence of denaturing agents like urea or guanidinium chloride. The stability under acidic condition in combination with the high rigidity enables potential applications in encapsulation and controlled drug release.

Rationally designed amphiphilic β-sheet rich sequences consisting of an alternating pattern of polar and nonpolar residues were shown to self-assemble at the air-water interface into amyloid-like fibrils.<sup>193</sup> Such self-assembled monolayers offer the potential for application as protein-based biomaterials. Ordered β-sheet lipopeptide monolayers served as templates for the biomineralization of calcium carbonate.<sup>194,195</sup> The self assembly of a

20-residue amphiphilic  $\beta$ -hairpin into a fibrous network could be reversibly triggered by changes in pH, ionic strength, temperature, and by UV irradiation.<sup>196,197</sup> Such a design could be employed to construct predictable responsive materials. Also, cell culture scaffolds were produced from amphiphilic peptides of alternating polar and nonpolar segments.<sup>198</sup> These peptide produce hydrogels with extremely high water content allowing applications in three-dimensional cell cultures, controlled cell differentiation, tissue engineering and regenerative medicine.<sup>198,199</sup>

This summary of a few potential applications shows the broad potential of amyloid-based materials. Proteinogenic amyloids have many features that could be of great value for the construction of advanced, functional, and environmentally responsive materials. The exploration of applications for amyloidogenic biomaterials, especially considering the possibilities offered by expanding the primary sequence space by introducing noncanonical amino acids, offers numerous exciting avenues for future studies.

## 4 Aliphatic fluorinated amino acids in peptides and proteins

Most of the studies in which fluorinated residues have been incorporated into peptides or proteins deal with analogues of aliphatic amino acids. One explanation could be that these amino acids are easier to synthesize due to the lack of other functional groups. A large number is even currently commercially available. Additionally, the properties of these amino acids have been well studied and the consequences upon fluorination of alkyl side chains, such as hydrophobicity, lipophilicity, and polarity are understood to a great extent. The fluorinated amino acids that were used in the present study are solely analogues of aliphatic amino acids. With this regard the following section will summarize some interesting examples in which fluorinated analogues of aliphatic amino acids were introduced into peptides or proteins to modify function, structure, or stability of the peptides.

### 4.1 Fluorinated amino acids in helical peptides

Fluorinated analogues of leucine, isoleucine, and valine were among the most commonly used nonnatural building blocks to modify peptides or proteins. Analogues of alanine have been synthesized as well but since the activated amino acids were found to be unstable,<sup>42</sup> their incorporation into peptides is rarely found.<sup>200-203</sup> Introducing fluorine substituents into an aliphatic side chain generates additional stereocentres (*Figure 4.1*) which offer the opportunity to study the effects of stereochemistry on protein structures.

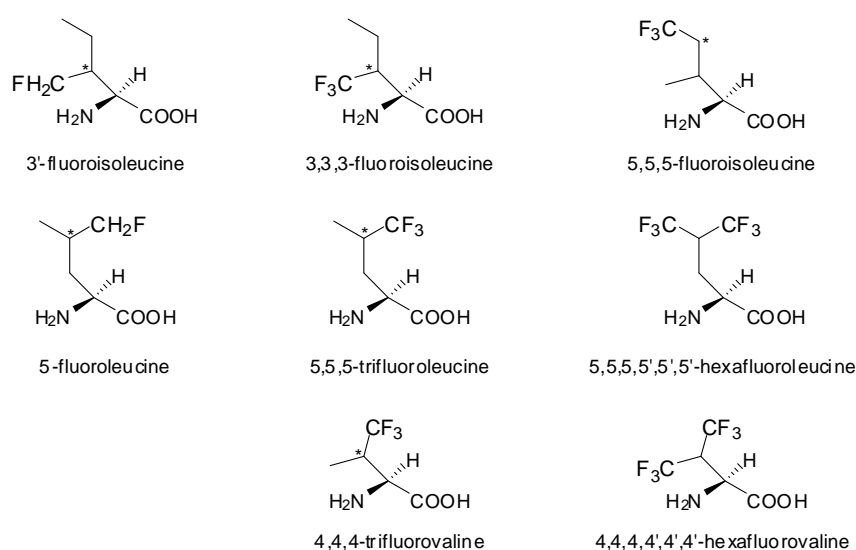


**Figure 4.1:** Fluorinated analogues of aliphatic amino acids that have been incorporated into peptides and proteins (modified with permission according to Salwiczek et al., Copyright © Royal Society of Chemistry).<sup>66</sup>

#### 4.1.1 *Proteolytic stability of fluorinated peptides*

One motivation to introduce fluorinated amino acids into peptides or proteins is to enhance the proteolytic stability of the fluorinated peptide, because the nonnatural amino acid is presumably not recognized and consequently not degraded by proteases. Some studies have shown that the incorporation of fluorinated building blocks indeed results in peptides with increased stability towards proteolytic cleavage.

Meng *et al.* incorporated hexafluoroleucine (HfL) instead of several residues into the helical glucagon-like peptide (GLP-1[7-36]) with the sequence: NH<sub>2</sub>-HAEGTFTSDVSSYLEGQAAKEFIAWLVKGR-CONH<sub>2</sub>.<sup>204</sup> The variants, containing HfL instead of Ala8, Glu9, and Gly10, in the highlighted positions, were more stable towards degradation of the protease dipeptidyl peptidase IV (DPP IV), which usually cleaves the peptide between Ala8 and Glu9. Also the double mutant containing HfL in both positions of the cleavage site (8 and 9) entirely resist degradation.

Gottler *et al.* substituted the leucines and isoleucines of pexiganan,<sup>205</sup> a synthetic analogue of magainin-2, an  $\alpha$ -helical AMP originally isolated from *Xenopus laevis*. They found enhanced interaction with bacterial membranes upon the incorporation of HfL. The fluorinated peptide retained its antimicrobial activity while remaining hemolytically inactive. Also, in this case the fluorinated variant showed improved stability towards proteolytic cleavage by trypsin and chymotrypsin in the presence of a membrane environment. This effect was, however, attributed to an increased tendency of the fluorinated peptide to self assemble within the lipid bilayer, because, in the absence of a membrane, the peptide was as rapidly degraded as its nonfluorinated variant.

Meng *et al.* studied fluorinated variants of two membrane peptides (buforin-2 and magainin-2), which have different binding mechanisms.<sup>206</sup> Several variants of both peptides containing different levels of HfL as substituents for Ile, Leu, and Val were investigated. All fluorinated variants except the globally fluorinated mangainin-2 variant showed similar or enhanced antimicrobial activity. In addition, a truncated buforin-2 variant that is inactive was found to become active upon fluorination. The hemolytic activity of buforin-2 analogues remained unchanged, while higher hemolytic activity was found for some magainin-2 variants. In contrast to the fluorinated pexiganan described by Gottler *et al.*,<sup>205</sup> the fluorinated peptides in this study remained proteolytically stable even in the absence of a membrane.

Recent studies by Asante and Kokschi, however, show that enhanced or reduced proteolytic stability of fluorinated peptides is strongly context-dependent and can not be easily extrapolated from one model to another.<sup>207</sup> The position with respect to the



cleavage side, the nature of the fluorinated amino acid, and also the type of protease were found to be factors that influence the rapidity of peptide degradation.

#### 4.1.2 *Hydrophobicity, packing, or the “fluorous effect”*

Another interesting ongoing discussion in the literature is whether the enhanced stability of peptides upon fluorination results from the higher hydrophobicity of fluorinated amino acids, or if better side chain packing offers a reasonable explanation.

Coiled-coil peptides have often been used as models to investigate the impact of fluorination on protein stability or protein-protein interactions. Their primary sequence comprises the so called heptad repeat (abcdefg)<sub>n</sub>. Hydrophobic amino acids in the **a** and **d** positions ensure the assembly of the helices in an aqueous environment.<sup>208</sup> Oppositely charged residues in **e** and **g** positions further stabilize the helical assembly due to electrostatic interactions.<sup>209</sup> The remaining **b**, **c**, and **f** positions are exposed to the solvent and therefore occupied by polar or charged amino acids. This design principle can be applied to the *de novo* design of helical assemblies of different oligomerization state.<sup>210</sup> A detailed description of the coiled coil design can be found in *section 7.1* of this thesis.

The coiled coil subdomain of the naturally occurring transcription factor GCN4 often serves as a template for the study of how fluorinated analogues of hydrophobic amino acids, when incorporated into the hydrophobic core, affect the structure and stability of this motif. The parallel alignment of the two helices leads to packing of the **d** positions of one strand against those of the other strand. The replacement of all Leu residues in **d** positions (*Figure 4.2*) with a diastereomeric mixture of trifluoroleucine (TfL) resulted in peptides with enhanced thermal stability and higher resistance towards denaturation with chaotropic agents.<sup>211</sup>

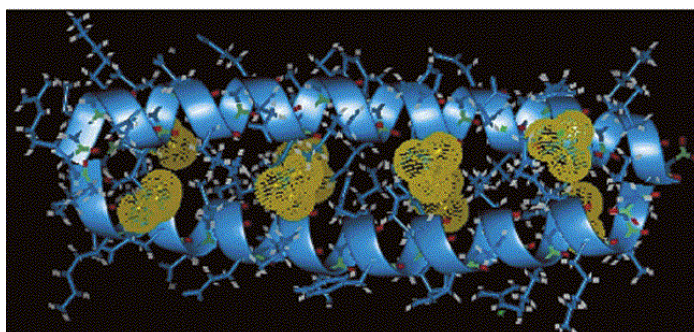


**Figure 4.2:** Modeled structure of GCN4 containing TfL at all **d** positions. Van der Waals radii of the fluorine atoms are indicated with yellow spheres (reproduced with permission from Tang et al. Copyright © American Chemical Society).<sup>211</sup>

The valine and isoleucine residues at the **a** positions were substituted with their fluorinated analogues, 5,5,5-trifluoroisoleucine (5TfI) and (2S,3R)-4,4,4-trifluorovaline (4TfV) during expression in *E. coli*.<sup>212</sup> Both fluorinated variants showed increased thermal stability, however to a different extent compared to their particular valine or isoleucine peptides. The substitution of Ile with 5TfI resulted in an eight-fold higher stabilization in comparison to the Val-to-4TfV substitution.<sup>212</sup> Steric clashes between the large  $\gamma$ -CF<sub>3</sub> group and the peptide backbone in close proximity were suggested to be the cause.

A version of GCN4 with a fully fluorinated core was studied by Bilgiçer *et al.*<sup>213</sup> At all **a** positions a diastereomeric mixture of TfV was introduced, and all **d** positions were occupied by 5TfL. Although thermal stabilization is observed for this highly fluorinated variant, the degree of stabilization is not greater than that observed for the incorporation of 5TfL solely at the **d** positions.<sup>212</sup> However, since the sequences of the GCN4 variants described here are not completely identical, a direct comparison should be made carefully.

The enhanced stabilities of the fluorinated variants with regard to their native structures were mainly explained on the basis of the increased hydrophobicity of the fluorinated amino acids in comparison to their hydrocarbon parent molecules. Since the substitutions in all these cases affect the hydrophobic core of the coiled coils, this argumentation seems viable. The assembly of the helices is driven by the hydrophobic nature of the residues in **a** and **d** positions. Thus residues with higher hydrophobicity positively affect this assembly. Comparative studies investigating 5TfL and HfL at the **d** positions of an artificial coiled coil revealed that the all-HfL variant is even more stable than the 5TfL analogue.<sup>214,215</sup> This indicates that enhanced stability and fluorine content could correlate with each other.

Also, the interaction of highly fluorinated molecules with hydrocarbon compounds was studied with the help of designed coiled coils.<sup>216,217</sup> A dimeric coiled coil containing solely Leu in all **a** and **d** positions (HH) was designed to be covalently linked by a disulfide bridge. Leu was replaced with HfL in either one or both helical strands in order to give the heterodimeric (HF), or the fully fluorinated variant (FF). Thermal stability of the three coiled coils increased in the following order HH < HF < FF. Under redox conditions the heterodimers (HF) tended to self sort into the homodimers (HH) and (FF). The authors argued that the fluorinated side chains disfavor an interaction with the hydrocarbon side chain, analogous to the observation of the immiscibility of hydrocarbon and perfluorinated solvents. The so called “fluorous effect” was invoked in this context to explain the segregation of the peptide variants. Interestingly, sedimentation analysis revealed that the variants with the highly fluorinated core switched to a tetrameric oligomerization state.

Similar segregation behavior was observed in the presence of membrane environments (Figure 4.3). The large increase in hydrophobicity and lipophobicity results in segregation of the peptides from either phospholipid bilayers,<sup>218</sup> or detergent micelles,<sup>219</sup> and as a consequence enhances the helix-helix interaction.

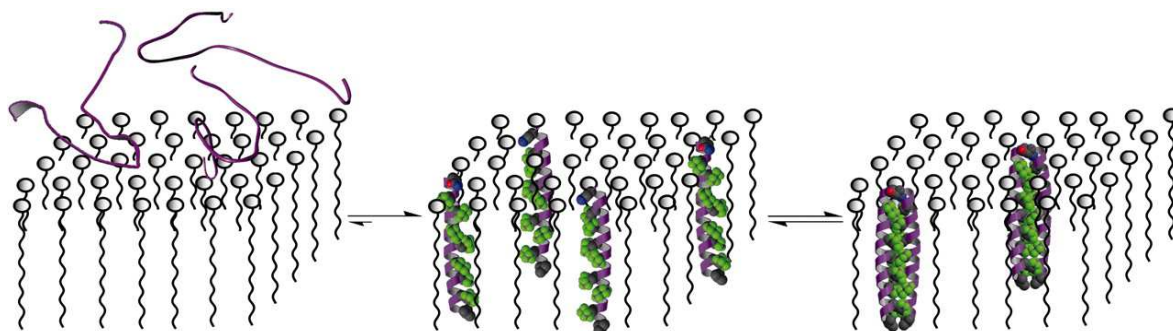


**Figure 4.3:** Schematic diagram showing the self-assembly of the designed highly fluorinated peptides in a membrane environment (according to Bilgiçer *et al.* Copyright © National Academy of Sciences).<sup>219</sup>

Whether a specific fluorine interaction in fact caused the observed segregation was further tested by the Marsh group. They used a tetrameric, antiparallel coiled-coil template in which the Leus at the hydrophobic core were replaced by HfLs in a layer-by-layer fashion.<sup>220,221</sup> Interestingly, the variant with the completely fluorinated core did not display the same increase in stability that was found for the other layers. In NMR experiments, these variants were found to be less dynamic due to an overpacking of the hydrophobic core as a result of the larger side chain of HfL in comparison to Leu; however, no self sorting behavior was observed, neither for the mixed forms, nor during the titration of fluorinated against the hydrocarbon variants. One explanation may be found in the different systems of Kumar and Marsch. The four-helix bundles assemble in an antiparallel fashion and the orientation of the helices determines the packing of side chain residues in the hydrophobic core of the coiled coil. Hence, the packing of the side chains may be favored for the mixed forms in contrast to the fully fluorinated coiled coils, which were shown to have overpacked cores due to steric reasons. This was also experimentally confirmed by Buer *et al.*<sup>222</sup> The same four-helix bundle was either substituted in **a** or **d** positions with HfL to create helix bundles in which Leu and HfL alternately pack against each other. The stabilization per HfL residue is higher for these variants than for the fully fluorinated coiled coil. That favorable packing might have induced the observed segregation behavior of the dimeric coiled coils studied by Kumar is supported by the fact that the fluorinated variants underwent the switch to the tetrameric oligomerization state. Perhaps the higher oligomerization state is better able to

compensate for the increased side chain volumes in the hydrophobic core than is the dimeric oligomerization state.

Recent crystal structures (*Figure 4.4*) of the four-helix bundles with different fluorinated amino acids incorporated at **a** positions confirmed that large numbers of fluorinated amino acids can be introduced into the tetrameric coiled coil while causing only small perturbations in structure, although the side chains of the fluorinated amino acids are notably larger than those of the native amino acid analogues.<sup>223</sup> Since the structures do not indicate any preferred fluorous interaction, the authors found an explanation for enhanced stability of the fluorinated peptides in increased hydrophobicity and efficient side chain packing.<sup>223,224</sup>

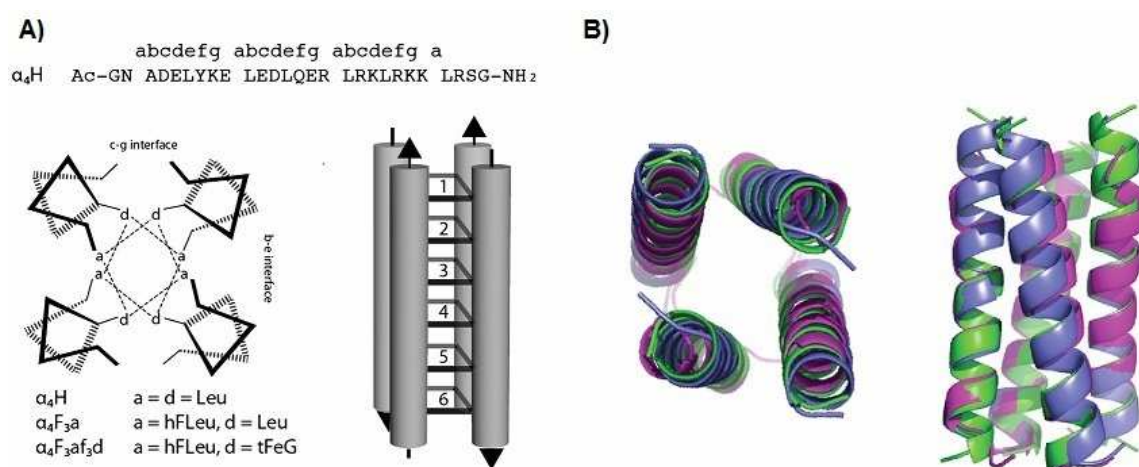


**Figure 4.4:** **A)** Sequence and helical wheel diagram of the fluorinated variants of the four helix bundle  $\alpha_4H$ . All four **a** positions contain HfL in case of  $\alpha_4F_3a$ . In the  $\alpha_4F_3af_3d$  variants all Leu in **a** positions were replaced by HfL and all Leu in **d** positions were substituted by tFeG, which is the trifluorinated analogue of aminobutyric acid (TfeGly). **B)** Overlay of the backbones determined from the crystal structures of  $\alpha_4H$  (green),  $\alpha_4F_3a$  (blue), and  $\alpha_4F_3af_3d$  (purple) indicating that the incorporation of large numbers of sterically demanding fluorinated residues induce only marginal structural perturbations in the helical assembly (according to Buer et al. Copyright © National Academy of Science).<sup>223</sup>

Favorable side chain packing can have a large contribution to the stability of coiled coils. This was shown in studies by Jäckel, Salwiczek and Kokschi investigating dimeric coiled coils that contain single substitutions of different fluorinated amino acids at the hydrophobic core.<sup>225-229</sup> The system investigated was a heteromeric coiled in which fluorine substituents were introduced solely into one of the two helices to study the interaction of the fluorine side chains within a natural environment. Analogues of  $\alpha$ -aminobutyric acid containing different stoichiometries of fluorine in their side chain were introduced either at a central **a** or **d** position as a replacement for Leu or Val in order to study the effect of increasing fluorine content on the coiled-coil interaction. Since even the trifluorinated Abu analogue (TfeGly) is less hydrophobic than the substituted Leu (*Figure*

2.1),<sup>49</sup> it is not surprising that all fluorinated variants suffered from a loss in thermal stability compared to the native coiled coil dimer. The effects of single substitutions were found to be strongly position dependent. While for substitutions at the **a** position of the heterodimer stability of the coiled coil strongly correlates with the size of the incorporated side chain, such clear trends were not found for the **d** position. Different side chain packing at the **a** and **d** positions were concluded to account for the observed effects. Fluorination of the  $\gamma$ -CH<sub>3</sub> group of Abu strongly polarizes the neighboring  $\beta$ -methylene unit due to fluorine's electron withdrawing effect. This polarized CH<sub>2</sub>-group points away from the hydrophobic core in the case of the **a** position, but into it in the case of the **d** position, hence weakening the hydrophobic interactions.

The few mentioned examples show that, although the properties of fluorinated aliphatic amino acids are fairly well understood, effects on peptide stability can not be generalized for different systems. Moreover, even similar systems, like the class of coiled coils described here, can be affected in different ways.

#### **4.1.3 Altered activity and function of fluorinated peptides**

The motivation to design fluorinated peptides that possess enhanced stability often involves the idea to discover peptides with improved functions.

Niemz and Tirrell investigated several fluorinated variants of the bee venom melittin.<sup>230</sup> They found increased membrane affinity for the fluorinated variants as a result of enhanced self-association behavior of the peptides. Some of the earlier mentioned fluorinated magainin-2 variants, that display higher proteolytic stability, also show enhanced antimicrobial activity.<sup>206</sup> The commonly used anti-cancer drug interleukin-2 was substituted with 5Tfl at five Ile positions in the hydrophobic core by applying *in vivo* procedures.<sup>231</sup> The EC<sub>50</sub> value for the fluorinated variant was about 30% higher compared to the native peptide; however, the fact that the fluorinated peptide shows an activity almost as high as the wild type indicates retention of folding.

Also, globular proteins like ubiquitin, green fluorescent protein (GFP), or chloramphenicol acetyltransferase (CAT) have been fluorinated to different extents.<sup>232-235</sup> In the case of ubiquitin, selective site specific incorporation of a monofluorinated leucine analogue were tested for its function as <sup>19</sup>F-reporter.<sup>232</sup> The overall fold of the fluorinated variant was comparable to the native protein structure. In the case of CAT, fluorinated variants of lower<sup>233</sup> and higher<sup>235</sup> stability have been reported. The same holds true for fluorinated GFP mutants in terms of reduced or enhanced fluorescence.<sup>234</sup>

## 4.2 Fluorinated amino acids in $\beta$ -sheet forming peptides

A property that is seldom considered during the discussion of the newly gained properties of fluorinated peptides is the intrinsic propensity of fluorinated amino acids for a certain secondary structure. Indeed, it was found that the fluorinated analogues of leucine (Leu), aminobutyric acid (Abu), and phenylalanine (Phe) exhibit a reduced  $\alpha$ -helix propensity compared to their hydrocarbon analogues,<sup>236,237</sup> hence, they may be more readily accommodated in  $\beta$ -sheet structures. Cheng *et al.* used a monomeric  $\alpha$ -helix model peptide Ac-YGG-KAAAAKAXAAKAAAAK-NH<sub>2</sub> in which X served as guest position for the amino acid of interest. The fluorinated amino acids were placed at this guest position and the  $\alpha$ -helix propensity values were calculated from CD data by using a modified Lifson-Roig theory and compared to their nonfluorinated analogues.<sup>238-240</sup> All fluorinated amino acids studied by Cheng *et al.* showed lower helix propensity values in comparison to their hydrocarbon analogues. This may in part result from unfavorable solvent interactions at the exposed positions of the monomeric helix; alternatively, increased side chain volumes, especially in the case of a CH<sub>3</sub>-to-CF<sub>3</sub> substitution for  $\beta$ -branched residues like Val or Ile, may induce clashes with the backbone and distort the helical conformation.<sup>241</sup> Until a larger sample set of fluorinated amino acids has been investigated using this system, general conclusions cannot be made.

The observation that fluorinated amino acids may indeed be better accommodated in a  $\beta$ -sheet environment was shown in studies in which residues at  $\beta$ -sheet positions of peptides or within  $\beta$ -sheet subdomains of proteins were specifically replaced by their fluorinated analogues, resulting in enhanced stability or activity.

Hong and Raleigh substituted two buried valine residues at  $\beta$ -sheet positions of the N-terminal domain of the ribosomal protein L9 (NTL9(1-56)) with diastereomeric mixtures of trifluorovaline (TfV).<sup>242</sup> The per residue increase in stability for the two fluorinated positions 3 and 21 was larger than for any known fluorinated helical protein. Kinetics of folding and unfolding of the protein was measured via stopped-flow experiments. Both fluorinated variants were found to unfold slower than the wild type indicating that the trifluoromethyl substitution stabilizes the native state relative to the transition state. The folding rates instead were increased for both fluorinated variants, suggesting a stabilization of the transition state by hydrophobic interactions. Monosubstitutions of six residues in the hydrophobic core with their particular fluorinated counterpart were conducted and the peptides were studied in an extensive fine structure analysis of the NTL9(1-56) folding transition state.<sup>243</sup> Here, the variant containing TfL instead of Leu30 in the short helical domain of the protein was found to destabilize the protein compared to the native one containing Leu. It is likely that steric clashes of the increased side chain within the densely



packed hydrophobic core induce the destabilization, reminiscent of the overpacked core of the highly fluorinated four-helix bundles described by the Marsh group.<sup>221</sup> However, the study of Horng investigated two buried positions of NTL9(1-56), thus it remains unclear whether higher hydrophobicity or a preferred  $\beta$ -sheet structure, as a consequence of lower  $\alpha$ -helix propensity, causes the increase in protein stability.

Chiu and coworkers used the GB1 domain as a model to study the intrinsic propensities of fluorinated amino acids to adopt  $\beta$ -sheet conformations.<sup>244</sup> They substituted the solvent exposed position 53 within the internal  $\beta$ -strand 4 (Figure 4.5) with several highly fluorinated analogues of Abu, Leu, and Phe and measured the stabilities of the fluorinated proteins during thermal denaturation. Increased stabilities were found for all fluorinated GB1 variants in comparison to the peptides containing the particular hydrocarbon analogue at position 53. This was attributed to increased hydrophobicity as well as steric effects of the fluorinated amino acids. The increase in stability observed here was less dramatic than that observed by Horng upon fluorination of NTL9. The position being substituted in GB1 is exposed to solvent, where hydrophobic amino acids would interact with the aqueous environment, and this somewhat counteracts the stabilizing effect. Nevertheless the study supports the idea that fluorinated amino acids could have a higher propensity for  $\beta$ -sheet structures.

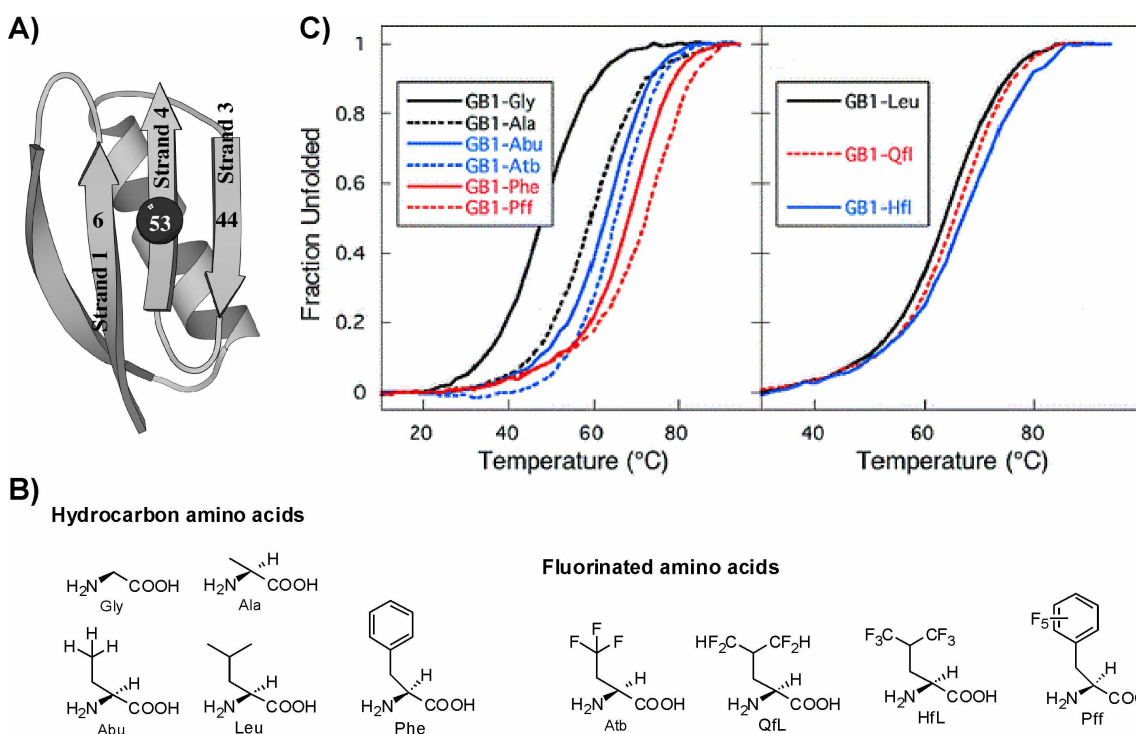


**Figure 4.5:** **A)** Ribbon diagram of protein GB1 domain with highlighted solvent exposed position 53 in  $\beta$ -strand 4. **B)** Fluorinated and hydrocarbon amino acids that were incorporated at position 53. **C)** Denaturation curves of GB1 variants showing the higher stability of all fluorinated peptides in comparison to the particular nonfluorinated variants (modified with permission according to Chiu et al. Copyright © American Chemical Society).<sup>244</sup>

In another study the biologically active  $\beta$ -hairpin *protegrin-1* was substituted at two important Val positions (Val 14 and Val 16) with either Leu or HfL to test for a correlation between increasing hydrophobicity and enhanced membrane activity.<sup>245</sup> The substitutions affected the hydrophobic interface of the hairpin dimer that *protegrin-1* adopts upon binding to a membrane. As expected, the substitutions stepwise increase the hydrophobicity of the peptide, with the HfL variant being the most hydrophobic one. Although both amino acids have also larger side chain volumes in comparison to Val, the substitutions do not cause any perturbation of the structure. While the hemolytic activity is not affected by the substitutions, the fluorinated variant appears to be less antimicrobially active. Interestingly, the Leu variants show enhanced activity against bacteria compared to the native hairpin. An additional interesting finding was the altered oligomerization state of the Leu and HfL variants during lipid-peptide interaction. While the native peptide, a monomer in solution, initially forms dimers upon interaction with a lipid surface, both the Leu and HfL variants adopt a tetrameric oligomerization state in the presence of a membrane. The binding isotherm of the fluorinated variant, however, exhibits a lower effective positive charge compared to the double Leu variant. This may explain the lower antimicrobial activity observed for the fluorinated peptide.

Recently, the effect of fluorinated and nonfluorinated side chain interactions on conformational stability was studied with the help of two  $\beta$ -hairpin scaffolds (*Figure 4.6 A*).<sup>246</sup> One scaffold (I), a non-hydrogen-bonded hairpin, stabilized with a disulfide bond connecting the C- and N-terminal side chains, contains two central leucines with side chains directly facing each other. In a series of all possible combinations these Leu residues were replaced by HfL in such a way as to achieve Leu-Leu, Leu-HfL, and HfL-HfL interactions. The other scaffold (II), a cross-strand H-bonded hairpin with an introduced Ati residue (a 1,2-Dihydro-3(6*H*)-pyridinone Unit) to restrict backbone flexibility, was substituted in the terminal positions to study cross strand interactions. The Gly and Leu residues in the two positions were replaced by HfL in a fashion that allows every possible combination of interacting side chains: LL2, LH2, HL2, HH2, HG2, LG2, GH2, and GG2.<sup>246</sup> The incorporation of the larger HfL residues into the short  $\beta$ -hairpin sequences did not cause any perturbation of the structures, as evidenced by NMR. The authors found that HfL-HfL interactions were weaker than Leu-Leu and Leu-HfL interactions (*Figure 4.6 B*), which seems surprising with regard to the higher hydrophobicity of HfL. This clearly demonstrates that hydrogen to fluorine substitutions go along with an interplay of several properties including polarizability, dipolar interactions, and hydrophobicity. The low polarizability relative to volume of CF<sub>3</sub> versus CH<sub>3</sub> presumably influences the interaction energies of HfL.<sup>247</sup> The HfL-Leu interface has been found to have an interaction energy similar to that of Leu-Leu in water, which was



attributed to dipolar interactions arising from the opposite dipoles of the C-F and the C-H bonds. Stabilization or destabilization of the scaffold structures upon the incorporation of HfL is strongly dependent on the substituted position. HfL incorporation at the C-terminus of scaffold (II) stabilizes the structure in comparison to the Leu variants whereas at the N-terminal position the opposite effect was found. These results show that structure stabilization also for  $\beta$ -sheet systems is fairly context dependent.

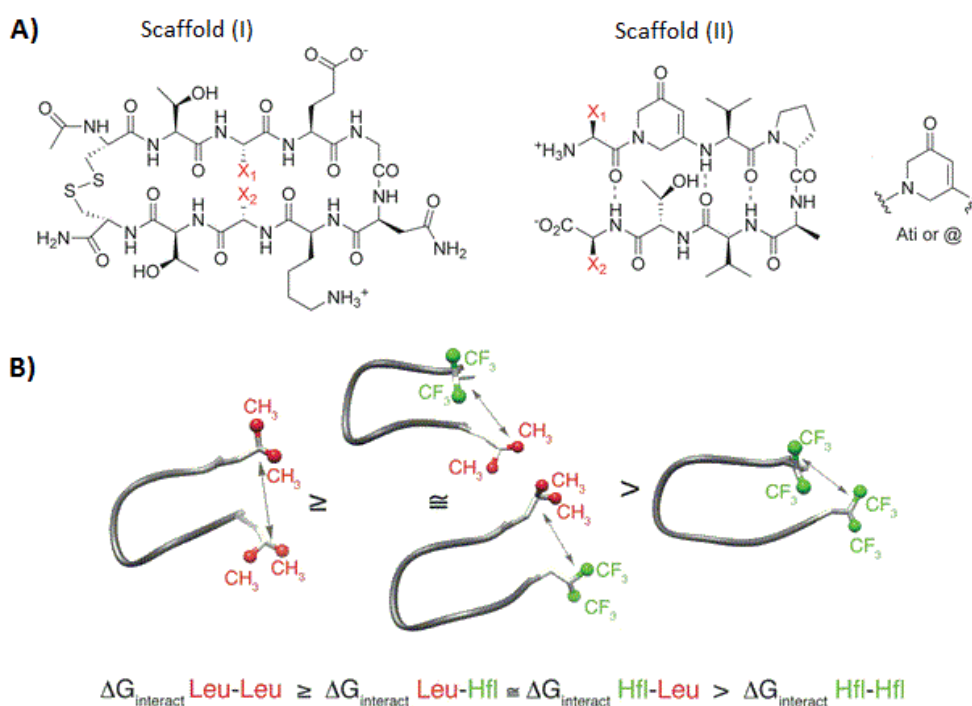


**Figure 4.6:** **A)** Structures of scaffold (I) and scaffold (II) with X1 and X2 representing the particular substituted positions in each  $\beta$ -hairpin. **B)** Variants of scaffold (II) ordered according to decreasing interaction energies of the two terminal functional groups (modified with permission according to Clark et al. copyright © American Chemical Society).<sup>246</sup>

This short summary of studies investigating  $\beta$ -sheet based peptides and proteins that contain fluorinated aliphatic amino acids shows the complexity associated with the incorporation of fluorinated amino acids into peptides and proteins. In general, fluorinated amino acids introduced at  $\beta$ -sheet positions stabilize these structures due to higher hydrophobicity and higher propensity for  $\beta$ -sheet structures compared to the particular replaced hydrocarbon analogue. However, the effects on structure, stability and function still remain position and system dependent. The GB1 protein was suggested to serve as a reference peptide to determine  $\beta$ -sheet propensities. However, the amino acids investigated in this context were distinguished according to their stabilizing effect on the protein ( $T_m$  and  $\Delta\Delta G$ ). No values for the  $\beta$ -sheet propensities of fluorinated amino acids, analogous to the values for  $\alpha$ -propensities calculated from CD-spectra of the Ala-based peptide sequence,<sup>236</sup> exist so far. Stabilization of GB1 on the other hand was found to

correlate with increasing hydrophobicity of the incorporated amino acids.<sup>248</sup> The observation that, in this regard, Ile would have a higher  $\beta$ -sheet propensity than Val is in conflict with the helix propensity measurements, where Ile was also found to more favorably adopt helical structures in comparison to Val.<sup>240</sup> The stabilization for the protein may be increased with increasing hydrophobicity, but drawing conclusions strictly on the basis of  $\beta$ -sheet propensities may be misleading.

As to what extent  $\beta$ -sheet propensity values are different for Leu and Ile could be interesting with regard to the similar hydrophobicity of both amino acids. With respect to their  $\alpha$ -helix propensity values they can be clearly distinguished, indicating that these values do not correlate simply with hydrophobicity. Also the conformations of side chains, including branching in close proximity to the peptide backbone, have been found to dictate the  $\alpha$ -helix propensity. Beta branched amino acids usually prefer  $\beta$ -sheet structures. Thus, Leu and Ile should favor the  $\beta$ -sheet structure to different extents. By only considering the hydrophobicity, which is equal for both amino acids, these differences can not be detected within the GB1 model.

Especially in cases when not only aliphatic amino acids are investigated a careful consideration of other factors, aside from the hydrophobicity, that contribute to the  $\beta$ -sheet propensity of an amino acid may become necessary. With regard to the fact that especially single fluorination may induce polarity, a discussion of  $\beta$ -sheet propensities based on solely the hydrophobicity of an amino acid may be imprecise. Since the investigations of fluorinated amino acids in  $\beta$ -sheet systems is restricted to a few examples so far, further studies of other sequences and other fluorinated derivatives are required for a better understanding of how fluorination alters such systems.

### **4.3 Fluorinated amino acids in amyloid forming peptides**

Fluorinated amino acids have rarely been investigated in amyloid forming sequences. This is surprising with regard to the fact that these structures usually contain high  $\beta$ -sheet content and fluorinated amino acids have been shown to positively alter these structures. In many studies of amyloid forming peptides, fluorinated amino acids were used as NMR-labels to give insights into the overall structure of amyloid fibrils or to study the pathway and intermediate species during aggregation processes. Nevertheless, how the incorporation of these non-natural amino acids with unique stereoelectronic properties may influence amyloid formation itself has not been investigated thus far. A first approach in this direction is given in the present work.

#### 4.3.1 Fluorinated amino acids as $^{19}\text{F}$ -NMR-labels in amyloid structures

Although the common method to detect amyloids is staining with Thioflavin T, this method can not discriminate between monomers, oligomers, and small non-fibrillar species that occur during fibril formation of most amyloidogenic proteins.<sup>131,132,135,249</sup> These pre-fibrillar intermediates are extensively discussed to be the actual toxic species.<sup>132,250-252</sup> Conformational changes, however, can be detected with NMR-analysis, when the label is incorporated at a position that experiences an environmental change upon structural rearrangement. The advantage of using fluorine as NMR-label is the excellent sensitivity and the large chemical shift dispersion, making it a great reporter for changes in the chemical environment.<sup>66,253</sup> In addition, the abundance of fluorine is rare in biological systems. Thus, there are no competing background signals, as is the case for other NMR-nuclei like  $^1\text{H}$ ,  $^{13}\text{C}$  or  $^{15}\text{N}$  or  $^{31}\text{P}$ .<sup>253,254</sup>

$^{19}\text{F}$ -NMR was used to gain quantitative information about structure and mechanism of fibrillation of  $\alpha$ -synuclein, the protein associated with Parkinson's disease.<sup>255</sup> The tyrosine residues at positions 39, 125, 133, and 136 were replaced by 3-fluorotyrosine during expression in *E.coli*. Conformational changes upon treatment of the protein with urea, spermine, and sodium dodecyl sulfate (SDS) were successfully detected by using  $^{19}\text{F}$ -NMR measurements. Accelerated aggregation in the presence of SDS and spermine was observed. Furthermore, the authors stated that no low molecular weight intermediates of high abundance appear during fibrillation, as these would have been detectable via  $^{19}\text{F}$ -analysis.

Similar approaches were later taken for other disease related amyloid forming proteins. The mechanism of amyloid formation for the diabetes-related islet amyloid polypeptide (IAPP) was studied by introducing a 4-trifluoromethylphenylalanine instead of Phe23 into the sequence.<sup>34</sup> This solvent-exposed residue of the monomeric species becomes buried during aggregation, making it sensitive to environmental changes. Using real-time  $^{19}\text{F}$ -NMR to detect the consumption of monomeric species in combination with Thioflavin T staining assays to detect fibril formation, the authors were able to show that IAPP aggregates without the buildup of non-fibrillar intermediates.<sup>34</sup>

The rate of monomer consumption closely matches the rate of amyloid formation (*Figure 4.7*), indicating that the monomer is directly converted into large,  $\beta$ -sheet rich compounds that are ThT-active. The absence of non-fibrillar oligomeric species during the aggregation pathway of IAPP is clearly distinguishable from the mechanism of fibril formation of other amyloidogenic proteins.<sup>256-258</sup>

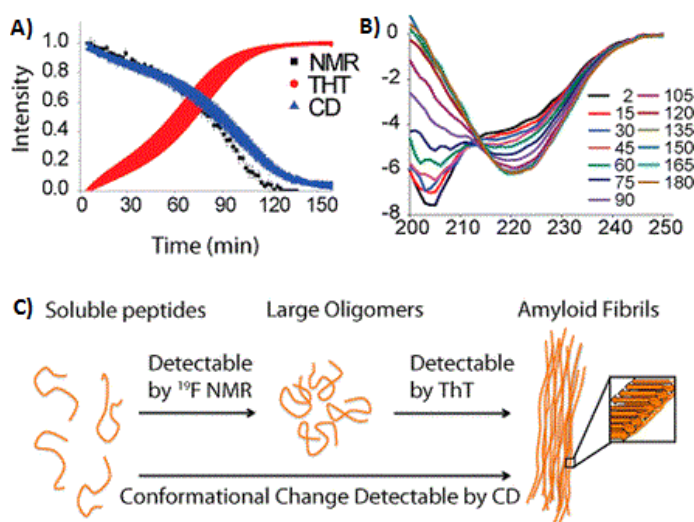


**Figure 4.7:** **A)** Rate of monomer consumption (black) determined by NMR-analysis versus rate of fibril formation obtained from ThT-assay (red) and CD-data (blue). **B)** CD spectra at different time points show the systematic conversion of an unfolded toward a  $\beta$ -sheet structure. **C)** Schematic indication of sensitivities of each particular method (adapted with permission from Suzuki et al. copyright © American Chemical Society).<sup>34</sup>

During amyloid formation of A $\beta$ , the protein widely accepted to be the causative agent of Alzheimer's disease, a minimum of six oligomeric species (Figure 4.8) were detected by applying similar  $^{19}\text{F}$ -NMR experiments.<sup>249</sup> Methionine 35 was replaced by trifluoromethionine during solid phase peptide synthesis, because the  $\text{CF}_3$  group on the flexible side chain should respond with significant changes in chemical shift and line-broadening upon changes of secondary structure or oligomerization state. The detection of several intermediates during the early phase of fibril formation indicates that the simple model of nucleation dependent polymerization is indeed more complex and consists of several distinct steps.

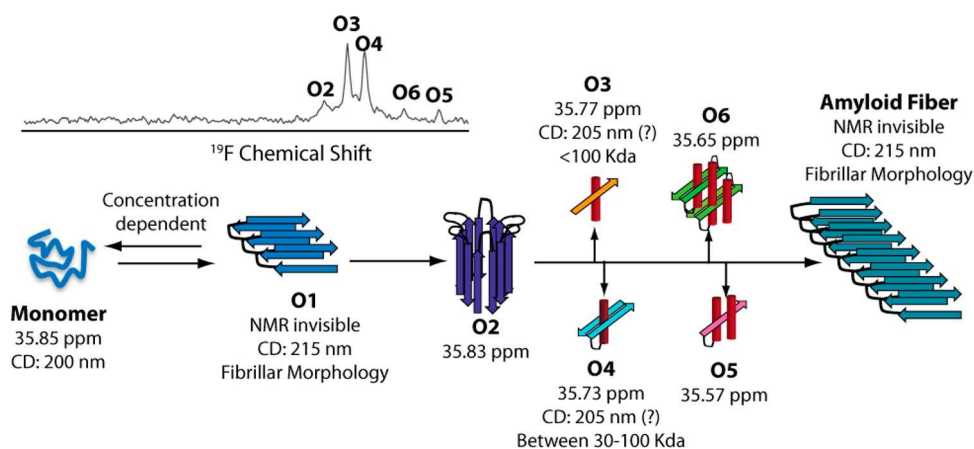


**Figure 4.8:** Cartoon of a potential aggregation pathway of A $\beta$  (1-40) indicating six individual oligomers detected with  $^{19}\text{F}$ -NMR that arise and disappear during the early phase of amyloid formation (reproduced with permission from Suzuki et al. copyright © American Chemical Society).<sup>249</sup>

Nevertheless, this method had its limitations, as it is not sensitive for detecting transient oligomers that do not accumulate to a significant extent. Also large oligomers whose concentration does not change appreciably in the lag phase can not be detected. These large oligomers would cause line broadening like amyloid fibrils do, making analysis with solution NMR methods impossible.

To overcome this, amyloid structures are commonly analyzed with solid state NMR.<sup>93,122,259</sup> Solid state NMR usually requires labelling of the sequence with non naturally abundant isotopes, like  $^{15}\text{N}$  or  $^{13}\text{C}$ . The lack of a natural abundance of fluorine in biomolecules renders such isotope labeling unnecessary. The combination of site specific incorporation of the fluorinated reporter group and the solid state  $^{19}\text{F}$ -NMR-analysis has been successfully used to study peptides in the presence of membranes.<sup>260-263</sup>

The sterically restrictive 4- $\text{CF}_3$ -phenylglycine ( $\text{CF}_3$ -Phg) was site specifically introduced as either the L- or D-enantiomer instead of Leu6, Leu8, Leu11, or Leu15 of an amphipathic model peptide (MAP: KLALKLALKALKALKLA-NH<sub>2</sub>) to allow or prevent  $\beta$ -sheet aggregation due to steric reasons.<sup>264</sup> The peptide was designed as an amphiphilic  $\alpha$ -helix able to transverse lipid bilayers and penetrate cells.<sup>265</sup> However, at high peptide concentrations a conformational switch from an  $\alpha$ -helical structure towards a  $\beta$ -sheet rich aggregate was observed. The incorporation of the D-form instead of Leu15 was found to inhibit this aggregation due to disruption of the hydrogen-bond pattern between the sheets, while the variant containing the L-form behaved similar to the parent peptide; namely showing helical conformation only at low peptide concentrations. The conformation of the side chain of only one residue discriminated in this case between a similar or different behavior of the peptide compared to the natural one.

The mechanism of amyloid formation in the presence of a membrane was later studied on a small cationic peptide [KIGAKI]<sub>3</sub> designed as an amphiphilic  $\beta$ -strand.<sup>33</sup> The antimicrobially active peptide shows in solution a random coil structure that change to a  $\beta$ -sheet conformation in the presence of lipid bilayers. In an extensive solid state  $^{19}\text{F}$ -NMR analysis of variants containing single substitutions of different residues along the sequence by the well studied NMR reporter 3-(trifluoromethyl)-L-bicyclopent-[1.1.1]-1-ylglycine ( $\text{CF}_3$ -L-Bpg) (*Figure 4.9*), the conformation, membrane alignment, and dynamic behaviour of the peptide was investigated. The transition from monomeric  $\beta$ -strands to fibrils consisting of H-bonded  $\beta$ -sheets was found to be concentration dependent (*Figure 4.9*). Since the C- $\text{CF}_3$  bond of the rigid side chain in this label is collinear with the  $\text{C}_\alpha$ - $\text{C}_\beta$  bond, the direction of the C- $\text{CF}_3$  bond vector reflects the orientation and mobility of the backbone segment to which it is rigidly attached. At low concentrations the peptide is found to exist in a flexible monomeric  $\beta$ -sheet conformation in the vicinity of the hydrophobic/hydrophilic interface of the membrane with the hydrophobic residues directed towards the inside of the lipid

bilayer. At high concentrations the  $\beta$ -strands self assemble into amphiphilic  $\beta$ -sheets in an amyloid-like fashion, lying immobile on the surface of the membrane.

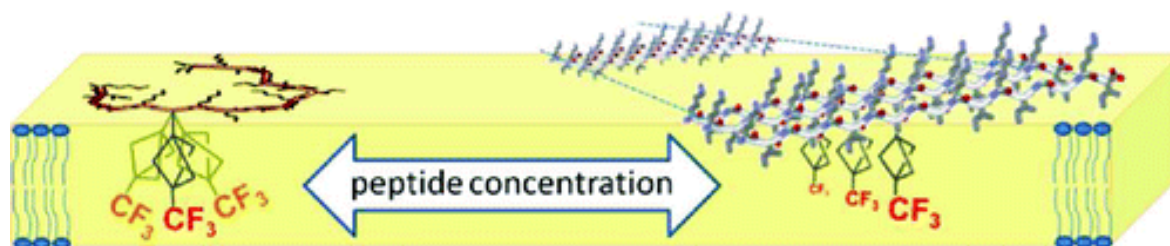


**Figure 4.9:** At low peptide concentrations of  $[KIGAKI]_3$  the rigid  $CF_3$ -l-Bpg side chain shows reduced dipolar splittings in ss  $^{19}F$ -NMR indicating a high flexibility of the amphiphilic  $\beta$ -strands that corresponds to monomeric  $\beta$ -strands that swim around freely in the hydrophilic/hydrophobic interface of the membrane. Upon concentration increases of the peptide, the peptides take on an amyloid-like structure which reduces the flexibility of the  $CF_3$ -l-Bpg side chains and give rise to stronger dipolar interactions in the ss  $^{19}F$ -NMR-measurements (reproduced with permission from Wadhvani et al. copyright © American Chemical Society).<sup>33</sup>

This solid state  $^{19}F$ -NMR approach enables monitoring of the concentration dependent self-assembly of disordered peptides into amyloid fibrils. However, this approach is based on studying the dynamic behavior of peptide segments, which is restricted to the rigid  $^{19}F$ -NMR label and the fixation of the peptide at a membrane. The presence of the membrane is thought to positively influence amyloid formation, also in the case of the Alzheimer's causing  $A\beta$ . Nevertheless, it is still not clear if amyloid formation occurs intra or extracellularly.<sup>266</sup> This might explain a concentration dependent effect on amyloid formation observed for  $A\beta$ .<sup>267-269</sup> Whether the solid state  $^{19}F$ -NMR approach can be transferred to the study of the amyloid formation process in the absence of a membrane remains to be shown.

#### 4.3.2 Fluorinated amino acids as tools to modulate amyloid fibrils

Using fluorinated amino acids as labels to follow amyloid formation relies on the assumptions that the label, on the one hand, location does not perturb the peptide structure, and, on the other hand, does not alter the pathway of aggregation in comparison to the unmodified sequence. In fact the modified properties of the fluorinated amino acid analogues, including changes in size, hydrophobicity, polarity, and acidity can influence both the structure and the aggregation behavior of the peptides.

This was unambiguously shown in two individual studies that investigated electrostatic, aromatic, hydrophobic, and steric effects on the self-assembly of short fragments derived from the well known aggregation prone region of  $A\beta$ .<sup>270,271</sup> Senguen and co-workers used the amyloid- $\beta$  fragment (16-22) with the well studied fibril structure consisting of antiparallel

aligned  $\beta$ -sheets.<sup>270</sup> The two central phenylalanine residues were substituted singly or multiply with Ala, Tyr, cyclohexylalanine (Cha), and the fully fluorinated analogue of Phe, pentafluorophenylalanine (F<sub>5</sub>-Phe). While the Ala and Tyr variants failed to undergo fibril formation, kinetic and thermodynamic investigations showed that both singly substituted F<sub>5</sub>-Phe variants aggregated at dramatically enhanced rates relative to the wild type. The double F<sub>5</sub>-Phe mutant exhibited additive thermodynamic effects. The elevated fibril formation of the fluorinated variants was not only attributed to the greater hydrophobicity of F<sub>5</sub>-Phe compared to Phe, but also to additional fluorine-fluorine interactions, based on the fact that highly fluorinated amino acids show strong self-aggregating properties.<sup>272</sup> A combination of aromatic effects, such as  $\pi$ -stacking of the aromatic side chains, and the notably higher propensity of F<sub>5</sub>-Phe for the  $\beta$ -sheet structure, observed by Cheng *et al.*,<sup>244</sup> were proposed to be factors that enhance amyloid formation rates.

Serpell *et al.* found similar results in their studies and also emphasized the impact of electrostatic interactions on amyloid formation.<sup>271</sup> They designed an aggregating model peptide based on the shortest known amyloid forming sequence KFFE by connecting two of these segments with a flexible hydrophobic linker region. The resulting sequence KFFEAAKKFFE was modified by certain amino acid substitutions. Although their study did not include any fluorinated amino acids, they found that any removal of the central Phe residues results in a complete loss of assembly ability, indicating the importance of a hydrophobic residue at this particular position. In addition, they observed alternative fibril morphologies as a consequence of altered  $\beta$ -sheet packing upon the incorporation of charged residues into the peptide sequence. This finding indicates that also electrostatic contributions can influence amyloid formation. This should be especially considered when partially fluorinated amino acids are incorporated into aggregating structures, because these can have different polar or electrostatic properties compared to aliphatic hydrocarbon amino acids.

These results show that any modification of a sequence needs to be studied carefully. Fluorinated amino acids come along with new intrinsic properties that can be different in comparison to those of the particular hydrocarbon analogue in terms of hydrophobicity, polarity, acidity/basicity, size, and physicochemical properties. The replacement of a natural amino acid with its fluorinated analogue thus has the potential to perturb the structure or alter the behavior of the peptides or proteins, which, depending on the aim of the study, may be beneficial. Special caution is necessary with regard to the modification of amyloid forming sequences, as the complex multi-step assembly process is influenced by a combination of several factors.





---

## 5 Aim of the work

The model peptide **VW18** was previously developed for the purpose of enabling systematic investigations of the molecular mechanisms that underlie the conformational change from a soluble  $\alpha$ -helical coiled coil structure to  $\beta$ -sheet rich amyloid fibrils. Prior studies with this system led to a molecular model of the internal fibril architecture by means of a glycine and proline scan to identify bend positions. The overarching aim of this work was to evaluate the impact of fluorine on amyloid formation in this model system. In keeping with this, initial studies focused on the role of proline had to first be conducted via the incorporation of proline chimeras in turn motifs. Moreover, the mechanism of the structural transition of **VW18** had to be further elucidated by determining the critical size of the nucleus that serves as a template for the attachment of further peptide strands. With this information in hand, amyloid formation promoting valine residues in **VW18** were replaced by diverse side chain fluorinated amino acids. The resulting fluorinated peptides were then analyzed by appropriate methods including CD spectroscopy, Thioflavin T fluorescence spectroscopy, TEM analysis, and solid state NMR measurements.



## 6 Applied Methods

The main part of the present thesis deals with the structural investigation of peptides that can undergo structural transitions upon modification of the primary sequence and under specific conditions. A set of techniques including high and low resolution methods was used for structural characterization of these peptides. The most important methods applied here are briefly described below. Additional methods that were used are summarized in the publications resulting from this thesis and in the references cited therein.

### 6.1 Circular dichroism spectroscopy

Circular dichroism (CD) spectroscopy is one of the most commonly applied low resolution techniques for investigating the secondary structures of peptides and proteins in solution.<sup>273</sup> This non-destructive method has become routine for the structural analysis of biological macromolecules because it is less demanding in terms of time and sample amount in comparison to high resolution methods, such as NMR-analysis or X-ray crystallography. CD spectroscopy furthermore allows a wide variety of experimental conditions like changes in pH, concentration, and the presence of metal ions, to name only a few. CD spectroscopy was extensively utilized to follow transitions between secondary structures of the peptides studied in the present thesis.

Unlike linearly polarized light that occurs when the electric field vector oscillates only in one plane, circularly polarized light occurs when the direction of the electric field vector rotates about its propagation direction while the vector retains constant magnitude. It can be obtained by superimposing two linearly polarized light beams that have a phase shift of  $\lambda/2$  and electrical field vectors that are perpendicular to each other. The resultant amplitude vector of the electrical field will then rotate on a spiral perpendicular to the direction of the propagating light wave (*Figure 6.1*).

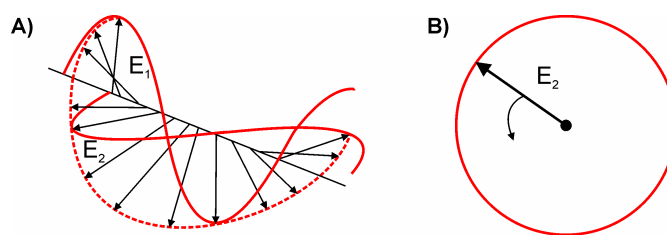


**Figure 6.1:** **A)** Generation of left circularly polarized light by superposition of polarized light. The electrical field vectors of the light waves are perpendicular to each other and the two waves have a phase difference of a quarter wavelength with  $E_1$  preceding  $E_2$ . If  $E_2$  would precede  $E_1$ , the resulting wave would be right circularly polarized. **B)** Circularly polarized light projected in the direction of proliferation.

When oppositely circular polarized light beams (right and left polarized light) pass through a chiral sample, the extent to which both are absorbed is different. This difference is defined as circular dichroism and can be expressed by the Beer Lambert law as:<sup>274</sup>

$$\Delta A = A_L - A_R = \epsilon_L c l - \epsilon_R c l = \Delta \epsilon c l \quad (6.1)$$

where  $A$  is the absorption,  $\epsilon$  the absorption coefficient,  $c$  is the molar concentration of the sample, and  $l$  the path length. The term  $\Delta \epsilon$  is defined as the circular dichroism.

Plane-polarized light consists of right- and left-circularly polarized light of equal intensity. The different absorption of both components by an optical active medium, converts plane-polarized light into elliptically polarized light. The semimajor axis is given by the sum of magnitudes of both components, while with the difference in magnitude gives the semiminor axis of the ellipse (Figure 6.2).

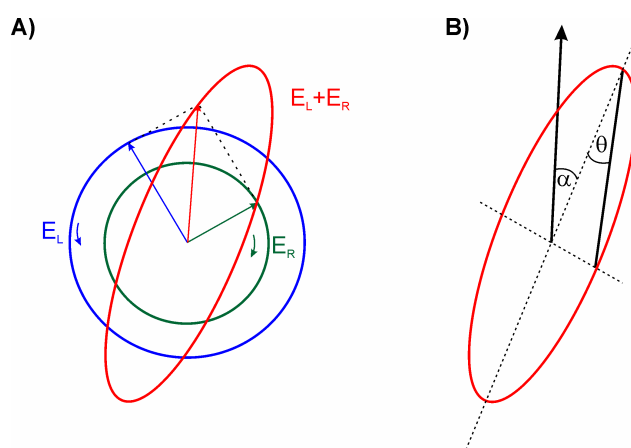


**Figure 6.2:** **A)** Elliptically polarized light formed by two oppositely circularly polarized light beams of unequal intensity after absorption of plane-polarized light by an optically active molecule. If the absorption of right-circularly polarized light is greater than that of left-circularly polarized light, then the result will be a left-elliptically polarized light beam. **B)** The ellipticity  $\theta$  is the angle between the minor and major axis of the ellipse whose ratio is equal to  $\tan \theta$ . The angle  $\alpha$  is the optical rotation, i.e. the angle between the major axis of the ellipse and the initial plane of the incident plane-polarized light (reproduced according Woody et al. copyright © Plenum Press).<sup>274</sup>

Since the differences in absorption are usually very small, CD is commonly reported by the ellipticity  $\theta$ , which is the angle between semiminor and semimajor axis of the ellipse. The ellipticity is directly proportional to the CD:<sup>274</sup>

$$\theta \text{ (deg)} = 180 \ln 10 \Delta A / 4\pi = 32,98 \Delta A \quad (6.2)$$

The removal of the trivial linear dependence on path length, concentration, and chain length enables a comparison of different proteins. The resulting molar residue ellipticity is defined as:

$$[\theta] = \theta / 10000 c n l \quad (6.3)$$

Where  $\theta$  is the measured ellipticity in mdeg,  $c$  is the sample concentration in mol/l,  $l$  is the path length in cm, and  $n$  is the number of residues.

The amide group is the most abundant chromophore of peptides and proteins, however also the amino acids (except for glycine) of which proteins are composed are enantiomeric. The most characteristic absorption bands of the peptide bond can be found in the far-UV region (160 – 250 nm) where the  $n \rightarrow \pi^*$  transition (around 220 nm), and the  $\pi \rightarrow \pi^*$  transition (around 190 nm) appears. Characteristic CD spectra can be distinguished for the three mainly adopted secondary structures of peptides and proteins (Figure 6.3)

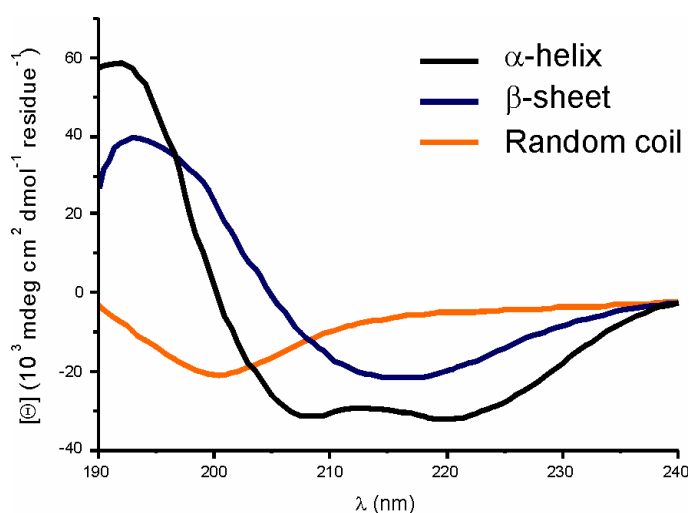


**Figure 6.3:** Characteristic far-UV spectra of  $\alpha$ -helix,  $\beta$ -sheet, and random coil.

The  $\alpha$ -helical structure gives CD spectra with two characteristic minima at 208 nm ( $\pi \rightarrow \pi^*$  transition) and 222 nm ( $n \rightarrow \pi^*$  transition). The characteristic maximum at 190 nm also

arises from the  $\pi \rightarrow \pi^*$  transition. In contrast,  $\beta$ -sheet structures show one broad minimum around 215 nm ( $\pi \rightarrow \pi^*$  transition), a maximum at 195-198 nm ( $n \rightarrow \pi^*$  transition) and another minimum at 175 nm ( $\pi \rightarrow \pi^*$  transition). Unordered structures usually have a minimum at 200 nm ( $n \rightarrow \pi^*$  transition). The spectra of isolated  $\alpha$ -helices,  $\beta$ -sheets, and coils were experimentally obtained from a variety of systems.<sup>275,276</sup> To analyze complex protein structures, deconvolution of the CD spectra with computational approaches is usually necessary.<sup>277</sup> In this way, the contributions of the three named and other secondary structures like polyproline II and  $\beta$ -turns can be obtained.

## 6.2 Dye Binding studies

CD spectroscopy can be used to follow secondary structural transitions, but it does not yield information about fibril forming. Dye binding is one of the common techniques used for the identification of amyloids and several dyes like Congo red, Thioflavin T (ThT) or NIAD-4 have been reported.<sup>278-280</sup> The dyes Congo red and Thioflavin T have their origin in the staining of histological samples<sup>278,281-283</sup> since the specific binding to Congo red has been declared as one of the common characteristics of amyloids.<sup>83</sup> However, the observation that Congo red can accelerate or inhibit the amyloid formation process,<sup>284,285</sup> and the much easier handling of Thioflavin T in contrast to Congo red established ThT as a more relying staining agent for amyloid structures. An additional advantage of ThT is its ability to yield quantitative information on the amount of amyloids present in the sample.<sup>286</sup> In addition it can be used *in vitro* and *in vivo*.<sup>279,287</sup> LeVine and Naiki showed that ThT bound to fibrils results in dramatic shifts in the excitation maximum (from 385 nm to 450 nm) and the emission maximum (from 445 nm to 485 nm).<sup>279,288,289</sup> The fluorescence emission intensity depends on the amount of aggregates and can thus be applied to monitor the transition from native to aggregated form. The specific recognition and modest binding affinity of ThT to amyloids make it a good scaffold for the elaboration of alternative amyloid stains, including reagents used for medical imaging of amyloid in living patients.<sup>290,291</sup>

Although there are many theories reported on how ThT binds to amyloid fibrils,<sup>292</sup> the mechanism is still not fully understood. The binding of ThT to fibrils is independent of the primary sequence of the peptide but linked to the presence of a cross- $\beta$  structure within the fibrils.<sup>279,288</sup> Such structures consist of repeating side chain interactions running across the  $\beta$ -strand within a  $\beta$ -sheet layer. The  $\beta$ -sheets are oriented perpendicular to the fibril axis and form extended channel-like motifs along the solvent exposed side parallel to the fibril axis. These channels could serve as a potential binding site for the Thioflavin-T

dye molecules (Figure 6.4),<sup>293</sup> a model later supported by molecular dynamics simulations.<sup>294,295</sup>

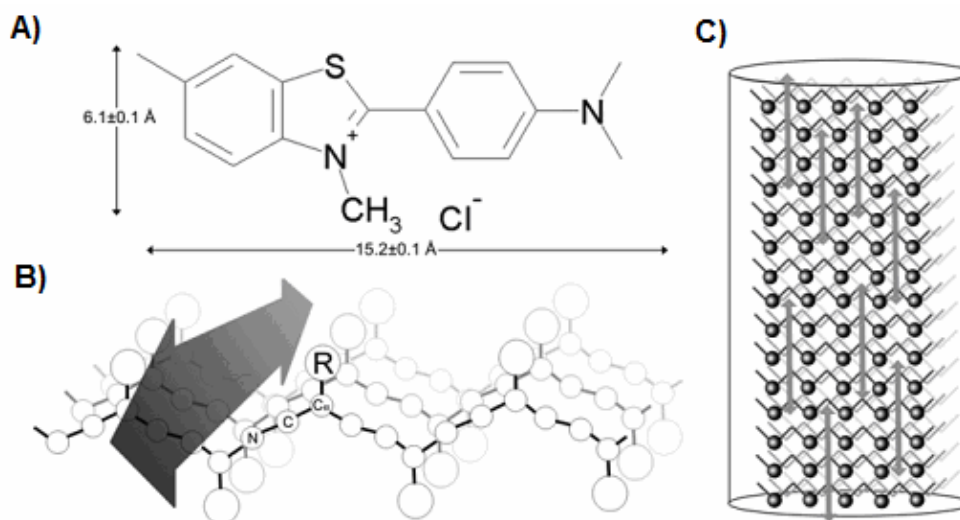


**Figure 6.4:** **A)** Chemical structure and dimensions of the Thioflavin T molecule. **B)** Schematic representation of a  $\beta$ -sheet with backbone atoms (N, C and Ca) and a side chain group (R) indicated. ThT binding is represented by a double headed arrow and occurs in a channel between the side chains. **C)** Schematic representation of a protofilament with ThT molecules (double headed arrows) bound parallel to the fibril axis and perpendicular to the  $\beta$ -strands (according to Krebs *et al.*, Copyright © Elsevier).<sup>293</sup>

That at least two molecules have to bind as excited dimers in the channels to gain a characteristic fluorescence signal was suggested by Groenning *et al.*<sup>296</sup> Aggregates having channels with diameters less than 8-9 Å and lengths less than 15.2 Å were able to bind only one ThT molecule per channel and did not show the specific shift in the absorption spectra.<sup>296</sup> However, ThT also shows binding affinity for hydrophobic pockets of non-fibrillar proteins.<sup>297,298</sup> Other studies discuss the loss of rotational freedom between the benzylamine and the benzothiazole ring in the ThT molecule upon interacting with the amino acid side chains in the fibril channels as a possible the reason for the strong fluorescence.<sup>299-302</sup> The fast rotation rapidly quenches excited states and thereby causes the low fluorescence emission of unbound ThT. Nevertheless, none of the models can explain why ThT binds parallel to the fibril axis.<sup>292</sup>

### 6.3 Size exclusion / static light scattering

Gel filtration or size exclusion chromatography (SEC) can be used to determine the molecular mass of peptides and proteins. The separation principle relies on different permeation of molecules of various sizes with a porous carrier material, the gel. The

elution volume of the molecule from a SEC column depends on the size of the molecule in an approximate relation to the Stokes radius.<sup>303</sup> Small molecules elute later than large molecules because they permeate even the narrow pores of the stationary phase. Large molecules instead do not interact with the gel and elute first. Once a SEC column has been calibrated with standard proteins of known molecular mass and Stokes radius, the elution volumes can be used to estimate the unknown Stokes radii of other proteins. Provided that the proteins have similar shape to the standard protein that was used for calibration, the elution volumes can be estimated from the size because the partial specific volumes of all soluble proteins are roughly the same. However this method has limitations for membrane proteins that contain a certain amount of associated detergent molecules. Also asymmetric particles or proteins with other conformation or shape compared to the standard protein cause uncertainties in the ratio of Stokes radius to elution volume.

More reliable methods to determine the molecular mass are analytical sedimentation equilibrium centrifugation or static light scattering. These methods can directly measure the absolute molecular mass independent of the shape of the molecule and without assumption of the amount of detergent bound.<sup>304</sup>

Static light scattering of a macromolecular solution is described by the classical Rayleigh relationship:

$$\Delta LS = \left( \frac{I_\theta}{I_0} \right)_{\text{solution}} - \left( \frac{I_\theta}{I_0} \right)_{\text{buffer}} = K \left( \frac{dn}{dc} \right)^2 M_w c \quad (6.4)$$

where  $I_\theta/I_0$  is the ratio of the intensities of the light scattered at angle  $\theta$  and the incident light.  $\theta$  is the angle between the direction of the incident and scattered light.  $\Delta LS$  is the excess of light scattered at a given angle by the solution containing the scattering protein in comparison to the light scattered by the buffer.  $M_w$  is the weight-averaged molecular mass of the scattering protein, which is to be determined and  $c$  is the concentration in mg/ml and can be directly measured by using concentration sensitive detectors. For proteins the concentration can be determined by measuring the absorption at 280 nm with a UV detector, if the extinction coefficient is known:<sup>304</sup>

$$c = \frac{\Delta UV_{280}}{A_{280}} = \frac{UV_{280\_solution} - UV_{280\_buffer}}{A_{280}} \text{ at 1 cm pathlength} \quad (6.5)$$

$dn/dc$  is the specific refractive index of the protein and can be experimentally determined using a UV detector for concentration determination, and a differential refractometer,



which measures the difference in the refractive index ( $\Delta RI$ ) between the macromolecular solution and the buffer:

$$\frac{dn}{dc} = \frac{\Delta RI}{(\Delta UV_{280} / A_{280})} = \frac{(RI_{solution} - RI_{buffer}) A_{280}}{\Delta UV_{280}} \quad (6.6)$$

If  $dn/dc$  is known, there is an alternative equation for determining the concentration with the help of the differential refractometer:

$$c = \frac{\Delta RI}{(dn/dc)} \quad (6.7)$$

For the majority of soluble proteins  $dn/dc$  has approximately the same value of 0.185 ml/g.<sup>304</sup>

$K$  is an instrument constant depending on the refractive index of the solution without macromolecule ( $n$ ), the wavelength of the light that is used ( $\lambda_0^2$ ), the angle between incident and scattered light ( $\theta$ ) and the distance between the scattering molecule and the detector ( $r$ );  $N_A$  is Avogadro's number:

$$K = \frac{2\pi^2 n^2}{\lambda_0^2 N_A} \left( \frac{1 + \cos^2 \theta}{r^2} \right) \quad (6.8)$$

Eq. (6.4) is an approximation which is valid for protein concentrations below 0.1 mg/ml and the proteins that are small (masses up to several million Dalton) compared to the wavelength of the light in order to not cause an angular dependency of the light scattering. Because  $dn/dc$  is known for soluble proteins, their molecular weight can be determined from Eq. (6.4) using a two detector setup: a LS detector and a concentration sensitive detector, which can be either the UV detector or the RI detector.

$$M_w = \frac{\Delta LS}{K \left( \frac{dn}{dc} \right)^2 \left( \frac{\Delta UV_{280}}{A_{280}} \right)} = \frac{A_{280} \Delta LS}{K \left( \frac{dn}{dc} \right)^2 \Delta UV_{280}} \quad (6.9a)$$

or:

$$M_w = \frac{\Delta LS}{K \left( \frac{dn}{dc} \right)^2 \left( \frac{\Delta RI}{dn/dc} \right)} = \frac{A_{280} \Delta LS}{K \left( \frac{dn}{dc} \right) \Delta RI} \quad (6.9b)$$

The determined molecular masses are weight-averaged molecular masses. If the protein solution is not monodisperse, the determined molecular masses are different from the real protein molecular mass. This requires that the detectors are connected in-line with a chromatography system. Thus, all three signals are measured continuously during a size exclusion run. This method is referred to as SEC-MALLS (Multi Angle Laser Light Scattering).<sup>305</sup> The size exclusion separates the different components of the sample and the molecular mass of each eluting component is determined with the in-line connected detectors. This enables a determination of different oligomerization states within a protein solution as shown in the overlay of all three spectra (UV, LS, RI) and the corresponding determined molecular mass of a BSA-sample (*Bovine Serum Albumine*), typically used as a standard protein for calibrating the SEC-MALLS instrument (*Figure 6.5*). The spectra show that three oligomerization states of BSA (monomer, dimer, and trimer) can be distinguished with the combination of SEC and SLS.<sup>304</sup>

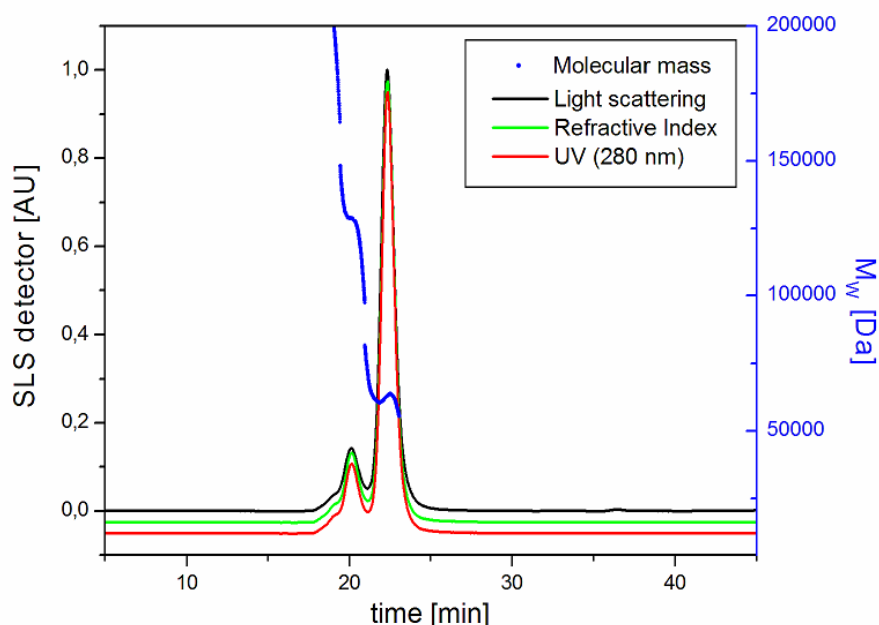


**Figure 6.5:** Example of a representative SEC/LS analysis of BSA.

## 6.4 Solid state $^{19}\text{F}$ -NMR

Isotopes or nuclides with an odd number of protons and/or of neutrons have an intrinsic magnetic moment and an angular momentum, in other words a nonzero spin. In contrast, nuclides with even proton and neutron numbers have a total spin of zero. When a nucleus carrying a nonzero spin is brought into a strong magnetic field, the possible orientation states of the nuclear spin with respect to that field are no longer identical in energy.<sup>306</sup> The effected splitting of energy levels allows the nucleus to perform transitions between spin

states that are connected to absorption or emission of radiation in the radio wavelength range (Figure 6.6).

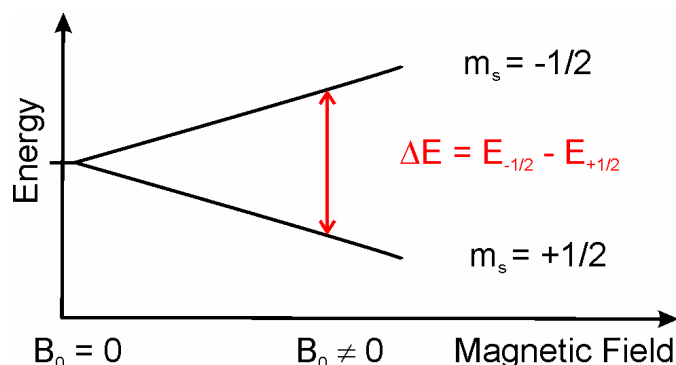


**Figure 6.6:** Splitting of nuclei spin states in an external magnetic field of nuclei which have a spin of one-half, like  $^1\text{H}$ ,  $^{13}\text{C}$ , or  $^{19}\text{F}$ .

Resonant absorption by nuclear spins only occurs when applied electromagnetic radiation matches the energy difference between the nuclear spin levels in a constant magnetic field of appropriate strength. Such magnetic resonance frequencies are typically in the range of radio frequency. The magnetic resonant absorption is detected in NMR.<sup>306</sup>

The effective field strength acting on a specific nucleus is dependent on the local electronic environment of the nucleus. The surrounding electron cloud can enhance or counteract the external magnetic field, thereby slightly shifting the resonance frequency observed. This effect is called chemical shielding and it allows conclusions about the chemical surrounding of the nucleus to be drawn. The shift in the NMR frequency to the external magnetic field is called chemical shift. If a nucleus is shielded to a higher degree due to higher electron density of its surrounding molecular orbital, then its NMR frequency is shifted "upfield". A less shielded nucleus will shift the NMR frequency "downfield".

Amyloid fibrils are intrinsically non-crystalline and insoluble, and therefore not assessable by conventional high resolution NMR in solution.<sup>307</sup> Solid state NMR-spectroscopy has become a powerful tool for the investigation of amyloid fibrils,<sup>93</sup> as well as biopolymers or membrane-associated proteins (compare also Section 3.1 and 4.3.1).<sup>308,309</sup>

In contrast to solution-state NMR, in which protons are the most commonly applied nuclei, in solid state they give very broad resonance, due to dipolar couplings. Solid state NMR thus requires a labelling of the peptide or protein with isotopes that are not naturally abundant, like  $^{15}\text{N}$  or  $^{13}\text{C}$ .<sup>308</sup> In contrast,  $^{19}\text{F}$  is an ideal nucleus for NMR-investigations, since it has a natural abundance of 100%.<sup>310</sup> On the other hand, fluorine does not naturally occur in biological samples, like membranes or proteins. The lack of a natural abundance background and the high sensitivity makes the  $^{19}\text{F}$ -isotope an interesting alternative label for proteins.<sup>311</sup> Like  $^1\text{H}$ ,  $^{13}\text{C}$ ,  $^{15}\text{N}$ , and  $^{31}\text{P}$ , the  $^{19}\text{F}$  nucleus possesses a

spin of  $I = 1/2$ , which makes it suitable and straightforward for structural investigations. Another benefit, beside and the large chemical shift range, is the high gyromagnetic ratio of  $^{19}\text{F}$ , which provides it with an exceptional NMR sensitivity and strong dipolar couplings, up to a distance of  $18\text{\AA}$ .<sup>309</sup>

In selectively labelled peptides, structural constraints can be obtained from two directionally dependent interactions commonly found in solid-state NMR; the *chemical shift anisotropy* (CSA) and the internuclear *dipolar coupling* (DC).<sup>309</sup> CSA is the orientation dependency of the chemical shift. The shielding effected by the electron cloud surrounding a nucleus will be different for different orientations of the molecule with respect to the external magnetic field. Anisotropic effects only become evident in NMR if the sample is sufficiently solid. When the motion of a molecule is restricted, the anisotropy of the electron cloud is reflected in the NMR-spectra. Especially the chemical shift is highly anisotropic and can be expressed as a function of the orientation of the molecule.

The second interaction relevant in solid state NMR involves two nuclei. The energy levels of one nucleus are influenced by the spin state of the other nucleus when they are in close proximity. This effect is called dipolar coupling.<sup>309</sup> The coupling strength depends on the distance between the two nuclei.

In solid state NMR, the anisotropic interactions cause broad lines that obscure the chemical-shift information. A common approach to overcome this problem and gain high resolution condition is rapid spinning of the sample at the magic angle (MAS).<sup>308</sup> By spinning the sample at a frequency between 1 and 70 kHz at the magic angle  $\theta_m$ , where  $\cos^2\theta_m = 1/3 = \text{ca. } 54.74^\circ$ , with respect to the direction of the magnetic field, the normally broad lines become narrower. If the sample is spun fast enough, anisotropic interactions are essentially averaged to zero which increases the resolution for better identification and analysis of the spectrum. However, this method also comes along with a loss of information that the anisotropic interactions contain.<sup>312</sup> To overcome this problem, radio frequency pulse sequences are commonly used in solid state NMR-methods to selectively recouple anisotropic interaction by irradiation. One exemplary method to gain information out of dipolar coupling with the help of a pulse sequence method is presented below.

#### **6.4.1 The CODEX experiment**

The CODEX (Centerband Only Detection of Exchange) experiment is based on recoupling the chemical shift anisotropy by means of two identical rotor synchronized pulse trains.<sup>312-</sup><sup>314</sup> The application of such rotor synchronized pulse trains leads to a stimulated echo at the end of the second pulse train (*Figure 6.7*)

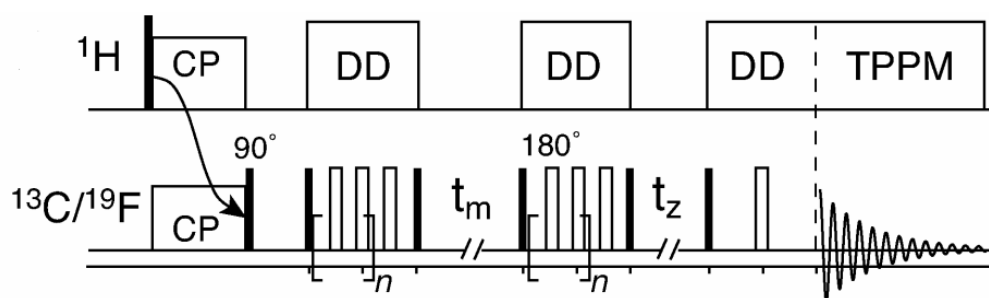


**Figure 6.7:** Pulse sequence for the CODEX experiment. Filled and open rectangles indicate  $90^\circ$  and  $180^\circ$  pulses, respectively, DD = dipolar decoupling and TPPM = two-pulse phase modulation (reproduced with permission from Buffy et. al. copyright © American Chemical Society).<sup>315</sup>

This experiment is sensitive to changes in the chemical shift, which generally reflect the orientation of the labeled segment with respect to the magnetic field, during a mixing time  $t_{\text{mix}}$ . Such changes can be caused either by a reorientation of the labeled molecular segment due to slow dynamics, or by magnetisation „diffusing“ between sites with different local orientation. Both processes lead to a reduction in the CODEX NMR signal.<sup>315</sup> Two spectra are recorded for a series of mixing times, one displaying the full intensity  $S_0$ , and a second one in which the intensity  $S$  after a certain mixing time is displayed. A distinct reduction in signal intensity is observed for the occurrence of slow molecular motions of the labeled segment or the presence of other nuclei in close proximity. When slow motion is eliminated through sample cooling, the CODEX experiment detects only spin diffusion.<sup>315</sup> In case of a nearby nuclei (for  $^{19}\text{F}$  nuclei within internuclear distances of  $\sim 10\text{-}15$  Å), the signal  $S/S_0$  is expected to asymptotically approach a non-zero constant for long mixing times  $t_{\text{mix}}$ , rather than decaying all the way down to zero. For homogeneous systems consisting of a single oligomeric species with  $M$  orientationally unique molecules, the constant value is identical to  $1/M$ , where  $M$  is the number of nuclei involved in the spin diffusion, such as the number of monomers in the case of a homo-oligomer.<sup>315</sup> Thus, by measuring the equilibrium value of a spin diffusion CODEX experiment, one can extract the size of a peptide aggregate and the number of interacting units. As spin diffusion only leads to a reduction in signal intensity when it occurs between non-equivalent sites with different orientation, the observed spin diffusion does not reflect neighbouring spins within the same protofilament. The labelled amino acids are essentially only shifted along the protofilament (but not rotated to any significant extent) and hence oriented the same way. Thus, a reduction in the signal intensity for long mixing times indicates couplings of spins that belong to different, adjacent protofilaments.



## 7 Results and discussion

### 7.1 The coiled coil as a model to study amyloid formation

The process of amyloid formation is very complex and influenced by many factors. Therefore the mechanism is often studied with the help of peptide models which have brought numerous advantages such as high synthetic accessibility and a simplified aggregation pathway in order to allow for detailed mechanistic analysis.<sup>316</sup>

There are several strategies for the *de novo* design of amyloid forming model peptides. Some of them are based on the short aggregation prone regions of prominent amyloid forming peptides, such as A $\beta$  or IAPP.<sup>103,270,271,317-319</sup> Hence, these models are often too short to allow the formation of other initial secondary structures.

Amyloid formation of several native proteins, however, involves the structural transition from an initial functional secondary structure towards another pathological one.<sup>320-322</sup> Studying this behavior with the help of models requires a design that allows the peptides to adopt at least two different secondary structures. One of the first approaches of such 'switch peptides' was established by Mutter *et al.*<sup>323</sup> Hydrophobic interactions have a major contribution in stabilizing amphiphilic  $\alpha$ -helical as well as  $\beta$ -sheet structures. Thus, Mutter and coworkers designed a repetitive pattern of hydrophobic and polar amino acids which resulted in an amphiphilic  $\beta$ -sheet. However, for this simple design an  $\alpha$ -helical arrangement was very unlikely as the hydrophobic residues would be solvent exposed around the helical cylinder. For that reason hydrophobic Leu residues on one side of the helical cylinder were replaced with the neutral amino acid alanine, which is neither polar nor hydrophobic, but possesses a large propensity for helical structures.<sup>324,325</sup> Doing so, the authors created a sequence that was amphiphilic with respect to  $\alpha$ -helical as well as  $\beta$ -sheet conformations and allowed for a switch between both structures depending on the experimental conditions. Based on this principle many switch peptides have been designed that react to environmental changes.<sup>326</sup>

One of most naturally abundant folding motifs, which is also used for the *de novo* design of model peptides that can undergo structural transitions, is the  $\alpha$ -helical coiled coil. This folding motif occurs in nature in very different functional proteins,<sup>327</sup> including transcription factors,<sup>328</sup> structural, and viral fusion proteins.<sup>329</sup> Classical coiled coils are composed of two to five right-handed helical strands that wrap around each other in order to give a left-handed helix bundle (*Figure 7.1 A/B*).<sup>330</sup> The primary sequence of coiled coils follows a general buildup principle that is based on a periodicity of seven residues giving the so

called heptad repeat (*Figure 7.1 C*), denoted  $(\mathbf{abcdefg})_n$ . Positions **a** and **d** are usually filled with hydrophobic amino acids, such as Leu, Ile, Val, and Met, that form the first recognition motif by a 'knobs-into-holes' packing of the hydrophobic side chains.<sup>330-332</sup> In an aqueous environment, this formation of a hydrophobic core is the main driving force of the assembly of the helical strands. Polar or charged amino acids are placed in the **e** and **g** positions to further stabilize the coiled coil by means of a second recognition motif of electrostatic interactions.<sup>209,333-337</sup> The remaining **b**, **c**, and **f** positions are exposed to the solvent and contain usually polar and charged amino acids as well. These **b**, **c**, and **f** positions can tolerate substitutions more easily than the other positions without altering the overall stability of the folding motif.

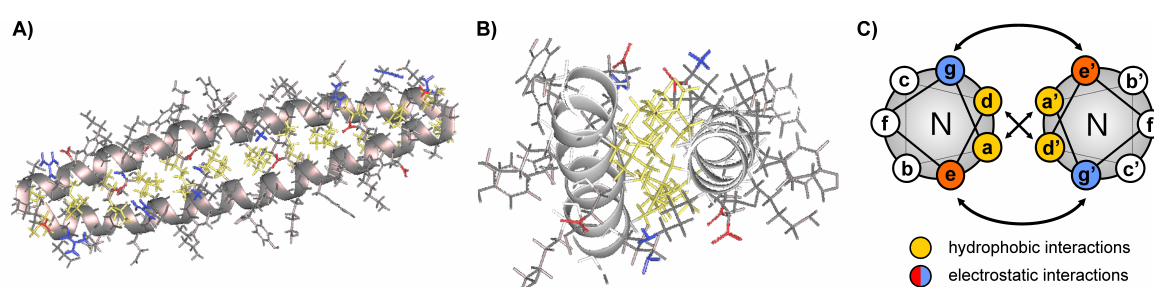


**Figure 7.1:** Schematic representation of the  $\alpha$ -helical coiled coil folding motif. **A)** Side view of a dimeric coiled coil. **B)** Top view along the helical cylinder. **C)** Helical wheel diagram representing a simplified top view of the coiled coil.

The oligomerization state of coiled coils is mainly influenced by the residues of the hydrophobic core. Harbury *et al.* found that the **a** and **d** positions of dimers, trimers, and tetramers that contain parallel aligned helices have different packing interactions (*Figure 7.2 A*).<sup>338</sup> The dimer **d** position resembles the tetramer **a** position with a perpendicular knobs-into-hole packing, whereas parallel packing interactions are found at the **a** positions of dimers and **d** positions of tetramers. Trimers show a third class of interaction, the so called acute knobs-into-hole packing. Leu was found to favor perpendicular packing while Ile prefers parallel side chain interactions. Hence, the placement of Leu or Ile in either **a** or **d** positions dictate a dimeric or tetrameric oligomerization. Trimers do not discriminate between the two amino acids but are preferably formed when both positions contain the same amino acid. Also, charged amino acids, which can build up hydrogen bonds in the hydrophobic core favor dimeric oligomerization.<sup>339</sup>

The occurrence of  $\beta$ -branched amino acids at the hydrophobic core of dimers can also affect the orientation of the helices. While Val at **a** positions favors a parallel dimeric or trimeric orientation, the complete Leu variant can also induce an antiparallel alignment of the helices.<sup>340</sup> Nevertheless, the orientation of the helices is mainly dictated by the electrostatic interactions between the **e** and **g** positions.



According to attractive or repulsive interhelical Coulomb interactions, a parallel or antiparallel orientation,<sup>334-337,341,342</sup> as well as a homo or heteromeric oligomerization, is favored (*Figure 7.2 B*).<sup>343</sup>

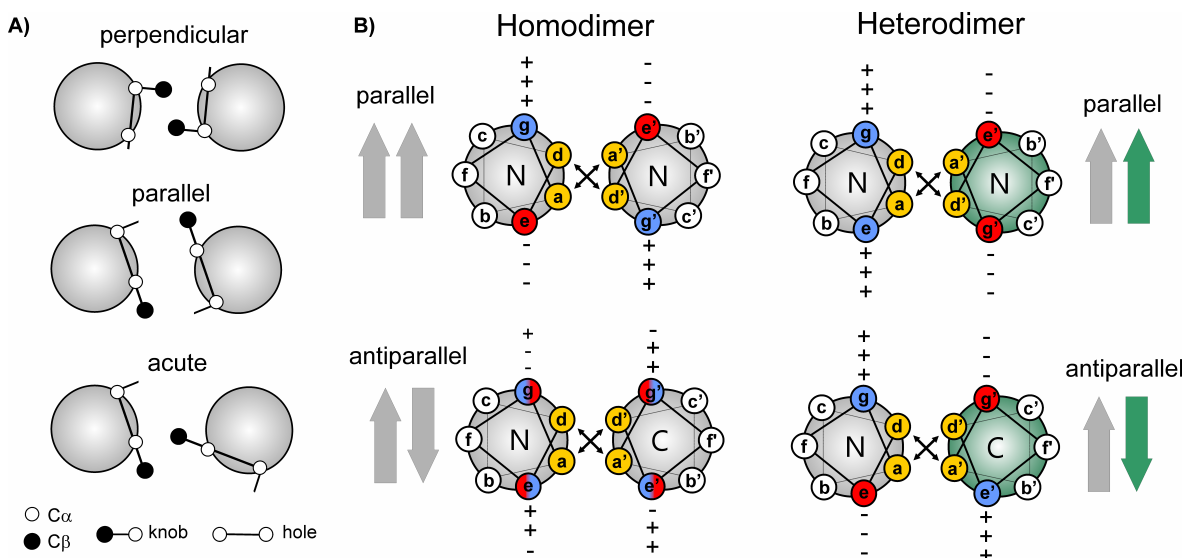


**Figure 7.2:** **A)** Three types of knobs into holes packing at the hydrophobic core of coiled coils (redrawn from Harbury *et al.*)<sup>338</sup> **B)** Possible orientations of helices in homo- and heterodimers directed by electrostatic interactions in **e** and **g** positions.

The well studied sequence-structure relationship of this folding motif led to the development of many amyloid forming model peptides based on the design principles of coiled coils featured with typically amyloid inducing elements, enabling the peptides to undertake structural conversion.<sup>111,326</sup>

The group of Mihara generated a 14 residue long coiled coil dimer which was covalently linked by disulfid bonds at the C-terminus.<sup>344</sup> Bulky adamantine groups were introduced at the N-termini of both helices in order to generate a hydrophobic domain (hydrophobic defect) that induces amyloid formation. By complexing the adamantine groups with  $\beta$ -cyclodextrin the authors inhibited amyloid formation. This peptide was further extensively studied under different experimental conditions.<sup>344-347</sup>

A different approach to induce an  $\alpha$ -to- $\beta$  structural transition at elevated temperatures was shown upon the introduction of hydrophobic amino acids at the solvent exposed positions of a coiled coil folding motif.<sup>348,349</sup> These peptides have been found to stabilize the  $\beta$ -sheet structure due to the formation of a hydrophobic patch consisting of amino acids in the **d**, **f**, and **a** positions.<sup>348</sup>

A similar approach of structural transition without the need of temperature as trigger was achieved in the group of Prof. Kokschi. Pagel *et al.* showed that the placement of valine residues at three solvent exposed positions (**b**, **c**, and **f**) induce spontaneous time-dependent amyloid formation out of initial disordered or coiled-coil structures.<sup>350-352</sup>

The hydrophobic  $\beta$ -branched side chain of valine prefers the adoption of  $\beta$ -sheet structures.<sup>324,325</sup> Thus, the formation of  $\beta$ -sheet amyloids is driven by an unfavorable interaction of the hydrophobic side chain with the aqueous environment and the preferred accommodation of the valine residues in a  $\beta$ -sheet conformation.

The model peptide **VW18** (Figure 7.3) which is able to undergo structural transition from an initial dimeric coiled coil fold into  $\beta$ -sheet rich amyloid fibrils was used in the present work to study different aspects of amyloid formation, including the influence of nonnatural, partially side chain fluorinated amino acids incorporated in the primary sequence.

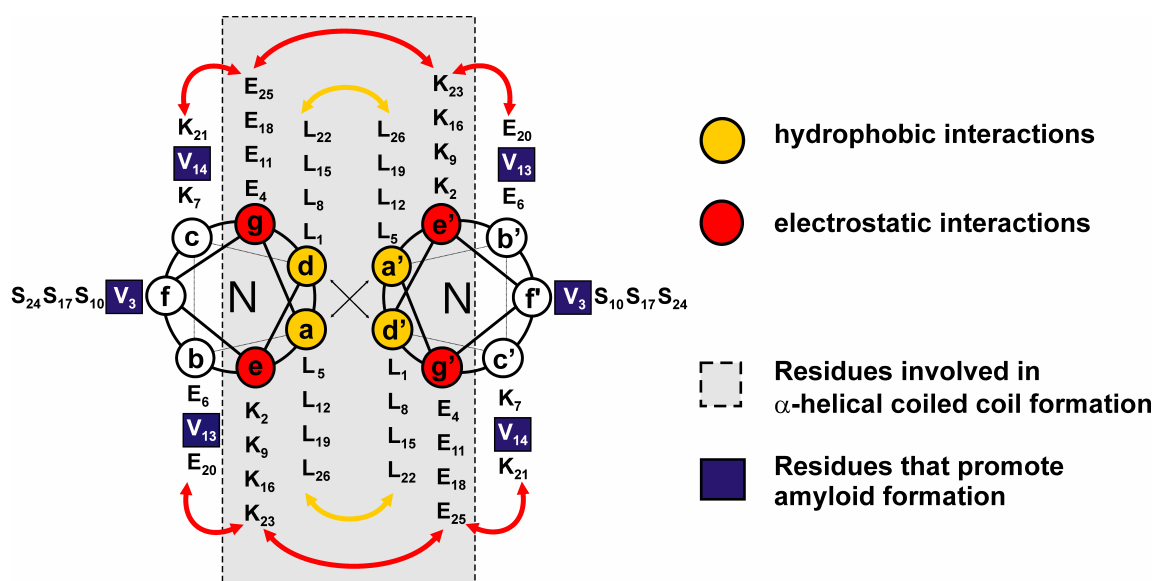


**Figure 7.3:** Helical wheel presentation and sequence of **VW18**. The design is based on two features: I) intact coiled coil interaction domains (grey frame) with hydrophobic interactions (yellow) and electrostatic interactions (red), and II) valine at the **b**, **c**, and **f** positions to generate an intrinsic amyloid forming propensity (blue).

Positions **a** and **d** are solely occupied by the hydrophobic amino acid leucine, forming the hydrophobic core that represents the primary recognition motif of the dimer. Positions **e** and **g** carry the oppositely charged amino acids glutamic acid and lysine, which are responsible for secondary recognition through interhelical electrostatic interactions, to further stabilize the coiled coil. The presence of oppositely charged flanking residues in the **e** and **g** positions ensure a parallel orientation of the two helices (compare Figure 7.2 B). The remaining positions **b**, **c**, and **f** are exposed to the solvent and occupied by the polar amino acid serine. In addition, three  $\beta$ -sheet preferring valines were incorporated at positions 3, 13, and 14 in this particular region. These are the key residues which induce the structural transition to a  $\beta$ -sheet rich amyloid structure within 24 hours under physiological conditions. **VW18** was previously studied in terms of inhibition due to helical co-assembly,<sup>353</sup> or induced by glycosidation<sup>354</sup> or phosphorylation<sup>355</sup> of the solvent exposed serine residues.

## 7.2 The internal fibril architecture of VW18

Studying the process of amyloid formation and how modifications in the primary sequence can affect the aggregation behavior requires sufficient knowledge of the peptide structure. **VW18** is a two-state system that initially adopts a stable  $\alpha$ -helical coiled coil structure, which undergoes a time-dependent structural reorganization towards  $\beta$ -sheet-rich amyloid fibrils (Figure 7.4). Thus, the initial coiled coil fold and the final fibril architecture had to be elucidated. Since the design of **VW18** is based on the bottom up principles of an ideal coiled coil motif the structure of the helix is well known (Figure 7.3). The dimeric oligomerization was proven with the help of size exclusion<sup>353</sup> and static light scattering (see also section 7.5).

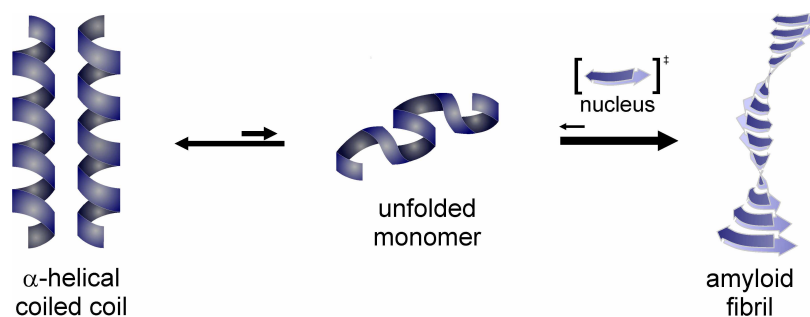


**Figure 7.4:** Schematic illustration of the two-state folding mechanism of **VW18**. The initial coiled coil motif undergoes a spontaneous structural transition towards  $\beta$ -sheet rich amyloid fibrils in an aqueous environment.

The arrangement of the respective  $\beta$ -strands within the fibril was elucidated during my master's thesis, which I performed in the group of Prof. Dr. Beate Kokschi.<sup>356</sup> Preliminary results initiating this study were produced during an internship I completed in the same group prior to my master's thesis.<sup>357</sup> For this purpose, a systematic replacement of residues in the sequence of **VW18** by glycine and proline was conducted (Gly- and Pro-scan).<sup>358</sup> In this context, proline and glycine substitutions are especially useful in determining the location of typical secondary structure elements.<sup>359,360</sup> Due to its rigid backbone, proline is rarely present in protein  $\alpha$ -helices and  $\beta$ -sheets, but is frequently found in turns or bends.<sup>361</sup> Glycine, on the other hand, shows the opposite behavior: the absence of a side chain results in outstanding backbone flexibility, which, in turns or bends, enables conformations that are energetically highly unfavorable for other amino acids.<sup>362,363</sup> With respect to amyloids, systematic proline<sup>364,365</sup> and combined proline / alanine scanning<sup>366</sup> have already been used to analyze internal fibrillar architecture. These scans provide information about the impact that particular replaced side chains and the changed backbone flexibility have on structure stabilization and the ability to form amyloid fibrils.<sup>367</sup> This is a very effective method to identify energetically important

backbone H-bonds and side chain interactions like hydrophobic or electrostatic interactions. Replacement of residues within the aggregation prone region,<sup>368,366</sup> or substitutions of crucial electrostatic interaction partners,<sup>369</sup> can have dramatic effects on folding behavior and protein stability.<sup>367</sup> Substitution of less important residues usually has a much less substantial effect on folding behavior.

A previous series of TEM, AFM, and X-ray fiber diffraction studies on **VW18** revealed twisted, ribbon-like fibrillar aggregates that are composed of multiple smaller units (*Figure 7.5 A*), the so-called protofilaments. The spacing within each protofilament unit was found to be approximately 3.3 nm by TEM analysis of the fibrils. The fact that this value was significantly lower than the length expected theoretically for a fully extended 26 residue  $\beta$ -strand of  $\sim 9$  nm indicated that the previously proposed structural model<sup>351</sup> needed careful revision. Based on the protofilament dimensions it was concluded that the peptide strands embedded in the protofilament must contain at least one bend. The distance of around  $\sim 3.3$  nm meant that no more than 9 to 10 residues could be involved in one extended region of the  $\beta$ -strand (*Figure 7.5 B*).

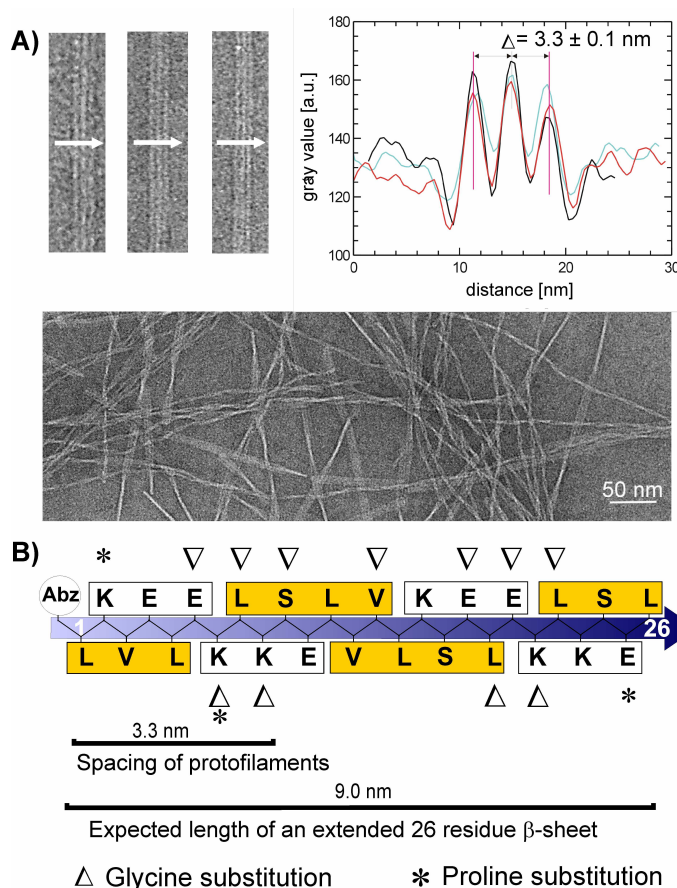


**Figure 7.5:** **A)** Example of a density profile measured on horizontally oriented fibrils perpendicular to their long fibril axis and the subsequent TEM image below. **B)** Extended  $\beta$ -strand of **VW18** showing substituted positions: glycine substitution (triangle), proline substitution (star). Hydrophobic and hydrophilic parts of the sequence are highlighted in yellow and white respectively (modified with permission according to Gerling et al. copyright © American Chemical Society).<sup>358</sup>

In the course of my internship and subsequent master's thesis a series of single glycine and proline mutants (*Figure 7.5 B, Table 7.1*) was synthesized using fully automated solid phase peptide synthesis (SPPS) and the folding and assembly behavior of each peptide was monitored directly using CD spectroscopy and Thioflavin T fluorescence staining. Substitution with glycine was conducted for amino acids 6 to 10 and 18 to 22, as the bends within the peptide strand were assumed to be in these positions. Placing glycine at the site of a bend should result in a faster structural transition to  $\beta$ -sheets and amyloids, as the formation of bends is facilitated due to higher flexibility of glycine.<sup>363</sup> Replacing valine in position 14 served as a negative control since it was known from previous design studies that the three valine residues in the solvent exposed positions are crucial for the structural transition into amyloids. In addition to glycine substitutions the residues close to N- and C-termini (2 and 25) were substituted with proline to explore the effect of these regions on amyloid formation. These particular segments were supposed to form extended  $\beta$ -strands that have a crucial impact on the core structure of amyloid fibrils, thus the incorporation of rigid, structure breaking proline should disrupt these structures and inhibit amyloid formation. Furthermore, the morphology of the resulting aggregates was characterized by TEM.

**Table 7.1:** Names and sequences of the VW18 variants containing Gly or Pro in the sequence.

Name	Sequence
VW18	Abz-LKVELEKLNKSELVVLKSELEKLNKSEL
VW18-K2P	Abz-LPVELEKLNKSELVVLKSELEKLNKSEL
VW18-E6G	Abz-LKVELGKLNKSELVVLKSELEKLNKSEL
VW18-E6P <sup>#</sup>	Abz-LKVELPKLNKSELVVLKSELEKLNKSEL
VW18-K7G	Abz-LKVELEGLNKSELVVLKSELEKLNKSEL
VW18-K7P	Abz-LKVELEPLKSELVVLKSELEKLNKSEL
VW18-L8G	Abz-LKVELEKGNKSELVVLKSELEKLNKSEL
VW18-K9G	Abz-LKVELEKLNKSELVVLKSELEKLNKSEL
VW18-S10G	Abz-LKVELEKLNKSELVVLKSELEKLNKSEL
VW18-E11P <sup>#</sup>	Abz-LKVELEKLNKSELVVLKSELEKLNKSEL
VW18-V14G	Abz-LKVELEKLNKSELVGLKSELEKLNKSEL
VW18-E18G	Abz-LKVELEKLNKSELVVLKSGLEKLNKSEL
VW18-E18P <sup>#</sup>	Abz-LKVELEKLNKSELVVLKSPLEKLNKSEL
VW18-L19G	Abz-LKVELEKLNKSELVVLKSEGEKLNKSEL
VW18-E20G	Abz-LKVELEKLNKSELVVLKSELGKLNKSEL
VW18-K21G	Abz-LKVELEKLNKSELVVLKSELEGLKSEL
VW18-L22G	Abz-LKVELEKLNKSELVVLKSELEKGNKSEL
VW18-E25P	Abz-LKVELEKLNKSELVVLKSELEKLNKSP
VW18-L8G,L19G*	Abz-LKVELEKGNKSELVVLKSEGEKLNKSEL

<sup>#</sup> These variants were synthesized during my internship under supervision of Dr. Kevin Pagel, 2008

\* This variant was synthesized in the context of this thesis

In the course of this PhD thesis, one double glycine mutant (*Table 7.1*) was synthesized containing glycine in both expected bend regions. This variant was necessary to determine whether one or two bends are present in the sequence. An extensive density profile analysis of the variants containing Gly at a potential bend position was also accomplished in this context.<sup>358</sup> These studies revealed that the diameters of protofilament units are equal for all of these variants, which represents a similar internal arrangement of the  $\beta$ -strands in the glycine variants and the unmodified **VW18** (*Figure 7.5*).

Compared to **VW18**, faster  $\beta$ -sheet formation and aggregation for variants containing glycine in positions 7, 8, 19, and 21 (*Figure 7.6*) were found. These mutants showed  $\beta$ -sheet structures already after four hours detected by CD spectroscopy. The double glycine variant (**VW18\_L8G;L19G**) underwent structural transition considerably faster in comparison to **VW18** and all other single glycine mutants, indicating that the  $\beta$ -sheet formation is facilitated due to the incorporation of highly flexible glycine at both potential bend positions. The remaining variants harboring glycine in positions 6, 9, 10, 18, and 22 showed no or a considerably slower transition into  $\beta$ -sheet structure compared to **VW18**. As assumed, for the glycine substitution in position 14 no structural conversion leading to amyloid formation was observed. Interestingly, the mutant containing Gly at position 20 showed a somewhat slower conversion rate compared to **VW18** (*Figure 7.6 B*). This effect was attributed to the removal of the negatively charged side chain (glutamic acid in the wild type sequence) upon glycine substitution. The glutamate in position 20 might be involved in crucial electrostatic interactions between the protofilaments. Interprotofilament interactions are often of an electrostatic or hydrophilic nature.<sup>370,371</sup> Due to the fact that the residues 19 and 21 are found to be involved in bend formation, it is very likely that residue 20 is involved in bend 2 as well.

As assumed, the variants containing proline at either position 2 or 25 did also not adopt a  $\beta$ -sheet structure or assemble into amyloids. CD spectroscopy revealed that both peptides retain their initial  $\alpha$ -helical structure for the entire observation period of one week.

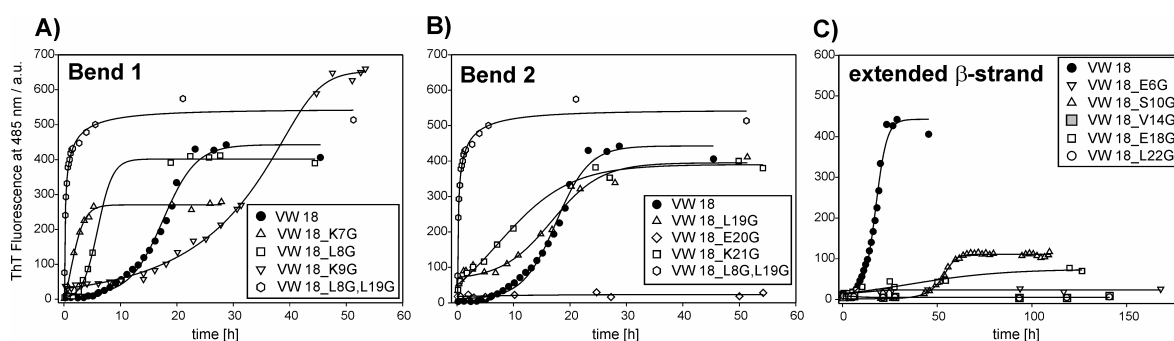


**Figure 7.6:** ThT fluorescence staining assay for glycine containing variants representing the following parts of the fibril architecture: **A)** Bend 1, **B)** Bend 2, and **C)** Extended  $\beta$ -strand (reproduced with permission from Gerling et al. copyright © American Chemical Society).<sup>358</sup>

Based on these findings, and as part of this PhD thesis, a structural model was proposed for **VW18**, representing the molecular arrangement within the protofilaments of the formed amyloid fibrils. The model (*Figure 7.7*) consists of three extended  $\beta$ -strand segments comprising residues 1 – 6, 10 – 18, and 22 – 26, and two bend regions comprising residues 7 - 9 and 19 - 21. In contrast to  $\beta$ -hairpin-like structures, where  $\beta$ -strands are connected via intramolecular main chain H-bonds, in the plane of the turn,<sup>372</sup> amyloid-like fibrils have their bend plane orthogonal to the fibril axis and main chain H-bonds connect the individual  $\beta$ -strands in an intermolecular fashion. Fibril growth can best be described as the stacking of centrally unfolded paperclips, one upon another. The interactions between the  $\beta$ -segments within the particular peptide strands are ensured by packing of the hydrophobic side chains.

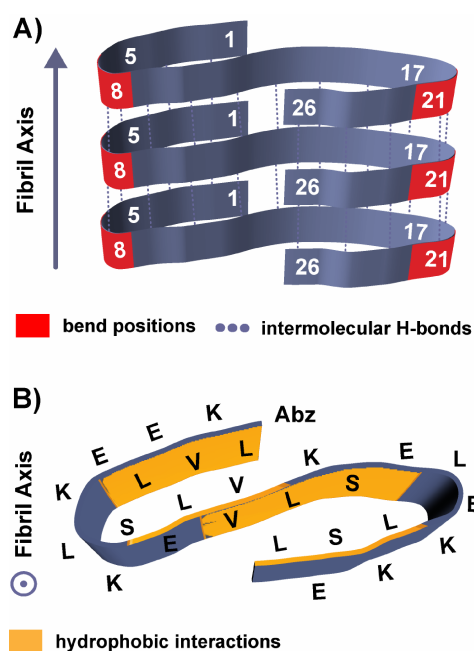


**Figure 7.7:** Proposed internal architecture of one protofilament in the amyloid fibril of **VW18**. **A)** Cartoon of a fibril composed of three stacked protofilament units; extended  $\beta$ -segments are displayed in blue, bend regions are highlighted in red. Vertical fibril growth is indicated by intermolecular H-bonds between the  $\beta$ -sheets (•••). **B)** View along the fibril axis showing the intramolecular hydrophobic interactions of the particular core residues (yellow) (reproduced with permission from Gerling et al. copyright © American Chemical Society).<sup>358</sup>

Due to the steric demand of the bulky hydrophobic side chains that are pointing towards the interior of the fibril, the bend regions must contain at least two or more residues. This is in good agreement with the present results. The proposed structural model implies that the charged residues point to the exterior of the fibril and interact with the aqueous environment, whereas the hydrophobic and uncharged residues are packed in the interior of the fibril. The segments proximal to the C- and N-terminus likely contribute to the hydrophobic core packing based on the results of the proline substitution experiments.

The results of the double glycine variant gained in the context of this thesis enabled the development of a solid structural model for the fibril architecture of **VW18**, which served as basis for investigating the impact of sequence modification on amyloid formation.

### 7.3 The impact of proline ring puckering on turn conformations

#### 7.3.1 *The different turn motifs of $\beta$ -hairpins and amyloids*

In the course of fibril architecture elucidation of **VW18** by systematic glycine and proline replacements, certain interesting phenomena were observed. The substitution of glutamic acid in position 20 by glycine results in a peptide variant that shows a slower structural conversion toward amyloids compared to **VW18** and the other glycine variants. According to the proposed structural model, position 20 is part of bend 2. Thus, the non-aggregating nature of this variant was attributed to the removal of the negatively charged glutamic acid side chain. Residue 20 might be involved in crucial electrostatic interactions between protofilaments, which are often electrostatic or hydrophilic in nature.<sup>370</sup> Alternatively, salt bridges located within a bend are not uncommon for amyloid structures. Substitutions of charged bend residues in aggregating peptides can have dramatic effects, as shown for  $A\beta_{42}$ ,<sup>371</sup> where a toxic conformer was formed as a consequence of glutamic acid replacement by lysine at bend position 22. However, to confirm this interpretation in the present case, additional studies were necessary.

Another interesting finding during this scanning approach was that the incorporation of proline at position 7 of **VW18**, having been identified as a bend region by glycine substitution, prevented aggregation into amyloid structures. This proline variant **VW18\_K7P** retained a disordered structure for more than ten days. Considering the fact that proline is mainly found in the type II  $\beta$ -turns of  $\beta$ -hairpin structures this finding is not completely surprising.<sup>361,373</sup> Amyloid forming peptides do not have the same structural features as  $\beta$ -hairpin structures (*Figure 7.8*). Their turn structure is better described by the  $\beta$ -bend<sup>374</sup> or the  $\beta$ -arch motif.<sup>375</sup>  $\beta$ -turns are stabilized by intramolecular main chain H-bonds between residues that are part of the formed turn. The connection via main chain H-bonding induces a sharp bend. The side chains of the contributing amino acids are oriented perpendicular to the plane of the turn. In contrast to that, the plane of H-bonds in amyloid structures is perpendicular to the plane of the turn (*Figure 7.8*). Here, the peptide chain folds back on itself as well, but the flanking extended  $\beta$ -strand segments interact via their side chains rather than main chain H-bonds. The resulting broader loop regions in amyloid-like structures are therefore more appropriately termed bends or arches.<sup>374,375</sup> For instance, within amyloid fibrils the hydrophobic side chains are coplanar with the bend,



resulting in a much broader turn motif compared to the tight kink in the backbone of  $\beta$ -hairpins. This explains why bends usually contain more than two residues, and why the rigid proline incorporated into **VW18** disrupted this conformation.

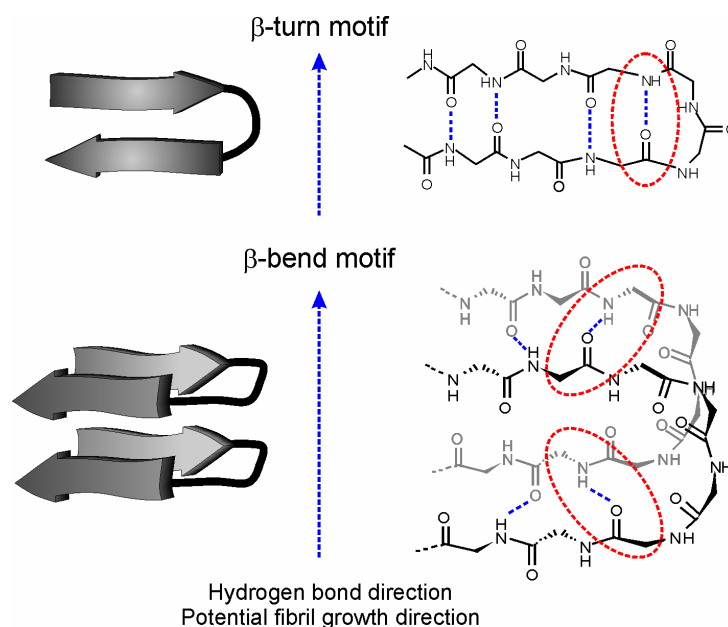


**Figure 7.8:** Comparison of the  $\beta$ -turn motif, found in hairpins with the  $\beta$ -bend motif occurring in amyloid fibrils. On the top:  $\beta$ -turn motif: The hydrogen bonds connect the  $\beta$ -strands of the same  $\beta$ -sheet. At the bottom:  $\beta$ -bend motif: The hydrogen bonds occur parallel to the fibril axis and connect the  $\beta$ -strands of different stacked  $\beta$ -sheets (redrawn from Zanuy et al. copyright © Elsevier).<sup>374</sup>

Although earlier proline scans of amyloid structures helped to identify bend regions,<sup>359,364,365</sup> this strategy was not successful for elucidating the fibril architecture of **VW18**. Furthermore, previously synthesized variants of **VW18** in which the glutamic acid residues at positions 6, 11, and 18 were replaced by proline were unable to adopt any ordered secondary structure. During the entire observation period of 10 days, these variants remained in a random coil conformation.<sup>356,357</sup> The hypothesis that any proline mutant of **VW18** would exist in an disordered state was disproven by the variants containing Pro proximal to the N- and C-termini.<sup>358</sup> Although these peptides do not form amyloids, they adopt the initial coiled coil structure. Thus, the behavior of the proline variants in which glutamic acid residues were replaced could be explained in two ways. Either the side chains of these residues are involved in interactions that are crucial for amyloid formation, or the relatively short sequence of **VW18**, with only 26 amino acids, is too sensitive for the incorporation of the structure disrupting proline residue.

With the aim of clarifying whether the removal of the side chain upon proline substitution causes the inability of the proline mutants to form amyloids, two proline chimera were synthesized in the group of Prof. Kokschi that contain a glutamic acid side chain, in *cis*- or *trans*-conformation, in the pyrrolidine ring (Figure 7.9).<sup>376</sup>

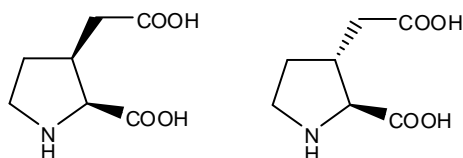


**Figure 7.9:** Chemical structure of *cis*- and *trans*-proline-glutamic acid chimeras.

These chimeras provide the turn inducing conformation of proline and, in addition bear the potential for electrostatic interactions due to the negatively charged side chain. However, since amyloid formation is a complex process that is influenced by several factors, the effects of the novel proline-glutamic acid chimeras were first tested on a simplified model. With regard to the fact that none of the investigated proline containing **VW18** variants ever showed amyloid formation, the idea was to find a system that contains proline at a turn position in the sequence to study the effect of the modified side chain. Since proline is mainly found in the tight turns of  $\beta$ -hairpins, the model for this investigation was a short  $\beta$ -hairpin, previously described by de Alba *et al.*<sup>377</sup> The design of this model and the results of this study are presented in the following sections.

### 7.3.2 The effect of a glutamate side chain on proline's ring conformation

The turn region of  $\beta$ -hairpins and thus the conformation of the adopted  $\beta$ -hairpin is strongly affected by the ring conformation of proline (see section 2.4).<sup>73</sup> Hydrogen bonding pattern between the interacting  $\beta$ -strands dictate the type of  $\beta$ -hairpin adopted. According to the type of the adopted turn the nomenclature of  $\beta$ -hairpins was introduced by Sibanda *et al.*<sup>378</sup> The turn type is defined by the H-bond pattern of the turn contributing residues which includes the number of H-bonds that connect these residues and defines which residue of the turn sequence forms an H-bond with the opposing  $\beta$ -strand (Figure 7.10).

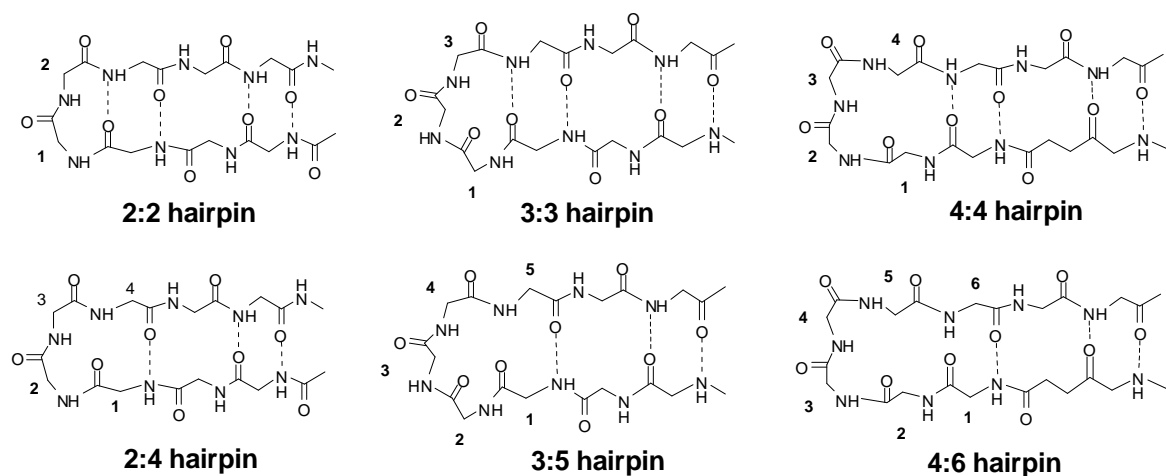


**Figure 7.10:** A selection of  $\beta$ -hairpin types differing in the number and pattern of hydrogen bonds that connect the turn contributing residues.

Introducing electron withdrawing substituents such as fluorine, hydroxyl, or acetyl residues on the pyrrolidine ring of proline strongly affects the ring puckering.<sup>71,74,77,379,380</sup> The effect that an electronegative glutamate side chain exerts on the ring conformation of proline and how this in turn affects the turn conformation of a short  $\beta$ -hairpin was to be tested in the present investigation. Basis for this study was a 10 residue long  $\beta$ -hairpin forming peptide IYSNPDGTWT (**P1\_P**) that contains a proline residue as one of four turn-contributing residues Asn-Pro-Asp-Gly (NPDG). The peptide was first described by de Alba *et al.*<sup>377</sup> who studied different variants of this  $\beta$ -hairpin with altered turn conformations resulting in several coexisting  $\beta$ -hairpin types with different H-bond patterns (*Figure 7.11*).<sup>381</sup> It is water soluble, non-aggregating in nature, and forms an equilibrium of two hairpin types in aqueous solution with a 3:5  $\beta$ -hairpin (type I  $\beta$ -turn) predominating over a 4:4  $\beta$ -hairpin conformation (G1  $\beta$ -bulge).

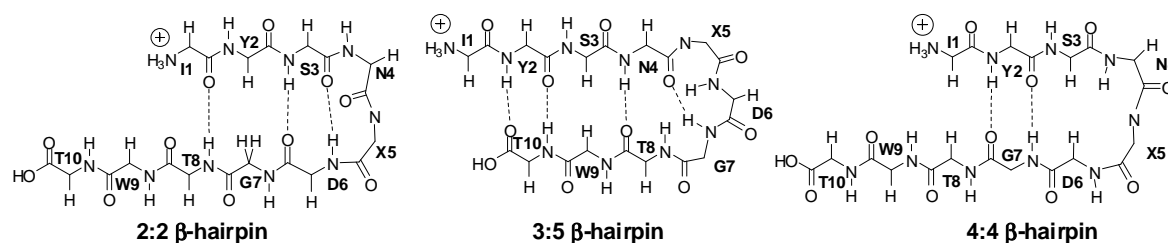


**Figure 7.11:** Types of  $\beta$ -hairpins that **P1\_P** can adopt. X5 is the position that was replaced in the study of de Alba *et al.* to study the effect of an altered turn motif on the  $\beta$ -hairpin conformation (based on de Alba *et al.*)<sup>381</sup>

Two proline chimeras, carrying a glutamic acid side chain in a *cis*- or *trans*-configuration on C3 of the pyrrolidine ring (*Figure 7.9*), were previously synthesized in our group.<sup>376</sup> Starting from *trans*-4-hydroxy proline, a straightforward synthesis yielded enantiomerically pure Fmoc protected 3-substituted *cis*- and *trans*-proline-glutamic acid chimeras, which were suitable for incorporation into peptide sequences via solid phase peptide synthesis (SPPS). Pro 5 of the model peptide **P1\_P** is part of the turn moiety and was replaced by either of the two diastereomers of the proline chimeras to result in the peptides **P1\_P**<sup>*cis*-E</sup> and **P1\_P**<sup>*trans*-E</sup>. The consequences of this modification were studied with 1D- and 2D-NMR analysis, CD spectroscopy, and a combined size exclusion chromatography / static light scattering analysis to elucidate the impact of the proline chimera's side chain on the turn region of the  $\beta$ -hairpin.<sup>382</sup>

*The results presented in chapter 7.3 have been published in:* J. Maity, U. I. M. Gerling, S. Vukelić, A. Schäfer, B. Kokschi, *Amino Acids* **2014**, *46*, 177-186.

The final publication is available at link.springer.com: <http://dx.doi.org/10.1007/s00726-013-1610-1>

### 7.3.2.1 <sup>1</sup>H-NMR analysis of the $\beta$ -hairpins

In collaboration with Dr. J. Maity and Dr. A. Schäfer, the <sup>1</sup>H-NMR spectra of the three peptides in aqueous solution were assigned using the standard sequential assignment procedure via total correlation spectroscopy (TOCSY).<sup>383,384</sup> Nuclear Overhauser effect spectroscopy (NOESY) and rotating frame nuclear Overhauser spectroscopy (ROESY) were used to gain information about the proximity of the protons. The peak arising from C<sub>δ</sub>H<sub>3</sub> (Ile) of the unmodified model peptide **P1\_P** was used as reference in the <sup>1</sup>H-NMR spectra for both peptides containing the proline chimera. The chemical shifts of the proton resonances for the peptides (**P1\_P**<sup>cis-E</sup> and **P1\_P**<sup>trans-E</sup>) in aqueous solution at 5 °C and pH 4.3 are listed in *Table 7.2* and *Table 7.3* respectively.

**Table 7.2:** Chemical shift assignments of peptide (*P1\_P*<sup>cis-E</sup>)

residue	NH	H <sub>α</sub>	H <sub>β</sub>	Other
Ile 1		3.8	1.91	C <sub>γ</sub> H 1.42, 1.14; C <sub>γ</sub> H <sub>3</sub> 0.93; C <sub>δ</sub> H <sub>3</sub> 0.86
Tyr 2	8.5	4.65	2.89, 2.78	C <sub>δ</sub> H 7.07; C <sub>ε</sub> H 6.78
Ser 3	8.18	4.26	3.62, 3.62	
Asn 4	8.44	4.72	2.81, 2.57	N <sub>δ</sub> H <sub>2</sub> 7.62, 7.00
Pro <sup>cis-E</sup>		4.44	2.79	C <sub>γ</sub> H 2.15, 1.72; C <sub>γ</sub> H 2.44, 2.37; C <sub>δ</sub> H 3.87, 3.66
Asp 6	8.78	4.59	2.98, 2.91	
Gly 7	7.98	3.85, 3.81		
Thr 8	7.96	4.28	4.11	C <sub>γ</sub> H <sub>3</sub> 1.08
Trp 9	8.35	4.78	3.30, 3.20	N <sub>ε1</sub> H 10.09; C <sub>δ1</sub> H 7.19; C <sub>ε3</sub> H 7.57; C <sub>ζ3</sub> H 7.09; C <sub>η2</sub> H 7.17; C <sub>ζ2</sub> H 7.44
Thr 10	7.99	4.24	4.2	C <sub>γ</sub> H <sub>3</sub> 1.06

**Table 7.3:** Chemical shift assignments of peptide (*P1\_P*<sup>trans-E</sup>)

residue	NH	H <sub>α</sub>	H <sub>β</sub>	Other
Ile 1		3.82	1.93	C <sub>γ</sub> H 1.43, 1.14; C <sub>γ</sub> H <sub>3</sub> 0.94; C <sub>δ</sub> H <sub>3</sub> 0.86
Tyr 2	8.52	4.63	2.89, 2.89	C <sub>δ</sub> H 7.07; C <sub>ε</sub> H 6.78
Ser 3	8.16	4.3	3.57, 3.57	
Asn 4	8.49	4.79	2.79, 2.64	N <sub>δ</sub> H <sub>2</sub> 7.64, 7.02
Pro <sup>trans-E</sup>		4.03	2.62	C <sub>γ</sub> H 2.23, 1.78; C <sub>γ</sub> H 2.60, 2.48; C <sub>δ</sub> H 3.96, 3.73
Asp 6	8.76	4.61	2.98, 2.92	
Gly 7	8.21	3.93, 3.88		
Thr 8	7.97	4.31	4.14	C <sub>γ</sub> H <sub>3</sub> 1.10
Trp 9	8.4	4.77	3.31, 3.20	N <sub>ε1</sub> H 10.11; C <sub>δ1</sub> H 7.21; C <sub>ε3</sub> H 7.55; C <sub>ζ3</sub> H 7.09; C <sub>η2</sub> H 7.19; C <sub>ζ2</sub> H 7.44
Thr 10	8.06	4.29	4.22	C <sub>γ</sub> H <sub>3</sub> 1.08

The chemical shift of the C<sub>α</sub> proton (H<sub>α</sub>) can be used to designate the secondary structure of peptides.<sup>384,385</sup> The particular amino acid experiences an α-<sup>1</sup>H upfield shift relative to the

random coil value when placed in a helical configuration, while the  $\alpha$ - $^1\text{H}$  chemical shift is found to move downfield when the residue is placed in a  $\beta$ -strand or extended configuration. Thus, the deviation of the chemical shift ( $(\Delta\delta\text{H}_\alpha) = \delta\text{H}_\alpha$  (observed) –  $\delta\text{H}_\alpha$  (random coil)) of  $\text{H}_\alpha$  of a certain amino acid from the random coil values is negative in turn or helical regions and positive in  $\beta$ -strand regions. This procedure was accomplished for all residues of  $\text{P1\_P}^{\text{cis-E}}$  and  $\text{P1\_P}^{\text{trans-E}}$ . In general all residues of both peptides show similar trends for  $\Delta\delta\text{H}_\alpha$  (Figure 7.12); however, variation with regard to the proline chimera moieties were found. The conformational shift  $\text{H}_\alpha$  was positive in case of  $\text{P}^{\text{cis-E}}$ , while for  $\text{P}^{\text{trans-E}}$  this value was negative. As the negative  $\Delta\delta\text{H}_\alpha$  values are more suitable with residues at a turn position of a  $\beta$ -hairpin, the  $\text{P}^{\text{trans-E}}$  moiety fits more appropriately into the  $\beta$ -turn position in contrast to the  $\text{P}^{\text{cis-E}}$  moiety.

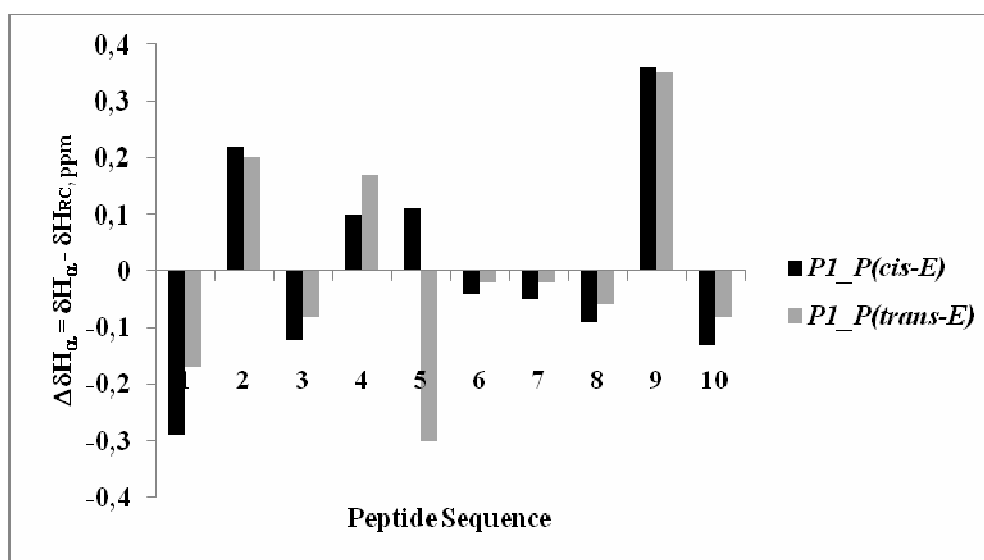
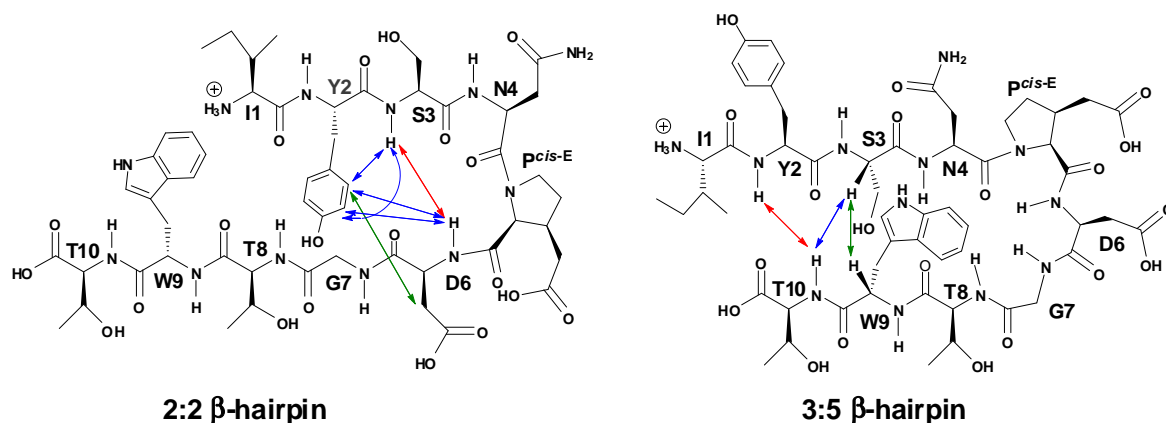


**Figure 7.12:** Histograms of the conformational shift values of the  $\text{H}_\alpha$  ( $\Delta\delta\text{H}_\alpha$ ) relative to random coil values in the peptides  $\text{P1\_P}^{\text{cis-E}}$  and  $\text{P1\_P}^{\text{trans-E}}$  at pH 4.3 and 5 °C in aqueous solution.

NOE spectra were recorded to gain information about the proximity of non-adjacent residues. For  $\text{P}^{\text{cis-E}}$  long range NOEs originating from the backbone protons,  $\text{NH}(\text{Y2})\text{-NH}(\text{T10})$ ,  $\text{H}_\alpha(\text{S3})\text{-NH}(\text{T10})$  and  $\text{H}_\alpha(\text{S3})\text{-H}_\alpha(\text{W9})$  were found, indicating the presence of a 3:5  $\beta$ -hairpin (

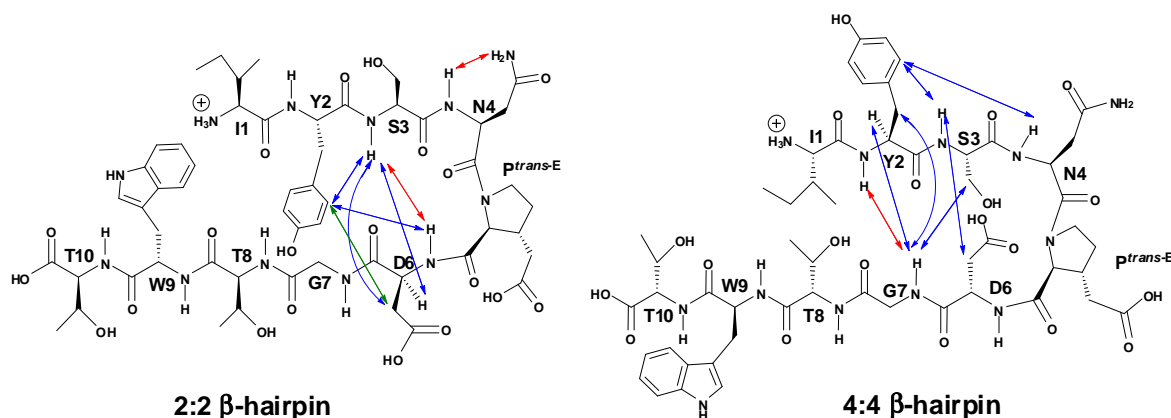
Figure 7.13 A). These cross peaks strongly suggest that the segment Y2-S3 of one  $\beta$ -strand faces toward the segment W9-T10 of the opposing  $\beta$ -strand. In addition to these backbone NOEs, strong NH-NH interaction of S3 and D6 were observed, which points to the formation of a 2:2  $\beta$ -hairpin (

Figure 7.13 B). However, the expected  $\text{H}_\alpha(\text{Y2})\text{-H}_\alpha(\text{G7})$  interaction was not observed. The data reveal that  $\text{P}^{\text{cis-E}}$  adopts two different types of  $\beta$ -hairpin (3:5 and 2:2) in aqueous solution, which are in equilibrium with each other.



**Figure 7.13:** Cross strand NOEs observed for  $P^{cis-E}$  at 5 °C in aqueous solutions at pH 4.3. NH-NH interactions are highlighted in red; HN-CH interactions are indicated by blue arrows and CH-CH proximities are given in green.

$P1\_P^{trans-E}$  showed long range NOEs between the NH's of S3 and D6 indicating the formation of a 2:2  $\beta$ -hairpin. Additionally, NH-NH NOEs of Y2 and G7 as well as  $H_{\alpha}(Y2)$ -NH(G7) interaction imply the presence of another species, the 4:4  $\beta$ -hairpin (Figure 7.14). However, the type of 4:4  $\beta$ -hairpin found for  $P1\_P^{trans-E}$  is not exactly the same that the reference peptide  $P1\_P$  forms (Figure 7.11). In case of  $P1\_P$  the distal residues are S3 and T8 and N4, P5, D6, and G7 form the turn region. In contrast, in  $P1\_P^{trans-E}$  the distal strand residues are Y2 and G7 and the four turn participating residues are S3, N4,  $P^{trans-E}$ , and D6.



**Figure 7.14:** Cross strand NOEs observed for  $P^{trans-E}$  at 5 °C in aqueous solutions at pH 4.3. NH-NH interactions are highlighted in red; HN-CH interactions are indicated by blue arrows and CH-CH proximities are given in green.

Vicinal coupling constant values ( $^3J_{NH\alpha H}$ ) have been considered as a means of verification for the  $\beta$ -sheet formation of peptides, where values greater than 6 Hz are characteristic for the  $\beta$ -strand structure. These values have been calculated for the  $P1\_P$  variants and are summarized in Table 7.4. Almost all of the residues have values larger than 6 Hz, indicating their existence in  $\beta$ -strand structures. The residues Asn, Asp, and Gly show

smaller values because they participate in the turn formation. For residues near the C and N-terminus of the peptide larger  $^3J_{\text{NHC}\alpha\text{H}}$  values were found as these residues adopt the extended  $\beta$ -strand structures.

**Table 7.4:**  $^3J_{\text{NHC}\alpha\text{H}}$  values for  $P1\_P^{\text{cis-E}}$  and  $P1\_P^{\text{trans-E}}$

Residue	$P1\_P^{\text{cis-E}}$	$P1\_P^{\text{trans-E}}$
	$^3J_{\text{NHC}\alpha\text{H}}$ (Hz)	$^3J_{\text{NHC}\alpha\text{H}}$ (Hz)
Tyr 2	7.8	7.3
Ser 3	7.8	7.8
Asn 4	6.9	6.4
Asp 6	6.4	6.4
Gly 7	4.3	5.6
Thr 8	7.8	8.2
Trp 9	7.3	7.4
Thr 10	8.6	8.6

NMR analysis of the modified peptides revealed that the substitution of Pro with  $P^{\text{cis-E}}$  results in an equilibrium of 2:2  $\beta$ -hairpins with 3:5  $\beta$ -hairpins, while the incorporation of  $P^{\text{trans-E}}$  leads to the formation of 2:2  $\beta$ -hairpins and 4:4  $\beta$ -hairpins. The reference peptide has been described to exist in an equilibrium of 3:5 and 4:4  $\beta$ -hairpins.<sup>377</sup> The stereochemistry of the glutamic acid side chain at C3 of the proline chimera as the only distinguishing factor between the peptides  $P1\_P^{\text{cis-E}}$  and  $P1\_P^{\text{trans-E}}$  was thus found to have a crucial impact on the ring conformation, which in turn affects the type of  $\beta$ -hairpin being adopted (*Figure 7.15*).

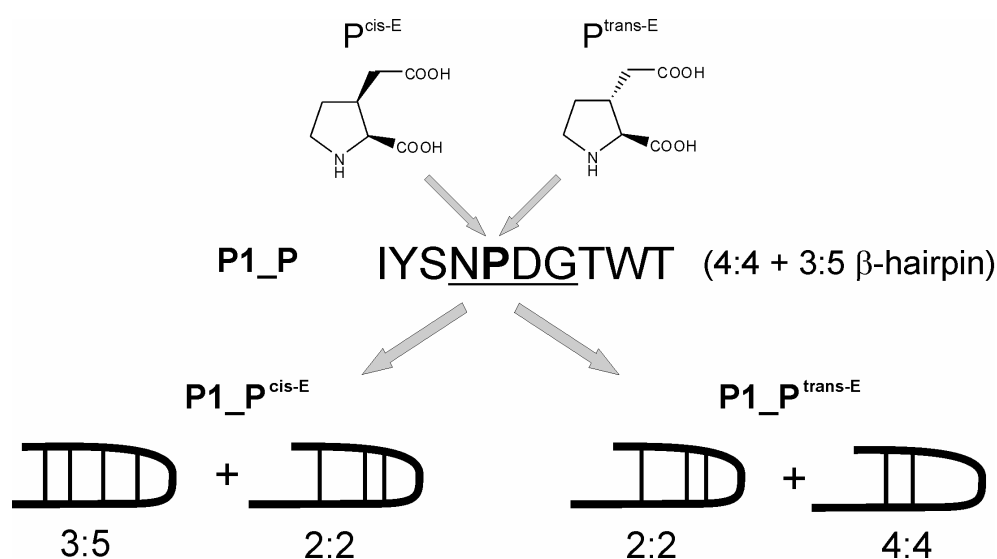


**Figure 7.15:** Schematic illustration of the altered  $\beta$ -hairpin conformations that results from incorporation of the two proline chimeras into the turn motif of  $P1\_P$ .

### 7.3.2.2 Conformational studies with CD spectroscopy

In addition to the NMR analysis, the conformations of the peptides were investigated by CD spectroscopy. Due to the short sequences of only 10 residues, no characteristic  $\beta$ -sheet spectra with a minimum around 216 nm were obtained (compare Figure 6.3, section 6.1). However, some specific secondary structure signatures were observed. For all types of  $\beta$ -hairpins found with NMR analysis, no more than three residues per strand are involved in stretched  $\beta$ -strands; thus, the obtained spectra of all three peptides resemble more a random coil-like structure (Figure 7.16 A). Nevertheless, a small minimum around 216 nm was observed, which increases with peptide concentration. Also, the characteristic random coil minimum at 198 nm is slightly shifted towards 201 nm for 300  $\mu$ M and 500  $\mu$ M samples, indicating a higher amount of ordered structures with increasing peptide concentration. The maximum between 220 and 230 nm indicates that the aromatic residues (Trp, Tyr) are part of ordered structures (Figure 7.16 B).<sup>386,387</sup> A systematic decrease in this maximum was observed at elevated temperatures, supporting this assumption. The obtained results, which are in good agreement with previously published CD spectra,<sup>377,386</sup> show that all three peptides adopt similar structures in aqueous solution. Indications for a  $\beta$ -hairpin conformation were found in the CD spectra, but a distinction between the different  $\beta$ -hairpin types that were found with NMR cannot be made with CD spectroscopy alone.

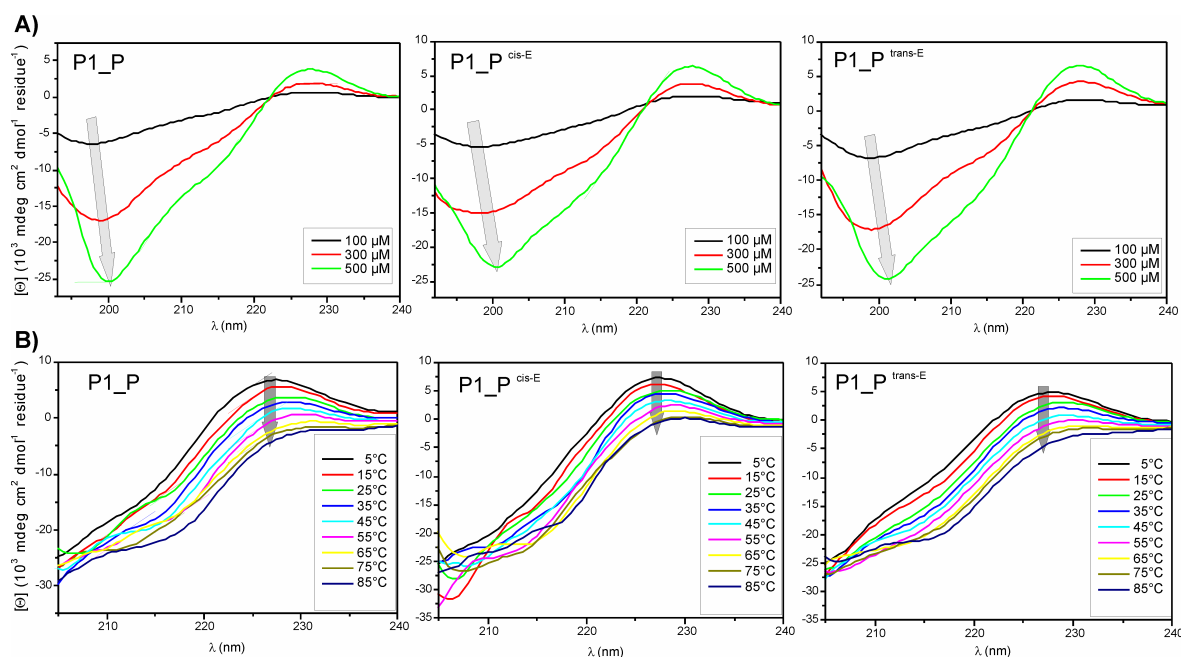


**Figure 7.16:** CD spectra of the **P1\_P** variants in aqueous solution at pH 4.3. **A)** Spectra of three different sample concentrations at 5 °C. **B)** Spectra of 300  $\mu$ M samples at increasing temperatures. The grey arrows indicate the shifts of the characteristic minima and maxima.



### 7.3.2.3 Determination of oligomerization state

To exclude higher oligomers or aggregates of peptides the oligomerization state of the **P1\_P** variants has been investigated by size exclusion (SEC) experiments coupled with static light scattering (SLS) analysis. The obtained results show that all peptides were found to be monomeric in solution, which is in good agreement with the NMR and CD results. Single species were found for all three peptides in the SEC experiments, and the corresponding molecular weights determined with SLS are comparable to the theoretical monomer masses (Table 7.5, Figure 7.17). The  $M_W$  values and SEC spectra, reported as the mean of three individual measurements, confirm that the observed  $\beta$ -hairpins consist of single peptide strands, and that the interaction found in the NMR measurements are indeed of intramolecular nature rather than occurring between two individual molecules.

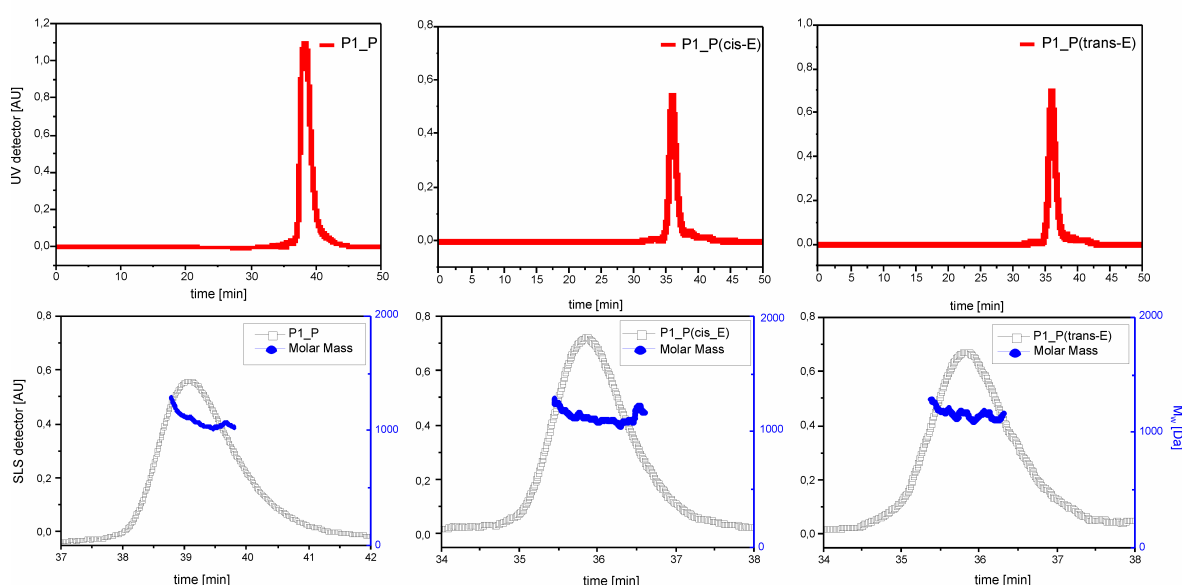


**Figure 7.17:** SEC/SLS chromatograms of **P1\_P** variants. Single peaks were detected with UV at 280 nm (red). Corresponding Rayleigh ratio (black) and molar mass distribution (blue) indicate monomeric species for all peptides.

**Table 7.5:** Theoretical and experimental determined molecular weights of the peptide variants.

Peptide	Theoretical monomer mass [Da]	SEC/SLS determined mass [Da]
<i>P1_P</i>	1153	1104 ± 145 Da
<i>P1_P</i> <sup>cis-E</sup>	1211	1188 ± 195 Da
<i>P1_P</i> <sup>trans-E</sup>	1211	1166 ± 130 Da

The results of this study clearly show the importance of the proline ring puckering on the conformation of the turn motif in  $\beta$ -hairpins. Even small alterations in this sensitive region

can have large consequences on the whole peptide conformation as the turn type dictates the type of  $\beta$ -hairpin that is formed. The puckering of the rigid pyrrolidine ring is very sensitive to modifications. Electronegative residues can shift the equilibrium of C<sup>Y</sup>-exo versus C<sup>Y</sup>-endo towards one preferred conformation. Thus, the proline chimeras that differ only at one single chiral center, can alter the  $\beta$ -hairpin structures of the corresponding peptides. This study has shown that even slight variations in side chain conformation can significantly influence the entire conformation of a peptide.

Based on the results of this study, the proline-glutamic acid chimeras should be incorporated into the sequence of **VW18** in order to explore the influence of charged residues at the bend positions of **VW18** on amyloid formation (future directions). Due to time constraints, these investigations were not accomplished in the context of this thesis.

#### **7.4 The role of oligomeric intermediates in the amyloid formation process of VW18**

Although the process of amyloid formation has been extensively studied over the years, the mechanism is still not fully understood. Numerous experimental<sup>136,388-391</sup> and theoretical<sup>392-396</sup> approaches have been developed to probe the structural and kinetic aspects of amyloid formation. By these means, the small precursor and intermediate species that occur at a very early stage of amyloid formation, rather than the mature fibrils, were found to be the neurotoxic species.<sup>397-399</sup> However, it has turned out that it is very challenging to characterize the early stages of this reaction, in particular the primary nucleation events and the formation of low relative molecular weight oligomers that often act as seeds or templates for fibril growth, and thus induce the actual cascade process.

Amyloid formation in general is understood to proceed via a nucleated growth mechanism. This is an activated process displaying certain characteristic properties: 1) a lag time before aggregates can be detected and 2) a maximum growth rate after nucleation is triggered.<sup>400-402</sup> Nucleation, which is generally found to be the rate-limiting step,<sup>402</sup> requires the system to overcome an energy barrier associated with the formation of the nucleus. Thus, nucleated growth is often characterized by a lag phase preceded by rapid fibril growth.<sup>403-406</sup> The multi-stage amyloid formation process includes a number of consecutive or parallel processes by which the soluble monomer is converted to large aggregates. This includes, for instance, partial unfolding or refolding, oligomerization, conformational conversion, elongation, condensation, and fragmentation.<sup>407,408</sup> A number of models describing aggregation have been proposed,<sup>408-414</sup> which result from the variety of kinetic behaviors depending on the protein and the experimental condition studied.

However, the formation of oligomeric intermediate species, which are normally soluble and sometimes structurally unstable or metastable, is a key step in the nucleation process.<sup>136,405,415-417</sup> Nucleation is mostly completed by the structural conversion of these small intermediate species into small prefibrillar structures that act as templates triggering the rapid fibril growth. Also, native or native-like structures can form the nucleus that consists of oligomeric aggregates, and the conversion to amyloids subsequently takes place within the aggregates.<sup>418,419</sup>

A wide range of experimental strategies is currently being developed in order to detect the actual nucleus size.<sup>409-412</sup> This usually requires a combination of several techniques that are processed in parallel, such as the combination of Thioflavin T fluorescence staining to monitor  $\beta$ -sheet fibril formation and dynamic light scattering to detect non-fibrillar intermediates.<sup>411</sup> Also, size exclusion, NMR-methods, or electrospray differential mobility analysis were used in concert, and several models describing the nucleation process of different proteins have been proposed.<sup>409,410,412</sup> Other approaches to develop a mechanistic model for the amyloid formation process uses theoretical approaches such as simulations, molecular dynamics, or model based calculations.<sup>413,414,420</sup>

The nucleus size can also be calculated from experimental data by applying the theory of nucleated growth polymerization.<sup>413,421-423</sup> Such an approach requires monitoring of the aggregation process at many different concentrations, as well as the determination of the critical concentration, which is the concentration of unpolymerized monomer that remains in solution after amyloid formation has reached the end point characterized by a typical plateau in a ThT-staining experiment. This strategy was used to define the size of the critical monomer for the here utilized model peptide **VW18**. Knowing the nucleus size enables conclusions to be drawn regarding the mechanism of structural conversion and amyloid formation of **VW18**, and gives information about potential intermediate species.

According to nucleated growth polymerization theory, the nucleus is the state in which the free energy (along the reaction coordinate) is maximized. The nucleus size,  $n_*$ , is the number of polymerizing units (peptides in our case) that form the nucleus. If the initial concentration of non-aggregated peptides in an aggregation kinetics experiment is  $c$ , then the rate at which the concentration of aggregated peptides,  $c_a$  initially grows, is:

$$\frac{dc_a}{dt} = k_+ c_n c \quad (7.1)$$

Where  $k_+$  is the second order rate constant for growth; the concentration of nuclei,  $c_n$ , grows at the following rate:

$$\frac{dc_n}{dt} = k_* c^{n_*} \quad (7.2)$$

Here  $k_*$  is the  $n_*^{\text{th}}$ -order rate constant for nucleation. Integrating Eq. 7.2 and inserting the result into Eq. 7.1 gives:

$$c_a = \frac{1}{2} k_+ k_* c^{n_*+1} t^2, \quad (7.3)$$

which allows the nucleus size to be determined in three steps:

First,  $c_a(t)$  is measured at various initial concentrations  $c$ . Second, for each  $c$ , the prefactor  $p(c) = \frac{1}{2} k_+ k_* c^{n_*+1}$  (in the initial stages of aggregation, that is, at the limit  $t \rightarrow 0$ ) is determined.

Finally,  $n_*$  is determined by finding the value that best matches these values of  $p(c)$ .

The ThT-binding has been used to assess the concentration of the aggregated peptides and it was assumed that the ThT-signal is linearly dependent on  $c_a$ .

The amyloid formation rates of **VW18** were monitored at various sample concentrations (Figure 7.18)

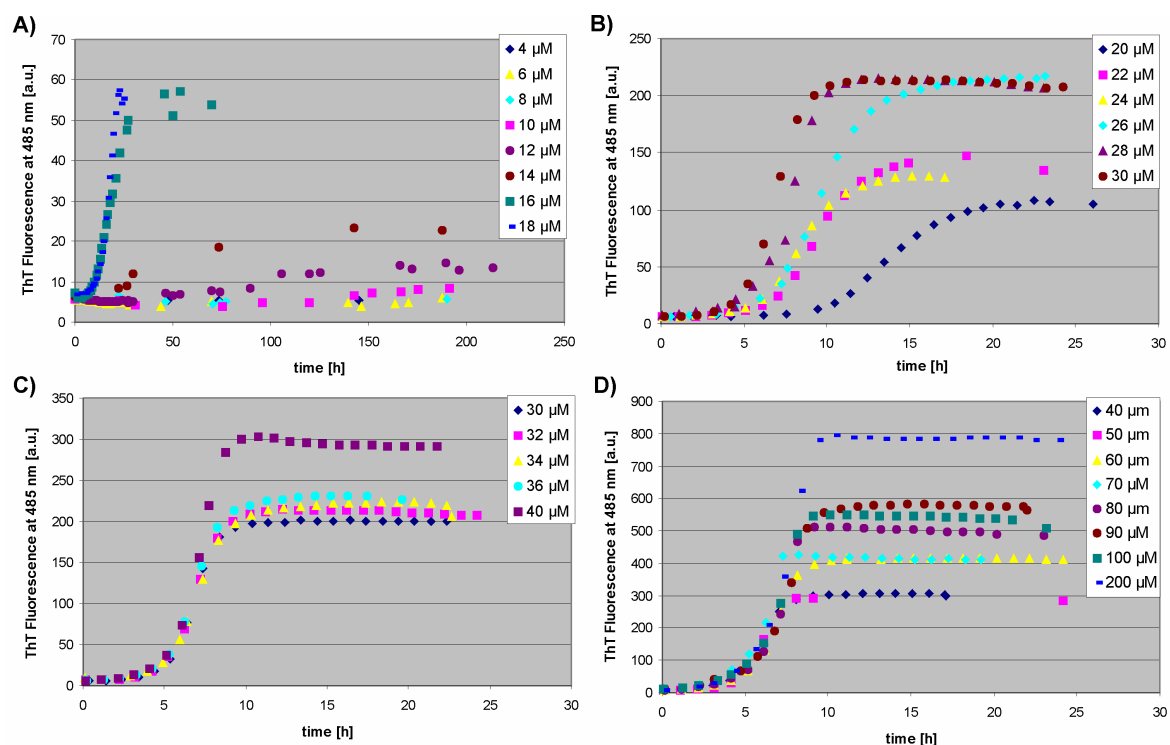


**Figure 7.18:** Measured ThT-intensity at 485 nm as a function of time for **VW18** at different initial sample concentrations.

At sample concentrations smaller than 12  $\mu\text{M}$ , no amyloid formation was observed for **VW18** for an incubation period of ten days (Figure 7.18 A). With increasing sample concentration, amyloid formation proceeded via a typical nucleated growth polymerization mechanism (Figure 7.18 B/C/D) demonstrated by a certain lag phase that is followed by a

rapid fibril growth phase, and a plateau stage indicating the endpoint of amyloid formation. At concentrations lower than 30  $\mu\text{M}$ , the length of the lag phase was found to depend upon the particular sample concentration (*Figure 7.18 B*). The amyloid formation rates of samples between 30  $\mu\text{M}$  and 200  $\mu\text{M}$  showed no differences regarding the length of the lag phase and the overall shape of the ThT curve, indicating a similar amyloid formation process for these samples.

Interestingly, reduced amyloid formation rates were observed for **VW18** samples of 300  $\mu\text{M}$  or higher concentrations (*Figure 7.19*). An explanation for this phenomenon might be the increasing viscosity of the samples. The highly viscous solutions might reduce the mobility of the molecules and thereby reduce the kinetics of amyloid formation. Mobility of the individual molecules contributes to amyloid formation which was proven in several studies that use agitated conditions during fibril formation.<sup>23,406,424-426</sup> Such an effect was also observed for **VW18** and several fluorinated variants and is described in detail in *section 7.5.4.1*

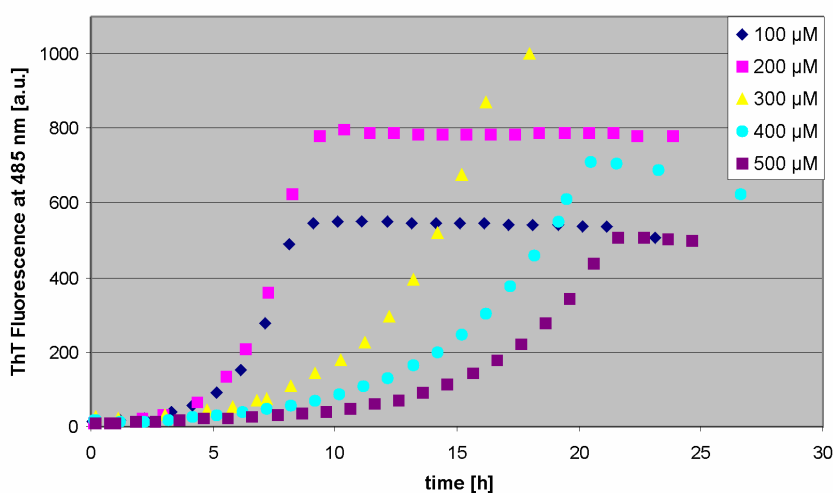


**Figure 7.19:** Measured ThT-intensity at 485 nm as a function of time for **VW18** at initial sample concentrations of 100  $\mu\text{M}$ , 200  $\mu\text{M}$ , 300  $\mu\text{M}$ , 400  $\mu\text{M}$ , and 500  $\mu\text{M}$ .

The critical concentration of non-aggregated monomer that remains in solution after fibril formation is completed was determined using an HPLC-based assay. After the endpoint of amyloid formation was detected with ThT-staining, the samples were incubated for further 24 hours. Afterwards the samples were thoroughly mixed and aliquots of 500  $\mu\text{L}$  were taken from each particular sample at the individual concentrations. The fibrils were quantitatively precipitated by centrifuging the samples at 30000 g (at 25  $^{\circ}\text{C}$ ) for around 18 hours using a microcentrifuge (MIKRO 220R, Hettich). A volume of 50  $\mu\text{L}$  of the supernatant solution was removed and diluted with 50  $\mu\text{L}$  ACN containing 0.1% TFA and analyzed by analytical HPLC using a linear  $\text{CH}_3\text{CN}/\text{H}_2\text{O}$  gradient. The monomer

concentration was calculated according to the corresponding peak area using the linear dependency on a calibration curve that was previously prepared for several non-aggregated **VW18** concentrations (*Figure 7.20*).

The critical concentration ( $c_{crit}$ ) was calculated as the mean of all investigated sample concentrations. The value of  $c_{crit} = 10.36 \mu\text{M}$  ( $\approx 10.4 \mu\text{M}$ ) correlates nicely with the observation that amyloid formation does not occur at sample concentrations below  $12 \mu\text{M}$  (*Figure 7.18 A*).

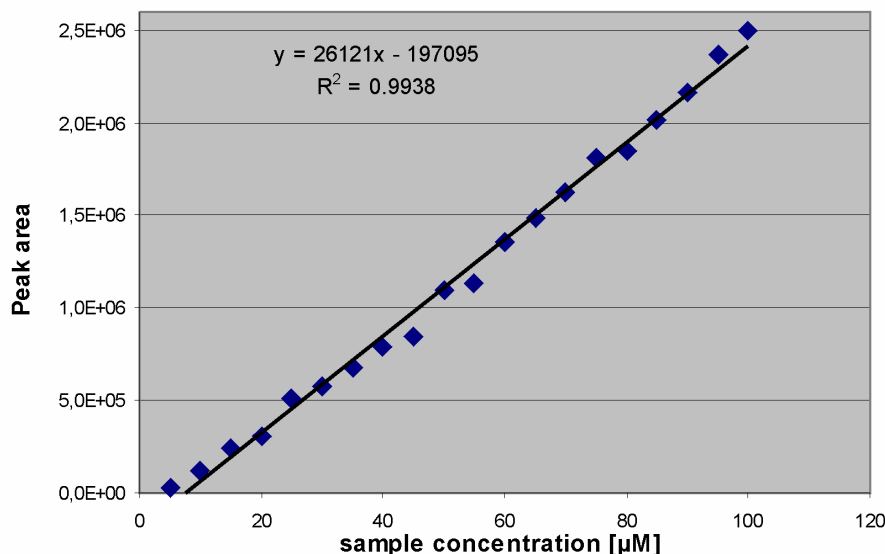


**Figure 7.20:** Calibration curve for determining the concentration of unpolymerized **VW18** monomer after completion of fibril formation.

For each of the sample concentrations ThT-binding was used to assess the time dependence of concentration of aggregated peptides, assuming the ThT-signal is linearly dependent on  $c_a$ . The measured ThT-signal for an initial concentration  $c = 100 \mu\text{M}$  (*Figure 7.21 A*) was used to extract  $c_a(t)$  (*Figure 7.20 B*) using the formula:

$$c_a(t) = \frac{\text{ThT}(t) - \text{ThT}(0)}{\text{ThT}(t \rightarrow \infty) - \text{ThT}(0)} (c - c_{crit}) \quad (7.4)$$

where  $c_{crit}$  is the critical concentration below which no aggregation takes place (measured to be  $c_{crit} = 10.4 \mu\text{M}$  for **VW18**). For a sample concentration of  $c = 100 \mu\text{M}$ ,  $\text{ThT}(0) = 11.57$  and  $\text{ThT}(t \rightarrow \infty) = 542.41$ . *Figure 7.21 C* shows the same data as *Figure 7.21 B*, but plotted as a function of  $t^2$ , and focusing on the aggregation of the first 10% of the total amount that will be aggregated. The linear fit for determining the prefactor  $p(100 \mu\text{M}) = 0.4329$  is also shown.

This procedure has been performed for all ThT curves at the indicated concentrations. Finally,  $\ln(p(c))$  as a function of  $\ln(c)$  for all investigated amyloid formation rates is shown in *Figure 7.21 D*. The solid line is a fit to the values between the dashed vertical lines. High concentrations were excluded because the data were presumably affected by the increase in viscosity of the sample solution. Low concentrations were excluded because  $c_{crit}$  was very likely slightly overestimated, which has a big effect at low concentrations. The slope of the fit is 1.9, which can be translated into a nucleus size of  $n^* = 1.9 - 1 = 0.9 \approx 1$ .

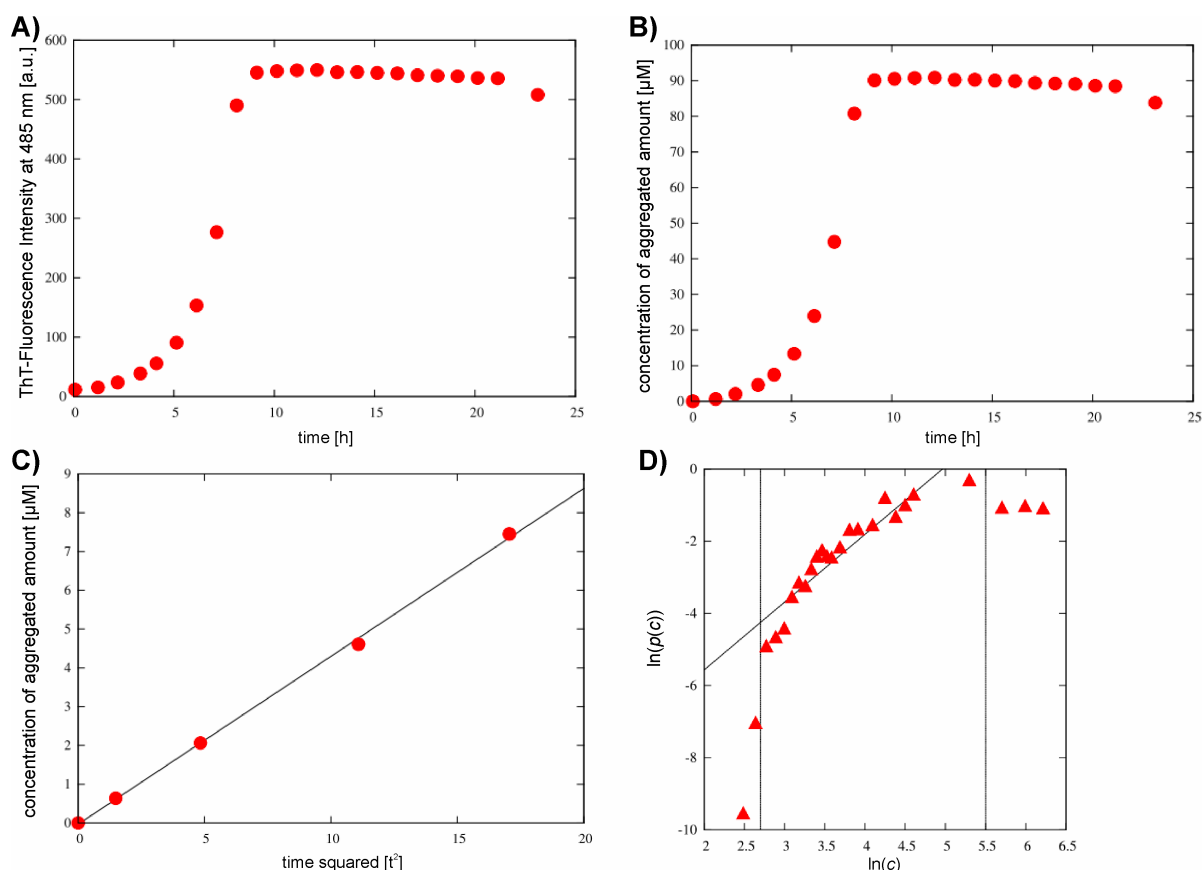


**Figure 7.21:** **A)** Measured ThT-intensity of 100 μM VW18 at  $\lambda = 485$  nm as a function of time. **B)** Concentration of aggregated peptide extracted from ThT-intensity displayed in A) by using equation 7.4. **C)** Concentration of aggregated peptide as a function of  $t^2$ . The slope of the fit gives  $p(100 \mu\text{M}) = 0.4329$ . **D)** Log-log plot of prefactors  $p(c)$  as a function of initial concentrations ( $c$ ). The fit is to the data between the vertical lines (slope of 1.9), corresponding to a nucleus size of one.

The calculated nucleus size of one can be interpreted to an amyloid formation mechanism of **VW18** that involves a disordered monomeric transition state. The separation of the two helices that form the initial dimeric coiled coil is then regarded as the energy barrier that the system has to overcome to form the nucleus (*Figure 7.22*). The attachment of further monomers to the formed nucleus is energetically downhill for the system due to the formation of hydrogen bonds between the molecules. The detailed structure of the nucleus could not be extracted from the results of the described method. Previous studies,

however, indicated that **VW18** adopts a three-stranded  $\beta$ -sheet conformation in the final fibril structure (Figure 7.7).<sup>358</sup> The intermediate species could, thus, either have a random coil-like structure or contain partially  $\beta$ -sheet content. The nucleus does not necessarily have to show the  $\beta$ -sheet arrangement found in the final fibril architecture. The conversion to the  $\beta$ -sheet rich structure can also take place within the aggregates during the process of monomer attachment.<sup>418,419</sup> Due to the fact that structural conversion of the coiled coil dimer towards the  $\beta$ -sheet rich amyloid structure is triggered by an unfavorable accommodation of the valines in the solvent exposed positions, it seems likely that during the process of nucleus formation intermediate species show structures in which the majority of hydrophobic residues are excluded from the aqueous environment. The optimized arrangement of hydrophobic residues being buried at the inside of the structure would correspond to the model of internal fibril architecture that has been previously proposed (Figure 7.7).<sup>358</sup> A nucleus size of one was also found for the Poly(Gln) protein related to Huntington's disease,<sup>421</sup> which was calculated according to the same strategy that was used here to determine the nucleus size of **VW18**. For Poly(Gln) the proposed model describes an unfavorable transition state for the nucleation process.<sup>421</sup> The nucleus is formed from an extended, statistical coil state that converts to a compact state. Fibril elongation is understood as an initial binding of the nucleus to a monomer of an extended conformation followed by a consolidation of the structure that generates a new binding site for a monomer. Thus, a rearrangement of the initial nucleus structure of **VW18** towards a more favorable conformation is not unlikely. Further molecular modeling investigations and molecular dynamic simulations addressing the conformation of the nucleus and the energetics of the amyloid formation process are currently in progress.

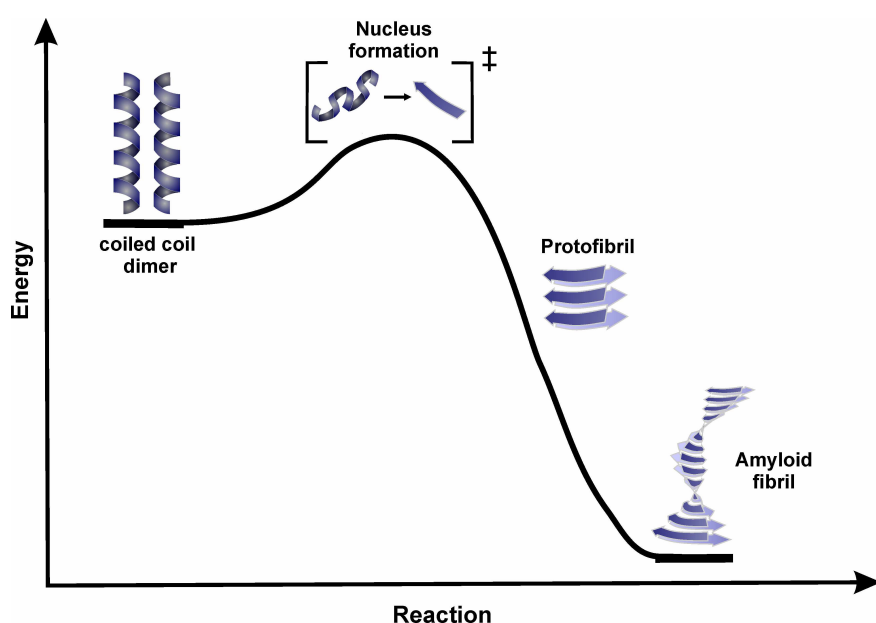


**Figure 7.22:** Suggested energy course for the structural transition of **VW18**.



## 7.5 Altering amyloid formation by fluorinated amino acids

Amyloid formation has been extensively studied for naturally occurring as well as for fully *de novo* designed peptides and proteins (*section 3*). One motivation for this investigation is an understanding of the aggregation mechanism and the factors that influence this process. The finding that amyloid fibrils are also used by nature for protective and storage purposes (*section 3.3*) has inspired researchers to investigate amyloids in terms of their potential application as biomaterials. Many natural and nonnatural building blocks have been used for this purpose. Nonnatural and fluorinated amino acids in particular have become a standard tool to modify the properties of peptides and proteins (*section 2 and 4*). This application of fluorine is based on its unique stereoelectronic properties, which combine small size, very low polarizability, and the strongest inductive effect among all chemical elements.<sup>48</sup> The presence of fluorine within a molecule can often favorably and predictably alter the biophysical and chemical properties, such as hydrophobicity, acidity / basicity, reactivity, and conformation,<sup>66</sup> and the substituents can be readily observed by <sup>19</sup>F-NMR.<sup>33</sup> Many studies in which peptides have been modified with fluorinated amino acids resulted in elaborated structures. This effect has been found for helical,<sup>228-428</sup> and  $\beta$ -sheet based scaffolds,<sup>242-245</sup> and was mainly explained by an increase in hydrophobicity of the fluorinated variants compared to their hydrocarbon analogues.<sup>217,220,223,224,429</sup> However, fluorinated amino acids have been rarely investigated in the context of amyloids.<sup>270</sup> One common application is the use of fluorinated amino acids as NMR-label to gain insights into the mechanism of structural conversion and amyloid formation.<sup>33,34,249,264,430,431</sup> The assumption in such NMR studies is that the fluorine label being introduced into the sequence does not significantly alter the fibril structure and the mechanism of amyloid formation to allow for adequate conclusions with respect to the unaltered structure. However, a systematic study that includes a consideration of the altered properties combined with fluorinated amino acids such as size, hydrophobicity, fluorine content, and secondary structure propensity as factors to influence folding and aggregation is still missing.

In the present thesis several partial side chain fluorinated amino acids have been investigated on their potential to influence the amyloid formation process. The basis for this study was the model peptide **VW18**, which was previously extensively studied in terms of structural modifications. Natural amino acids within the sequence of **VW18** were substituted with a set of fluorinated amino acids that contain different fluorine content in

their side chains. This approach enables a systematic evaluation of fluorine's impact on amyloid formation.<sup>432</sup>

### 7.5.1 The fluorinated building blocks

The fluorinated amino acids that were used to study fluorine's impact on amyloid formation are derivatives of  $\alpha$ -L-aminobutyric acid (Abu) in which one, two, or three hydrogen atoms of the  $\gamma$ -methyl group have been replaced by fluorine (*Figure 7.23*). A single fluorine atom was introduced in monofluoroethylglycine MfeGly (1). The racemic <sup>t</sup>Bu ester was provided by the group of Prof. Haufe (University Muenster). With the help of Acylase I, it was converted to the enantiomerically pure L-amino acid, in our group. Subsequent Fmoc protection of the L-form gave a product suitable for peptide incorporation. Double and triple fluorination of the ethyl side chain of Abu led to difluoroethylglycine DfeGly (2) and trifluoroethylglycine TfeGly (3), respectively. Two diastereoisomers of trifluorovaline, (2*S*,3*S*)-TfV (4) and (2*S*,3*R*)-TfV (5) were synthesized as Boc-protected derivatives in the group of Dr. Czekelius (Holger Erdbrink). The Boc-protected amino acids were converted to Fmoc-species in order to allow incorporation into peptides via SPPS. The synthesis of the amino acids has been described elsewhere and will not be discussed in detail here.<sup>241,433-436</sup> However, the synthetic procedures are given in the Experimental Section.

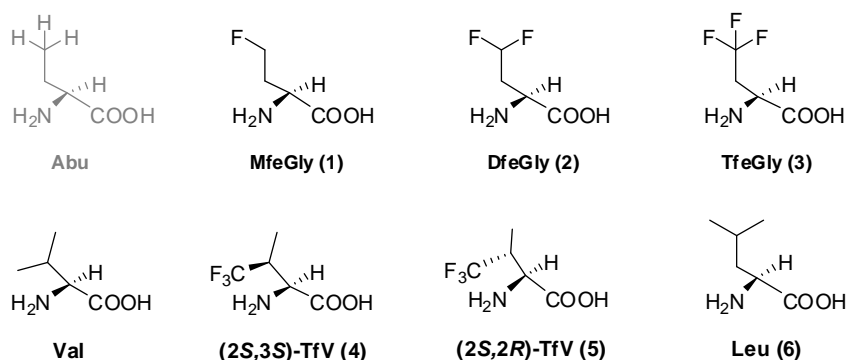


**Figure 7.23:** Chemical structure and names of the amino acids investigated in the present study. Abu was not incorporated into **VW18**; the properties of this amino acid (hydrophobicity and helix propensity), which were compared to the fluorinated derivatives, were taken from previous studies.<sup>49,236</sup> Val is the amino acid to be replaced in the sequence of **VW18**.

**VW18** contains three valine residues, at positions 3, 13, and 14, which are initially exposed to the solvent when the peptide adopts the coiled coil fold (*Figure 7.3*, section 7.1).<sup>358</sup> The valines at positions 13 and 14 were individually substituted with a series of fluorinated  $\alpha$ -L-aminobutyric acid analogues (1-3) (*Figure 7.24*). The diastereoisomers of trifluorovaline (4, 5), were only introduced instead of valine 14 to see if the orientation of the CF<sub>3</sub> group alters the amyloid formation process. In addition, both valine residues (13

and 14) were replaced by the nonfluorinated amino acid leucine (6) to create a second set of reference peptides. Since Leu is the most hydrophobic amino acid among the canonical aliphatic amino acids, it was used to study the impact of hydrophobicity on amyloid formation, to be compared with the results obtained for the fluorinated amino acids. Simultaneous substitution of all three valines (3, 13, and 14) was only carried out for the highly fluorinated amino acid TfeGly (3) and for the nonfluorinated amino acid Leu (6) (Figure 7.23).

The single substitutions of the neighboring valines 13 and 14 were found to affect the central  $\beta$ -strand of the proposed internal fibril folding motif (Figure 7.24 B).<sup>358</sup> Due to the fact that the side chains of the neighboring residues in the central  $\beta$ -strand are oriented in different directions, an effect on the interaction with the hydrophobic side chains of the flanking  $\beta$ -strands was expected. The consequences of the incorporation of fluorinated amino acids into the sequence of **VW18** were studied with several analytical methods, and the results are discussed in the following sections.

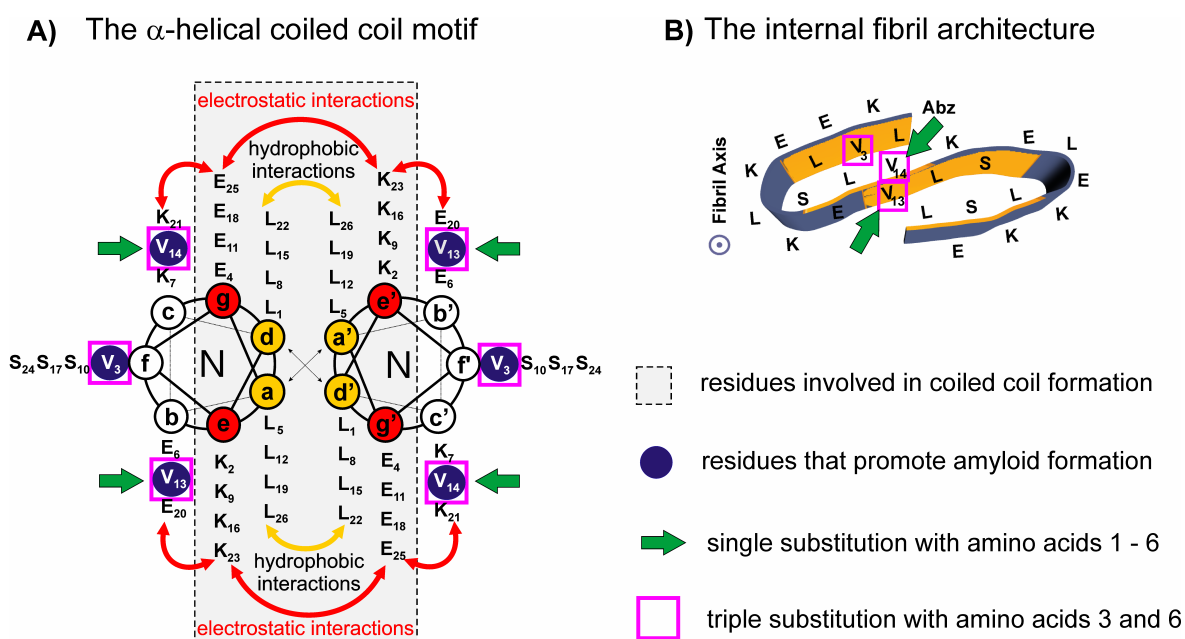


**Figure 7.24:** **A)** Helical wheel diagram of peptide **VW18**. Valines 13 and 14 were individually replaced by amino acids 1 – 6 (green arrows). All three valines were simultaneously replaced by TfeGly (3) or by Leu (6) (purple square). **B)** Proposed model of the internal architecture of the peptide strands within the fibrils of **VW18**.<sup>358</sup> The top view along the fibril axis show the intramolecular hydrophobic interactions of the particular core residues (yellow) and the positions of substituted valine residues (green arrows and purple squares).

### 7.5.2 Hydrophobicity and spatial demand of fluorinated amino acids

Although hydrogen and fluorine atoms are often discussed as being isosteric, the  $\text{CF}_3$  group occupies approximately twice the van der Waals volume of a  $\text{CH}_3$  group, and the

steric effect of the  $\text{CF}_3$  group is close to that of an isopropyl group (see section 2.1).<sup>46,437</sup> That the size of amino acid side chains closely correlate with their hydrophobicity has been previously shown by Samsonov *et al.*<sup>49</sup> They investigated the relationship between side chain volume (van der Waals volume) and hydrophobicity of some fluorinated amino acids in comparison to the natural aliphatic hydrophobic amino acids with the help of an RP-HPLC assay. The impact of increasing fluorine content of the  $\alpha$ -L-aminobutyric acid analogues on the hydrophobicity of aliphatic amino acids was shown to vary non-linearly with the increase in steric size by elongation and branching of the side chain (Figure 7.25). TfeGly (3) was found to be very similar to the canonical amino acid valine with regard to its properties, hydrophobicity and van der Waals volume. DfeGly (2) is less hydrophobic compared to valine but still more hydrophobic than the nonfluorinated Abu analogue. Single fluorination of Abu, however, induced a loss in hydrophobicity. Although being larger than Abu with regard to the side chain volume, MfeGly (1) is nevertheless less hydrophobic. The induced dipole moment endows this amino acid with a more hydrophilic or polar character.

For this thesis this study was extended to include the fluorinated valine analogues (2S,3S)-TfV (4) and (2S,3R)-TfV (5). These two amino acids were found to be comparable to Leu and Ile with regard to both properties.

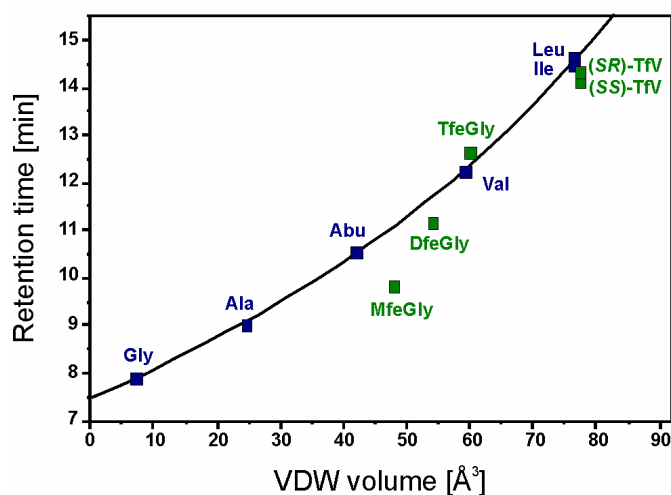


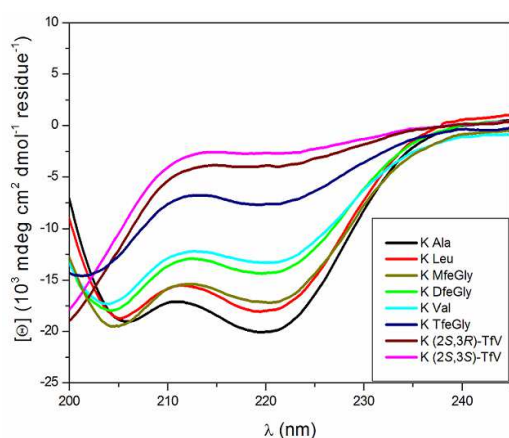
**Figure 7.25:** Retention times of the Fmoc-amino acids plotted against the van der Waals volume of the side chains. Nonfluorinated amino acids are represented by blue squares, the correlation between them is shown with a black line, and fluorinated amino acids are represented by green squares.

### 7.5.3 The $\alpha$ -helix propensity of fluorinated amino acids

The intrinsic propensity of canonical amino acids to promote certain secondary structures is an important factor in peptide and protein folding. Cheng and coworkers investigated

the  $\alpha$ -helix propensities of several canonical amino acids and their fluorinated analogues using an alanine-based peptide sequence Ac-YGGKAAAAKA-**Xaa**-AAKAAAAK-NH<sub>2</sub> that forms a monomeric  $\alpha$ -helix.<sup>236-240</sup> The amino acid of interest was placed at the guest position **Xaa**, and the  $\alpha$ -helix propensity was calculated from the corresponding CD data by using a modified Lifson-Roig theory.<sup>238-240</sup> The authors stated that fluorinated amino acids exhibit a reduced  $\alpha$ -helix propensity compared to their hydrocarbon analogues. Analogous to the design and methods of Cheng *et al.*,<sup>236,438</sup> the  $\alpha$ -helix propensities of the fluorinated amino acids 1 – 5 (Figure 7.23) were investigated. It was found that increases in the fluorine content per side chain additively reduce the  $\alpha$ -helix propensity (Figure 7.26; Table 7.6). Introducing a single fluorine atom into the Abu side chain in case of MfeGly (1) resulted already in a decrease of the helix propensity in comparison to the nonfluorinated Abu. However, the value for MfeGly (1) is still twice as high as the one for valine. Thus, MfeGly is presumably better accommodated in the initial  $\alpha$ -helical structure of **VW18** than Val. The value of DfeGly (2) is comparable to Val, and TfeGly (3) has a very low, almost nonexistent,  $\alpha$ -helix propensity, which is consistent with the findings of Cheng *et al.*<sup>236</sup>

**Table 7.6:** Mean residue ellipticity ( $\theta_{222}$ ), fraction helix ( $f_{\text{helix}}$ ), and helix propensity ( $\omega$ ) of **KXaa** peptides for various amino acids. The values for Abu (grey) have been taken from Cheng *et al.*<sup>236</sup>



Amino acid	$[\theta_{222 \text{ nm}}]$	$f_{\text{helix}}$	$\omega$
Abu <sup>236</sup>	-18100 ± 200	0.52 ± 0,01	1.22 ± 0.14
MfeGly	-16814 ± 379	0.48 ± 0,01	0.873 ± 0.068
DfeGly	-13969 ± 569	0.40 ± 0,02	0.497 ± 0.060
TfeGly	-7469 ± 475	0.22 ± 0,01	0.057 ± 0.022
Leu	-17457 ± 465	0.50 ± 0,01	0.994 ± 0.093
Val	-13054 ± 452	0.38 ± 0,01	0.411 ± 0.041
(2S,3S)-TfV	-2685 ± 526	0.08 ± 0,02	0
(2S,3R)-TfV	-3887 ± 547	0.11 ± 0,02	0

**Figure 7.26:** CD spectra of the **KXaa** peptides at pH 7 in 1 mM phosphate, borate, and citrate with 1 M NaCl at 0 °C. The displayed spectra represent the mean of three independent measurements at concentrations of 80  $\mu$ M, 50  $\mu$ M, and 30  $\mu$ M. The ellipticity ( $\theta$ ) value at 222 nm was used to calculate the fractional helical content ( $f_{\text{helix}}$ ) and the subsequent  $\alpha$ -helix propensity ( $\omega$ ).

The trifluorinated valine analogues (4, 5) incorporated at the guest position of the referred peptide sequence resulted in disordered structures with a very low fractional helical content ( $f_{\text{helix}}$ ). The calculation of the helix propensity ( $\omega$ ) resulted in slightly negative values and were thus interpreted as zero.<sup>241</sup> Since valine was already declared as a  $\beta$ -sheet preferring amino acid,<sup>248</sup> it was not surprising that the fluorination of one of the methyl groups increases this effect even further. The large CF<sub>3</sub> group in close proximity to the backbone is highly unfavorable for the formation of  $\alpha$ -helical structures, hence

explaining the absence of a propensity for  $\alpha$ -helical structures of both diastereoisomers of TfV (*Table 7.6*).<sup>241</sup>

The monomeric oligomerization state, which is a requirement for correct  $\alpha$ -helix propensity calculation based on the Lifson-Roig theory, was demonstrated for all peptide variants with SEC/SLS analysis (*Figure 7.27, Table 7.7*). Obtained results show monomeric oligomerization of all peptides variants. Single peaks were found for all Ala based peptides during SEC, containing species with a molecular weight comparable to the theoretical monomer masses.

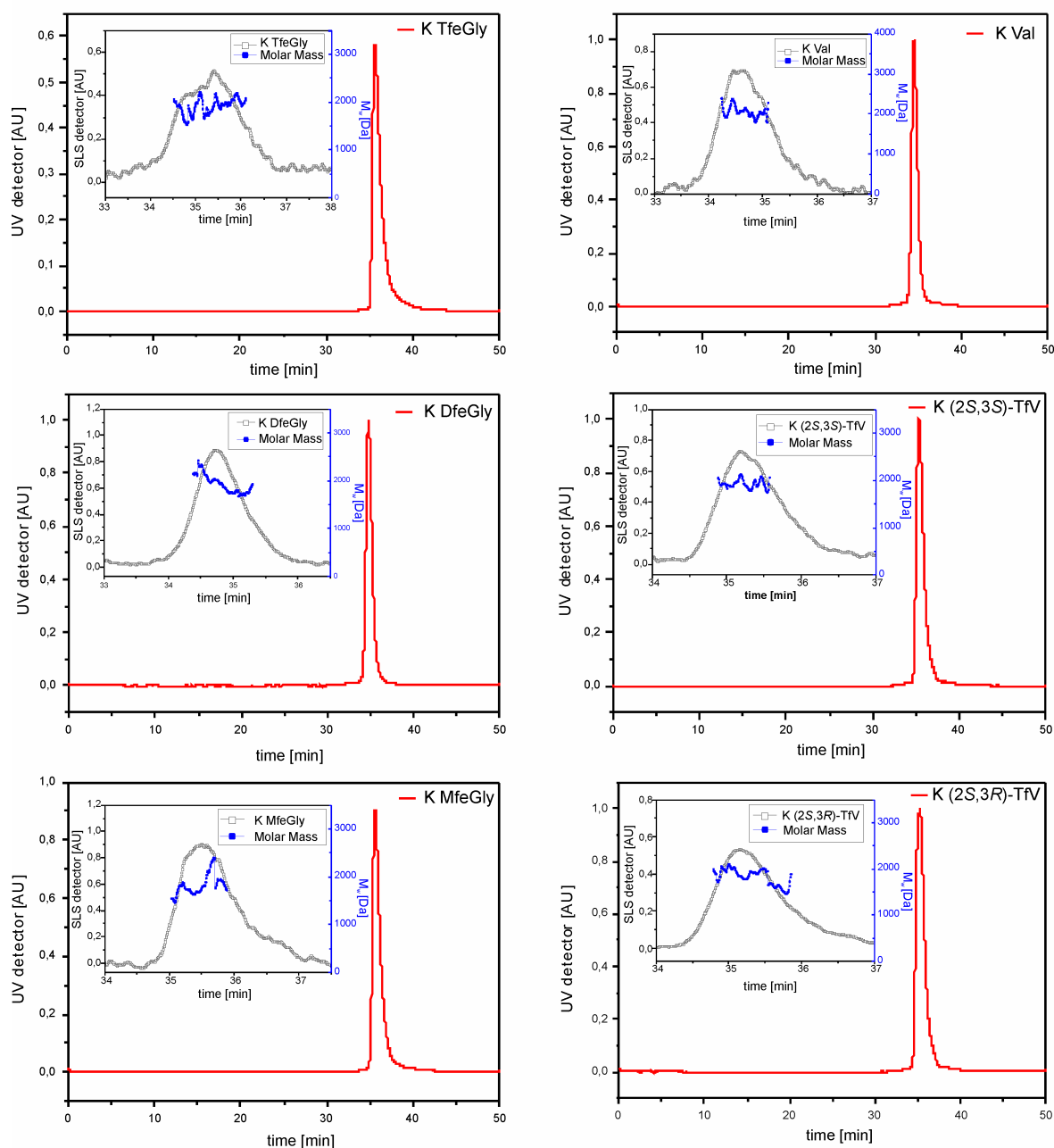


**Figure 7.27:** SEC/SLS chromatograms of *KXaa* peptides. Single peaks were detected with UV at 230 (red). Corresponding Rayleigh ratio (black) and molar mass distribution (blue) indicate monomeric species for all peptide variants.

**Table 7.7:** Theoretical and experimental determined molecular weights of **KXaa** peptides.

Peptide	theoretical monomer mass [Da]	SEC/SLS determined mass [Da]
K TfeGly	1771	1950 ± 220
K DfeGly	1752	1948 ± 236
K MfeGly	1733	1909 ± 226
K Val	1729	2029 ± 143
K (2S,3S)-TfV	1782	1998 ± 183
K (2S,3R)-TfV	1783	1919 ± 243

The results show that the helix propensity of fluorinated amino acids depends on the extent of side chain fluorination. Thus, the statement of Cheng *et al.*<sup>236</sup> that fluorinated analogues indeed display reduced propensities for helical conformations compared to the hydrocarbon variants could be confirmed. However, the measurements of this study show that the decrease in helix propensity occurs stepwise with increasing fluorine content.

However, the interpretation that decreased  $\alpha$ -helix propensity values are a result of increased side chain volumes and hydrophobicities would be misleading. This has been clearly demonstrated in a comparative study investigating the helix propensities of several fluorinated isoleucine analogues. Nyakatura, and Kokschi studied the hydrophobicity and helix propensity of (2S,3S)-5-F<sub>3</sub>Ile and compared the results to the previously investigated (2S,3S)-4'-F<sub>3</sub>Ile<sup>241</sup> and the nonfluorinated reference isoleucine (Figure 7.28).<sup>439</sup>

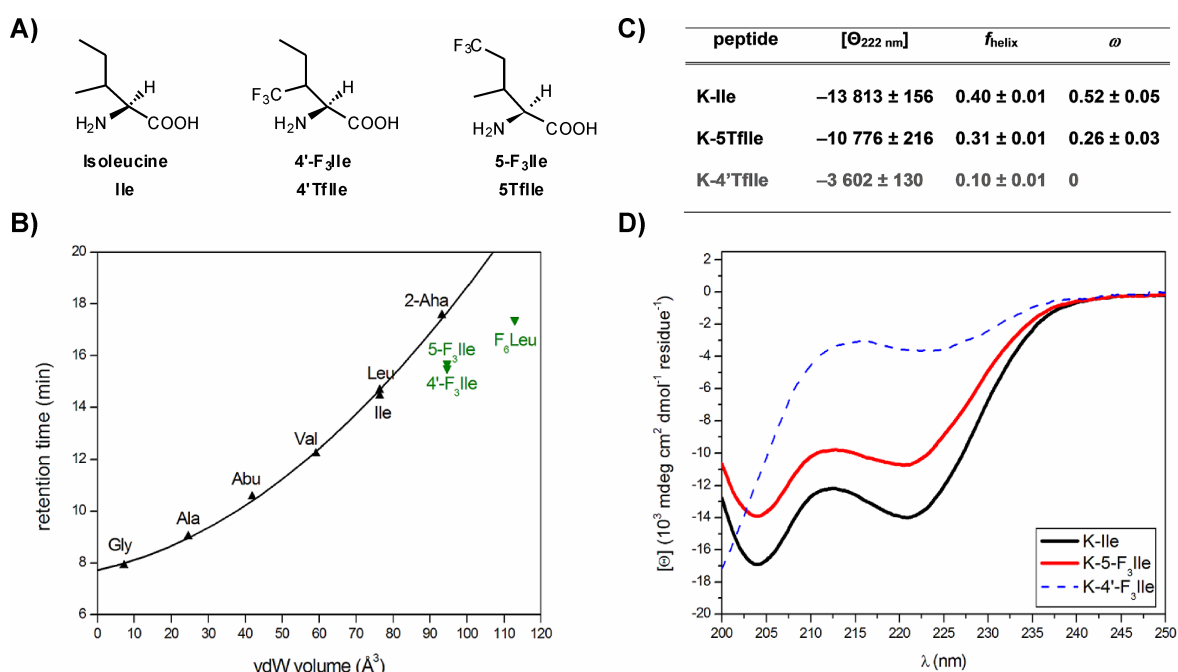


**Figure 7.28:** **A)** Chemical structures and Names of isoleucine and the trifluorinated analogues. **B)** Retention times of the Fmoc-amino acids plotted against the van der Waals volume of the side chains showing the increased size and hydrophobicity of 4'-F<sub>3</sub>Ile and 5-F<sub>3</sub>Ile in comparison to Ile. **C)** Mean residue ellipticity ( $\theta_{222}$ ), fraction helix ( $f_{helix}$ ), and helix propensity ( $w$ ) of the **KXaa** peptides containing the Ile variants and **D)** according CD spectra of **KXaa** peptides that were used to calculate the fractional helix content and the helix propensity (according to Erdbrink *et al.*).<sup>439</sup>

Both fluorinated analogues show increased side chain volumes and hydrophobicities compared to Ile. The fluorinated analogues differ only in the position in which they carry the CF<sub>3</sub> group (*Figure 7.28 A*); hence, their hydrophobicity is equal (*Figure 7.28 B*). Nevertheless, their helix propensities are strikingly different. The value of (2S,3S)-5'-F<sub>3</sub>Ile, albeit lower than that of Ile, is significantly increased in comparison to (2S,3S)-4'-F<sub>3</sub>Ile (*Figure 7.28 C/D*). Thus, not the hydrophobicity discriminates the helix propensity in this case, but the distance of the fluorine substituents from the amino acid backbone. This effect is similar for the canonical amino acids Leu and Ile that have equal hydrophobicity and side chain volumes but different helix propensities based on the different shape of their side chains. The  $\beta$ -branched side chain of Ile is unfavorable for adopting helical structures but more suitable for  $\beta$ -sheet conformations. That helix propensity does not correlate with hydrophobicity can also be seen for Abu and its monofluorinated analogue MfeGly (1). Although being less hydrophobic than Abu, MfeGly also possesses the lower helix propensity (*Figure 7.26, Table 7.6*).

These results clearly show that the helix propensities of fluorinated amino acids cannot be easily predicted. Since this property, however, is a crucial factor for the formation of secondary structures it should be generally considered during the investigation of fluorinated amino acids in peptide environments. The fact that the model peptide **VW18**, being modified with fluorinated residues, initially adopts an  $\alpha$ -helical coiled coil structure requires the knowledge of the helix propensity values of the utilized amino acids.

#### **7.5.4 Amyloid formation rates of fluorinated VW18 variants**

By replacing valine with TfeGly (3), size and hydrophobicity were kept similar, thus having the opportunity to study the impact of fluorine on the amyloid formation process of the model peptide. The reduction of fluorine content in the side chains of DfeGly (2) and MfeGly (1) led to amino acids that are less hydrophobic compared to valine. In contrast, the two reference peptides that contain a single Leu instead of Val at one of the two positions (13 or 14) are even more hydrophobic than **VW18**. This set of peptides allowed a systematic comparison of the influence of hydrophobicity and spatial demand of the side chain on amyloid formation of **VW18**. As Leu is larger with regard to the van der Waals volume and also more hydrophobic than the replaced valine, the leucine containing peptides were expected to fold faster into amyloids than the valine containing parent peptide. This assumption was based on the design of the coiled coil model peptide where placement of hydrophobic residues at the solvent exposed positions of the coiled coil triggers the structural transition into amyloids.<sup>351,358</sup>



The structural transition of all peptides was investigated under non-agitated conditions with CD spectroscopy, and the amyloid formation rates were determined with Thioflavin T fluorescence staining assays. Except for the two TfV containing peptides (*Figure 7.30*), all **VW18** variants show clear initial helical structures in the CD spectra with characteristic minima at 208 and 222 nm, which time dependently change over to  $\beta$ -sheet structures with a characteristic minimum around 216 nm (*Figure 7.29*).

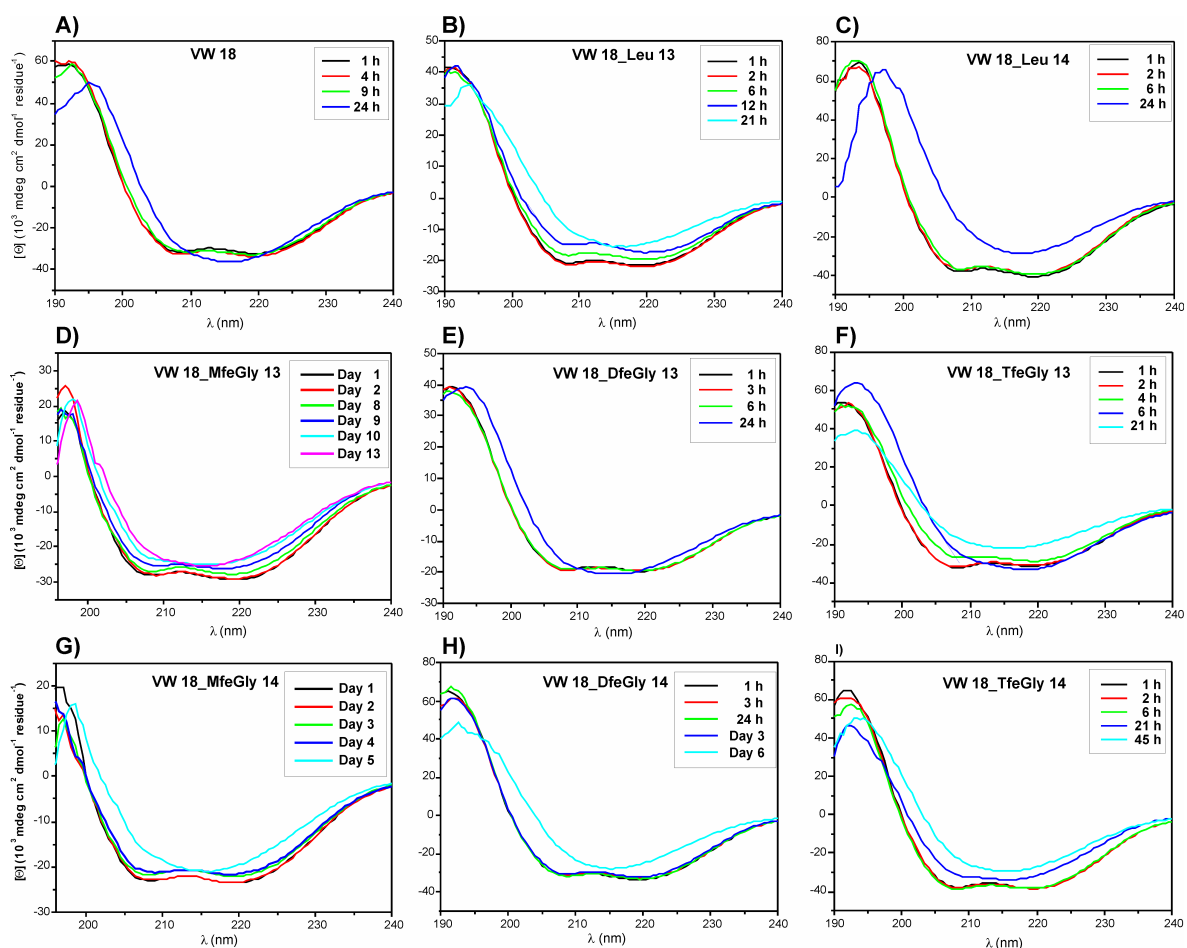


**Figure 7.29:** CD spectra of **VW18** and single substituted variants ( $100 \mu\text{M}$  each) after different periods of incubation in  $10 \text{ mM}$  phosphate buffer at  $\text{pH } 7.4$ .

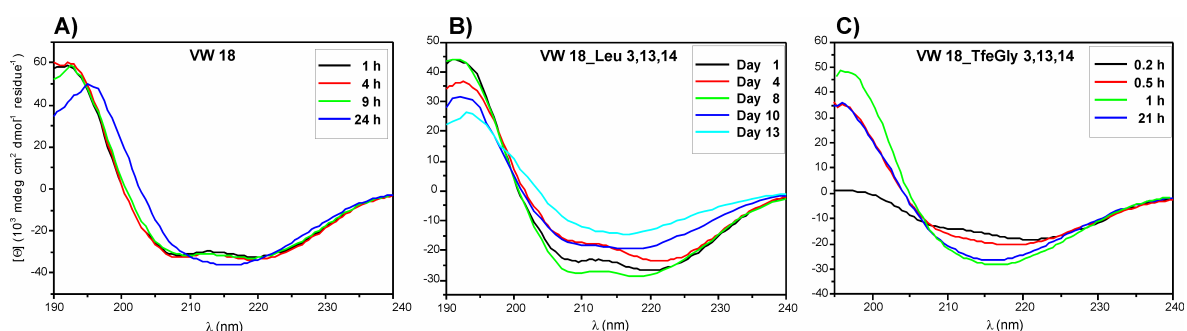


**Figure 7.30:** CD spectra of **VW18** and triple substituted variants ( $100 \mu\text{M}$  each) after different periods of incubation in  $10 \text{ mM}$  phosphate buffer at  $\text{pH } 7.4$ .

The amyloid formation rates of the fluorinated peptide variants were found to be strongly influenced by the nature of the incorporated amino acid. Reducing fluorine content per side chain (TfeGly (3) > DfeGly (2) > MfeGly (1)) dramatically reduced amyloid formation rates were observed (Figure 7.31). While the structural transition occurred within only a few hours in case of a single TfeGly (3) substitution, it took several days for the MfeGly (1) peptides (Figure 7.31 A/B). This effect was observed for both positions, 13 and 14, although the absolute folding rates show a dependency on the particular position substituted (discussed in section 7.5.5). The overall structural conversion of peptides containing TfeGly and DfeGly in position 14 was found to be slower in comparison to the peptides containing the same amino acids in position 13. However, within each set of substitutions the same trend of amyloid formation rates was found for both positions independently, with TfeGly variants aggregating faster than DfeGly peptides, which in turn aggregate faster than MfeGly variants.

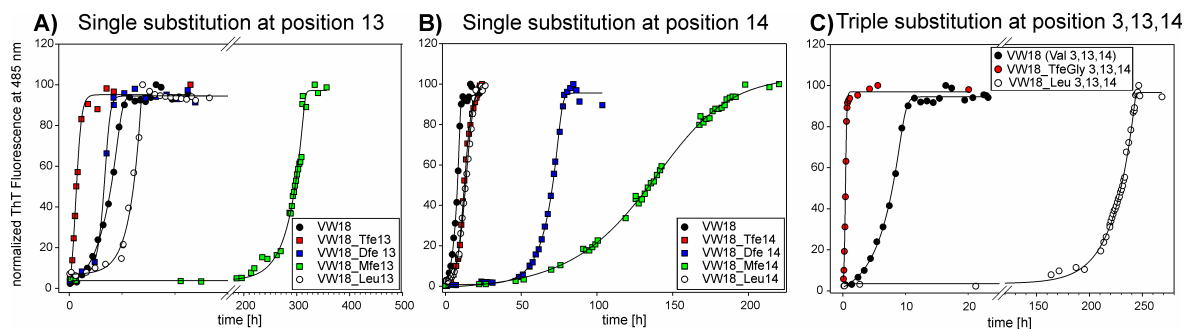


**Figure 7.31:** ThT fluorescence staining assay for peptide variants compared to **VW18** (●) and the Leu containing reference peptides (○). Single substitution of valine 13 (A) and valine 14 (B) with fluorinated analogues of L-amino butyric acid: TfeGly (■), DfeGly (■), and MfeGly (■). C) Simultaneous substitution of all three valine residues with TfeGly (●), and Leu (○).

A decrease in fluorine content per side chain for the series TfeGly (3), DfeGly (2), and MfeGly (1) led to a systematic decrease in hydrophobicity and side chain volume (van der Waals volume) of the latter two fluorinated amino acids (Figure 7.25). DfeGly (2) and MfeGly (1) are less hydrophobic and smaller than the replaced canonical amino acid valine. At first glance, it seems obvious that these factors are the reason for reduced amyloid formation rates. However, reduced hydrophobicity and size are obviously not the main reasons for the reduced amyloid formation kinetics, because also the Leu (6) containing reference peptides (**VW18\_Leu 13** and **VW18\_Leu 14**), which are even more hydrophobic than **VW18**, showed reduced amyloid formation rates. The effects found for single TfeGly (3) and single Leu (6) substitutions were even enhanced in the triply substituted variants (Figure 7.31 C). The peptide in which TfeGly (3) was substituted for all three valine residues (**VW18\_TfeGly 3,13,14**) showed even faster structural conversion into amyloids than the single TfeGly (3) variants. The triple Leu (6) variant (**VW18\_Leu**

**3,13,14**) undergoes amyloid formation with a reduced rate compared to the single leucine mutants (*Figure 7.31 A/B/C*). Thus, hydrophobicity and side chain volume are not the only driving forces for the structural rearrangement and amyloid formation of **VW18**.

The fluorinated amino acids have been found to have a strong impact on the amyloid formation rates of the model peptide. Taking into account the previously described helix propensity measurements of the fluorinated amino acids, it can be stated that the fluorinated amino acids significantly influence the initially formed  $\alpha$ -helical coiled coil structure of **VW18**. A stabilizing or destabilizing effect of this folding motif as a result of different  $\alpha$ -helix propensities of the particularly incorporated amino acids strongly correlates with reduced or enhanced structural transition to the amyloid structure.

#### 7.5.4.1 Altered fibril forming conditions

Experimental conditions and sample handling are also crucial factors determining the rate of amyloid formation. This was investigated with the series of peptides in which position 13 was replaced. The samples were continuously agitated, and the influence on the amyloid formation kinetics was determined (*Figure 7.32*).

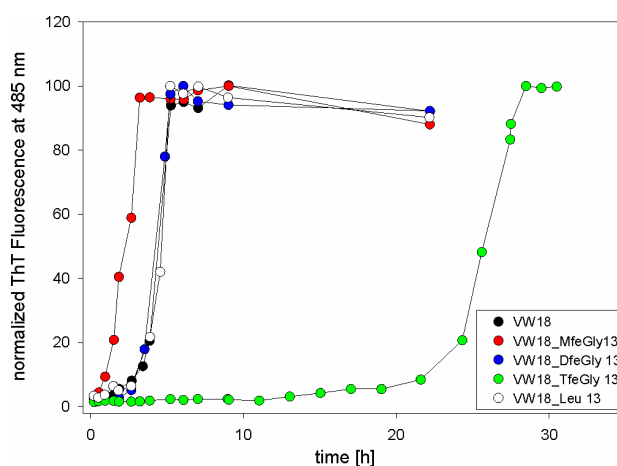


**Figure 7.32:** ThT fluorescence staining assay under constantly agitated conditions for **VW18** (●) and the variants containing TfeGly (●), DfeGly (●), MfeGly (●), and Leu (○) in position 13.

Agitation of the samples was found to significantly reduce the lag phase and increases amyloid formation rates in every case, which was in good agreement with other studies.<sup>23,406,424-426</sup> However, the same trend of folding rates was observed for the peptides modified in position 13 compared to the non-agitated conditions and, thus concluded that the mechanism of structural transition is the same for all investigated **VW18** variants. The observed trend of amyloid formation rates of the studied peptide variants was independent of the conditions under which the fibrils were formed, but appeared as a result of the particularly incorporated fluorinated amino acids.

### 7.5.4.2 The orientation of the fluorine substituents as a discriminating factor

Whether the local orientation of the  $\text{CF}_3$  group influences the amyloid formation of **VW18**, due to structural differences in the internal fibril packing (Figure 7.7, section 7.2), was tested with two diastereomers of trifluorovaline (TfV). Valine in position 14 was replaced with either (2*S*,3*S*)-TfV (4) or (2*S*,3*R*)-TfV (5). The unfavorable  $\alpha$ -helix propensity of the two TfV-isomers (Table 7.6) discussed in section 7.5.3,<sup>241</sup> was significant enough to completely disrupt the initial coiled coil motif that **VW18** usually adopts, even though only a single valine residue was replaced. Both peptide variants containing TfV show an initially unfolded structure (Figure 7.33 A/B) that rapidly assembles into amyloid aggregates (Figure 7.33 C). Interestingly, this effect is stronger than that observed for any of the other fluorinated **VW18** variants. TfeGly (3), for instance, has a very low  $\alpha$ -helix propensity as well (Table 7.6), but all TfeGly peptide variants adopt clear initial  $\alpha$ -helical coiled coil structures (Figure 7.29 F/I; Figure 7.30 C).

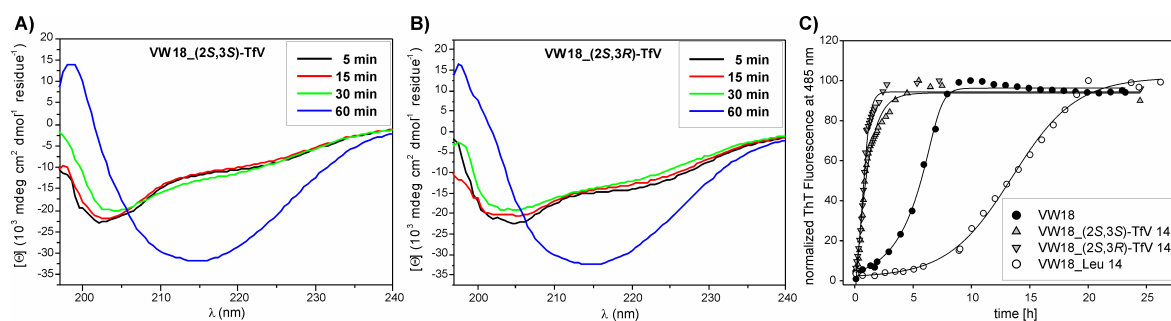


**Figure 7.33:** CD spectra of **VW18** and the variants containing (2*S*,3*S*)-TfV (A), and (2*S*,3*R*)-TfV (B) in position 14. Sample concentration was 100  $\mu\text{M}$  each at different time points of incubation in 10 mM phosphate buffer at pH 7.4. C) ThT fluorescence staining assay for TfV variants compared to the control peptides **VW18** and **VW18\_Leu 14**.

These findings support the hypothesis that the particular incorporated fluorinated amino acid influences the initial coiled coil structure of **VW18**, and that the rate of structural conversion is strongly dependent on the stability of that initial motif. Consequently, the destabilized, or rather non-existing, initial  $\alpha$ -helical structure of the TfV-variants results in very rapid amyloid formation (within one hour). Although van der Waals volume and hydrophobicities of (2*S*,3*S*)-TfV (4) and (2*S*,3*R*)-TfV (5) are comparable to Leu (6) (Figure 7.25), the leucine containing variant (**VW18\_Leu 14**) shows a notably slower structural transition into amyloids (Figure 7.33 C). The much higher  $\alpha$ -helix propensity of Leu (6) compared to Val and TfV (Table 7.6) offers a reasonable explanation. However, an influence of the local orientation of the  $\text{CF}_3$  group on amyloid formation, due to different packing patterns in the fibril, has not been observed for the particularly replaced position

14 of **VW18**. Both peptide variants **VW18\_(2S,3S)-TfV 14** and **VW18\_(2S,3R)-TfV 14** show almost the same rate of amyloid formation (*Figure 7.33 C*).

## 7.5.5 Analysis of the overall VW18 fibril structure by solid state $^{19}\text{F}$ -NMR

### 7.5.5.1 Chemical shift analysis

The **VW18** variants containing MfeGly (1) in either position 13 or 14 have been used to gain further insights in the fibril structure with the help of solid state  $^{19}\text{F}$ -NMR measurements. These investigations have been accomplished in collaboration with the group of Prof. Dr. A. Ulrich at the Karlsruhe Institute of Technology (KIT) in Karlsruhe.

The NMR chemical shift and dipolar couplings are sensitive to the local chemical environment and presence of nearby spins. In particular, due to the large dispersion of the  $^{19}\text{F}$  chemical shift and the large gyromagnetic ratio of  $^{19}\text{F}$ , small differences in the molecular environment can be readily picked up, and  $^{19}\text{F}$ - $^{19}\text{F}$  distances up to 10-15 Å are detectable.

The two MfeGly variants (**VW18\_MfeGly 13** and **VW18\_MfeGly 14**) were analyzed using magic angle spinning experiments with 25 kHz spinning speed to obtain high resolution in the  $^{19}\text{F}$  chemical shift region (see *section 6.4*). The  $^{19}\text{F}$ -NMR spectra of both types of labeled fibrils show two resolved signals each, at -215.8 ppm and -218.9 ppm in the case of **VW18\_MfeGly 13** (*Figure 7.34 A*), and at -216.3 ppm and -218.1 ppm in the case of **VW18\_MfeGly 14** (*Figure 7.34 B*).

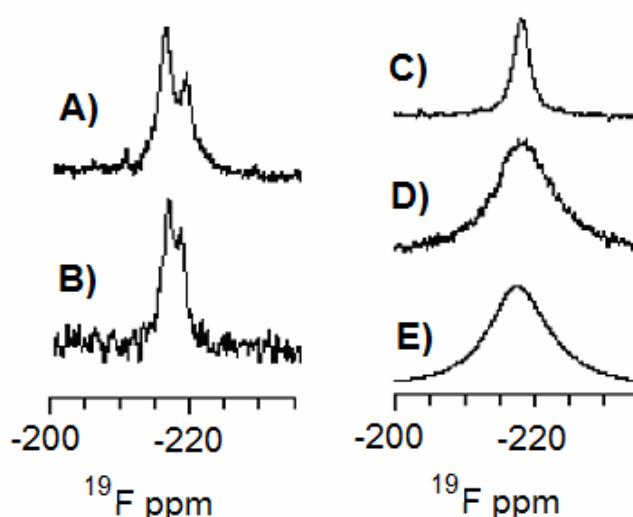


**Figure 7.34:** Solid state  $^{19}\text{F}$ -NMR spectra under 25 kHz magic angle spinning of **VW18\_MfeGly 13** fibrils (**A**), **VW18\_MfeGly 14** fibrils (**B**), the pure amino acid MfeGly (**C**), dry **VW18\_MfeGly 13** powder (**D**) and dry **VW18\_MfeGly 14** powder (**E**). Both fluorine-substituted analogues display two signals, one with a similar chemical shift as the micro-crystalline amino acid (-218.5 ppm).

Comparing the  $^{19}\text{F}$ -NMR spectra of these two fibrils with the respective spectra of the dry peptide powders of **VW18\_MfeGly 13** (*Figure 7.34 D*), and **VW18\_MfeGly 14** (*Figure 7.34 E*), much wider lines were noted for the dry powder samples, reflecting a considerable local heterogeneity of chemical environments, as is often found in amorphous materials. The comparatively narrow lines observed in the fibrillar samples (*Figure 7.34 A/B*) indicate a much lower structural variation, as typically found in NMR studies of fibrils, thus confirming that fibrils have indeed formed throughout. Remarkably, two signals are observed for both variants in the decoupled spectra, although only one position was labeled. This indicates that the  $^{19}\text{F}$ -label on MfeGly has to be exposed to two different local chemical environments. The signal intensities differ, in both cases the left (downfield) resonance is stronger and exceeds the upfield signal by a factor of 1.9 for **VW18\_MfeGly 13**, and 2.9 for **VW18\_MfeGly 14**, respectively. This observation of two different chemical environments, of which one is more abundant in the fibrils, is most likely a signature of the internal structure of the amyloids. The fibrils are known to consist of a ribbon of typically three protofilaments, which was shown previously in TEM-studies (see *section 7.2*).<sup>358</sup>

The two outer protofilaments must experience different solvent exposure than the inner ones. Thus, the two outer protofilaments could give rise to the more intense downfield signal, while the inner protofilament would be shielded more from the solvent and give rise to the  $^{19}\text{F}$  chemical shift corresponding to the smaller upfield signal. In the case of **VW18\_MfeGly 13**, the intensity ratio of approximately 2:1 would agree with such an assembly of two types of protofilaments. For **VW18\_MfeGly 14**, the observed ratio may have a larger error due to lower resolution of the peaks. However, the assumption is further supported by the almost identical  $^{19}\text{F}$  chemical shift of the smaller, upfield signal of MfeGly incorporated in the **VW18** fibrils (*Figure 7.34 A*, -218.9 ppm, and *Figure 7.34 B*, -218.1 ppm), and that of the free amorphous MfeGly amino acid (*Figure 7.34 C*, -218.5 ppm). Also the center of the signals of the dry peptide powder appears at a similar chemical shift (*Figure 7.34 D/E*, approx. -218 ppm). In both cases, the inner protofilament and the microcrystalline packing of the dry amino acid, the fluorine substituent would be surrounded by a similar, rather crystalline-like environment, whereas the outer protofilaments are influenced more by the solvent.

### 7.5.5.2 Evaluation of dipolar couplings

In addition to the chemical shift evaluation, the CODEX (Centerband Only Detection of Exchange) experiment was employed to probe potential dipolar couplings between non-equivalent spins.<sup>313,315</sup> Using this experiment, potential contacts between different protofilament units can be evaluated, as this experiment is sensitive to changes in the

chemical shift, which generally reflect the orientation of the labeled segment with respect to the magnetic field, during a mixing time  $t_{\text{mix}}$ . Such changes can be caused either by a reorientation of the labeled molecular segment due to slow dynamics, or by magnetization „diffusing“ between sites with different local orientation. These processes lead to a reduction of the CODEX NMR signal.

Two spectra were recorded for a series of mixing times, one displaying the full intensity  $S_0$ , and a second one of intensity  $S$  that is reduced by slow dynamics or spin diffusion during the mixing time. As an example, the CODEX spectra of **VW18\_MfeGly 13** and **VW18\_MfeGly 14** for  $t_{\text{mix}}=400$  ms are shown in *Figure 7.35 A and B*, respectively. A distinct reduction in signal intensity is observed for both amyloid analogues, indicating the occurrence of slow molecular motions or the presence of  $^{19}\text{F}$  nuclei in close proximity.

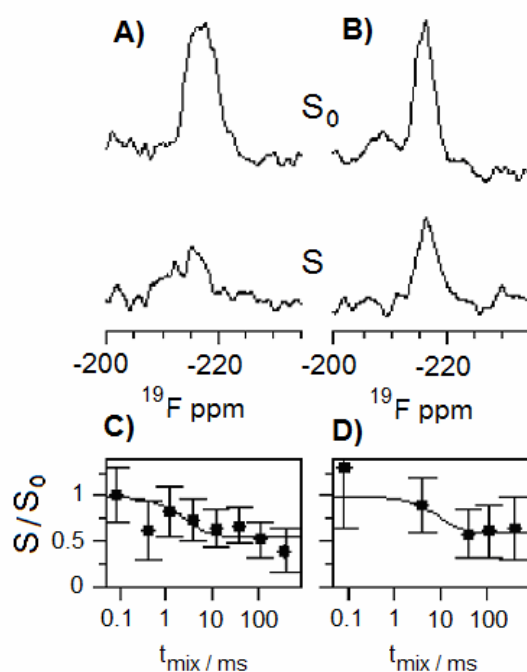


**Figure 7.35:** The CODEX experiment was used to examine spin diffusion and probe for proximities of non-equivalent  $^{19}\text{F}$  nuclei in **VW18\_MfeGly 13** (A/C) and **VW18\_MfeGly 14** (B/D). As an example, the full spectra without spin diffusion (denoted by  $S_0$ ) and spectra with reduced intensity indicating the presence of spin diffusion (denoted by  $S$ ) for a mixing time of 400 ms, are shown for **VW18\_MfeGly 13** (A) and **VW18\_MfeGly 14** (B). The ratio  $S/S_0$  was measured for different mixing times  $t_{\text{mix}}$  (C/D) and fitted as described in the Experimental section (solid line).

CODEX experiments have been used to study slow dynamics, e.g. in soft polymers, but the hydrogen-bonded architecture of amyloid fibrils is much more rigid compared to polymers. Solid state  $^{19}\text{F}$ -NMR studies of  $[\text{KIGAKI}]_3$  amyloid-like assemblies and  $^{13}\text{C}$ -NMR analyses of the dynamics of  $\text{A}\beta$  amyloids have shown very rigid core structures of the fibrils.<sup>33,440</sup> Since the positions 13 and 14, labeled in **VW18**, are located in the center of the fibrils (*Figure 7.7 B*), they should experience only very low flexibility as well. A further possibility to explain the CODEX decay by mobility could be exchange between different



side chain rotamer conformations on a timescale of ~10ms. In a recent study of side chain mobility in amyloids, motion on this timescale has indeed been observed but has been attributed to the overall mobility of monomers.<sup>441</sup> Otherwise a large range of timescales ranging from ns to s has been reported for side chain mobility, an interconversion rate just in the range affecting the CODEX experiment, hence seems not probable. Thus, dynamics is unlikely to be the main cause of the observed signal reduction in the CODEX experiment. The decay of the signal ratio  $S/S_0$  as a function of the mixing time  $t_{\text{mix}}$  (Figure 7.35 C/D) is indeed much better explained by spin diffusion between nearby  $^{19}\text{F}$  nuclei (within internuclear distances of ~10-15 Å). In this case, the signal  $S/S_0$  is expected to asymptotically approach a non-zero constant for long mixing times  $t_{\text{mix}}$ , rather than decaying all the way down to zero, which was observed for both **VW18** variants.<sup>315</sup> The constant value is identical to  $1/M$ , where  $M$  is the number of nuclei involved in the spin diffusion, such as the number of monomers in the case of a homo-oligomer.<sup>315</sup> For **VW18\_MfeGly13** and **VW18\_MfeGly14** it was observed that  $S/S_0$  approached a finite value corresponding to  $M=1.8$  and  $M=1.6$ , respectively.

As spin diffusion only leads to a reduction in signal intensity when it occurs between non-equivalent sites with different orientation, the observed spin diffusion does not reflect neighbouring spins within the same protofilament (along the fibril axis). That is because the  $^{19}\text{F}$ -labelled amino acids are essentially only shifted along the protofilament but not rotated to any significant extent. Hence, they are oriented the same way and do not give rise to spin diffusion. The slight macroscopic twist of the fibrillar ribbon, found in TEM-studies (Figure 7.36), is presumably too small to lead to a significant difference in orientation that would cause an appreciable effect in the CODEX experiment. Hence, the results seem to indicate couplings of spins that belong to different, adjacent protofilaments. Thus, the CODEX experiment and the two signals observed in the  $^{19}\text{F}$ -NMR spectra support the formation of fibrils consisting of several - most likely three - protofilaments, as also found for **VW18** in previous TEM-studies (compare section 7.2).<sup>358</sup>

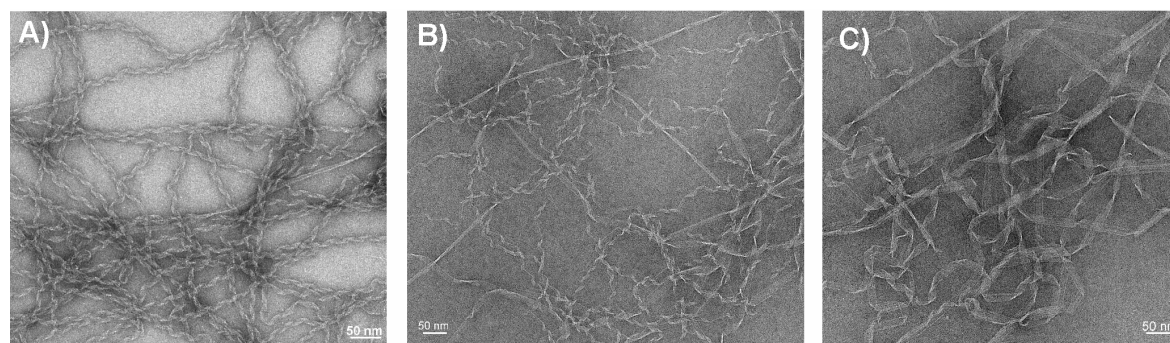


**Figure 7.36:** TEM micrographs of PTA stained fibrils of **A) VW18**, **B) VW18\_MfeGly 13**, and **C) VW18\_MfeGly 14**.



A further issue addressed by  $^{19}\text{F}$ -NMR concerns the substitution of positions 13 and 14 by MfeGly, as the two pairs of signals (*Figure 7.34 A/B*) exhibit slight differences in their chemical shifts. A small variation in the chemical environment is expected, given the different neighbouring residues in the  $\beta$ -strand. Slightly different folding rates have also been observed depending on the particular replaced position (*see Figure 7.31*). On the other hand, both analogues give rise to two components in the  $^{19}\text{F}$ -NMR spectra, with roughly the same intensity distribution. In the CODEX experiment (*Figure 7.35*), the decay of MfeGly in position 13 is similar to that in position 14. Overall, the  $^{19}\text{F}$ -NMR results suggest a rather similar architecture of the two peptide variants. In the end, despite the dramatic influence on the kinetics of fibril formation, the final fibril structure appears to be much less affected by the fluorine substitution.

### 7.5.6 The importance of the initial structure on amyloid formation rates

**VW18** is a two-state system having the opportunity to adopt two stable conformations ( $\alpha$ -helical coiled coil and  $\beta$ -sheet-rich amyloid fibrils). However, to compare the amyloid formation rates of all variants, the folding mechanism should be identical. If fluorine incorporation, for instance, alters the oligomerization state of the initial coiled coil, a potentially different folding mechanism could be assumed, which might not follow the same pathway of structural transition compared to unmodified **VW18**. To exclude that the observed folding rates of the fluorinated variants are the consequence of an altered initial coiled coil assembly, the oligomerization state was determined with SEC/SLS analysis. The variants containing TfeGly, DfeGly, MfeGly, and Leu in position 13 or 14, as well as the all-Leu variant initially form dimeric coiled coils (*Table 7.8, Figure 7.37, Figure 7.38*).

**Table 7.8:** Theoretical and experimentally determined molecular weights of **VW18** variants.

peptide	theoretical dimer mass [Da]	SEC/SLS determined mass [Da]
VW18	6286	6317 $\pm$ 539
VW18_TfeGly 13	6366	6277 $\pm$ 502
VW18_TfeGly 14	6366	6198 $\pm$ 475
VW18_DfeGly 13	6330	6160 $\pm$ 441
VW18_DfeGly 14	6330	5911 $\pm$ 654
VW18_MfeGly 13	6294	6055 $\pm$ 401
VW18_MfeGly 14	6294	6191 $\pm$ 495
VW18_Leu 13	6314	6092 $\pm$ 509
VW18_Leu 14	6314	6115 $\pm$ 488
VW18_Leu 3,13,14	6370	6203 $\pm$ 447

\* The oligomerization of the Tfv variants and the all-TfeGly variant could not be detected due to fast amyloid formation of these peptides.

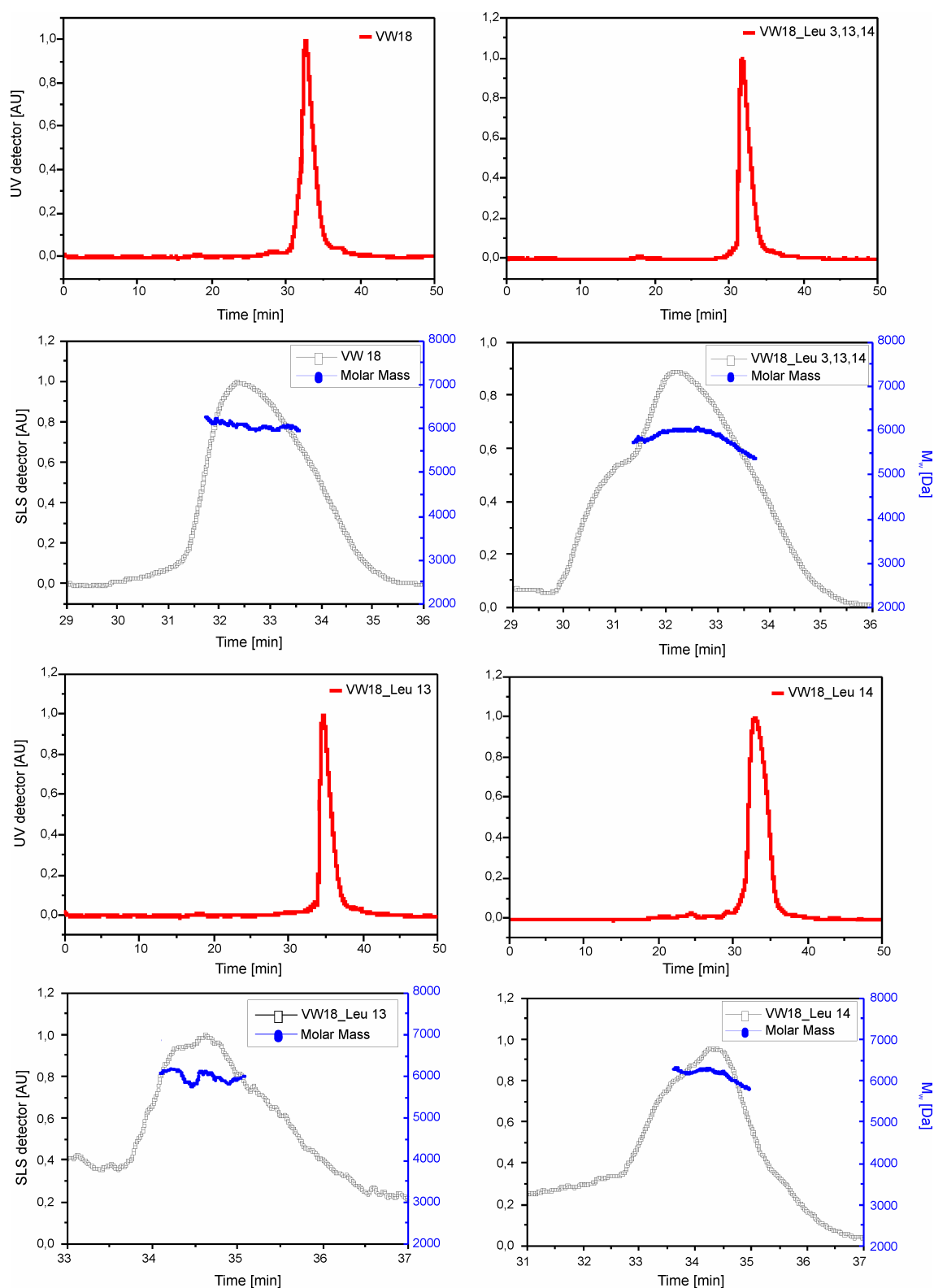


**Figure 7.37:** SEC/SLS chromatograms of **VW18**, the variants containing single Leu in either position 13 14, and of the all-Leu variant. Single peaks were detected with UV at 230 (red). Corresponding Rayleigh ratio (black) and molar mass distribution (blue) show an initial dimeric species for all peptides.

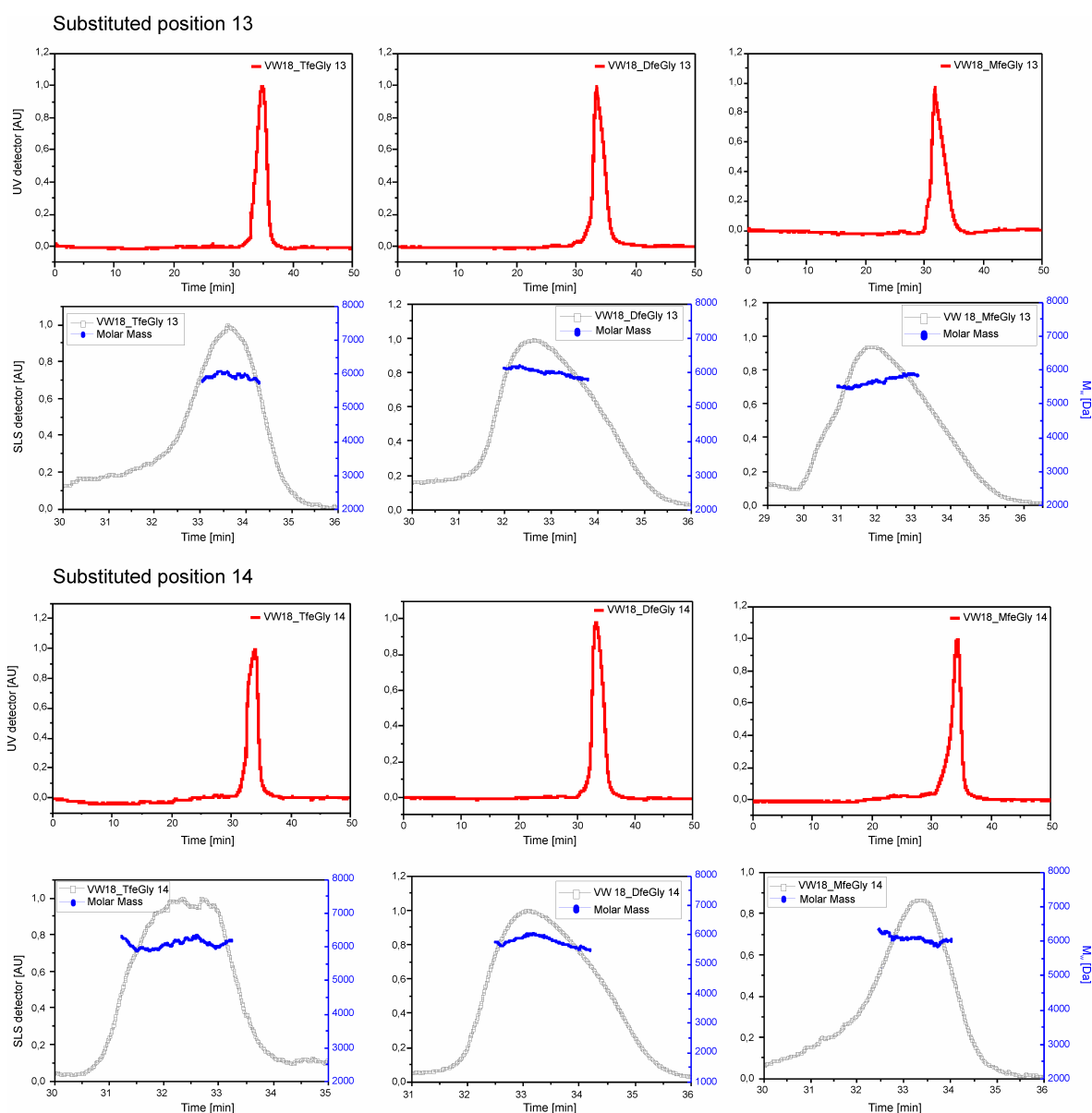


**Figure 7.38:** SEC/SLS chromatograms of **VW18** variants containing *TfeGly*, *DfeGly*, or *MfeGly* in either position 13 or 14. Single peaks were detected with UV at 230 (red). Corresponding Rayleigh ratio (black) and molar mass distribution (blue) show an initial dimeric species for all peptides.

Thus, the oligomerization state of the initial coiled coil was not affected by the substitution of the valine residues. However, helix propensity measurements revealed that the stability of the initial  $\alpha$ -helical structure was found to be strongly associated with the folding rates towards the  $\beta$ -sheet rich amyloid structure.

Two intrinsic properties of the particular incorporated amino acids influence the stability of the  $\alpha$ -helical starting structure; the hydrophobicity and the helix propensity. An amino acid with a high  $\alpha$ -helix propensity stabilizes the coiled coil structure, whereas placing a highly hydrophobic amino acid at the water exposed position 13 or 14 leads to destabilization due to unfavorable water exposure of the hydrophobic side chain. Thus, even slight differences in these two intrinsic properties of the particular incorporated amino acids can

affect the structural transition process. The bar chart (Figure 7.39) illustrates the relationships between  $\alpha$ -helix propensity and hydrophobicity for the studied fluorinated and nonfluorinated amino acids. It can easily be seen that the  $\alpha$ -helix propensities of the amino acids systematically decrease with increasing fluorine content, while the hydrophobicity gradually increases.

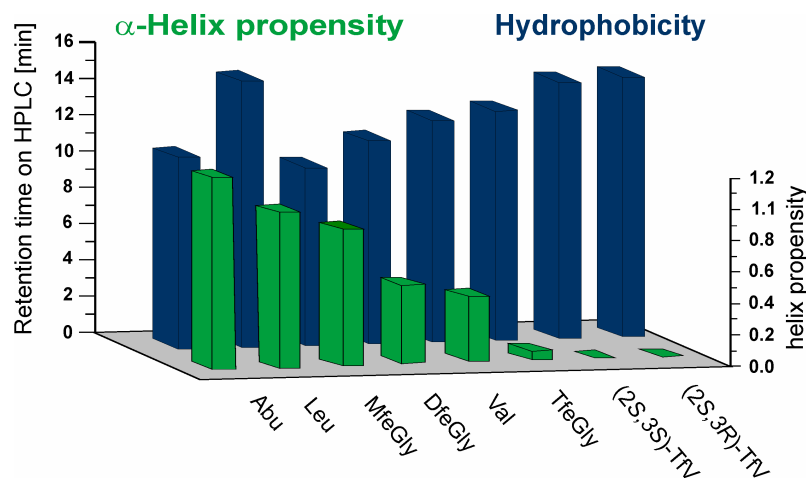


**Figure 7.39:** Relative comparison of selected hydrocarbon amino acids with their fluorinated analogues in terms of two intrinsic amino acid properties: helix propensity (green) and hydrophobicity (blue). The values for helix propensity and hydrophobicity are shown in Figure 7.24 and Table 7.5, respectively.

The exception is leucine, having both high  $\alpha$ -helix propensity and large hydrophobicity. The single leucine variants were found to aggregate faster into amyloids compared to the single MfeGly variants; even though leucine has a slightly higher  $\alpha$ -helix propensity compared to MfeGly (Table 7.6) and should, according to the previous statement, aggregate slower. The fact that leucine is much more hydrophobic compared to MfeGly (Figure 7.25 and Figure 7.39) offers a reasonable explanation for the enhanced amyloid formation rates of the single leucine variants. MfeGly possesses a strong dipole moment due to the electron-withdrawing single fluorine atom. This induced polarity makes MfeGly relatively hydrophilic, even more so than the nonfluorinated Abu derivative (Figure 7.25). Thus, MfeGly should be considered as a polar amino acid rather than a hydrophobic one. From the design of the ideal coiled coil, it is easily understandable that MfeGly is much better accommodated in a water exposed environment than is the hydrophobic leucine, thus explaining the greater stability of the MfeGly peptide in the initial coiled coil formation. In contrast, TfeGly has a very low  $\alpha$ -helix propensity (Figure 7.39 front row), lower than the substituted valine residue; hence, it destabilizes the initial  $\alpha$ -helical coiled coil structure. Peptide variants containing TfeGly therefore show fast structural transitions into  $\beta$ -sheet rich amyloids (Figure 7.31 A/B), although the size and hydrophobicity are

comparable to the replaced valine residue (*Figure 7.25*). This destabilizing effect is further enhanced when all three valines are replaced by TfeGly (*Figure 7.31 C*).

DfeGly possesses a similar  $\alpha$ -helix propensity compared to the replaced valine (*Table 7.6*) but is less hydrophobic (*Figure 7.39 back row*). Thus DfeGly containing peptides show similar or somewhat slower amyloid formation rates (*Figure 7.31 A/B*).

Amyloid formation rates were observed to depend on which residue is substituted, position 13 or 14. The overall structural conversion of peptides containing TfeGly and DfeGly in position 14 was found to be slower in comparison to the peptides containing the same amino acids in position 13. This position dependent effect might be explained by the different environments of the two positions in helical, as well as in fibril structures.  $^{19}\text{F}$ -NMR results also indicated such differences between the positions in the fibril structure. However, within each set of substitutions, the same trend of amyloid formation rates was found for both positions independently, which can be attributed to the particular incorporated amino acids and the subsequently altered intrinsic properties.

The influence of fluorine on amyloid formation has been systematically investigated using an engineered two-state model peptide. While fluorination shows only marginal effects on the structure itself, it significantly influences the kinetics of the structural transition. Since the complex process of amyloid formation is affected by many factors, any modification of the primary sequence requires a careful consideration of all intrinsic properties that could be potentially altered upon sequence variation. However, *de novo* designed peptide materials based on the self-assembly of amyloid-like structures could benefit from the variety of property modulations offered by the incorporation of fluorinated amino acids. Since fluorinated amyloid forming peptides have been rarely investigated so far, the results achieved from this study should offer valuable information for the design of such materials.



## 8 Summary

The aim of this thesis was to study the impact of fluorinated amino acids on amyloid formation. Secondary structure formation of peptides and proteins is strongly dictated by the intrinsic properties of the amino acids that make up the primary sequence. Aliphatic amino acids that are partially fluorinated have unique stereoelectronic and physicochemical properties that influence peptide conformation, stability, and folding behavior. Amyloid formation is a complex process that is caused by the interplay of several factors. A well studied model peptide (**VW18**) has been used to examine the influence of size, hydrophobicity, and secondary structure propensity on the amyloid formation process.

The model peptide **VW18** represents an ideal tool for this study, as it adopts a well defined  $\alpha$ -helical starting structure based on the design principles of a coiled coil folding motif, and can fold into  $\beta$ -sheet rich amyloids under specific conditions. The internal fibril architecture was elucidated by a systematic glycine- and proline-scanning approach. The concept of this study can be summarized according to *Figure 8.1*.

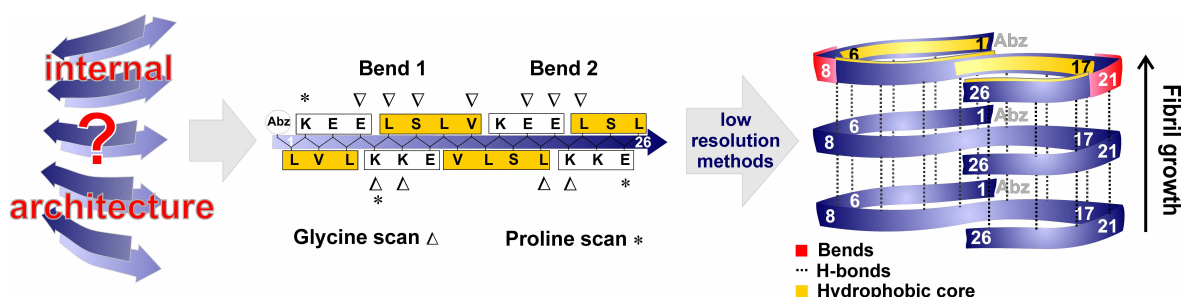


**Figure 8.1:** Concept of elucidating the internal fibril architecture of **VW18** by a systematic scan.

By glycine scanning two bend regions were identified in the sequence, within residues 7 – 9 and residues 19 – 21. With the help of proline substitutions at positions 2 and 25, the residues proximal to the N- and C-terminus, respectively, were found to be part of short  $\beta$ -sheet segments that are likely crucial for core packing within the amyloid fibril. Based on the findings a structural model was developed for **VW18**, representing the molecular arrangement within the protofilaments of the formed amyloid fibrils. The model consists of three extended  $\beta$ -strand segments, residues 1 – 6, residues 10 – 18, and residues 22 – 26, and two bend regions between. During proline substitution at a bend position of **VW18** these regions were found to differ from the turns typically found in  $\beta$ -hairpin-like structures. Whereas in  $\beta$ -hairpins  $\beta$ -strands are connected via intramolecular main chain H-bonds, in the plane of the turn, amyloid fibrils have their bend plane orthogonal to the fibril axis, and main chain H-bonds connect the individual  $\beta$ -strands in an intermolecular fashion.

With the help of two proline-glutamic acid chimeras that differ only in the configuration (*cis* or *trans*) of their side chain the sensitivity of the turn motif in  $\beta$ -hairpin structures were further evaluated. Even small alterations of the side chain were found to significantly influence the conformation of  $\beta$ -hairpin peptides. This strong influence can be attributed to an altered ring puckering of Pro due to the introduced electronegative side chain. The ring conformation of prolines within turn sequences dictates which  $\beta$ -hairpin type will be adopted. In future studies these building blocks should help to evaluate the influence that a side chain at a bend position has on amyloid formation potential of **VW18**.

A potential mechanism for the structural transition of **VW18** from the helical coiled coil motif toward the  $\beta$ -sheet rich amyloid structure was proposed by calculating the critical nucleus size that provides the basis for the amyloid formation process. The identified nucleus size of one indicates a disordered transition state during the structural transition of **VW18**. This nucleation process, which can be conceptualized according to *Figure 8.2*, includes disassembly of the initial dimeric coiled coil which can be understood as an energy barrier that the system must overcome. Reorganization of the unfolded monomers into a three stranded  $\beta$ -sheet containing the bend regions found in the Gly- and Pro-sequence has not yet been fully elucidated. Although the single  $\beta$ -strand motif is presumably unstable, it may serve as a template for further stacking  $\beta$ -sheets. This process can be regarded as energetically downhill, and could include a systematic structural reorganization towards the proposed model of the internal fibril architecture.

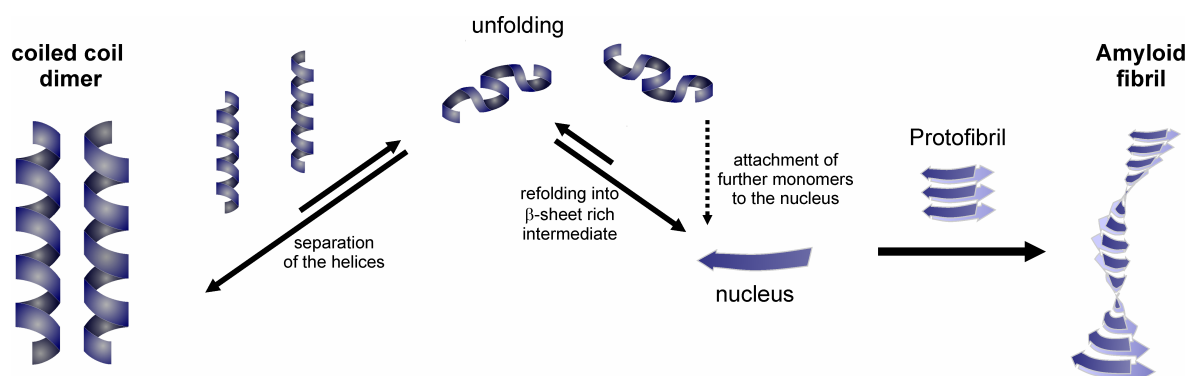


**Figure 8.2:** Suggested aggregation pathway of **VW18**. The nucleation phase includes the separation and unfolding of the coiled coil dimer and the refolding of the monomer into a  $\beta$ -sheet rich intermediate that serves as template for the attachment of further peptide strands.

The detailed structural information that were gained from **VW18** provided an ideal platform to study the influence of fluorinated amino acids on the process of amyloid formation.



The correlation of side chain volume and hydrophobicity of the utilized fluorinated amino acids MfeGly, DfeGly, TfeGly, (2S,3S)-TfV, (2S,3R)-TfV, and (2S,3S)-4'-TfL has been systematically evaluated. A RP-HPLC assay expressing this relation was previously established by our group.<sup>49</sup> This assay was expanded for the newly introduced fluorinated analogues of valine and isoleucine. The fluorinated amino acids were found, albeit being generally more hydrophobic than their hydrocarbon analogues, to be less hydrophobic than their surface area would suggest at first sight. This behavior results from the fact that fluoroalkyl side chains possess two seemingly contrary physicochemical properties, hydrophobicity and polarity which in combination explain the observed effects. The increasing polar character is exemplified by the monofluorinated amino acid MfeGly, which is actually less hydrophobic than the nonfluorinated parent Abu even though it possesses a larger side chain.

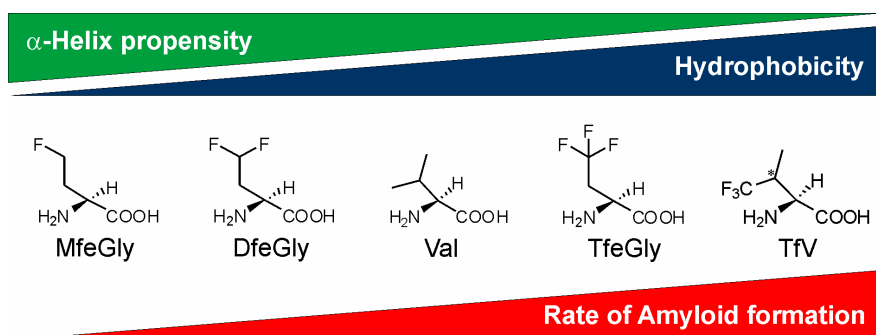
The  $\alpha$ -helix propensities of the fluorinated amino acids were determined and compared to aliphatic nonfluorinated amino acids. The observation that fluorinated amino acids contain reduced helix propensities compared to their hydrocarbon analogues, made previously,<sup>236</sup> was also true for the fluorinated amino acids investigated here. Additionally, the decrease in helix propensity was found to occur in a stepwise fashion. With an increase in the fluorine content per side chain for MfeGly, DfeGly, and TfeGly, additively reduced  $\alpha$ -helix propensity values were detected.

In terms of amyloid formation it was found that the fluorine content of fluorinated amino acids significantly influences the kinetics of this process. Two aggregation promoting valine residues in the primary sequence of **VW18** were systematically replaced by the fluorinated amino acids. A strong correlation between increasing fluorine content and amyloid formation was found. Differences in the intrinsic amino acid properties, like size (van der Waals volume), hydrophobicity, and  $\alpha$ -helix propensity of the fluorinated amino acids were carefully considered as factors that influence amyloid formation. The stability of the initial  $\alpha$ -helical coiled coil structure of **VW18** was found to be strongly influenced by the nature of the fluorinated amino acid, and the observed structural transition towards  $\beta$ -sheet-rich amyloids was attributed to a stabilization or destabilization of this initial state. The  $\alpha$ -helix propensity of the particularly incorporated amino acid was found to play a key role in the amyloid formation process of our two-state model system.

The final fibril structure, studied by solid-state <sup>19</sup>F-NMR of the variants containing MfeGly in either position 13 or 14, was shown to be much less affected by the substitutions than the amyloid formation rates. The fluorinated amino acid in the particular position of the sequence is exposed to two different chemical environments. The observed intensity ratio of 2:1 suggests two types of protofilaments, which is in good agreement with the formation of ribbons of three (two outer and one inner) protofilaments also found previously for

**VW18** fibrils in TEM-experiments. Contacts between the protofilaments were also indicated in spin diffusion experiments. Thus, with the help of solid state NMR studies it could be confirmed that the fibrils containing the MfeGly substitution seem to have the same overall architecture as the fibrils of **VW18**.

In conclusion, the impact of side chain fluorination on amyloid formation kinetics was successfully evaluated. Secondary structure propensities play a key role in amyloid formation and should, besides other properties of fluorinated amino acids, generally be considered in the design of fluorinated peptides and proteins. With these results, which can be summarized according to *Figure 8.3*, a credible prediction of the outcome of a peptide or protein modification with these investigated fluorinated amino acids within a  $\beta$ -sheet forming entity of arbitrary sequences may be possible for the first time.



If these amino acids are introduced at solvent-exposed positions of coiled coil sequences.

**Figure 8.3:** General observed trend for the amyloid formation rates of **VW18** variants, containing one of the displayed amino acid in position 13 or 14, which result from the interplay of the intrinsic properties of the particularly incorporated amino acid.

The results gained within this thesis complement the current understanding of fluorine's ability to modulate the structures and properties of peptides. This knowledge of how partially side chain fluorinated amino acids can influence conformation and the kinetics of structural transitions and amyloid formation will help to define general criteria for the design of fluorinated peptides with beneficial properties for medicinal and industrial applications.

## 9 Outlook

In the context of this thesis, the effect of fluorination of canonical aliphatic side chains on the formation of amyloid fibrils from an  $\alpha$ -helical starting structure in a peptide model system was determined. We used analogues of Abu that were fluorinated to different extents, and found that their  $\alpha$ -helical propensity decreases and their hydrophobicity increases with increasing fluorine content. Peptides containing higher degrees of fluorination tend to form amyloid fibrils faster, and this trend varies directly or inversely with the  $\alpha$ -helix propensity and hydrophobicity of the judiciously placed nonnatural building blocks. Future studies of these systems should focus on the following main aspects: a) additional structural studies, b) systematically introducing higher degrees of fluorination, c) investigating other peptide systems, especially sequences of known biomaterials, d) investigating the impact of fluorination on biologically and industrially relevant proteins, and e) exploiting fluorine's unique properties in analytical techniques at surfaces or membranes, especially in mixed peptide polymer systems.

a) Further structural investigations of **VW18** will be needed. Although the  $^{19}\text{F}$ -NMR results of the MfeGly variants seem to support our suggested internal fibril architecture of **VW18**, the model of the protofilaments is still based on conclusions drawn from low resolution techniques. Independent confirmation of the internal fibril packing could be achieved in solid state NMR-measurements of  $^{13}\text{C}$  or  $^{15}\text{N}$  labeled **VW18** variants. The successful elucidation of the **VW18** fibril structure would offer greater insight into our existing structural model by providing more detail on the arrangement of peptide strands inside the fibril. In addition the influence of the charged residues at the bend positions of **VW18** on the process of amyloid formation should be investigated by incorporating the two proline chimera into the sequence.

b) The extent to which fluorination can drive the formation of supramolecular aggregates, such as fibrils, remains to be determined, especially in the case of multiple fluorine atoms. In the present thesis, only one variant of **VW18** was synthesized that contained the highly fluorinated amino acid TfeGly in multiple positions of the sequence. For this variant, we observed an increased folding rate compared to the respective singly substituted variants. It could be valuable to test how further fluorination of the sequence influences the behavior of **VW18**, not only in terms of amyloids but also with respect to the initial coiled coil folding motif. The replacement of all leucine residues, providing the hydrophobic core of the coiled coil motif, would possibly lead to an assembly in which the core packing is

---

provided solely by fluorinated amino acids, similar to the GCN4 variant studied by Kumar.<sup>213</sup> The behavior of such so called 'Teflon proteins' in aqueous, organic, or fluorous solvents is certainly worth studying.<sup>442</sup> Depending on the solvent environment, perhaps the arrangement of the assembly could be controlled, analogous to the formation of several phases as observed in mixtures of water, organic, and fluorinated media.

c) Fluorine's impact on the structure and properties of peptide-based materials should be more broadly evaluated. Amyloids have been used for a variety of biomaterial applications (see *section 3.3*), and their assembly is known to mainly be driven by the hydrophobic effect. Partial or complete fluorination of the amino acid side chain strongly influences hydrophobicity and polarity, thus, fluorinated amino acids that differ with regard to this property could be used to fine tune the assembly behavior of amyloid forming peptides. This effect could be tested on a more synthetically accessible model, such as the amyloid stretch of the A $\beta$  protein, consisting of a sequence of only five amino acids (KLVFF). For this model, the  $\alpha$ -helix propensity values determined for our fluorinated amino acids could be neglected, as the short motif is unable to form helical conformations. Amyloid formation rates would, thus, mainly depend upon hydrophobicity/polarity and fluorine content of the particular amino acid.

d) A long-term goal would be the development of fluorinated proteins. Larger proteins are not accessible with solid phase peptide synthesis, instead their synthesis requires *in vivo* incorporation strategies. Efforts toward enabling the incorporation different fluorinated amino acids via tRNA activation are currently in progress in a collaboration project with the laboratory of Prof. Dr. N. Budisa (TU-Berlin).

e) Fluorine as an additional orthogonal functionality in fibril structures could also serve as a powerful tool. The most obvious application is its utility as a reporter group for analytical techniques, to follow processes like interactions with surfaces or membranes. Whether the fluorinated side chains displayed on the surface of a fibril could be used in specific interactions might be interesting to test. Highly fluorinated aliphatic hydrocarbon chains show specific noncovalent interactions. Such 'fluorous tags' have been used in many applications ranging from separation<sup>443,444</sup> and purification approaches<sup>445,446</sup> to large functional supramolecular complexes.<sup>447</sup> Perfluoroalkyl chains have also been used to modulate the self assembly of insulin upon complexation with Zn<sup>II</sup> and phenol which are based on intermolecular fluorous interactions.<sup>448</sup> Perfluorinated alkyl chains of varying length were attached to the amino side chain functionality of a C-terminal lysine residue. The peptide variants showed different scenarios of aggregation depending on the chain length of the particularly attached fluorous tag. The group of Prof. Dr. R. Haag (FU-Berlin)

---

has shown that large dendrimeric complexes can be formed via the interaction of perfluorinated alkyl chains.<sup>449</sup> The size of the complexes could be fine-tuned by varying the length of the fluorine tags. It could be interesting to test whether similar interactions could be achieved between fluorinated amyloid fibrils and fluorinated polymer chains. Fibrils consisting of parallel stacked  $\beta$ -sheets would contain the fluorinated amino acid at the same position of neighboring peptide strands. This would result in an alignment of the fluorinated side chains in a pearl necklace arrangement on the fibril surface. Perhaps these multiple fluorine side chains would resemble a perfluorinated alkyl chain and, thus, could also specifically interact with other perfluorinated molecules such as polymers or dendrimers. If fluorinated amino acids that typically contain one or two  $\text{CF}_3$ -groups are not sufficient for such an interaction, one could think of incorporating building blocks containing perfluorinated alkyl side chains into the peptide sequence.



## 10 Experimental Section

### 10.1 General Methods

Solvents used for peptide synthesis (DMF, NMP) were obtained 'synthesis grade' from VWR or Acros Organics. Water used for HPLC and to prepare buffers was purified with a MilliPore device. Acetonitrile (HPLC grade), Piperidine (99%, extra pure) and DIPEA (98%) were purchased from VWR or Acros Organics. TFA for HPLC (Uvasol® grade) and DBU (synthesis grade) were obtained from Merck.

Resins for peptide synthesis were purchased from NovaBiochem. Fmoc- and orthogonal side chain protected amino acids and coupling reagents were obtained from Iris Biotech, NovaBiochem, Fa. Gehardt, Sigma Aldrich, Opregen, or VWR and applied without further purification.

Solvents used for synthesis of the fluorinated amino acids were dried with the solvent purification system MB-SPS 800 from M. Braun, or freshly distilled according to standard laboratory methods.

All syntheses involving air- and moisture-sensitive compounds were carried out using standard Schlenk-type glassware under an atmosphere of argon.

$^1\text{H}$  and  $^{19}\text{F}$  NMR spectra were recorded at room temperature using a Bruker AC 250, JEOL ECX 400, JEOL Eclipse 500, or Bruker Advance 3 (700 MHz).  $^1\text{H}$  NMR and  $^{13}\text{C}$  NMR: chemical shift ( $\delta$ ) is given relative to TMS and referenced to the solvent signal.  $^{19}\text{F}$  NMR: chemical shift ( $\delta$ ) is given relative to  $\text{CFCl}_3$  (external reference). The order of citation in parentheses is a) multiplicity (s = singlet, d = doublet, t = triplet, q = quartet, m = multiplet, br = broad), b) coupling constant, c) number of nuclei, and d) assignment. Coupling constants ( $J$ ) are reported in Hertz (Hz).

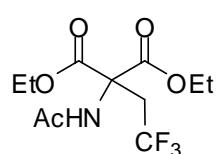
### 10.2 Synthesis of fluorinated amino acids

The fluorinated amino acid (S)-2-amino-4,4-difluorobutanoic acid (**DfeGly, (2)**) was synthesized according to Winkler *et al.*<sup>435</sup> and kindly provided as the Fmoc protected derivative by Dr. Cosimo D. Cadicamo.

### 10.2.1 Synthesis of (S)-2-amino-4,4,4-trifluorobutanoic acid (TfeGly) (**3**)<sup>433,236</sup>

#### 10.2.1.1 Synthesis of diethyl 2-acetamido-2-(2,2,2-trifluoroethyl) malonate (**3a**)

According to Tsushima *et al.*<sup>433</sup> diethyl 2-acetamido-2-(2,2,2-trifluoroethyl) malonate (1.0 eq.; 9.30 g, 43.0 mmol) and potassium tert-butoxide (1.0 eq.; 4.80 g, 43.0 mmol) were dissolved in dry THF (80 mL), heated to 60 °C and refluxed for approximately two hours. The mixture was cooled to room temperature, and trifluoromethyl 2,2,2-trifluoroethanesulfonate (1.1 eq.; 6.77 mL, 47.0 mmol) was added via cannula. The suspension was refluxed for two days. The mixture was cooled to room temperature and concentrated *in vacuo*. The reaction was quenched with 1M HCl (50 mL) and extracted with ethyl acetate (4 x 50 mL). The organic phases were combined, washed with water (2 x 20 mL), dried over sodium sulfate, and concentrated *in vacuo*. The crude product was purified by column chromatography on silica gel using a mixture of hexane and ethyl acetate (Hexane / EtOAc = 3:1) as eluent. The yellow solid was recrystallized from diethylether and hexane, and the product was obtained as white needle-like crystals. **Yield:** 5.40 g (23.6 mmol, 42%). The obtained spectra accorded to the literature.<sup>433</sup>

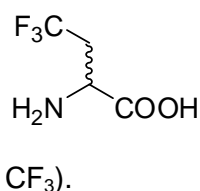


<sup>1</sup>H NMR (400 MHz, 298 K, CDCl<sub>3</sub>): δ [ppm] = 6.91 (s, 1H, NH), 4.27 (q,  $J_{\text{HH}} = 7.2$  Hz, 4H, 2 x CH<sub>2</sub>), 3.31 (q,  $J_{\text{HH}} = 10.5$  Hz, 2H, CH<sub>2</sub>CF<sub>3</sub>), 2.08 (s, 3H, COCH<sub>3</sub>), 1.28 (t,  $J_{\text{HH}} = 7.1$  Hz, 6H, 2 x CH<sub>3</sub>).

<sup>19</sup>F NMR (376 MHz, 298 K, CDCl<sub>3</sub>): δ [ppm] = -62.01 (t,  $^1J_{\text{HF}} = 5.3$  Hz, 3F, CF<sub>3</sub>).

#### 10.2.1.2 Synthesis of 2-amino-4,4,4-trifluorobutanoic acid (**3b**)

According to Tsushima *et al.*<sup>433</sup> compound **3a** (5.40 g, 23.6 mmol) was dissolved in concentrated HCl (5 mL) and refluxed overnight. The mixture was concentrated *in vacuo*, and the residue was lyophilized. **Yield:** 3.61 g (22.98 mmol, 97%) The obtained spectra accord to the literature.<sup>433</sup>



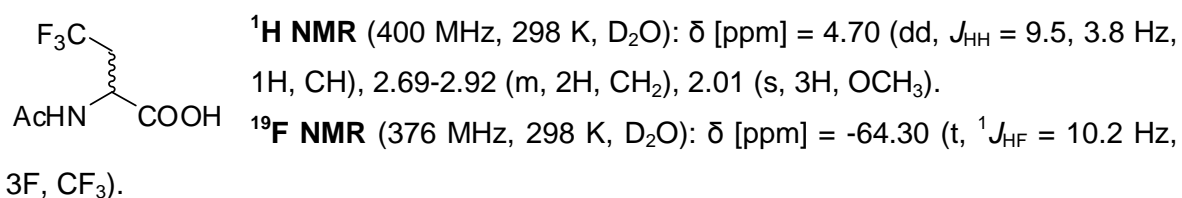
<sup>1</sup>H NMR (400 MHz, 298 K, D<sub>2</sub>O): δ [ppm] = 4.39 (dd,  $J_{\text{HH}} = 8.1, 4.0$  Hz, 1H, CH), 2.89-3.13 (m, 2H, CH<sub>2</sub>).

<sup>19</sup>F NMR (376 MHz, 298 K, D<sub>2</sub>O): δ [ppm] = -64.06 (t,  $^1J_{\text{HF}} = 10.2$  Hz, 3F, CF<sub>3</sub>).



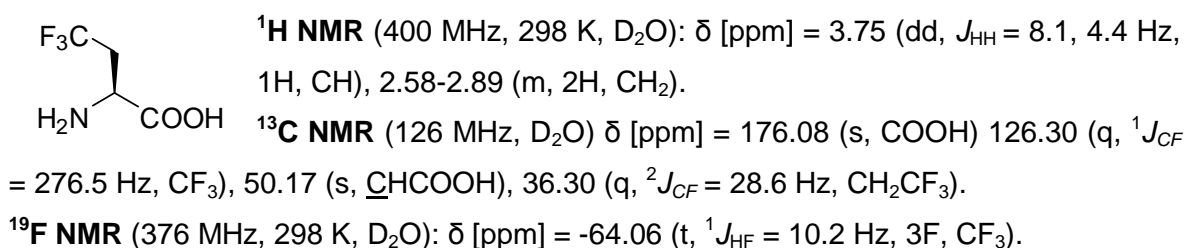
### 10.2.1.3 Synthesis of 2-acetamido-4,4,4-trifluorobutanoic acid (**3c**)<sup>236</sup>

According to Chiu *et al.*<sup>236</sup> the racemic amino acid **3b** (1.0 eq.; 2.60 g, 16.6 mmol) was dissolved in water (50 mL, Millipore) and the pH was adjusted to 9. The solution was cooled to 0 °C in an ice bath. Acetic anhydride (1.0 eq.; 1.72 mL, 18.2 mmol) was added dropwise, and the pH was adjusted to 8-9 using a WTW pH526 pH-meter and an InLab® microelectrode (Mettler Toledo). The mixture was stirred for 30 min in an ice bath, warmed to room temperature, and stirred another two hours at room temperature. Then the reaction was slowly acidified to pH 2 using conc. HCl, and extracted with ethyl acetate (5 x 50 mL). The organic layers were combined, dried over sodium sulfate, and concentrated *in vacuo*. The product was obtained as a white solid. **Yield:** 2.00 g (10.1 mmol, 61%) The obtained spectra accord to the literature.<sup>236</sup>



### 10.2.1.4 Synthesis of (S)-2-amino-4,4,4-trifluorobutanoic acid (**3d**)<sup>236</sup>

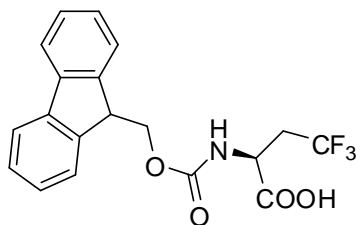
According to Chiu *et al.*<sup>236</sup> the N-acetylated amino acid **3c** (1.0 eq.; 2.00 g, 10.1 mmol) was dissolved in water (Millipore) to give a 50 mM final concentration. The pH was first adjusted to 11 using 1N NaOH, then adjusted to pH 7 using 10% AcOH, to produce a buffer system. Acylase I (0.10 g, grade II, 553 units / mg) was allowed to hydrate for 5 min in 5 mL water, after which it was added to the amino acid solution. The pH was readjusted to 7.0 using 0.1% AcOH or 0.01 N NaOH. The mixture was gently stirred at 36 °C for a few hours, then overnight at room temperature. The mixture was brought to pH 4 using 10% AcOH and filtered through an ion exchange resin (Dowex 50W X8; 100-200 mesh). The resin was washed with Millipore water until the eluting solution had a neutral pH. Afterwards the free L-amino acid was eluted from the resin using 1N NH<sub>3</sub>. All fractions containing amino acid (positive Ninhydrin reaction) were combined, and the product lyophilized. The product was obtained as a white powder. **Yield:** 0.76 g (4.84 mmol, 48%)



### 10.2.1.5 Synthesis of (S)-2-(((9H-fluoren-9-yl)methoxy)carbonylamino)-4,4,4-trifluorobutanoic acid (**3e**)<sup>236</sup>

According to Chiu *et al.*<sup>236</sup> the L-enantiomer of amino acid **3d** (1.0 eq.; 0.76 g, 4.84 mmol) was dissolved in 10% Na<sub>2</sub>CO<sub>3</sub> (5 mL) and cooled to 0 °C using an ice bath. Dioxane (1 mL) was added dropwise via cannula. After stirring the suspension for 15 min at 0 °C, Fmoc-succinimide (1.1 eq.; 1.79 g, 5.32 mmol) was added. The mixture was stirred for three hours at 0 °C, then at room temperature overnight.

The reaction was quenched with water (50 mL) and extracted with diethylether (1x 50 mL). The aqueous phase was cooled in an ice-bath and the pH was carefully adjusted to 2 using conc. HCl. Precipitation of a white solid was observed. The suspension was extracted with DCM (4 x 50 mL), and the combined organic phases were washed with water (1 x 50 mL), dried over sodium sulfate, and concentrated *in vacuo*. The crude product was purified using preparative HPLC (Knauer; see section 10.2.5) with a Phenomenex ® Luna C8 10 µm (250 mm x 21.2 mm) reverse phase column. HPLC runs were performed with a flow rate of 20 mL/min applying a linear eluent gradient of H<sub>2</sub>O (solvent A) and ACN (solvent B) containing 0.1% TFA (solvent B: 30% → 100% in 30 min), with UV-detection at λ<sub>abs</sub> = 280 nm. The fractions containing the pure Fmoc-amino acid were combined and ACN was removed *in vacuo*. The pure product was obtained as a white solid after lyophilization and identified by ESI-ToF MS. **Yield:** 1.43 g (3.77 mmol, 78%).



**<sup>1</sup>H NMR** (400 MHz, 298 K, CDCl<sub>3</sub>): δ [ppm] = 7.77 (d, *J*<sub>HH</sub> = 7.5 Hz, 2H, Ar (Fmoc)), 7.58 (d, *J*<sub>HH</sub> = 7.4 Hz, 2H, Ar (Fmoc)), 7.42 (t, *J*<sub>HH</sub> = 7.4 Hz, 2H, Ar (Fmoc)), 7.38 (t, *J*<sub>HH</sub> = 7.4, 1.0 Hz, 2H, Ar (Fmoc)), 5.53 (d, *J*<sub>HH</sub> = 9.4 Hz, 1H, NH), 4.64 (dd, *J*<sub>HH</sub> = 8.1, 4.4 Hz, 1H, CH), 4.42-4.25 (m, 2H, COOCH<sub>2</sub> (Fmoc)), 4.23 (t, *J*<sub>HH</sub> = 6.1 Hz, 1H, COOCH<sub>2</sub>CH (Fmoc)), 2.85-2.72 (m, 2H, CH<sub>2</sub>CF<sub>3</sub>).

**<sup>13</sup>C NMR** (126 MHz, CDCl<sub>3</sub>) δ [ppm] = 168.75 (s, COOH), 151.67 (s, C=O), 142.54 (s, Ar-C), 141.42 (s, Ar-C), 128.33 (s, Ar-C), 127.91 (q, <sup>1</sup>*J*<sub>CF</sub> = 276.2 Hz, CF<sub>3</sub>), 127.56 (s, Ar-C), 125.33 (s, Ar-C), 120.29 (s, Ar-C), 73.06 (s, COOCH<sub>2</sub>CH), 57.37 (s, HO<sub>2</sub>CCH), 46.46 (s, CHCOOH), 25.56 (q, <sup>2</sup>*J*<sub>CF</sub> = 28.2 Hz, CH<sub>2</sub>CF<sub>3</sub>).

**<sup>19</sup>F NMR** (376 MHz, 298 K, CDCl<sub>3</sub>): δ [ppm] = -62.92 (t, <sup>1</sup>*J*<sub>HF</sub> = 10.2 Hz, 3 F, CF<sub>3</sub>).

**HRMS (ESI):** found *m/z*: 378.1091, calcd. for [C<sub>19</sub>H<sub>15</sub>F<sub>3</sub>NO<sub>4</sub>]<sup>-</sup>: 378.0959.

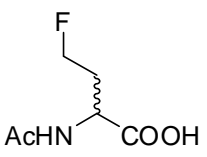
## 10.2.2 Synthesis of (S)-2-amino-4-fluorobutanoic acid (MfeGly) (1)

An enantiomeric mixture of the tert-butylester (4-amino-6-fluoro-2,2-dimethylhexan-3-one) was synthesized by Malte Behrends,<sup>450,436</sup> and kindly provided by the group of Prof. Dr. G. Haufe (University of Muenster) for this study.

### 10.2.2.1 2-acetamido-4-fluorobutanoic acid (1a)

4-amino-6-fluoro-2,2-dimethylhexan-3-one (1.0 eq.; 0.3 g, 1.7 mmol) was dissolved in DCM (10 mL) and cooled to 0 °C using an ice bath. After adding DIPEA (1.0 eq; 0.29 mL, 1.7 mmol) via cannula and freshly distilled acetic anhydride (1.1 eq.; 177  $\mu$ L, 1.87 mmol) dropwise using a 200 mL Eppendorf® pipette, the mixture was stirred for three hours at room temperature. The mixture was quenched with 0.1 M HCl (50 mL) and extracted with ethyl acetate (4 x 50 mL). The organic phases were combined, dried over sodium sulfate, and concentrated *in vacuo*.

The residue was stirred in DCM / TFA (3 mL / 3 mL) for three hours at room temperature and the solvent was removed *in vacuo*. The residue was dissolved in distilled water (50 mL). The pH was adjusted to 2 using 0.1 M HCl and the product extracted with ethyl acetate (4 x 50 mL). The organic phases were combined, dried over sodium sulfate, and concentrated *in vacuo*. The product was obtained as a yellow solid. Yield: 0.27 g (1.65 mmol, 97%), crude, over two steps.

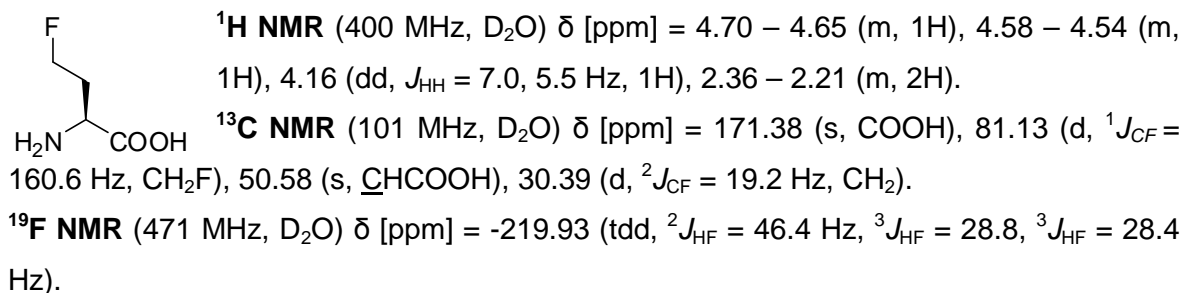
 **<sup>1</sup>H NMR** (400 MHz, 298 K, D<sub>2</sub>O):  $\delta$  [ppm] = 6.74 (d,  $J_{\text{HH}}$  = 6.9 Hz, 1H, NH), 4.75 (dd,  $J_{\text{HH}}$  = 12.3, 6.6 Hz, 1H, CH), 4.66 (t,  $J_{\text{HH}}$  = 5.0 Hz, 1H, CH<sub>2</sub>F), 4.54 (t,  $J_{\text{HH}}$  = 5.0 Hz, 1H, CH<sub>2</sub>F), 2.42-2.29 (m, 2H, CH<sub>2</sub>), 2.14 (s, 3H, CH<sub>3</sub>).

**<sup>13</sup>C NMR** (126 MHz, D<sub>2</sub>O)  $\delta$  [ppm] = 175.32 (s, COOCH<sub>3</sub>), 174.44 (s, COOH), 81.35 (d,  $^1J_{\text{CF}}$  = 160.7 Hz, CH<sub>2</sub>F), 49.80 (s, CHCOOH), 31.49 (d,  $^2J_{\text{CF}}$  = 19.8 Hz, CH<sub>2</sub>), 21.76 (s, CH<sub>3</sub>).

**<sup>19</sup>F NMR** (471 MHz, D<sub>2</sub>O)  $\delta$  [ppm] = -219.98 (tdd,  $^2J_{\text{HF}}$  = 46.8 Hz,  $^3J_{\text{HF}}$  = 23.1,  $^3J_{\text{HF}}$  = 23.9 Hz).

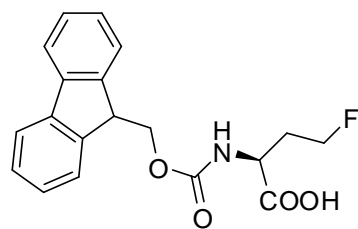
### 10.2.2.2 Synthesis of (S)-2-amino-4-fluorobutanoic acid (1b)

2-acetamido-4-fluorobutanoic acid **1a** (0.27 g, 1.65 mmol) was dissolved in water (30 mL, Millipore), and the separation of the two enantiomers was accomplished similar to the procedure described in for TfeGly (section 9.3.1.4). **Yield:** 94.4 mg (0.78 mmol, 47%).



### 10.2.2.3 Synthesis of (S)-2-(((9H-fluoren-9-yl)methoxy)carbonylamino)-4-fluorobutanoic acid (1c)

The Fmoc protection of the free L-amino acid was conducted similar to the procedure described in section 10.3.1.5. **Yield:** 208.4 mg (0.61 mmol, 78%).



**<sup>1</sup>H NMR** (500 MHz, 298 K, CDCl<sub>3</sub>): δ [ppm] = 7.76 (d,  $J_{\text{HH}} = 7.2$  Hz, 2H, Ar (Fmoc)), 7.58 (d,  $J_{\text{HH}} = 7.2$  Hz, 2H, Ar (Fmoc)), 7.40 (t,  $J_{\text{HH}} = 7.3$  Hz, 2H, Ar (Fmoc)), 7.31 (t,  $J_{\text{HH}} = 7.4$  Hz, 2H, Ar (Fmoc)), 5.37 (d,  $J_{\text{HH}} = 5.7$  Hz, 1H, NH), 4.41 (t,  $J_{\text{HH}} = 7.1$  Hz, 1H, COOCH<sub>2</sub>CH (Fmoc)), 4.27 – 4.17 (m, 2H, COOCH<sub>2</sub> (Fmoc)) 4.08-4.02 (m, 2H, CH<sub>2</sub>F), 3.47 (dd,  $J_{\text{HH}} = 11.7, 5.8$  Hz, 1H, CH), 2.61-2.59 (m, 2H, CH<sub>2</sub>).

**<sup>13</sup>C NMR** (126 MHz, CDCl<sub>3</sub>) δ [ppm] = 174.51 (s, COOH), 154.83 (s, COOCH<sub>2</sub>), 144.39 (s, Ar-C), 141.63 (s, Ar-C), 127.70 (s, Ar-C), 127.19 (s, Ar-C), 124.78 (s, Ar-C), 120.17 (s, Ar-C), 80.35 (d,  $^1J_{\text{CF}} \sim 160$  Hz, CH<sub>2</sub>F), 65.27 (s, COOCH<sub>2</sub>CH), 50.43 (CHCOOH), 31.79 (d,  $^2J_{\text{CF}} = 19.4$  Hz, CH<sub>2</sub>).

**<sup>19</sup>F NMR** (471 MHz, CDCl<sub>3</sub>) δ [ppm] = -219.96 (tdd,  $^2J_{\text{HF}} = 40.5$  Hz,  $^3J_{\text{HF}} = 22.9$ ,  $^3J_{\text{HF}} = 23.1$  Hz).

**HRMS (ESI):** found m/z: 342.1162, calcd. for [C<sub>19</sub>H<sub>17</sub>FNO<sub>4</sub>]: 342.1147.

### 10.2.3 Synthesis of Fmoc protected TfV and TfI

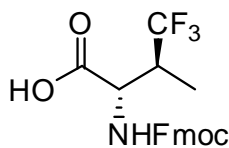
The enantiomerically pure, Boc protected amino acids (2S, 3S)-TfV, (2S, 3R)-TfV, and (2S, 3R)-4'-TfI were synthesized by Holger Erdbrink,<sup>241</sup> and kindly provided by the group of PD. Dr. C. Czekelius (Freie Universität Berlin). Boc deprotection and Fmoc protection was accomplished for all three amino acids according to the following general procedure:

The Boc protected amino acids were stirred in a 1:1 mixture of DCM / TFA for three hours at room temperature. DCM and TFA were removed under reduced pressure. The remaining brown oil was dissolved in 10% Na<sub>2</sub>CO<sub>3</sub> and Dioxane. The mixture was cooled

to 0 °C, and 1.1 eq. Fmoc-OSu was added. The reaction was stirred for three hours at 0 °C, then overnight at room temperature. The reaction was quenched with water and acidified with HCl to pH 2. The aqueous phase was extracted with DCM (4 x 50 mL). The combined organic phases were dried over sodium sulfate, filtered, and concentrated *in vacuo*. The crude product was purified by reversed-phase preparative HPLC using linear CH<sub>3</sub>CN/H<sub>2</sub>O gradients containing 0.1% trifluoroacetic acid (TFA), and identified by ESI-ToF MS.

### 10.2.3.1 Synthesis of (2S,3S)-2-(((9H-fluoren-9-yl)methoxy)carbonyl)amino)-4,4,4-trifluoro-3-methylbutanoic acid (4)

According to the described general procedure, the corresponding Boc protected amino acid (120 mg, 0.443 mmol) was stirred in DCM / TFA (3 mL / 3 mL) for three hours at room temperature, and the solvent was removed *in vacuo*. The residue was dissolved in 10% Na<sub>2</sub>CO<sub>3</sub> and dioxane, cooled to 0 °C, and Fmoc-OSu (164,2 mg, 0,487 mmol) was added. After stirring the reaction mixture overnight, and the subsequent workup, the product was obtained as a white solid. **Yield:** 63.4 mg (0.161 mmol, 36%).



**<sup>1</sup>H NMR** (500 MHz, 298 K, CDCl<sub>3</sub>): δ [ppm] = 7.76 (d, *J*<sub>HH</sub> = 7.5 Hz, 2H, Ar (Fmoc)), 7.58 (d, *J*<sub>HH</sub> = 7.3 Hz, 2H, Ar (Fmoc)), 7.40 (t, *J* = 7.4 Hz, 2H, Ar (Fmoc)), 7.31 (t, *J*<sub>HH</sub> = 7.5, 1.0 Hz, 2H, Ar (Fmoc)), 5.42 (d, *J*<sub>HH</sub> = 9.4 Hz, 1H, NH), 4.89 (dd, *J*<sub>HH</sub> = 9.2, 2.8 Hz, 1H, CHCO<sub>2</sub>H), 4.63-4.34 (m, 2H, COOCH<sub>2</sub> (Fmoc)), 4.24 (t, *J*<sub>HH</sub> = 7.0 Hz, 1H, COOCH<sub>2</sub>CH (Fmoc)), 3.02-2.85 (m, 1H, CHCF<sub>3</sub>), 1.21 (d, *J*<sub>HH</sub> = 7.2 Hz, 3H, CH<sub>3</sub>).

**<sup>13</sup>C NMR** (101 MHz, Acetone-D<sub>6</sub>): δ [ppm] = 173.45 (s, COOH), 157.09 (s, COOCH<sub>2</sub>), 143, 62 (s, Ar-C), 142.05 (s, Ar-C), 128.32 (s, Ar-C), 128.20 (q, <sup>1</sup>*J*<sub>FC</sub> ~ 280 Hz, CF<sub>3</sub>), 127.89 (s, Ar-C), 125.46 (s, Ar-C), 120.71 (s, Ar-C), 67.46 (s, CO<sub>2</sub>CH<sub>2</sub>CH), 53.34 (m<sub>C</sub>, HO<sub>2</sub>CCH), 47.80 (s, CO<sub>2</sub>CH<sub>2</sub>CH), 40.16 (q, <sup>2</sup>*J*<sub>FC</sub> = 26.5 Hz), 8.67 (q, <sup>1</sup>*J* = 2.4 Hz, CH<sub>3</sub>).

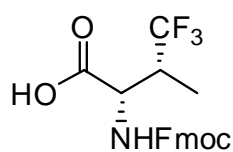
**<sup>19</sup>F NMR** (376 MHz, 298 K, CDCl<sub>3</sub>): δ [ppm] = -70.5 (d, *J*<sub>HF</sub> = 8.6 Hz, 3F, CF<sub>3</sub>).

**HRMS (ESI):** found *m/z*: 393.1197, calcd. for [C<sub>20</sub>H<sub>18</sub>F<sub>3</sub>NO<sub>4</sub>]<sup>-</sup>: 393.1188.

### 10.2.3.2 Synthesis of (2S,3R)-2-(((9H-fluoren-9-yl)methoxy)carbonyl)amino)-4,4,4-trifluoro-3-methylbutanoic acid (5)

According to the described general procedure, the corresponding Boc protected amino acid (150 mg, 0.553 mmol) was stirred in DCM / TFA (3 mL / 3mL) for three hours at room temperature, and the solvent was removed *in vacuo*. The residue was dissolved in 10% Na<sub>2</sub>CO<sub>3</sub> and dioxane, cooled to 0 °C, and Fmoc-OSu (205.3 mg, 0,609 mmol) was added.

After stirring the reaction mixture overnight, and the subsequent workup, the product was obtained as a white solid. **Yield:** 65.2 mg (0.166 mmol, 30%).



**<sup>1</sup>H NMR** (500 MHz, 298 K, CDCl<sub>3</sub>): δ [ppm] = 7.76 (d,  $J_{\text{HH}} = 7.4$  Hz, 2H, Ar (Fmoc)), 7.58 (d,  $J_{\text{HH}} = 7.2, 2.6$  Hz, 2H, Ar (Fmoc)), 7.40 (t,  $J_{\text{HH}} = 7.4$  Hz, 2H, Ar (Fmoc)), 7.31 (t,  $J_{\text{HH}} = 7.4$  Hz, 2H, Ar (Fmoc)), 5.36 (d,  $J_{\text{HH}} = 9.7$  Hz, 1H, NH), 4.68 (dd,  $J_{\text{HH}} = 9.8, 3.7$  Hz, 1H,  $\text{CHCO}_2\text{H}$ ), 4.49-4.37 (m, 2H,  $\text{COOCH}_2$  (Fmoc)), 4.24 (t,  $J_{\text{HH}} = 7.0$  Hz, 1H,  $\text{COOCH}_2\text{CH}$  (Fmoc)), 3.07 (m, 1H,  $\text{CHCF}_3$ ), 1.27 (d,  $J_{\text{HH}} = 7.2$  Hz, 3H,  $\text{CH}_3$ ).

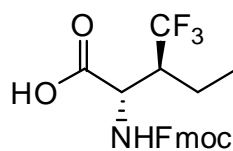
**<sup>13</sup>C NMR** (101 MHz, Acetone-D<sub>6</sub>): δ [ppm] = 171.20 (s, COOH), 157.17 (s,  $\text{COOCH}_2$ ), 144, 91 (s, Ar-C), 142.04 (s, Ar-C), 128.54 (s, Ar-C), 128.27 (q,  $^1J_{\text{FC}} \sim 280$  Hz,  $\text{CF}_3$ ), 127.91 (s, Ar-C), 126.13 (s, Ar-C), 120.80 (s, Ar-C), 67.58 (s,  $\text{CO}_2\text{CH}_2\text{CH}$ ), 54.58 (m,  $\text{HO}_2\text{CCH}$ ), 47.87 (s,  $\text{CO}_2\text{CH}_2\text{CH}$ ), 40.94 (q,  $^2J_{\text{FC}} = 25.8$  Hz,  $\text{CHCF}_3$ ), 11.19 (q,  $^1J = 2.7$  Hz,  $\text{CH}_3$ ).

**<sup>19</sup>F NMR** (376 MHz, 298 K, CDCl<sub>3</sub>): δ [ppm] = -68.08 (d,  $J_{\text{HF}} = 8.5$  Hz, 3F,  $\text{CF}_3$ ).

**HRMS (ESI):** found  $m/z$ : 393.1120, calcd. for [C<sub>20</sub>H<sub>18</sub>F<sub>3</sub>NO<sub>4</sub>]: 393.1188.

### 10.2.3.3 Synthesis of (2R,3R)-2-(((9H-fluoren-9-yl)methoxy)carbonyl)amino)-4,4,4-trifluor-3-methylbutanoic acid (6)

According general procedure 7, the corresponding Boc protected amino acid (100 mg, 0.351 mmol) was stirred in DCM / TFA (3 mL / 3 mL) for three hours at room temperature, and the solvent was removed *in vacuo*. The residue was dissolved in 10% Na<sub>2</sub>CO<sub>3</sub> and dioxane, cooled to 0 °C, and Fmoc-OSu (130.1 mg, 0.386 mmol) was added. After stirring the reaction mixture overnight, and the subsequent workup, the product was obtained as a white solid. **Yield:** 116.7 mg (0.287 mmol, 82%).



**<sup>1</sup>H NMR** (500 MHz, 298 K, CDCl<sub>3</sub>): δ [ppm] = 7.76 (d,  $J_{\text{HH}} = 7.5$  Hz, 2H, Ar (Fmoc)), 7.57 (d,  $J_{\text{HH}} = 7.4$  Hz, 2H, Ar (Fmoc)), 7.40 (t,  $J_{\text{HH}} = 7.5$  Hz, 2H, Ar (Fmoc)), 7.31 (t,  $J_{\text{HH}} = 7.4$  Hz, 2H, Ar (Fmoc)), 5.42 (d,  $J_{\text{HH}} = 9.2$  Hz, 1H, NH), 4.89 (dd,  $J_{\text{HH}} = 9.3, 2.4$  Hz, 1H,  $\text{CHCO}_2\text{H}$ ), 4.43 (m, 2H,  $\text{COOCH}_2$  (Fmoc)), 4.24 (t,  $J_{\text{HH}} = 7.0$  Hz, 1H,  $\text{COOCH}_2\text{CH}$  (Fmoc)), 2.72 (m, 1H,  $\text{CHCF}_3$ ), 1.81 (tt,  $J_{\text{HH}} = 14.5, 7.4$  Hz, 1H,  $\text{CH}_2\text{CH}_3$ ), 1.66 (tt,  $J_{\text{HH}} = 14.7, 7.4$  Hz, 1H,  $\text{CH}_2\text{CH}_3$ ), 1.09 (t,  $J_{\text{HH}} = 7.4$  Hz, 3H,  $\text{CH}_3$ ).

**<sup>13</sup>C NMR** (126 MHz, Acetone-D<sub>6</sub>) δ [ppm] = 206.26 (s), 171.77 (s, COOH), 156.91 (s,  $\text{COOCH}_2$ ), 144.67 (s, Ar-C), 141.81 (s, Ar-C), 128.31 (s, Ar-C), 128.14 (q,  $^1J_{\text{CF}} \sim 280$  Hz,  $\text{CF}_3$ ), 127.69 (s, Ar-C), 125.92 (s, Ar-C), 120.56 (s, Ar-C), 67.32 (s,  $\text{CO}_2\text{CH}_2\text{CH}$ ), 52.58

(m<sub>c</sub>, HO<sub>2</sub>CCH), 47.65 (s, CO<sub>2</sub>CH<sub>2</sub>CH), 46.65 (q, <sup>2</sup>J<sub>CF</sub> = 23.9 Hz, CHCF<sub>3</sub>), 18.19 (s, CH<sub>2</sub>CH<sub>3</sub>), 12.08 (s, CH<sub>3</sub>).

<sup>19</sup>F NMR (471 MHz, 298 K, CDCl<sub>3</sub>): δ [ppm] = -67.8 (d, J<sub>HF</sub> = 8.3 Hz, 3F, CF<sub>3</sub>).

HRMS (ESI): found *m/z*: 407.0975, calcd. for [C<sub>21</sub>H<sub>20</sub>F<sub>3</sub>NO<sub>4</sub>]<sup>-</sup>: 407.1344.

## 10.3 Peptide synthesis, purification and characterization

### 10.3.1 Automated peptide synthesis

All peptides were synthesized from the C-terminal to the N-terminal end using the following protected derivatives of the standard canonical amino acids:

Fmoc-L-Ala-OH (alanine), Fmoc-L-Glu(OtBu)-OH (glutamic acid), Fmoc-L-Gly-OH (glycine), Fmoc-L-Ile-OH (isoleucine), Fmoc-L-Leu-OH (leucine), Fmoc-L-Lys-OH (lysine), Fmoc-L-Pro-OH (proline), Fmoc-L-Ser(tBu)-OH (serine), Fmoc-L-Thr(tBu)-OH (threonine), Fmoc-L-Trp(tBu)-OH (tryptophan), Fmoc-L-Tyr(tBu)-OH (tyrosine), Fmoc-Val-OH (valine).

All fluorinated and non-fluorinated variants of **VW18**, and all **KXaa**-analogues, were synthesized according to the standard Fmoc strategy using 10 mL polypropylene reactors in a Multi-Syntech Syro XP peptide synthesizer (MultiSynTech GmbH, Witten, Germany).

For the **VW18** variants, a preloaded Fmoc-Leu-OWang resin (0.64 mmol/g, 0.05 mmol scale) or preloaded Fmoc-Leu-NovaSyn®TGA resin (0.2 mmol/g, 0.05 mmol scale) was used. All **VW18** derivatives were N-terminally labeled with anthranilic acid (Abz) to enable photometric concentration determination.

For the **KXaa**-peptides that were used for α-helix propensity measurements, a NovaSyn®TGR-resin was preloaded with the first amino acid Fmoc-Lys(Boc)-OH (0.23 mmol/g, 0.025 mmol scale). The N-terminal amino group was acetylated using acetic anhydride (*see capping, section 10.3.3*)

All peptides were synthesized using 4 eq. of Fmoc-amino acid. C-terminal activation was carried out using 4 eq. TBTU / HOBt and 8 eq. DIPEA. Fmoc deprotection was achieved by treatment of the resin with 2% piperidine and 2% DBU (4x5 min). The chaotropic salt NaClO<sub>4</sub><sup>-</sup> (0.8 mM) was added to the dissolved amino acid to avoid on-resin aggregation during peptide synthesis. The standard protocol applied with the particular synthesizer is given in *Table 10.1*.

The fluorinated amino acid, and the residue immediately succeeding it in the sequence, were coupled manually using 2 eq. amino acid and HOAt / DIC activation with coupling times of 2 x 8 h.

**Table 10.1:** SPPS standard protocol applied on Multi-Syntech Syro XP peptide synthesizer.

procedure		reagent	duration
Double coupling start	swelling	2.5 mL DMF	2 x 15 min
	Fmoc deprotection	2 mL 2% Pip / 2% DBU in DMF	4 x 5 min
	washing	2.5 mL DMF	6 x 1 min
Double coupling	coupling	4 eq. Fmoc-X-OH and HOBt in DMF 4 eq. TBTU in DMF 8 eq. DIPEA in NMP	30 min
	washing	2.5 mL DMF	1 x 1 min
	coupling	4 eq. Fmoc-X-OH and HOBt in DMF 4 eq. TBTU in DMF 8 eq. DIPEA in NMP	30 min
	washing	2.5 mL DMF	3 x 1 min
	Fmoc deprotection	2 mL 2% Pip / 2% DBU in DMF	4 x 5 min
	washing	2.5 mL DMF	6 x 1 min

### 10.3.2 Manual peptide synthesis

The Fmoc protected building blocks (*cis*- and *trans*-proline-glutamic acid chimeras) were synthesized and kindly provided by Dr. Jyotirmoy Maity,<sup>376</sup> for incorporation into the peptide sequences and the conformational study of the resulting  $\beta$ -hairpins.

**P1\_P** peptides, and the two analogues (**P1\_P<sup>cis-E</sup>**, **P1\_P<sup>trans-E</sup>**) containing the proline chimeras, were manually synthesized according to the standard Fmoc strategy. A NovaSyn®TGA-resin was preloaded with the first amino acid Fmoc-Thr-(<sup>t</sup>Bu)-OH (0.35 mmol/g, 0.05 mmol scale). C-terminal activation was carried out using 4 eq. Dic / HOBt. The Fmoc protected proline chimera, and the amino acid directly succeeding it in the sequence, were coupled manually for 2 x 8 h using 2 eq. amino acid and HOAt / DIC activation. Gly (7) was introduced carrying a DMB protecting group on the amino function to avoid aspartimide formation with the neighboring Asp (6) under basic conditions during



Fmoc deprotection steps. Fmoc deprotection was achieved by treatment of the resin with 20% piperidine in DMF.

### **10.3.3 Capping**

For capping of the free amino groups with acetic anhydride, a solution of Ac<sub>2</sub>O (10% (v/v)) and DIPEA (10% (v/v)) in DMF (3 mL) was added to the resin in three batches. The reaction was shaken for 3 x 10 min. Afterwards, the resin was washed with 5 mL DMF (3 x 1 min) and 5 mL DCM (3 x 1 min).

### **10.3.4 Cleavage from the resin**

Peptides based on the sequence of **VW18** and all **KXaa** variants were cleaved from the resin by treatment with 2 mL of a solution containing triisopropylsilane (10%, w/v), water (1%, w/v), and TFA (89%, w/v). The resin was shaken for 3 h and then filtered into a 100 mL flask. The resin was washed with 0.5 mL TFA and 0.5 mL DCM, and the washing solutions were combined with the cleavage solution. DCM was removed under a gentle stream of argon, and the peptides were precipitated by the addition of 80 mL ice-cold diethylether. The supernatant of the suspension was removed by centrifugation, and the precipitated raw peptide was washed with 15 mL ice-cold diethylether. The crude peptide was dried before purification.

**P1\_P** peptides and its analogues were cleaved from the resin with 2 mL of a solution containing triisopropylsilane (10%, w/v), water (1%, w/v), and TFA (89%, w/v). To cleave the ethyl ester of the proline chimera side chain, the crude peptide was stirred in 1M LiOH solution at room temperature overnight. Afterwards the peptide was precipitated in cold ether and handled in a manner similar to the other peptides, as described above.

### **10.3.5 Preparative HPLC**

The crude peptides were dissolved in a mixture of H<sub>2</sub>O and ACN containing 01 % TFA, and purified by reversed-phase preparative HPLC using a Knauer high-pressure-gradient system, with Smartline Manager 5000 interface with solvent degasser, two Smartline 1000 pumps (one for each eluent), variable UV-detector 2500, injection valve, high-pressure-gradient mixer, and a 5 mL sample loop. Separation was accomplished with a Phenomenex ® Luna C8 10 µm (250 mm x 21.2 mm) reversed-phase column. HPLC runs were performed with a flow rate of 20 mL/min, applying linear eluent gradients of

H<sub>2</sub>O (solvent A) and ACN (solvent B) containing 0.1% TFA, with UV-detection at  $\lambda_{\text{abs}} = 320$  nm for **VW18** based peptides containing Abz and  $\lambda_{\text{abs}} = 280$  nm for **KXaa** and **P1\_P** peptide variants containing the aromatic amino acid tyrosine (Tyr).

**VW18** variants containing MfeGly in position 13 or 14 that were used for solid state <sup>19</sup>F-NMR experiments were purified under TFA free conditions to avoid background <sup>19</sup>F-signals. Gradients of water / acetonitrile supplemented with 5 mM HCL instead of 0.1% TFA were used as previously described in detail.<sup>451</sup>

After separation, the purity of the collected fractions was determined by analytical HPLC. Fractions with sufficient purity were combined, and ACN was removed by rotary evaporation. Lyophilization of the remaining aqueous solution yielded the pure peptide.

### 10.3.6 Analytical HPLC

The purity of the synthesized peptides was determined by analytical HPLC. Analytical HPLC was performed on either a computer-controlled high-pressure-gradient LaChrom-HPLC-system (Merck-Hitachi), with L-7000 interface; two L-7100 pumps (one for each eluent); diode array detector L-7450; autosampler L-7200 with 100  $\mu$ L sample loop; solvent degasser L-7612; high-pressure gradient mixer; Rheodyne injection valve 7725i, 20  $\mu$ L sample loop, or on a computer-controlled high-pressure-gradient Elite LaChrom-HPLC-system (VWR-Hitachi) with two pumps L-2130 (one for each eluent); diode array detector L-2455; a fluorescence detector L-2485; autosampler L-2200 with 100  $\mu$ L sample loop, and a solvent degasser L-7612. HPLC runs were performed with a flow rate of 1 mL/min applying linear eluent gradients of H<sub>2</sub>O (solvent A) and ACN (solvent B) containing 0.1% TFA. UV-detection was set to  $\lambda_{\text{abs}} = 320$  nm for **VW18** based peptides containing Abz,  $\lambda_{\text{abs}} = 280$  nm for **KXaa** and **P1\_P** peptide variants containing the aromatic amino acid tyrosine (Tyr), and  $\lambda_{\text{abs}} = 220$  nm for both unlabeled peptide fragments and for purity control of the final peptides. Data analysis was accomplished using the LaChrome Software version 4.0.

The following reversed phase columns were used:

Phenomenex® Jupiter C4 5  $\mu$ M (250 mm x 4.6 mm), Phenomenex® Luna C8 (2) 5  $\mu$ M (250 mm x 4.6 mm), Phenomenex® Luna C8(2) 10  $\mu$ M (250 mm x 4.6 mm), Capcell C18 5  $\mu$ M (250 mm x 4.6 mm).

### 10.3.7 Characterization by ESI-ToF

Peptides were identified by ESI-ToF MS using an Agilent 6210 ESI-ToF LC-MS spectrometer (Agilent Technologies Inc., Santa Clara, CA, USA) with manual sample injection via a syringe pump (Harvard Apparatus 11 Plus) at a flow rate of 0.2 mL/min.

The peptides **VW18\_MfeGly 13** and **VW18\_MfeGly 14**, used for solid state  $^{19}\text{F}$ -NMR experiments were identified using an Agilent 1100 LC series coupled to a Bruker  $\mu\text{TOF}$  mass spectrometer.

## 10.4 Synthesized peptides

The peptide sequences summarized in *Table 10.2 – 10.4* were synthesized within the scope of the present thesis and identified by ESI-ToF mass spectrometry.

**Table 10.2:** Names, sequences, and identification of synthesized **VW18** variants.

Name	Sequence	observed	calculated
		[M+3] <sup>3+</sup>	[M+3] <sup>3+</sup>
<b>VW18</b>	Abz-LKVELEKLNKSELVVLKSELEKLNKSEL	1048.6149	1048.6177
<b>VW18_G8,G19</b>	Abz-LKVELEKLNKSELVVLKSELEKLNKSEL	1011.2523	1011.2359
<b>VW18_TfeGly 13</b> <sup>3</sup>	Abz-LKVELEKLNKSEL-TfeGly-VLKSELEKLNKSEL	1061.9436	1061.9582
<b>VW18_TfeGly 14</b> <sup>1</sup>	Abz-LKVELEKLNKSELV-TfeGly-LKSELEKLNKSEL	1061.9501	1061.9582
<b>VW18_DfeGly 13</b>	Abz-LKVELEKLNKSEL-DfeGly-VLKSELEKLNKSEL	1055.9345	1055.9615
<b>VW18_DfeGly 14</b>	Abz-LKVELEKLNKSELV-DfeGly-LKSELEKLNKSEL	1055.9358	1055.9615
<b>VW18_MfeGly 13</b>	Abz-LKVELEKLNKSEL-MfeGly-VLKSELEKLNKSEL	1049.9629	1049.9649
<b>VW18_MfeGly 14</b>	Abz-LKVELEKLNKSELV-MfeGly-LKSELEKLNKSEL	1049.9597	1049.9649
<b>VW18_Leu 13</b> <sup>4</sup>	Abz-LKVELEKLNKSEL-Leu-VLKSELEKLNKSEL	1053.2982	1053.2895
<b>VW18_Leu 14</b> <sup>2</sup>	Abz-LKVELEKLNKSELV-Leu-LKSELEKLNKSEL	1053.2890	1053.2895
<b>VW18_TfeGly 3,13,14</b>	Abz-LK-TfeGly-ELEKLNKSEL-TfeGly-TfeGly-LKSELEKLNKSEL	1088.5842	1088.6392
<b>VW18_Leu 3,13,14</b>	Abz-LK-Leu-ELEKLNKSEL-Leu-Leu-LKSELEKLNKSEL	1062.6406	1062.6333
<b>VW18_(SS)-TfV 14</b>	Abz-LKVELEKLNKSELV-(2S,3S)-TfV-LKSELEKLNKSEL	1066.6173	1066.6315
<b>VW18_(SR)-TfV 14</b>	Abz-LKVELEKLNKSELV-(2S,3R)-TfV-LKSELEKLNKSEL	1066.6172	1066.6315

<sup>3</sup> Synthesized by Olaf Wagner during an internship under my supervision, 2010.

<sup>4</sup> Synthesized by Kristin Folmert during an internship under my supervision, 2010.

**Table 10.3:** Names, sequences, and identification of synthesized **KXaa** peptide variants.

Name	Sequence	observed	calculated
		[M+2] <sup>2+</sup>	[M+2] <sup>2+</sup>
<b>K Ala</b> <sup>5</sup>	Ac-YGGKAAAAKA- <b>Ala</b> -AAKAAAAK-NH <sub>2</sub>	851.4915	851.4920
<b>K Leu</b> <sup>3</sup>	Ac-YGGKAAAAKA- <b>Leu</b> -AAKAAAAK-NH <sub>2</sub>	872.5213	872.5155
<b>K Val</b> <sup>4</sup>	Ac-YGGKAAAAKA- <b>Val</b> -AAKAAAAK-NH <sub>2</sub>	865.5041	865.5077
<b>K MfeGly</b> <sup>6</sup>	Ac-YGGKAAAAKA- <b>MfeGly</b> -AAKAAAAK-NH <sub>2</sub>	867.4920	867.5285
<b>K DfeGly</b> <sup>3</sup>	Ac-YGGKAAAAKA- <b>DfeGly</b> -AAKAAAAK-NH <sub>2</sub>	876.4890	876.5235
<b>K TfeGly</b> <sup>3</sup>	Ac-YGGKAAAAKA- <b>TfeGly</b> -AAKAAAAK-NH <sub>2</sub>	885.4880	885.5185
<b>K (2S,3S)-TfV</b> <sup>4</sup>	Ac-YGGKAAAAKA- <b>(2S,3S)-TfV</b> -AAKAAAAK-NH <sub>2</sub>	892.4904	892.5285
<b>K (2S,3R)-TfV</b> <sup>4</sup>	Ac-YGGKAAAAKA- <b>(2S,3R)-TfV</b> -AAKAAAAK-NH <sub>2</sub>	892.4919	892.5285
<b>K Ile</b> <sup>7</sup>	Ac-YGGKAAAAKA- <b>Ile</b> -AAKAAAAK-NH <sub>2</sub>	872.0341	872.5177
<b>K (2S,3S)-TfI</b> <sup>9</sup>	Ac-YGGKAAAAKA- <b>(2S,3S)-TfI</b> -AAKAAAAK-NH <sub>2</sub>	899.5220	899.5485

**Table 10.4:** Names, sequences, and identification of the **P1\_P** peptide variants.

Name	Sequence	observed	calculated
		[M+1] <sup>1+</sup>	[M+1] <sup>1+</sup>
<b>P1_P</b>	IYSNPDGTWT	1153.5219	1153.5165
<b>P1_P</b> <sup>cis-E</sup>	IYSNP <sup>cis-E</sup> DGTWT	1211.5259	1211.6303
<b>P1_P</b> <sup>trans-E</sup>	IYSNP <sup>trans-E</sup> DGTWT	1211.5269	1211.6303

## 10.5 Folding studies

### 10.5.1 Sample preparation and concentration determination

#### 10.5.1.1 Fibril forming peptides (VW18 variants)

Lyophilized peptide was dissolved in HFIP and sonicated for 15 minutes at room temperature. An aliquot of the stock solution was taken, and the HFIP was removed under a gentle stream of argon. The resulting film was dissolved in 1 mL 10 mM phosphate buffer (pH 7.4), and the concentration was determined by UV spectroscopy at 320 nm using a Varian Cary 50 spectrophotometer (Varian Medical Systems, Palo Alto, CA, USA) and PMMA cuvettes (10 mm path length, 1.5 mL, Plastibrand®, VWR International GmbH, Darmstadt, Germany). Prior to analysis, a calibration curve with Abz-Gly-OH (Bachem GmbH, Weil am Rhein, Germany) in phosphate buffer (10 mM, pH 7.4) was recorded at

<sup>5</sup> Synthesized by Sarah Chebli during her bachelor thesis under the supervision of Mario Salwiczek, **2010**; kindly provided for this study by Mario Salwiczek.

<sup>6</sup> Synthesized by Sergej Schwagerus during his bachelor thesis under my supervision, **2011**.

<sup>7</sup> Synthesized by Christian Knoll during an internship under my supervision, **2012**.

different concentrations. The desired amount of peptide stock solution was aliquoted and the HFIP was removed. Samples were stored at -20 °C until use. Prior to the experiments, peptides were dissolved in freshly prepared phosphate buffer (10 mM, pH 7.4). Unless reported differently, samples of 100 µM peptide concentration were prepared for all fibril forming peptides. Fibrils were formed by incubation of the samples at 25 °C under stationary or agitated conditions.

### 10.5.1.2 KXaa peptides used for $\alpha$ -helix propensity measurements

The lyophilized peptide was dissolved in 1 M NaCl, 1 mM sodium phosphate, 1 mM sodium citrate, and 1 mM sodium borate buffer (pH 7.0). The concentration of peptide stock solutions was determined using tyrosine absorbance in 6 M guanidinium hydrochloride ( $\epsilon_{276\text{ nm}} = 1,455 \text{ mol}^{-1}\text{cm}^{-1}$ ) using a Varian Cary 50 spectrophotometer (Varian Medical Systems, Palo Alto, CA, USA) and PMMA cuvettes (10 mm path length, 1.5 mL, Plastibrand®, VWR International GmbH, Darmstadt, Germany). Stock solutions of 1 mM concentration were prepared for each peptide.

### 10.5.1.3 P1\_P peptide variants used for $\beta$ -hairpin conformational studies

For preparation of the NMR-samples, the lyophilized peptide was dissolved in either H<sub>2</sub>O / D<sub>2</sub>O = 9:1 or pure D<sub>2</sub>O to obtain a 5 mM stock solution. The concentration of peptide stock solutions was determined in aqueous 6 M guanidine hydrochloride by adding 100 µL of the stock solution to 7 M guanidine hydrochloride solution, which was further diluted with water to result in a final guanidine hydrochloride concentration of 6 M. The absorbance of tyrosine and tryptophan were determined using a Varian Cary 50 spectrophotometer (Varian Medical Systems, Palo Alto, CA, USA) and PMMA cuvettes (10 mm path length, 1.5 mL, Plastibrand®, VWR International GmbH, Darmstadt, Germany). The concentration of the stock solution was calculated using the known extinction coefficients of Tyr and Trp ( $\epsilon_{\text{Tyr}}$  at 280 nm = 1.200 mol<sup>-1</sup>cm<sup>-1</sup>,  $\epsilon_{\text{Trp}}$  at 280 nm = 5.560 mol<sup>-1</sup>cm<sup>-1</sup>) according to *equation 10.1*:

$$c = \frac{A}{[n \cdot (\epsilon_{\text{Tyr}}) + n \cdot (\epsilon_{\text{Trp}})] \cdot l} \quad (10.1)$$

with  $A$  = absorption at 280 nm,  $l$  = path length (1 cm),  $n$  = number of times the particular residue appears in the sequence, and  $\epsilon$  = extinction coefficient.

The stock solutions were diluted to the desired concentrations required for NMR or CD experiments, and the pH was adjusted to 4.3 as described below.

## 10.5.2 pH adjustment

The pH of the buffer solutions and all peptide samples were adjusted using a WTW pH526 pH-Meter and an InLab® microelectrode (Mettler Toledo).

## 10.5.3 CD spectroscopy

### 10.5.3.1 VW18 variants

CD spectra of fibril forming peptide variants were recorded with a Jasco J-810 spectropolarimeter equipped with RCS-Lauda Thermo-Regulator (LAUDA Dr. R. Wobser GmbH & Co. KG) according to the parameters summarized below. Quartz cells (1.0 mm path length) were used throughout. Sample concentration of all peptide solutions was adjusted to 100  $\mu\text{M}$  in 10 mM phosphate buffer at pH 7.4. The spectra were obtained as the average of three scans that had been background-corrected by subtracting the corresponding buffer spectra. The measured CD data in mdeg were converted into molar ellipticity per residue  $[\theta] = (10^3 \cdot \text{mdeg} \cdot \text{cm}^2 \cdot \text{dmol}^{-1} \cdot \text{residue}^{-1})$ .

#### Parameters:

<i>Start wavelength:</i>	<i>240 nm</i>	<i>Response:</i>	<i>2 s</i>
<i>End wavelength:</i>	<i>190 nm</i>	<i>Band width:</i>	<i>2 nm</i>
<i>Step resolution:</i>	<i>0.5 nm</i>	<i>Temperature:</i>	<i>20 °C</i>
<i>Scan speed:</i>	<i>100 nm / min</i>	<i>Accumulation:</i>	<i>3</i>

### 10.5.3.2 P1\_P peptide variants

The peptide stock solutions ( $\text{H}_2\text{O} / \text{D}_2\text{O} = 9:1$ ; pH 4.3) were diluted to give solutions with final concentrations of 100  $\mu\text{M}$ , 300  $\mu\text{M}$ , and 500  $\mu\text{M}$ . CD spectra of the peptide variants were recorded with a Jasco J-810 spectropolarimeter at 5 °C. Quartz cells (0.2 mm path length for 300  $\mu\text{M}$  and 500  $\mu\text{M}$  samples, and 1.0 mm path length for 100  $\mu\text{M}$  samples) were used throughout. The spectra were the average of three scans obtained by collecting data from 240 to 190 nm at 0.5 nm intervals, 2 nm bandwidth, and 2 s response times. Spectra were background-corrected by subtracting the corresponding  $\text{H}_2\text{O} / \text{D}_2\text{O} = 9:1$  spectra.

### 10.5.3.3 *KXaa variants*

CD spectra were recorded with a Jasco J-810 spectropolarimeter at 0 °C. Quartz cuvettes (1.0 mm path length) were used. CD measurements were performed at peptide concentrations of 30, 50, and 80  $\mu\text{M}$ . Each reported CD value represents the mean of at least 3 independent measurements. Data were collected from 250 nm to 200 nm at 0.2 nm intervals, 2 nm bandwidth, and 2 s response time. Spectra were background-corrected by subtracting the corresponding buffer spectra. The measured CD data in mdeg were converted into molar ellipticity per residue  $[\theta] = (10^3 \cdot \text{mdeg} \cdot \text{cm}^2 \cdot \text{dmol}^{-1} \cdot \text{residue}^{-1})$ . The mean residue molar ellipticity was independent of peptide concentration (30-80  $\mu\text{M}$ ) for all peptides.

### 10.5.4 $\alpha$ -helix propensity measurements

The fractional helical content ( $f_{\text{helix}}$ ) of the **KXaa** peptides was calculated from the mean residue molar ellipticity of the CD data at 222 nm. The number of backbone amides ( $N$ ) is 19, and  $f_{\text{helix}}$  was calculated using *equation 10.2*.

$$f_{\text{helix}} = \frac{[\theta]_{222}}{40000 \cdot \left(1 - \frac{2.5}{N}\right)} \quad (10.2)$$

The helix propensity ( $w$ ) of the amino acid at the guest position was calculated from the  $f_{\text{helix}}$  of the corresponding peptide based on modified Lifson-Roig theory.<sup>238,239</sup> Four parameters need to be considered for each residue: helix propensity ( $w$ ), nucleation ( $v$ ), N-terminal capping propensity ( $n$ ), and C-terminal capping propensity ( $c$ ).<sup>239</sup> For all residues,  $v$  was set to 0.048,<sup>239</sup> and  $c$  was set to 1.<sup>239</sup> Literature values were used for  $w$  and  $n$  of the host residues.<sup>238</sup> For the residue in the guest position,  $w$  was simply calculated with  $n$  set to 1.<sup>236,438</sup>

### 10.5.5 HPLC assay to estimate the hydrophobicity and side chain volume of the Fmoc-amino acids

The impact of fluorination on the correlation of amino acid side chain volume and hydrophobicity was investigated with the help of an HPLC assay that was previously established in our group.<sup>49</sup> Fmoc-protected analogues of Gly, Ala, Abu, Val, Leu, and Ile, as well as those of MfeGly, DfeGly, TfeGly, (2S,3S)-TfV, and (2S,3R)-TfV were used, and

their retention times determined on a C18 column (Capcell C18, 5  $\mu\text{m}$ ). Approximately 10  $\mu\text{mol}$  of the respective Fmoc-amino acid was dissolved in 5 mL of a mixture of 40% acetonitrile (99.9%, HPLC gradient grade, VWR) in deionized water containing 0.1% TFA (Uvasol, Merck) and filtered over a syringe filter with 0.2  $\mu\text{m}$  pore size. The retention times on the C18 column were determined. A linear gradient from 40% to 70% ACN over 30 min was applied at room temperature, and all experiments were performed in triplicate. The van der Waals volumes of the side chains were calculated according to Zhao *et al.*<sup>452</sup> All atom and bond contributions (from  $\text{C}_\beta$  outward) of the side chain were considered for the calculation according to *equation 10.3* with  $N_B$  representing the number of bonds.

$$V_{\text{vdV}} = \sum \text{all atom contributions} - 5.92 N_B \quad (10.3)$$

The values in *Table 10.5* were used for the atom contributions.

**Table 10.5:** atom volumes

atom	$V_{\text{vdV}}$ ( $\text{\AA}^3$ )
H	7.24
C	20.58
F	13.31

### 10.5.6 Size exclusion / static light scattering

The oligomerization state of the peptides was determined by applying size exclusion chromatography (SEC) in combination with static light scattering (SLS). Size exclusion (SEC) analysis was performed using a WTC-015S5 column (5  $\mu\text{m}$ , 150  $\text{\AA}$ , 7.8 x 300 mm, Wyatt Technology) connected to a high-performance liquid chromatography (HPLC) workstation (La Chrom, VWR, Hitachi, L-2130). The separation was carried out at a velocity of 0.3 mL/min at room temperature in an aqueous buffer consisting of 10 mM sodium phosphate and 150 mM sodium chloride at pH 7.3. Elution of peptides was monitored by UV detection (VWR, Hitachi, L-2400) at 230 nm. The concentration of all injected **VW18** variants was 100  $\mu\text{M}$ , the sample concentration of the **KXaa** analogues was 80  $\mu\text{M}$ , and all **P1\_P** variants were injected at a sample concentration of 150  $\mu\text{M}$ . The injection volume was 100  $\mu\text{l}$  in each case. Static light scattering experiments were performed at 25  $^\circ\text{C}$  by using a Dawn Heleos 8 light scattering photometer and an Optilab rEX refractive index detector (Wyatt Technology). Molecular weight values were calculated by using a  $\text{dn}/\text{dc}$  value of 0.185 mL/g. All experiments were performed in



triplicate, and the data were analyzed with ASTRA software version 5.3.4.20 (Wyatt Technology).

### 10.5.7 Thioflavin T fluorescence staining assay

All fibril forming peptides (**VW18** and its variants) were prepared as described in the section (*sample preparation*). Fluorescence spectra were measured with a luminescence spectrometer LS 50B (Perkin–Elmer, Boston, MA, USA) using quartz cells (1.4 mL, 2 mm path length). Samples were prepared by incubating the peptide solution (480 mL, 100 μM, 10 mM phosphate buffer, pH 7.4) with a solution of Thioflavin T (20 μL, 100 μM, 10 mM phosphate buffer, pH 7.4) at 25 °C under stationary or agitated conditions for several days, or until completion of fibril formation (plateau phase in the ThT fluorescence staining assay). Spectra were measured by accumulating 10 scans from 470 nm to 520 nm with an excitation wavelength of 450 nm, and background-corrected by subtracting the free-dye spectrum. The given aggregation traces are plots of ThT fluorescence intensity at 485 nm ( $I_{485}^F$ ) versus the incubation time ( $t$ ). The data were fitted to a sigmoidal four parameter curve according to *equation 10.4*:

$$I^F = I_0^F + \frac{a}{1 + \exp\left[-\frac{(t - t_0)}{b}\right]} \quad (10.4)$$

### 10.5.8 Transmission electron microscopy

#### *Negative staining TEM*

Samples for staining electron microscopy were prepared by absorbing 7 μL aliquots of peptide solution to glow-discharged carbon-coated collodium films on 400-mesh copper grids. The grids were blotted, stained with 1% phosphotungstic acid (PTA), and air dried. TEM micrographs were taken at a primary magnification of 58300× using a defocus of 0.6 μm.

#### *Cryo-TEM*

The samples for cryo-TEM were prepared by placing a droplet of 10 μL peptide solution on a hydrophilized perforated carbon filmed grid (60 s plasma treatment at 8 W using a BALTEC MED 020 device) at room temperature. For obtaining an ultrathin layer of the

sample solution spanning the holes of the carbon film, the supernatant fluid was removed with filter paper. The grids were immediately vitrified in liquid ethane at its freezing point (-184 °C) using a standard plunging device. The vitrified samples were transferred under liquid nitrogen into a Philips CM12 transmission electron microscope by using the Gatan cryo holder and stage (model 626). Microscopy was carried out at a sample temperature of -175 °C by using the low-dose protocol of the microscope at a primary magnification of 58300x with a defocus of 1.5µm.

### **10.5.9 Solution <sup>1</sup>H-NMR spectroscopy of P1\_P variants**

<sup>1</sup>H-NMR and two dimensional-NMR (TOCSY, NOESY, and ROESY) spectral measurements were recorded in a sample volume of 0.6 mL of H<sub>2</sub>O / D<sub>2</sub>O (9:1 ratio by volume) or in pure D<sub>2</sub>O at 275 K on an AVANCE III 700 MHz pulse spectrometer from Bruker equipped with a cryo probe. Peptide concentrations for NMR experiments were 5 mM. The pH of the samples was adjusted to 4.3 with a minute amount of HCl or NaOH, DCl or NaOD, respectively, and no correction for the isotope effect was made.

One dimensional spectra were acquired by using a 90° pulse of 6.7 microsecond at 7W. Phase sensitive two-dimensional correlation spectroscopy (COSY),<sup>453</sup> total correlation spectroscopy (TOCSY),<sup>454</sup> nuclear Overhauser effect spectroscopy (NOESY),<sup>455,456</sup> and rotating frame nuclear Overhauser effect spectroscopy (ROESY)<sup>457,458</sup> were recorded by standard techniques using presaturation of water signal and the time proportional phase incrementation mode. A mixing time of 200 ms was used for NOESY spectra, whereas a spinlock pulse of 200 ms at 24 mW was used for ROESY spectra. TOCSY spectra were recorded using spinlock pulses of 400 ms. Additional NOESY and ROESY experiments were performed on peptide samples in pure D<sub>2</sub>O to facilitate the observation of the H<sub>α</sub>-H<sub>α</sub> NOE cross peaks close to the water signal. Obtained data were processed using Bruker TOPSPIN software.

### **10.5.10 Solid-state <sup>19</sup>F-NMR of VW18 variants containing MfeGly**

The fibrils of the peptides **VW18\_MfeGly 13** and **VW18-MfeGly 14** were investigated using solid-state <sup>19</sup>F-NMR. The local chemical operating at 564.68 MHz <sup>19</sup>F resonance frequency (600 MHz for <sup>1</sup>H) after single pulse excitation (2.5 µs pulse length) under 25 kHz magic angle spinning and 50 kHz <sup>1</sup>H-decoupling at a temperature of 25 °C. Approximately 5000-10000 scans separated by a recycle delay of 2s were accumulated for a typical spectrum. The <sup>19</sup>F-NMR spectra were referenced indirectly using the <sup>1</sup>H-NMR

water signal, and - in cases where two lines were present - fitted with two lineshapes composed of 50% Lorentzian and 50% Gaussian profile to deconvolute their relative intensities.

Internuclear proximities between non-equivalent  $^{19}\text{F}$ -substituents were probed using the CODEX (Centerband Only Detection of Exchange) experiment<sup>313,315</sup> with an extended phase cycle.<sup>314</sup> A chemical shift recoupling period of 240  $\mu\text{s}$ , z-filter of 80  $\mu\text{s}$ , and mixing times between 80  $\mu\text{s}$  and 400 ms were used. Scans acquiring the full signal  $S_0$ , and the signal reduced due to spin diffusion  $S$ , were collected in an interleaved fashion to assure identical conditions for both data sets. The ratio  $S/S_0$  was fitted to  $(1-1/M) \exp(t_{\text{mix}}/t_{\text{diff}}) + 1/M$ , assuming environment of the fluorine-labeled amino acid (MfeGly) and fluorine-fluorine contacts between different  $^{19}\text{F}$  nuclei were examined using solid state  $^{19}\text{F}$ -NMR under magic angle spinning. For the measurements, the amyloid suspensions were ultracentrifuged, and the pellet transferred into 2.5 mm outer diameter rotors.  $^{19}\text{F}$ -NMR spectra were acquired using a Bruker Avance spectrometer a spin diffusion amongst  $M$  equivalent sites with a spin diffusion time constant  $t_{\text{diff}}$ .



## 11 Literature

1. K. A. Jellinger, *J. Neural. Transm.* **2006**, *113*, 1603-1623.
2. D. J. Selkoe, *Nature* **2003**, *426*, 900-904.
3. C. M. Dobson, M. Karplus, *Curr. Opin. Struct. Biol.* **1999**, *9*, 92-101.
4. C. M. Dobson, *Nature* **2002**, *418*, 729-730.
5. M. Stefani, C. M. Dobson, *J. Mol. Med.* **2003**, *81*, 678-699.
6. C. M. Dobson, *Nature* **2003**, *426*, 884-890.
7. J. I. Guijarro, M. Sunde, J. A. Jones, I. D. Campell, C. M. Dobson, *Proc. Natl. Acad. Sci. U.S.A* **1998**, *95*, 4224-4228.
8. A. Wimo, B. Winblad, L. Jönsson, *Alzheimers Dement.* **2010**, *6*, 98-103.
9. S. M. de la Monte, J. R. Wands, *J. Diabetes Sci. Technol.* **2008**, *2*, 1101-1113.
10. L. Li, C. Hölscher, *Brain Res. Rev.* **2007**, *56*, 384-402.
11. E. Steen, B. M. Terry, E. J. Rivera, J. L. Cannon, T. R. Neely, R. Tavares, X. J. Xu, J. R. Wands, S. M. de la Monte, *J. Alzheimers Dis.* **2005**, *7*, 63-80.
12. E. J. Rivera, A. Goldin, N. Fulmer, R. Tavares, J. R. Wands, S. M. de la Monte, *J. Alzheimers Dis.* **2005**, *8*, 247-268.
13. S. Craft, *Neurobiol. Aging* **2005**, *26*, 65-69.
14. M. Schubert, D. Gautam, D. Surjo, K. Ueki, S. Baudler, D. Schubert, T. Kondo, J. Alber, N. Galldiks, E. Küstermann, S. Arndt, A. H. Jacobs, W. Krone, C. R. Kahn, J. C. Brüning, *Proc. Natl. Acad. Sci. U.S.A* **2004**, *101*, 3100-3105.
15. M. Schubert, D. P. Brazil, D. J. Burks, J. A. Kushner, J. Ye, C. L. Flint, J. Farhang-Fallah, P. Dikkes, X. M. Warot, C. Rio, G. Corfas, M. F. White, *J. Neurosci.* **2003**, *23*, 7084-7092.
16. I. Grundke-Iqbal, K. Iqbal, Y. C. Tung, M. Quinlan, H. M. Wisniewski, L. I. Binder, *Proc. Natl. Acad. Sci. U.S.A* **1986**, *83*, 4913-4917.
17. A. Verdelho, S. Madureira, J. M. Ferro, A.-M. Basile, H. Chabriat, T. Erkinjuntti, F. Fazekas, M. Hennerici, J. O'Brien, L. Pantoni, *J. Neurol. Neurosurg. Psychiatry* **2007**, *78*, 1325-1330.
18. F. Pasquier, A. Boulogne, D. Leys, P. Fontaine, *Diabetes Metab.* **2006**, *32*, 403-414.
19. P. Lewczuk, J. Hornegger, R. d. Zimmermann, M. Otto, J. Wiltfang, J. Kornhuber, *Eur. Arch. Psychatry Clin. Neurosci.* **2008**, *258*, 44-49.
20. C. L. Maarouf, T. M. Andacht, T. A. Kokjohn, E. M. Castano, L. I. Sue, T. G. Beach, A. E. Roher, *Curr. Alzheimer Res.* **2009**, *6*, 399-406.
21. K. A. Jellinger, B. Janetzky, J. Attems, E. Kienzl, *J. Cell. Mol. Med.* **2008**, *12*, 1094-1117.
22. C. P. R. Hackenberger, D. Schwarzer, *Angew. Chem. Int. Ed.* **2008**, *47*, 10030-10074.
23. W. S. Gosal, I. J. Morten, E. W. Hewitt, D. A. Smith, N. H. Thomson, S. E. Radford, *J. Mol. Biol.* **2005**, *351*, 850-864.
24. V. J. McParland, N. M. Kad, A. P. Kalverda, A. Brown, P. Kirwin-Jones, M. G. Hunter, M. Sunde, S. E. Radford, *Biochemistry* **2000**, *39*, 8735-8746.
25. H. Zhao, E. K. J. Tuominen, P. K. J. Kinnunen, *Biochemistry* **2004**, *43*, 10302-10307.
26. I. Cherny, E. Gazit, *Angew. Chem. Int. Ed.* **2008**, *47*, 4062-4069.
27. H. A. Lashuel, S. R. LaBrenz, L. Woo, L. C. Serpell, J. W. Kelly, *J. Am. Chem. Soc.* **2000**, *122*, 5262-5277.
28. C. E. MacPhee, D. N. Woolfson, *Curr. Opin. Solid State Mater. Sci.* **2004**, *8*, 141-149.
29. B. C. Buer, E. N. G. Marsh, *Protein Sci.* **2012**, *21*, 453-462.
30. N. C. Yoder, K. Kumar, *Chem. Soc. Rev.* **2002**, *31*, 335-341.
31. K. Müller, C. Faeh, F. o. Diederich, *Science* **2007**, *317*, 1881-1886.

32. S. Purser, P. R. Moore, S. Swallow, V. Gouverneur, *Chem. Soc. Rev.* **2008**, *37*, 320-330.
33. P. Wadhvani, E. Strandberg, N. Heidenreich, J. Bürck, S. Fanghänel, A. S. Ulrich, *J. Am. Chem. Soc.* **2012**, *134*, 6512-6515.
34. Y. Suzuki, J. R. Brender, K. Hartman, A. Ramamoorthy, E. N. G. Marsh, *Biochemistry* **2012**, *51*, 8154-8162.
35. S. R. Choi, G. Golding, Z. Zhuang, W. Zhang, N. Lim, F. Hefti, T. E. Benedum, M. R. Kilbourn, D. Skovronsky, H. F. Kung, *J. Nucl. Med.* **2009**, *50*, 1887-1894.
36. D. O'Hagan, C. Schaffrath, S. L. Cobb, J. T. G. Hamilton, C. D. Murphy, *Nature* **2002**, *416*, 279-279.
37. H. Deng, D. O'Hagan, C. Schaffrath, *Nat. Prod. Rep.* **2004**, *21*, 773-784.
38. C. Dong, F. Huang, H. Deng, C. Schaffrath, J. B. Spencer, D. O'Hagan, J. H. Naismith, *Nature* **2004**, *427*, 561-565.
39. M. B. van Niel, I. Collins, M. S. Beer, H. B. Broughton, S. K. F. Cheng, S. C. Goodacre, A. Heald, K. L. Locker, A. M. MacLeod, D. Morrison, C. R. Moyes, D. O'Connor, A. Pike, M. Rowley, M. G. N. Russell, B. Sohal, J. A. Stanton, S. Thomas, H. Verrier, A. P. Watt, J. L. Castro, *J. Med. Chem.* **1999**, *42*, 2087-2104.
40. C. W. Thornber, *Chem. Soc. Rev.* **1979**, *8*, 563-580.
41. L. M. Lima, E. J. Barreiro, *Curr. Med. Chem.* **2005**, *12*, 23-49.
42. A. Sutherland, C. L. Willis, *Nat. Prod. Rep.* **2000**, *17*, 621-631.
43. X.-L. Qiu, W.-D. Meng, F.-L. Qing, *Tetrahedron* **2004**, *60*, 6711-6745.
44. D. O'Hagan, *Chem. Soc. Rev.* **2008**, *37*, 308-319.
45. G. Bott, L. D. Field, S. Sternhell, *J. Am. Chem. Soc.* **1980**, *102*, 5618-5626.
46. T. Nagai, G. Nishioka, M. Koyama, A. Ando, T. Miki, I. Kumadaki, *J. Fluorine Chem.* **1992**, *57*, 229-237.
47. J. M. Kovacs, C. T. Mant, R. S. Hodges, *Pept. Sci.* **2006**, *84*, 283-297.
48. B. E. Smart, *J. Fluorine Chem.* **2001**, *109*, 3-11.
49. S. A. Samsonov, M. Salwiczek, G. Anders, B. Koksich, M. T. Pisabarro, *J. Phys. Chem. B* **2009**, *113*, 16400-16408.
50. K. M. Biswas, D. R. DeVido, J. G. Dorsey, *J. Chromatogr.* **2003**, *1000*, 637-655.
51. M. C. J. Wilce, M.-I. Aguilar, M. T. W. Hearn, *Anal. Chem.* **1995**, *67*, 1210-1219.
52. R. S. Hodges, B.-Y. Zhu, N. E. Zhou, C. T. Mant, *J. Chromatogr.* **1994**, *676*, 3-15.
53. B. E. Smart, *Characteristics of CF systems*, Plenum Press: New York, **1994**.
54. C. J. Wilson, D. A. Wilson, A. E. Feiring, V. Percec, *J. Polym. Sci., Part A: Polym. Chem.* **2010**, *48*, 2498-2508.
55. M. Cametti, B. Crousse, P. Metrangolo, R. Milani, G. Resnati, *Chem. Soc. Rev.* **2012**, *41*, 31-42.
56. H. M. Walborsky, J. H. Lang, *J. Am. Chem. Soc.* **1956**, *78*, 4314-4316.
57. M. Schlosser, *Angew. Chem. Int. Ed.* **1998**, *37*, 1496-1513.
58. C. J. Pace, J. Gao, in *Acc. Chem. Res.*, Vol. 46, American Chemical Society, **2013**, pp. 907-915.
59. M. A. Danielson, J. J. Falke, *Annu. Rev. Bioph. Biom.* **1996**, *25*, 163-195.
60. M. G. Woll, E. B. Hadley, S. Mecozzi, S. H. Gellman, *J. Am. Chem. Soc.* **2006**, *128*, 15932-15933.
61. C. A. Hunter, J. K. M. Sanders, *J. Am. Chem. Soc.* **1990**, *112*, 5525-5534.
62. M. L. Waters, *Curr. Opin. Chem. Biol.* **2002**, *6*, 736-741.
63. M. L. Waters, *Biopolymers* **2004**, *76*, 435-445.
64. H. Zheng, J. Gao, *Angew. Chem. Int. Ed.* **2010**, *49*, 8635-8639.
65. N. Voloshchuk, A. Y. Zhu, D. Snyder, J. K. Montclare, *Bioorg. Med. Chem. Lett.* **2009**, *19*, 5449-5451.
66. M. Salwiczek, E. K. Nyakatura, U. I. M. Gerling, S. Ye, B. Koksich, *Chem. Soc. Rev.* **2012**, *41*, 2135-2171.
67. M. Mae, H. Amii, K. Uneyama, *Tetrahedron Lett.* **2000**, *41*, 7893-7896.
68. A. Yaron, F. Naider, *Crit. Rev. Biochem. Mol. Biol.* **1993**, *28*, 31-81.

69. G. Vanhoof, F. Goossens, I. De Meester, D. Hendriks, S. Scharpe, *FASEB J.* **1995**, *9*, 736-744.
70. C. R. S. Briggs, D. O'Hagan, J. A. K. Howard, D. S. Yufit, *J. Fluorine Chem.* **2003**, *119*, 9-13.
71. M. L. DeRider, S. J. Wilkens, M. J. Waddell, L. E. Bretscher, F. Weinhold, R. T. Raines, J. L. Markley, *J. Am. Chem. Soc.* **2002**, *124*, 2497-2505.
72. M. S. Weiss, A. Jabs, R. Hilgenfeld, *Nat. Struct. Mol. Biol.* **1998**, *5*, 676-676.
73. E. J. Milner-White, L. H. Bell, P. H. Maccallum, *J. Mol. Biol.* **1992**, *228*, 725-734.
74. L. E. Bretscher, C. L. Jenkins, K. M. Taylor, M. L. DeRider, R. T. Raines, *J. Am. Chem. Soc.* **2001**, *123*, 777-778.
75. W. Kim, K. I. Hardcastle, V. P. Conticello, *Angew. Chem. Int. Ed.* **2006**, *45*, 8141-8145.
76. W. Kim, R. A. McMillan, J. P. Snyder, V. P. Conticello, *J. Am. Chem. Soc.* **2005**, *127*, 18121-18132.
77. N. Panasik, E. S. Eberhardt, A. S. Edison, D. R. Powell, R. T. Raines, *Int. J. Pept. Protein Res.* **1994**, *44*, 262-269.
78. I. W. Hamley, *Angew. Chem. Int. Ed.* **2007**, *46*, 8128-8147.
79. E. D. Eanes, G. G. Glenner, *J. Histochem. Cytochem.* **1968**, *16*, 673-677.
80. D. A. Kirschner, C. Abraham, D. J. Selkoe, *Proc. Natl. Acad. Sci. U.S.A* **1986**, *83*, 503-507.
81. M. Sunde, L. C. Serpell, M. Bartlam, P. E. Fraser, M. B. Pepys, C. C. F. Blake, *J. Mol. Biol.* **1997**, *273*, 729-739.
82. O. S. Makin, L. C. Serpell, *FEBS J.* **2005**, *272*, 5950-5961.
83. P. Divry, M. Florkin, *C. R. Soc. Biol.* **1927**, *97*, 1808-1810.
84. L. C. Serpell, M. Sunde, M. D. Benson, G. A. Tennent, M. B. Pepys, P. E. Fraser, *J. Mol. Biol.* **2000**, *300*, 1033-1039.
85. B. H. Toyama, J. S. Weissman, *Annu. Rev. Biochem.* **2011**, *80*, 557-585.
86. C. Ritter, M. L. Maddelein, A. B. Siemer, T. Luhrs, M. Ernst, *Nature* **2005**, *435*, 844-848.
87. B. H. Toyama, M. J. Kelly, J. D. Gross, J. S. Weissman, *Nature* **2007**, *449*, 233-237.
88. P. T. Lansbury, P. R. Costa, J. M. Griffiths, E. J. Simon, M. Auger, *Nat. Struct. Biol.* **1995**, *2*, 990-998.
89. R. Tycko, K. L. Sciarretta, J. P. Orgel, S. C. Meredith, *Biochemistry* **2009**, *48*, 6072-6084.
90. J. J. Balbach, Y. Ishii, O. N. Antzutkin, R. D. Leapman, N. W. Rizzo, *Biochemistry* **2000**, *39*, 13748-13759.
91. R. Tycko, *Curr. Opin. Struct. Biol.* **2004**, *14*, 96-103.
92. R. Tycko, *Protein. Pept. Lett.* **2006**, *13*, 229-234.
93. R. Tycko, *Annu. Rev. Phys. Chem.* **2011**, *62*, 279-299.
94. T. Luhrs, C. Ritter, M. Adrian, D. Riek-Loher, B. Bohrmann, *Proc. Natl. Acad. Sci. USA* **2005**, *102*, 17342-17347.
95. A. T. Petkova, Y. Ishii, J. J. Balbach, O. N. Antzutkin, R. D. Leapman, F. Delaglio, R. Tycko, *Proc. Natl. Acad. Sci. U.S.A* **2002**, *99*, 16742-16747.
96. A. T. Petkova, R. D. Leapman, Z. Guo, W. M. Yau, M. P. Mattson, R. Tycko, *Science* **2005**, *307*, 262-265.
97. M. I. Apostol, M. R. Sawaya, D. Cascio, D. Eisenberg, *J. Biol. Chem.* **2010**, *285*, 29671-29675.
98. M. R. Sawaya, S. Sambashivan, R. Nelson, M. I. Ivanova, S. A. Sievers, M. I. Apostol, M. J. Thompson, M. Balbirnie, J. J. W. Wiltzius, H. T. McFarlane, A. O. Madsen, C. Riek, D. Eisenberg, *Nature* **2007**, *447*, 453-457.
99. M. I. Ivanova, S. A. Sievers, M. R. Sawaya, J. S. Wall, D. Eisenberg, *Proc. Natl. Acad. Sci. U.S.A* **2009**, *106*, 18990-18995.
100. M. J. Thompson, S. A. Sievers, J. Karanicolas, M. I. Ivanova, D. Baker, D. Eisenberg, *Proc. Natl. Acad. Sci. U.S.A* **2006**, *103*, 4074-4078.

101. R. Nelson, M. R. Sawaya, M. Balbirnie, A. O. Madsen, C. Riek, R. Grothe, D. Eisenberg, *Nature* **2005**, *435*, 773-778.
102. L. O. Tjernberg, J. Naslund, F. Lindqvist, J. Johansson, A. R. Karlstrom, J. Thyberg, L. Terenius, C. Nordstedt, *J. Biol. Chem.* **1996**, *271*, 8545-8548.
103. M. T. Pastor, A. Esteras-Chopo, L. Serrano, *Prion* **2007**, *1*, 9-14.
104. A. Esteras-Chopo, L. Serrano, M. L. p. de la Paz, *Proc. Natl. Acad. Sci. U.S.A* **2005**, *102*, 16672-16677.
105. K. Tenidis, M. Waldner, J. Bernhagen, W. Fischle, M. Bergmann, M. Weber, M. L. Merkle, W. Voelter, H. Brunner, A. Kapurniotu, *J. Mol. Biol.* **2000**, *295*, 1055-1071.
106. M. von Bergen, P. Friedhoff, J. Biernat, J. Heberle, E. M. Mandelkow, E. Mandelkow, *Proc. Natl. Acad. Sci. U.S.A* **2000**, *97*, 5129-5134.
107. M. I. Ivanova, M. R. Sawaya, M. Gingery, A. Attinger, D. Eisenberg, *Proc. Natl. Acad. Sci. U.S.A* **2004**, *101*, 10584-10589.
108. S. Ventura, J. Zurdo, S. Narayanan, M. Parreno, R. Mangués, B. Reif, F. Chiti, E. Giannoni, C. M. Dobson, F. X. Aviles, L. Serrano, *Proc. Natl. Acad. Sci. U.S.A* **2004**, *101*, 7258-7263.
109. T. Takahashi, H. Mihara, *Acc. Chem. Res.* **2008**, *41*, 1309-1318.
110. M. Lopez de la Paz, K. Goldie, J. Zurdo, E. Lacroix, C. M. Dobson, A. Hoenger, L. Serrano, *Proc. Natl. Acad. Sci. U.S.A* **2002**, *99*, 16052-16057.
111. R. A. Kammerer, D. Kostrewa, J. Zurdo, A. Detken, C. Garcia-Echeverria, J. D. Green, S. A. Muller, B. H. Meier, F. K. Winkler, C. M. Dobson, M. O. Steinmetz, *Proc. Natl. Acad. Sci. U.S.A* **2004**, *101*, 4435-4440.
112. T. Kosaka, M. Imagawa, K. Seki, H. Arai, H. Sasaki, S. Tsuji, A. Asami-Odaka, T. Fukushima, K. Imai, T. Iwatsubo, *Neurology* **1997**, *48*, 741-745.
113. T. C. Gamblin, F. Chen, A. Zambrano, A. Abraha, S. Lagalwar, A. L. Guillozet, M. Lu, Y. Fu, F. Garcia-Sierra, N. LaPointe, R. Miller, R. W. Berry, L. I. Binder, V. L. Cryns, *Proc. Natl. Acad. Sci. U.S.A* **2003**, *100*, 10032-10037.
114. E. Cerasoli, B. K. Sharpe, D. N. Woolfson, *J. Am. Chem. Soc.* **2005**, *127*, 15008-15009.
115. K. Pagel, T. Seri, H. v. Berlepsch, J. Griebel, R. Kirmse, C. Böttcher, B. Koks, *ChemBioChem* **2008**, *9*, 531-536.
116. A. I. Bush, *Curr. Opin. Chem. Biol.* **2000**, *4*, 184-191.
117. F. E. Ali, F. Separovic, C. J. Barrow, R. A. Cherny, F. Fraser, A. I. Bush, C. L. Masters, K. J. Barnham, *J. Pept. Sci.* **2005**, *11*, 353-360.
118. W. Liu, J. M. Prausnitz, H. W. Blanch, *Biomacromolecules* **2004**, *5*, 1818-1823.
119. A. Jha, S. Narayan, J. B. Udgaonkar, G. Krishnamoorthy, *Biophys. J.* **2012**, *103*, 797-806.
120. J.-C. Rochet, P. T. Lansbury, *Curr. Opin. Struct. Biol.* **2000**, *10*, 60-68.
121. F. Chiti, C. M. Dobson, *Annu. Rev. Biochem.* **2006**, *75*, 333-366.
122. R. Nelson, D. Eisenberg, *Curr. Opin. Struct. Biol.* **2006**, *16*, 260-265.
123. R. Krishnan, S. L. Lindquist, *Nature* **2005**, *435*, 765-772.
124. P. Sikorski, E. Atkins, *Biomacromolecules* **2004**, *6*, 425-432.
125. G. G. Glenner, C. W. Wong, *Biochem. Biophys. Res. Commun.* **1984**, *120*, 885-890.
126. K. S. Kosik, C. L. Joachim, D. J. Selkoe, *Proc. Natl. Acad. Sci. USA* **1986**, *83*, 4044-4048.
127. J. Kang, H. G. Lemaire, A. Unterbeck, J. M. Salbaum, C. L. Masters, *Nature* **1987**, *325*, 733-736.
128. M. P. Lambert, A. K. Barlow, B. A. Chromy, C. Edwards, R. Freed, M. Liosatos, T. E. Morgan, I. Rozovsky, B. Trommer, K. L. Viola, P. Wals, C. Zhang, C. E. Finch, G. A. Krafft, W. L. Klein, *Proc. Natl. Acad. Sci. U.S.A* **1998**, *95*, 6448-6453.
129. D. M. Walsh, D. M. Hartley, Y. Kusumoto, Y. Fezoui, M. M. Condron, A. Lomakin, G. B. Benedek, D. J. Selkoe, D. B. Teplow, *J. Biol. Chem.* **1999**, *274*, 25945-25952.



130. K. A. Conway, S.-J. Lee, J.-C. Rochet, T. T. Ding, R. E. Williamson, P. T. Lansbury, *Proc. Natl. Acad. Sci. U.S.A* **2000**, *97*, 571-576.
131. S. T. Ferreira, M. N. N. Vieira, F. G. De Felice, *IUBMB Life* **2007**, *59*, 332-345.
132. S. Zraika, R. L. Hull, C. B. Verchere, A. Clark, K. J. Potter, P. E. Fraser, D. P. Raleigh, S. E. Kahn, *Diabetologia* **2010**, *53*, 1046-1056.
133. L. Haataja, T. Gurlo, C. J. Huang, P. C. Butler, *Endocr. Rev.* **2008**, *29*, 303-316.
134. N. Suzuki, T. T. Cheung, X. D. Cai, A. Odaka, L. Otvos, C. Eckman, T. E. Golde, S. G. Younkin, *Science* **1994**, *264*, 1336-1340.
135. S. G. Amara, E. Bamberg, B. Fleischmann, T. Gudermann, S. C. Hebert, R. Jahn, W. J. Lederer, R. Lill, A. Miyajima, S. Offermanns, R. Zechner, R. S. Harrison, P. C. Sharpe, Y. Singh, D. P. Fairlie, in *Reviews of Physiology, Biochemistry and Pharmacology, Vol. 159*, Springer Berlin Heidelberg, **2007**, pp. 1-77.
136. G. Bitan, M. D. Kirkitadze, A. Lomakin, S. S. Vollers, G. B. Benedek, D. B. Teplow, *Proc. Natl. Acad. Sci. U.S.A* **2003**, *100*, 330-335.
137. C. G. Glabe, *J. Biol. Chem.* **2008**, *283*, 29639-29643.
138. M. Sakono, T. Zako, *FEBS J.* **2010**, *277*, 1348-1358.
139. M. Bucciantini, G. Calloni, F. Chiti, L. Formigli, D. Nosi, C. M. Dobson, M. Stefani, *J. Biol. Chem.* **2004**, *279*, 31374-31382.
140. M. Bucciantini, E. Giannoni, F. Chiti, F. Baroni, L. Formigli, J. S. Zurdo, N. Taddei, G. Ramponi, C. M. Dobson, M. Stefani, *Nature* **2002**, *416*, 507-511.
141. C. G. Glabe, *Neurobiol. Aging* **2006**, *27*, 570-575.
142. M. Goedert, M. G. Spillantini, *Science* **2006**, *314*, 777-781.
143. M. Citron, *Nat. Rev. Drug Discov.* **2010**, *9*, 387-398.
144. C. Haass, B. D. Strooper, *Science* **1999**, *286*, 916-919.
145. T. Hamaguchi, K. Ono, M. Yamada, *Cell. Mol. Life Sci.* **2006**, *63*, 1538-1552.
146. F. M. Laird, H. Cai, A. V. Savonenko, M. H. Farah, K. He, T. Melnikova, H. Wen, H.-C. Chiang, G. Xu, V. E. Koliatsos, *J. Neurosci.* **2005**, *25*, 11693-11709.
147. Y. Luo, B. Bolon, S. Kahn, B. D. Bennett, S. Babu-Khan, P. Denis, W. Fan, H. Kha, J. Zhang, Y. Gong, L. Martin, J.-C. Louis, Q. Yan, W. G. Richards, M. Citron, R. Vassar, *Nat. Neurosci.* **2001**, *4*, 231-232.
148. A. K. Ghosh, M. Brindisi, J. Tang, *J. Neurochem.* **2012**, *120*, 71-83.
149. M. S. Wolfe, *J. Neurochem.* **2012**, *120*, 89-98.
150. F. Panza, V. Frisardi, B. P. Imbimbo, C. Capurso, G. Logroscino, D. Sancarlo, D. Seripa, G. Vendemiale, A. Pilotto, V. Solfrizzi, *CNS Neurosci. Ther.* **2010**, *16*, 272-284.
151. S. F. Lichtenthaler, *J. Neurochem.* **2011**, *116*, 10-21.
152. K. Furukawa, B. L. Sopher, R. E. Rydel, J. G. Begley, D. G. Pham, G. M. Martin, M. Fox, M. P. Mattson, *J. Neurochem.* **1996**, *67*, 1882-1896.
153. H. Meziane, J. C. Dodart, C. Mathis, S. Little, J. Clemens, S. M. Paul, A. Ungerer, *Proc. Natl. Acad. Sci. U.S.A* **1998**, *95*, 12683-12688.
154. T. D. Stein, N. J. Anders, C. DeCarli, S. L. Chan, M. P. Mattson, J. A. Johnson, *J. Neurosci.* **2004**, *24*, 7707-7717.
155. D. J. Selkoe, *Trends Neurosci.* **1993**, *16*, 403.
156. C. A. McLean, R. A. Cherny, F. W. Fraser, S. J. Fuller, M. J. Smith, V. Konrad, A. I. Bush, C. L. Masters, *Ann. Neurol.* **1999**, *46*, 860-866.
157. J. Wang, D. W. Dickson, J. Q. Trojanowski, V. M. Y. Lee, *Exp. Neurol.* **1999**, *158*, 328-337.
158. D. Schenk, R. Barbour, W. Dunn, G. Gordon, H. Grajeda, T. Guido, K. Hu, J. Huang, K. Johnson-Wood, K. Khan, D. Kholodenko, M. Lee, Z. Liao, I. Lieberburg, R. Motter, L. Mutter, F. Soriano, G. Shopp, N. Vasquez, C. Vandevent, S. Walker, M. Wogulis, T. Yednock, D. Games, P. Seubert, *Nature* **1999**, *400*, 173-177.
159. D. Morgan, D. M. Diamond, P. E. Gottschall, K. E. Ugen, C. Dickey, J. Hardy, K. Duff, P. Jantzen, G. DiCarlo, D. Wilcock, K. Connor, J. Hatcher, C. Hope, M. Gordon, G. W. Arendash, *Nature* **2000**, *408*, 982-985.

160. R. Dodel, H. Hampel, C. Depboylu, S. Lin, F. Gao, S. Schock, S. Jäckel, X. Wei, K. Buerger, C. Höft, B. Hemmer, H.-J. Möller, M. Farlow, W. H. Oertel, N. Sommer, Y. Du, *Ann. Neurol.* **2002**, *52*, 253-256.
161. R. Dodel, K. Balakrishnan, K. Keyvani, O. Deuster, F. Neff, L.-C. Andrei-Selmer, S. Röskam, C. Stüer, Y. Al-Abed, C. Noelker, *J. Neurosci.* **2011**, *31*, 5847-5854.
162. N. N. Nalivaeva, C. Beckett, N. D. Belyaev, A. J. Turner, *J. Neurochem.* **2011**, *120*, 167-185.
163. T. Saito, N. Iwata, S. Tsubuki, Y. Takaki, J. Takano, S.-M. Huang, T. Suemoto, M. Higuchi, T. C. Saido, *Nat. Med.* **2005**, *11*, 434-439.
164. M. A. Leissring, W. Farris, A. Y. Chang, D. M. Walsh, X. Wu, X. Sun, M. P. Frosch, D. J. Selkoe, *Neuron* **2003**, *40*, 1087-1093.
165. B. Spencer, R. A. Marr, R. Gindi, R. Potkar, S. Michael, A. Adame, E. Rockenstein, I. M. Verma, E. Masliah, *PLoS ONE* **2011**, *6*, e16575.
166. M. A. Leissring, *J. Biol. Chem.* **2008**, *283*, 29645-29649.
167. R. Wetzel, S. Shivaprasad, A. D. Williams, *Biochemistry* **2007**, *46*, 1-10.
168. M. B. Linder, G. R. Szilvay, T. Nakari-Setälä, M. E. Penttilä, *FEMS Microbiol. Rev.* **2005**, *29*, 877-896.
169. M. Gebbink, D. Claessen, B. Bouma, L. Dijkhuizen, H. A. B. Wosten, *Nat. Rev. Microbiol.* **2005**, *3*, 333-341.
170. N. J. Talbot, *Curr. Biol.* **2003**, *13*, R696-R698.
171. H. A. B. Wösten, M.-A. van Wetter, L. G. Lugones, H. C. van der Mei, H. J. Busscher, J. G. H. Wessels, *Curr. Biol.* **1999**, *9*, 85-88.
172. M. Hammar, Z. Bian, S. Normark, *Proc. Natl. Acad. Sci. U.S.A* **1996**, *93*, 6562-6566.
173. M. R. Chapman, L. S. Robinson, J. S. Pinkner, R. Roth, J. Heuser, M. Hammar, S. Normark, S. J. Hultgren, *Science* **2002**, *295*, 851-855.
174. X. Wang, D. R. Smith, J. W. Jones, M. R. Chapman, *J. Biol. Chem.* **2007**, *282*, 3713-3719.
175. J. F. Berson, A. C. Theos, D. C. Harper, D. Tenza, G. Raposo, M. S. Marks, *J. Cell Biol.* **2003**, *161*, 521-533.
176. D. M. Fowler, A. V. Koulov, C. Alory-Jost, M. S. Marks, W. E. Balch, J. W. Kelly, *PLoS Biol.* **2006**, *4*, e6.
177. J. M. Kenney, D. Knight, M. J. Wise, F. Vollrath, *Eur. J. Biochem.* **2002**, *269*, 4159-4163.
178. U. Slotta, S. Hess, K. Spieß, T. Stromer, L. Serpell, T. Scheibel, *Macromol. Biosci.* **2007**, *7*, 183-188.
179. T. Scheibel, R. Parthasarathy, G. Sawicki, X. M. Lin, H. Jaeger, S. L. Lindquist, *Proc. Natl. Acad. Sci. U.S.A* **2003**, *100*, 4527-4532.
180. Y. J. Song, S. R. Challa, C. J. Medforth, Y. Qiu, R. K. Watt, D. Pena, J. E. Miller, F. van Swol, J. A. Shelhutt, *Chem. Commun.* **2004**, 1044-1045.
181. O. Carny, D. E. Shalev, E. Gazit, *Nano Lett.* **2006**, *6*, 1594-1597.
182. M. Reches, E. Gazit, *J. Nanosci. Nanotechnol.* **2007**, *7*, 2239-2245.
183. M. Reches, E. Gazit, *Science* **2003**, *300*, 625-627.
184. H. Kodama, S. Matsumura, T. Yamashita, H. Mihara, *Chem. Commun.* **2004**, *0*, 2876-2877.
185. U. Baxa, V. Speransky, A. C. Steven, R. B. Wickner, *Proc. Natl. Acad. Sci. U.S.A* **2002**, *99*, 5253-5260.
186. A. J. Baldwin, R. Bader, J. Christodoulou, C. E. MacPhee, C. M. Dobson, P. D. Barker, *J. Am. Chem. Soc.* **2006**, *128*, 2162-2163.
187. A. Aggeli, M. Bell, N. Boden, J. N. Keen, P. F. Knowles, T. C. B. McLeish, M. Pitkeathly, S. E. Radford, *Nature* **1997**, *386*, 259-262.
188. A. Aggeli, M. Bell, L. M. Carrick, C. W. G. Fishwick, R. Harding, P. J. Mawer, S. E. Radford, A. E. Strong, N. Boden, *J. Am. Chem. Soc.* **2003**, *125*, 9619-9628.
189. Y. Zhang, H. W. Gu, Z. M. Yang, B. Xu, *J. Am. Chem. Soc.* **2003**, *125*, 13680-13681.

190. Z. M. Yang, G. L. Liang, L. Wang, B. Xu, *J. Am. Chem. Soc.* **2006**, *128*, 3038-3043.
191. A. Mahler, M. Reches, M. Rechter, S. Cohen, E. Gazit, *Adv. Mater.* **2006**, *18*, 1365-1370.
192. V. Jayawarna, M. Ali, T. A. Jowitt, A. E. Miller, A. Saiani, J. E. Gough, R. V. Ulijn, *Adv. Mater.* **2006**, *18*, 611-614.
193. M. H. Hecht, A. Das, A. Go, L. H. Bradley, Y. Wei, *Protein Sci.* **2004**, *13*, 1711-1723.
194. S. Cavalli, J. W. Handgraaf, E. E. Tellers, D. C. Popescu, M. Overhand, K. Kjaer, V. Vaiser, N. Sommerdijk, H. Rapaport, A. Kros, *J. Am. Chem. Soc.* **2006**, *128*, 13959-13966.
195. S. Cavalli, D. C. Popescu, E. E. Tellers, M. R. J. Vos, B. P. Pichon, M. Overhand, H. Rapaport, N. A. J. M. Sommerdijk, A. Kros, *Angew. Chem.* **2006**, *118*, 753-758.
196. J. P. Schneider, D. J. Pochan, B. Ozbas, K. Rajagopal, L. Pakstis, J. Kretsinger, *J. Am. Chem. Soc.* **2002**, *124*, 15030-15037.
197. L. A. Haines, K. Rajagopal, B. Ozbas, D. A. Salick, D. J. Pochan, J. P. Schneider, *J. Am. Chem. Soc.* **2005**, *127*, 17025-17029.
198. X. J. Zhao, S. G. Zhang, *Macromol. Biosci.* **2007**, *7*, 13-22.
199. S. G. Zhang, *Nat. Biotechnol.* **2003**, *21*, 1171-1178.
200. A. K. Mitra, I. Ostashevsky, C. F. Brewer, *Int. J. Pept. Protein Res.* **1983**, *22*, 495-501.
201. O. D. Hensens, R. F. White, R. T. Goegelman, E. S. Inamine, A. A. Patchett, *J. Antibiot.* **1992**, *45*, 133-135.
202. A. A. Patchett, D. Taub, O. D. Hensens, R. T. Goegelman, L. Yang, F. Dumont, L. Peterson, N. H. Sigal, *J. Antibiot.* **1992**, *45*, 94-102.
203. H. R. Hoveyda, J.-F. Pinault, *Org. Lett.* **2006**, *8*, 5849-5852.
204. H. Meng, S. T. Krishnaji, M. Beinborn, K. Kumar, *J. Med. Chem.* **2008**, *51*, 7303-7307.
205. L. M. Gottler, H. Y. Lee, C. E. Shelburne, A. Ramamoorthy, E. N. G. Marsh, *ChemBioChem* **2008**, *9*, 370-373.
206. H. Meng, K. Kumar, *J. Am. Chem. Soc.* **2007**, *129*, 15615-15622.
207. V. Asante, J. Mortier, H. Schlüter, B. Kokschi, *Bioorg. Med. Chem.* **2013**, *21*, 3542-3546.
208. J. M. Mason, K. M. Arndt, *ChemBioChem* **2004**, *5*, 170-176.
209. P. Burkhard, S. Ivaninskii, A. Lustig, *J. Mol. Biol.* **2002**, *318*, 901-910.
210. D. N. Woolfson, a. J. M. S. David A. D. Parry, *Advances in Protein Chemistry* **2005**, *Volume 70*, 79-112.
211. Y. Tang, G. Ghirlanda, N. Vaidehi, J. Kua, D. T. Mainz, W. A. Goddard, W. F. DeGrado, D. A. Tirrell, *Biochemistry* **2001**, *40*, 2790-2796.
212. S. Son, I. C. Tanrikulu, D. A. Tirrell, *ChemBioChem* **2006**, *7*, 1251-1257.
213. B. Bilgiçer, A. Fichera, K. Kumar, *J. Am. Chem. Soc.* **2001**, *123*, 4393-4399.
214. Y. Tang, G. Ghirlanda, W. A. Petka, T. Nakajima, W. F. DeGrado, D. A. Tirrell, *Angew. Chem. Int. Ed.* **2001**, *40*, 1494-1496.
215. Y. Tang, D. A. Tirrell, *J. Am. Chem. Soc.* **2001**, *123*, 11089-11090.
216. B. Bilgiçer, X. Xing, K. Kumar, *J. Am. Chem. Soc.* **2001**, *123*, 11815-11816.
217. B. Bilgiçer, K. Kumar, *Tetrahedron* **2002**, *58*, 4105-4112.
218. N. Naarmann, B. Bilgiçer, H. Meng, K. Kumar, C. Steinem, *Angew. Chem. Int. Ed.* **2006**, *45*, 2588-2591.
219. B. Bilgiçer, K. Kumar, *Proc. Natl. Acad. Sci. U.S.A* **2004**, *101*, 15324-15329.
220. K.-H. Lee, H.-Y. Lee, M. M. Slutsky, J. T. Anderson, E. N. G. Marsh, *Biochemistry* **2004**, *43*, 16277-16284.
221. H.-Y. Lee, K.-H. Lee, H. M. Al-Hashimi, E. N. G. Marsh, *J. Am. Chem. Soc.* **2006**, *128*, 337-343.
222. B. C. Buer, R. de la Salud-Bea, H. M. Al Hashimi, E. N. G. Marsh, *Biochemistry* **2009**, *48*, 10810-10817.

223. B. C. Buer, J. L. Meagher, J. A. Stuckey, E. N. G. Marsh, *Proc. Natl. Acad. Sci. U.S.A* **2012**, *109*, 4810-4815.
224. B. C. Buer, B. J. Levin, E. N. G. Marsh, *J. Am. Chem. Soc.* **2012**, *134*, 13027-13034.
225. C. Jäckel, W. Seufert, S. Thust, B. Koksich, *ChemBioChem* **2004**, *5*, 717-720.
226. C. Jäckel, M. Salwiczek, B. Koksich, *Angew. Chem. Int. Ed.* **2006**, *45*, 4198-4203.
227. M. Salwiczek, S. Samsonov, T. Vagt, E. Nyakatura, E. Fleige, J. Numata, H. Colfen, M. T. Pisabarro, B. Koksich, *Chem. Eur. J.* **2009**, *15*, 7628-7636.
228. M. Salwiczek, B. Koksich, *ChemBioChem* **2009**, *10*, 2867-2870.
229. M. Salwiczek, *Biophysical Aspects of Single Fluoroalkylamino acid Substitutions within a Natural Polypeptide Environment*, Dissertation thesis, Freie Universität Berlin (Berlin), **2010**.
230. A. Niemz, D. A. Tirrell, *J. Am. Chem. Soc.* **2001**, *123*, 7407-7413.
231. P. Wang, Y. Tang, D. A. Tirrell, *J. Am. Chem. Soc.* **2003**, *125*, 6900-6906.
232. D. Alexeev, P. N. Barlow, S. M. Bury, J. D. Charrier, A. Cooper, D. Hadfield, C. Jamieson, S. M. Kelly, R. Layfield, R. J. Mayer, H. McSparron, N. C. Price, R. Ramage, L. Sawyer, B. A. Starkmann, D. Uhrin, J. Wilken, D. W. Young, *ChemBioChem* **2003**, *4*, 894-896.
233. T. Panchenko, W. W. Zhu, J. K. Montclare, *Biotechnol. Bioeng.* **2006**, *94*, 921-930.
234. T. H. Yoo, A. J. Link, D. A. Tirrell, *Proc. Natl. Acad. Sci. U.S.A* **2007**, *104*, 13887-13890.
235. J. K. Montclare, D. A. Tirrell, *Angew. Chem. Int. Ed.* **2006**, *45*, 4518-4521.
236. H.-P. Chiu, Y. Suzuki, D. Gullickson, R. Ahmad, B. Kokona, R. Fairman, R. P. Cheng, *J. Am. Chem. Soc.* **2006**, *128*, 15556-15557.
237. H.-P. Chiu, R. P. Cheng, *Org. Lett.* **2007**, *9*, 5517-5520.
238. A. Chakrabarty, T. Kortemme, R. L. Baldwin, *Protein Sci.* **1994**, *3*, 843-852.
239. A. J. Doig, A. Chakrabarty, T. M. Klingler, R. L. Baldwin, *Biochemistry* **1994**, *33*, 3396-3403.
240. N. H. Andersen, H. Tong, *Protein Sci.* **1997**, *6*, 1920-1936.
241. H. Erdbrink, I. Peuser, U. I. M. Gerling, D. Lentz, B. Koksich, C. Czekelius, *Org. Biomol. Chem.* **2012**, *10*, 8583-8586.
242. J.-C. Horng, D. P. Raleigh, *J. Am. Chem. Soc.* **2003**, *125*, 9286-9287.
243. B. Anil, S. Sato, J.-H. Cho, D. P. Raleigh, *J. Mol. Biol.* **2005**, *354*, 693-705.
244. H.-P. Chiu, B. Kokona, R. Fairman, R. P. Cheng, *J. Am. Chem. Soc.* **2009**, *131*, 13192-13193.
245. L. M. Gottler, R. de la Salud Bea, C. E. Shelburne, A. Ramamoorthy, E. N. G. Marsh, *Biochemistry* **2008**, *47*, 9243-9250.
246. G. A. Clark, J. D. Baleja, K. Kumar, *J. Am. Chem. Soc.* **2012**, *134*, 17912-17921.
247. J. D. Dunitz, *ChemBioChem* **2004**, *5*, 614-621.
248. D. L. Minor, P. S. Kim, *Nature* **1994**, *367*, 660-663.
249. Y. Suzuki, J. R. Brender, M. T. Soper, J. Krishnamoorthy, Y. Zhou, B. T. Ruotolo, N. A. Kotov, A. Ramamoorthy, E. N. G. Marsh, *Biochemistry* **2013**, *52*, 1903-1912.
250. P. T. Lansbury, H. A. Lashuel, *Nature* **2006**, *443*, 774-779.
251. S. M. Vaiana, R. Ghirlando, W.-M. Yau, W. A. Eaton, J. Hofrichter, *Biophys. J.* **2008**, *94*, L45-L47.
252. R. Kaye, E. Head, J. L. Thompson, T. M. McIntire, S. C. Milton, C. W. Cotman, C. G. Glabe, *Science* **2003**, *300*, 486-489.
253. S. L. Cobb, C. D. Murphy, *J. Fluorine Chem.* **2009**, *130*, 132-143.
254. C. Li, G.-F. Wang, Y. Wang, R. Creager-Allen, E. A. Lutz, H. Scronce, K. M. Slade, R. A. S. Ruf, R. A. Mehl, G. J. Pielak, *J. Am. Chem. Soc.* **2009**, *132*, 321-327.
255. C. Li, E. A. Lutz, K. M. Slade, R. A. S. Ruf, G.-F. Wang, G. J. Pielak, *Biochemistry* **2009**, *48*, 8578-8584.
256. J. Lee, E. K. Culyba, E. T. Powers, J. W. Kelly, *Nat. Chem. Biol.* **2011**, *7*, 602-609.
257. M. D. Kirkitadze, M. M. Condron, D. B. Teplow, *J. Mol. Biol.* **2001**, *312*, 1103-1119.

- 
258. H. Ding, P. T. Wong, E. L. Lee, A. Gafni, D. G. Steel, *Biophys. J.* **2009**, *97*, 912-921.
259. S. Luca, W.-M. Yau, R. Leapman, R. Tycko, *Biochemistry* **2007**, *46*, 13505-13522.
260. S. Afonin, P. K. Mikhailiuk, I. V. Komarov, A. S. Ulrich, *J. Pept. Sci.* **2007**, *13*, 614-623.
261. R. W. Glaser, C. Sachse, U. H. N. Dürr, P. Wadhvani, A. S. Ulrich, *J. Magn. Reson.* **2004**, *168*, 153-163.
262. S. L. Grage, A. V. Suleymanova, S. Afonin, P. Wadhvani, A. S. Ulrich, *J. Magn. Reson.* **2006**, *183*, 77-86.
263. E. Strandberg, A. S. Ulrich, *Concept Magn. Reson. A* **2004**, *23A*, 89-120.
264. P. Wadhvani, J. Bürck, E. Strandberg, C. Mink, S. Afonin, A. S. Ulrich, *J. Am. Chem. Soc.* **2008**, *130*, 16515-16517.
265. Y. Wolf, S. Pritz, S. d. Abes, M. Bienert, B. Lebleu, J. Oehlke, *Biochemistry* **2006**, *45*, 14944-14954.
266. J. J. M. Hoozemans, S. M. Chafekar, F. Baas, P. Eikelenboom, W. Scheper, *Curr. Med. Chem.* **2006**, *13*, 2599.
267. B. O'Nuallain, S. Shivaprasad, I. Kheterpal, R. Wetzal, *Biochemistry* **2005**, *44*, 12709.
268. T. H. J. Huang, D. S. Yang, P. E. Fraser, A. Chakrabarty, *J. Biol. Chem.* **2000**, *275*, 36436.
269. R. P. Friedrich, K. Tepper, R. Roznicke, M. Soom, M. Westermann, K. Reymann, C. Kaether, M. Fandrich, *Proc. Natl. Acad. Sci. U.S.A.* **2010**, *107*, 1942.
270. F. T. Senguen, N. R. Lee, X. Gu, D. M. Ryan, T. M. Doran, E. A. Anderson, B. L. Nilsson, *Mol. BioSyst.* **2011**, *7*, 486-496.
271. K. E. Marshall, K. L. Morris, D. Charlton, N. O'Reilly, L. Lewis, H. Walden, L. C. Serpell, *Biochemistry* **2011**, *50*, 2061-2071.
272. E. Neil, G. Marsh, *Chem. Biol.* **2000**, *7*, R153-R157.
273. G. D. Fasman, *Circular Dichroism and the Conformational Analysis of Biomolecules*, Plenum Press, New York, **1996**.
274. R. W. Woody, *Circular Dichroism and the Conformational Analysis of Biomolecules*, Plenum Press, New York, **1996**.
275. N. J. Greenfield, G. D. Fasman, *Biochemistry* **1969**, *8*, 4108-4116.
276. J. Reed, T. A. Reed, *Anal. Biochem.* **1997**, *254*, 36-40.
277. N. J. Greenfield, *Anal. Biochem.* **1996**, *235*, 1-10.
278. H. Puchtler, F. Sweat, M. Levine, *J. Histochem. Cytochem.* **1962**, *10*, 355-364.
279. H. Naiki, K. Higuchi, M. Hosokawa, T. Takeda, *Anal. Biochem.* **1989**, *177*, 244-249.
280. E. Brandenburg, H. v. Berlepsch, B. Koksche, *Mol. BioSyst.* **2012**, *8*, 557-564.
281. G. T. Westermark, K. H. Johnson, P. Westermark, *Methods Enzymol.* **1999**, *309*, 3-25.
282. Q. Li, J. S. Lee, C. Ha, C. B. Park, G. Yang, W. B. Gan, Y. T. Chang, *Angew. Chem. Int. Ed.* **2004**, *43*, 6331-6335.
283. P. S. Vassar, C. F. Culling, *Arch. Pathol.* **1959**, *68*, 487-498.
284. A. Lorenzo, B. A. Yankner, *Proc. Natl. Acad. Sci. U.S.A* **1994**, *91*, 12243-12247.
285. W. G. Turnell, J. T. Finch, *J. Mol. Biol.* **1992**, *227*, 1205-1223.
286. H. LeVine III, *Methods Enzymol.* **1999**, *309*, 274-284.
287. E. E. Nesterov, J. Skoch, B. T. Hyman, W. E. Klunk, B. J. Bacskai, T. M. Swager, *Angew. Chem. Int. Ed.* **2005**, *44*, 5452-5456.
288. H. Levine III, *Protein Sci.* **1993**, *2*, 404-410.
289. H. Naiki, K. Higuchi, K. Kitagawa, A. Shimada, W.-H. Chen, M. Hosokawa, K. Nakakuki, T. Takeda, in *Amyloid and Amyloidosis 1990*, Springer, **1991**, pp. 393-396.
290. L. Cai, R. B. Innis, V. W. Pike, *Curr. Med. Chem.* **2007**, *14*, 19-52.
291. W. E. Klunk, Y. Wang, G.-f. Huang, M. L. Debnath, D. P. Holt, C. A. Mathis, *Life Sci.* **2001**, *69*, 1471-1484.

292. M. Biancalana, S. Koide, *Biochim. Biophys. Acta* **2010**, 1804, 1405.
293. M. R. H. Krebs, E. H. C. Bromley, A. M. Donald, *J. Struct. Biol.* **2005**, 149, 30-37.
294. M. Biancalana, K. Makabe, A. Koide, S. Koide, *J. Mol. Biol.* **2009**, 385, 1052-1063.
295. C. Wu, Z. Wang, H. Lei, W. Zhang, Y. Duan, *J. Am. Chem. Soc.* **2007**, 129, 1225-1232.
296. M. Groenning, L. Olsen, M. van de Weert, J. M. Flink, S. Frokjaer, F. S. Jørgensen, *J. Struct. Biol.* **2007**, 158, 358-369.
297. M. Groenning, M. Norrman, J. M. Flink, M. van de Weert, J. T. Bukrinsky, G. Schluckebier, S. Frokjaer, *J. Struct. Biol.* **2007**, 159, 483-497.
298. P. Sen, S. Fatima, B. Ahmad, R. H. Khan, *Spectrochim. Acta A Mol. Biomol. Spectrosc.* **2009**, 74, 94-99.
299. M. Lindgren, K. Sörgjerd, P. Hammarström, *Biophys. J.* **2005**, 88, 4200-4212.
300. V. I. Stsiapura, A. A. Maskevich, V. A. Kuzmitsky, V. N. Uversky, I. M. Kuznetsova, K. K. Turoverov, *J. Phys. Chem. B* **2008**, 112, 15893-15902.
301. V. I. Stsiapura, A. A. Maskevich, S. A. Tikhomirov, O. V. Buganov, *J. Phys. Chem. A* **2010**, 114, 8345-8350.
302. P. K. Singh, M. Kumbhakar, H. Pal, S. Nath, *J. Phys. Chem. B* **2009**, 113, 8532-8538.
303. Y. Nozaki, N. M. Schechter, J. A. Reynolds, C. Tanford, *Biochemistry* **1976**, 15, 3884-3890.
304. D. J. Slotboom, R. H. Duurkens, K. Olieman, G. B. Erkens, *Methods* **2008**, 46, 73-82.
305. P. J. Wyatt, *Anal. Chim. Acta.* **1993**, 272, 1-40.
306. F. Lottspeich, H. Zorbas, *Bioanalytik*, Spektrum Akademischer Verlag, Heidelberg-Berlin, **1998**.
307. H. Heise, *ChemBioChem* **2008**, 9, 179-189.
308. R. K. Harris, P. Jackson, *Chem. Rev.* **1991**, 91, 1427-1440.
309. A. S. Ulrich, *Prog. Nucl. Magn. Reson. Spectrosc.* **2005**, 46, 1-21.
310. S. A. Carss, U. Scheler, R. K. Harris, P. Holstein, R. A. Fletton, *Magn. Reson. Chem.* **1996**, 34, 63-70.
311. A. S. Ulrich, in *Modern magnetic resonance*, Springer, **2006**, pp. 261-267.
312. I. Fischbach, T. Pakula, P. Minkin, A. Fechtenkötter, K. Müllen, H. W. Spiess, K. Saalwächter, *J. Phys. Chem. B* **2002**, 106, 6408-6418.
313. E. R. deAzevedo, W. G. Hu, T. J. Bonagamba, K. Schmidt-Rohr, *J. Am. Chem. Soc.* **1999**, 121, 8411-8412.
314. D. Reichert, T. J. Bonagamba, K. Schmidt-Rohr, *J. Magn. Reson.* **2001**, 151, 129-135.
315. J. J. Buffy, A. J. Waring, M. Hong, *J. Am. Chem. Soc.* **2005**, 127, 4477-4483.
316. M. T. Pastor, A. Esteras-Chopo, M. L. de la Paz, *Curr. Opin. Struct. Biol.* **2005**, 15, 57-63.
317. E. Hughes, R. M. Burke, A. J. Doig, *J. Biol. Chem.* **2000**, 275, 25109-25115.
318. N. Sureshbabu, R. Kirubakaran, H. Thangarajah, E. J. P. Malar, R. Jayakumar, *J. Mol. Neurosci.* **2010**, 41, 368-382.
319. A. Mazzaglia, N. Micali, L. M. Scolaro, F. Attanasio, A. Magrí, G. Pappalardo, V. Villari, *J. Phys. Chem. B* **2009**, 114, 705-713.
320. J. L. Jiménez, E. J. Nettleton, M. Bouchard, C. V. Robinson, C. M. Dobson, H. R. Saibil, *Proc. Natl. Acad. Sci. U.S.A* **2002**, 99, 9196-9201.
321. J. L. Jimenez, J. I. Guijarro, E. Orlova, J. Zurdo, C. M. Dobson, M. Sunde, H. R. Saibil, *Embo J.* **1999**, 18, 815-821.
322. C. d. Govaerts, H. Wille, S. B. Prusiner, F. E. Cohen, *Proc. Natl. Acad. Sci. U.S.A* **2004**, 101, 8342-8347.
323. M. Mutter, R. Gassmann, U. Buttkus, K. H. Altmann, *Angew. Chem. Int. Ed.* **1991**, 30, 1514-1516.
324. P. Y. Chou, G. D. Fasman, *Biochemistry* **1974**, 13, 211-222.
325. P. Y. Chou, G. D. Fasman, *Annu. Rev. Biochem.* **1978**, 47, 251-276.

326. K. Pagel, B. Kokschi, *Curr. Opin. Chem. Biol.* **2008**, *12*, 730-739.
327. F. H. C. Crick, *Nature* **1952**, *170*, 882-883.
328. E. K. O'Shea, J. D. Klemm, P. S. Kim, T. Alber, *Science* **1991**, *254*, 539-544.
329. W. Weissenhorn, A. Dessen, S. C. Harrison, J. J. Skehel, D. C. Wiley, *Nature* **1997**, *387*, 426-430.
330. D. N. Woolfson, a. J. M. S. David A. D. Parry, in *Advances in Protein Chemistry, Vol. Volume 70*, Academic Press, **2005**, pp. 79-112.
331. C. Cohen, D. A. D. Parry, *Proteins: Struct. Funct. Bioinf.* **1990**, *7*, 1-15.
332. A. Lupas, M. Van Dyke, J. Stock, *Science* **1991**, *252*, 1162-1164.
333. M. Meier, A. Lustig, U. Aebi, P. Burkhard, *J. Struct. Biol.* **2002**, *137*, 65-72.
334. N. E. Zhou, C. M. Kay, R. S. Hodges, *Protein Eng.* **1994**, *7*, 1365-1372.
335. N. E. Zhou, C. M. Kay, R. S. Hodges, *J. Mol. Biol.* **1994**, *237*, 500-512.
336. W. D. Kohn, O. D. Monera, C. M. Kay, R. S. Hodges, *J. Biol. Chem.* **1995**, *270*, 25495-25506.
337. W. D. Kohn, C. M. Kay, R. S. Hodges, *J. Pept. Sci.* **1997**, *3*, 209-223.
338. P. B. Harbury, T. Zhang, P. S. Kim, T. Alber, *Science* **1993**, *262*, 1401-1407.
339. L. Gonzalez, D. N. Woolfson, T. Alber, *Nat. Struct. Mol. Biol.* **1996**, *3*, 1011-1018.
340. D. N. Woolfson, a. J. M. S. David A. D. Parry, in *Advances in Protein Chemistry, Vol. 70*, Academic Press, **2005**, pp. 79-112.
341. D. L. McClain, J. P. Binfeet, M. G. Oakley, *J. Mol. Biol.* **2001**, *313*, 371-383.
342. O. D. Monera, C. M. Kay, R. S. Hodges, *Biochemistry* **1994**, *33*, 3862-3871.
343. T. J. Graddis, D. G. Myszkka, I. M. Chaiken, *Biochemistry* **1993**, *32*, 12664-12671.
344. Y. Takahashi, A. Ueno, H. Mihara, *Chem. Eur. J.* **1998**, *4*, 2475-2484.
345. H. Mihara, Y. Takahashi, *Curr. Opin. Struct. Biol.* **1997**, *7*, 501-508.
346. Y. Takahashi, A. Ueno, H. Mihara, *Bioorg. Med. Chem.* **1999**, *7*, 177-185.
347. Y. Takahashi, T. Yamashita, A. Ueno, H. Mihara, *Tetrahedron* **2000**, *56*, 7011-7018.
348. H. Dong, J. D. Hartgerink, *Biomacromolecules* **2007**, *8*, 617-623.
349. B. Ciani, E. G. Hutchinson, R. B. Sessions, D. N. Woolfson, *J. Biol. Chem.* **2002**, *277*, 10150-10155.
350. K. Pagel, T. Vagt, B. Kokschi, *Org. Biomol. Chem.* **2005**, *3*, 3843-3850.
351. K. Pagel, S. C. Wagner, K. Samedov, H. von Berlepsch, C. Böttcher, B. Kokschi, *J. Am. Chem. Soc.* **2006**, *128*, 2196-2197.
352. K. Pagel, S. C. Wagner, R. Rezaei Araghi, H. von Berlepsch, C. Böttcher, B. Kokschi, *Chem. Eur. J.* **2008**, *14*, 11442-11451.
353. E. Brandenburg, H. von Berlepsch, U. I. M. Gerling, C. Böttcher, B. Kokschi, *Chem. Eur. J.* **2011**, *17*, 10651-10661.
354. J. A. Falenski, U. I. M. Gerling, B. Kokschi, *Bioorg. Med. Chem.* **2010**, *18*, 3703-3706.
355. M. Broncel, J. A. Falenski, S. C. Wagner, C. P. R. Hackenberger, B. Kokschi, *Chem. Eur. J.* **2010**, *16*, 7881-7888.
356. U. I. M. Gerling, *Strukturelle Charakterisierung eines coiled coil-basierten Amyloid-bildenden Modellsystems*, Master thesis, Freie Universität Berlin (Berlin), **2009**.
357. U. I. M. Gerling, *Untersuchungen der Internen Struktur eines Amyloid-Modellsystems durch Prolin-Modifikationen*, Practical Research thesis, Freie Universität Berlin (Berlin), **2008**.
358. U. I. M. Gerling, E. Brandenburg, H. v. Berlepsch, K. Pagel, B. Kokschi, *Biomacromolecules* **2010**, *12*, 2988-2996.
359. D. F. Moriarty, D. P. Raleigh, *Biochemistry* **1999**, *38*, 1811-1818.
360. S. J. Wood, R. Wetzel, J. D. Martin, M. R. Hurle, *Biochemistry* **1995**, *34*, 724.
361. P. Y. Chou, G. D. Fasman, *J. Mol. Biol.* **1977**, *115*, 135-175.
362. K. Takano, Y. Yamagata, K. Yutani, *Biochemistry* **2000**, *39*, 8655-8665.
363. S. R. Trevino, S. Schaefer, J. M. Scholtz, C. N. Pace, *J. Mol. Biol.* **2007**, *373*, 211-218.

364. A. Morimoto, K. Irie, K. Murakami, Y. Masuda, H. Ohigashi, M. Nagao, H. Fukuda, T. Shimizu, T. Shirasawa, *J. Biol. Chem.* **2004**, *279*, 52781-52788.
365. A. D. Williams, E. Portelius, I. Kheterpal, J.-T. Guo, K. D. Cook, Y. Xu, R. Wetzel, *J. Mol. Biol.* **2004**, *335*, 833-842.
366. A. D. Williams, S. Shivaprasad, R. Wetzel, *J. Mol. Biol.* **2006**, *357*, 1283-1294.
367. M. Jäger, M. Dendle, J. W. Kelly, *Protein Sci.* **2009**, *18*, 1806-1813.
368. A. Fox, T. Snollaerts, C. Errecart Casanova, A. Calciano, L. A. Nogaj, D. A. Moffet, *Biochemistry* **2010**, *49*, 7783-7789.
369. A. K. Buell, G. G. Tartaglia, N. R. Birkett, C. A. Waudby, M. Vendruscolo, X. Salvatella, M. E. Welland, C. M. Dobson, T. P. J. Knowles, *ChemBioChem* **2009**, *10*, 1309-1312.
370. T. Fujii, A. H. Iwane, T. Yanagida, K. Namba, *Nature* **2010**, *467*, 724-728.
371. Y. Masuda, A. Nakanishi, R. Ohashi, K. Takegoshi, T. Shimizu, T. Shirasawa, K. Irie, *Biosci. Biotechnol. Biochem.* **2008**, *72*, 2170-2175.
372. E. J. Milner-White, R. Poet, *Biochem. J.* **1986**, *240*, 289-292.
373. K. Guruprasad, S. Rajkumar, *J. Biosci.* **2000**, *25*, 143-156.
374. D. Zanuy, K. Gunasekaran, A. M. Lesk, R. Nussinov, *J. Mol. Biol.* **2006**, *358*, 330-345.
375. J. Hennesin, B. Jullian, A. C. Steven, A. V. Kajava, *J. Mol. Biol.* **2006**, *358*, 1094-1105.
376. J. Maity, P. Saha, U. I. M. Gerling, D. Lentz, B. Koksich, *Synthesis* **2012**, *44*, 3063-3070.
377. E. d. de Alba, M. A. Jiménez, M. Rico, J. L. Nieto, *Fold Des.* **1996**, *1*, 133-144.
378. B. L. Sibanda, T. L. Blundell, J. M. Thornton, *J. Mol. Biol.* **1989**, *206*, 759-777.
379. C. Renner, S. Alefelder, J. H. Bae, N. Budisa, R. Huber, L. Moroder, *Angew. Chem. Int. Ed.* **2001**, *40*, 923-925.
380. J. T. Gerig, R. S. McLeod, *J. Am. Chem. Soc.* **1973**, *95*, 5725-5729.
381. E. de Alba, M. A. Jiménez, M. Rico, *J. Am. Chem. Soc.* **1997**, *119*, 175-183.
382. J. Maity, U. I. M. Gerling, S. Vukelić, A. Schäfer, B. Koksich, *Amino Acids* **2014**, *46*, 177-186.
383. K. Wüthrich, M. Billeter, W. Braun, *J. Mol. Biol.* **1984**, *180*, 715-740.
384. K. Wüthrich, *NMR of proteins and nucleic acids*, John Wiley & Sons, New York, **1986**.
385. D. S. Wishart, B. D. Sykes, F. M. Richards, *J. Mol. Biol.* **1991**, *222*, 311-333.
386. A. M. Fernández-Escamilla, S. Ventura, L. Serrano, M. A. Jiménez, *Protein Sci.* **2006**, *15*, 2278-2289.
387. R. Lakshminarayanan, I. Yoon, B. G. Hegde, D. Fan, C. Du, J. Moradian-Oldak, *Proteins: Struct. Funct. Bioinf.* **2009**, *76*, 560-569.
388. J. Danielsson, J. Jarvet, P. Damberg, A. Gräslund, *FEBS J.* **2005**, *272*, 3938-3949.
389. E. Hellstrand, B. Boland, D. M. Walsh, S. Linse, *ACS Chem. Neurosci.* **2009**, *1*, 13-18.
390. T. P. J. Knowles, W. Shu, G. L. Devlin, S. Meehan, S. Auer, C. M. Dobson, M. E. Welland, *Proc. Natl. Acad. Sci. U.S.A* **2007**, *104*, 10016-10021.
391. J. Kardos, A. Micsonai, H. Pál-Gábor, É. Petrik, L. Gráf, J. Kovács, Y.-H. Lee, H. Naiki, Y. Goto, *Biochemistry* **2011**, *50*, 3211-3220.
392. C. H. Davis, M. L. Berkowitz, *J. Phys. Chem. B* **2009**, *113*, 14480-14486.
393. C. H. Davis, M. L. Berkowitz, *Proteins: Struct. Funct. Bioinf.* **2010**, *78*, 2533-2545.
394. J. A. Lemkul, D. R. Bevan, *Arch. Biochem. Biophys.* **2008**, *470*, 54-63.
395. M. Yang, D. B. Teplow, *J. Mol. Biol.* **2008**, *384*, 450-464.
396. T. P. J. Knowles, C. A. Waudby, G. L. Devlin, S. I. A. Cohen, A. Aguzzi, M. Vendruscolo, E. M. Terentjev, M. E. Welland, C. M. Dobson, *Science* **2009**, *326*, 1533-1537.
397. C. Haass, D. J. Selkoe, *Nat. Rev. Mol. Cell. Biol.* **2007**, *8*, 101-112.
398. D. M. Walsh, I. Klyubin, J. V. Fadeeva, W. K. Cullen, R. Anwyl, M. S. Wolfe, M. J. Rowan, D. J. Selkoe, *Nature* **2002**, *416*, 535-539.



399. M. Bucciantini, E. Giannoni, F. Chiti, F. Baroni, L. Formigli, J. Zurdo, N. Taddei, G. Ramponi, C. M. Dobson, M. Stefani, *Nature* **2002**, *416*, 507-511.
400. S. B. Padrick, A. D. Miranker, *Biochemistry* **2002**, *41*, 4694-4703.
401. F. A. Ferrone, J. Hofrichter, W. A. Eaton, *J. Mol. Biol.* **1985**, *183*, 611-631.
402. J. T. Jarrett, P. T. Lansbury Jr, *Cell* **1993**, *73*, 1055-1058.
403. A. K. Thakur, M. Jayaraman, R. Mishra, M. Thakur, V. M. Chellgren, I.-J. L. Byeon, D. H. Anjum, R. Kodali, T. P. Creamer, J. F. Conway, A. M Gronenborn, R. Wetzel, *Nat. Struct. Mol. Biol.* **2009**, *16*, 380-389.
404. A. Lomakin, D. S. Chung, G. B. Benedek, D. A. Kirschner, D. B. Teplow, *Proc. Natl. Acad. Sci. U.S.A* **1996**, *93*, 1125-1129.
405. T. R. Serio, A. G. Cashikar, A. S. Kowal, G. J. Sawicki, J. J. Moslehi, L. Serpell, M. F. Arnsdorf, S. L. Lindquist, *Science* **2000**, *289*, 1317-1321.
406. W.-F. Xue, S. W. Homans, S. E. Radford, *Proc. Natl. Acad. Sci. U.S.A* **2008**, *105*, 8926-8931.
407. C. J. Roberts, *Biotechnol. Bioeng.* **2007**, *98*, 927-938.
408. J. M. Andrews, C. J. Roberts, *J. Phys. Chem. B* **2007**, *111*, 7897-7913.
409. D. Ruzafa, B. Morel, L. Varela, A. I. Azuaga, F. Conejero-Lara, *PLoS ONE* **2012**, *7*, e49690.
410. A. Nayak, M. Sorci, S. Krueger, G. Belfort, *Proteins: Struct. Funct. Bioinf.* **2009**, *74*, 556-565.
411. A. M. Streets, Y. Sourigues, R. R. Kopito, R. Melki, S. R. Quake, *PLoS ONE* **2012**, *8*, e54541.
412. L. F. Pease III, M. Sorci, S. Guha, D.-H. Tsai, M. R. Zachariah, M. J. Tarlov, G. Belfort, *Biophys. J.* **2010**, *99*, 3979-3985.
413. N. S. Bieler, T. P. J. Knowles, D. Frenkel, R. Vácha, *PLoS Comput. Biol.* **2012**, *8*, e1002692.
414. S. Auer, C. M. Dobson, M. Vendruscolo, *HFSP J.* **2007**, *1*, 137-146.
415. A. Orte, N. R. Birkett, R. W. Clarke, G. L. Devlin, C. M. Dobson, D. Klenerman, *Proc. Natl. Acad. Sci. U.S.A* **2008**, *105*, 14424-14429.
416. A. J. Modler, K. Gast, G. Lutsch, G. Damaschun, *J. Mol. Biol.* **2003**, *325*, 135-148.
417. R. Bader, R. Bamford, J. s. Zurdo, B. F. Luisi, C. M. Dobson, *J. Mol. Biol.* **2006**, *356*, 189-208.
418. E. J. Nettleton, P. Tito, M. Sunde, M. Bouchard, C. M. Dobson, C. V. Robinson, *Biophys. J.* **2000**, *79*, 1053-1065.
419. G. Plakoutsi, N. Taddei, M. Stefani, F. Chiti, *J. Biol. Chem.* **2004**, *279*, 14111-14119.
420. J. Nasica-Labouze, N. Mousseau, *PLoS Comput. Biol.* **2012**, *8*, e1002782.
421. S. Chen, F. A. Ferrone, R. Wetzel, *Proc. Natl. Acad. Sci. U.S.A* **2002**, *99*, 11884-11889.
422. F. Ferrone, *Methods Enzymol.* **1999**, *309*, 256-274.
423. F. Oosawa, M. Kasai, *J. Mol. Biol.* **1962**, *4*, 10-21.
424. L. Nielsen, R. Khurana, A. Coats, S. Frokjaer, J. Brange, S. Vyas, V. N. Uversky, A. L. Fink, *Biochemistry* **2001**, *40*, 6036-6046.
425. J. Pronchik, X. He, J. T. Giurleo, D. S. Talaga, *J. Am. Chem. Soc.* **2010**, *132*, 9797-9803.
426. Y. Yoshimura, Y. Lin, H. Yagi, Y.-H. Lee, H. Kitayama, K. Sakurai, M. So, H. Ogi, H. Naiki, Y. Goto, *Proc. Natl. Acad. Sci. U.S.A* **2012**, *109*, 14446-14451.
427. C. Jäckel, M. Salwiczek, B. Koks, *Angew. Chem. Int. Ed.* **2006**, *45*, 4198-4203.
428. M. A. Molski, J. L. Goodman, C. J. Craig, H. Meng, K. Kumar, A. Schepartz, *J. Am. Chem. Soc.* **2010**, *132*, 3658-3659.
429. L. M. Gottler, R. de la Salud-Bea, E. N. G. Marsh, *Biochemistry* **2008**, *47*, 4484-4490.
430. C. Li, E. A. Lutz, K. M. Slade, R. A. S. Ruf, G.-F. Wang, G. J. Pielak, *Biochemistry* **2009**, *48*, 8578-8584.
431. G.-F. Wang, C. Li, G. J. Pielak, *ChemBioChem* **2010**, *11*, 1993-1996.

432. U. I. M. Gerling, M. Salwiczek, C. D. Cadicamo, H. Erdbrink, C. Czekelius, S. L. Grage, P. Wadhvani, A. S. Ulrich, M. Behrends, G. Haufe, B. Kokschi, *Chem. Sci.* **2014**, *5*, 819-830.
433. T. Tsushima, K. Kawada, S. Ishihara, N. Uchida, O. Shiratori, J. Higaki, M. Hirata, *Tetrahedron* **1988**, *44*, 5375-5387.
434. S. N. Osipov, T. Lange, P. Tsouker, J. Spengler, L. Hennig, B. Kokschi, S. Berger, S. M. El-Kousy, K. Burger, *Synthesis* **2004**, *2004*, 1821-1829.
435. D. Winkler, K. Burger, *Synthesis* **1996**, *1996*, 1419-1421.
436. K. W. Laue, C. Mück-Lichtenfeld, G. Haufe, *Tetrahedron* **1999**, *55*, 10413-10424.
437. M. Zanda, *New J. Chem.* **2004**, *28*, 1401-1411.
438. R. P. Cheng, P. Girinath, Y. Suzuki, H.-T. Kuo, H.-C. Hsu, W.-R. Wang, P.-A. Yang, D. Gullickson, C.-H. Wu, M. J. Koyack, *Biochemistry* **2010**, *49*, 9372-9384.
439. H. Erdbrink, E. K. Nyakatura, S. Huhmann, U. I. M. Gerling, D. Lentz, B. Kokschi, C. Czekelius, *Beilstein J. Org. Chem.* **2013**, *9*, 2009-2014.
440. H. A. Scheidt, I. Morgado, S. Rothemund, D. Huster, *J. Biol. Chem.* **2012**, *287*, 2017-2021.
441. J. Krishnamoorthy, J. R. Brender, S. Vivekanandan, N. Jahr, A. Ramamoorthy, *J. Phys. Chem. B* **2012**, *116*, 13618-13623.
442. N. Budisa, O. Pipitone, I. Siwanowicz, M. Rubini, P. P. Pal, T. A. Holak, M. L. Gelmi, *Chem. Biodiversity* **2004**, *1*, 1465-1475.
443. D. P. Curran, Z. Luo, *J. Am. Chem. Soc.* **1999**, *121*, 9069-9072.
444. Z. Luo, Q. Zhang, Y. Oderaotoshi, D. P. Curran, *Science* **2001**, *291*, 1766-1769.
445. F. A. Jaipuri, B. Y. M. Collet, N. L. Pohl, *Angew. Chem.* **2008**, *120*, 1731-1734.
446. F. A. Jaipuri, N. L. Pohl, *Org. Biomol. Chem.* **2008**, *6*, 2686-2691.
447. M. Zieringer, M. Wyszogrodzka, K. Biskup, R. Haag, *New J. Chem.* **2012**, *36*, 402-406.
448. L. Malik, J. Nygaard, R. Hoiberg-Nielsen, L. Arleth, T. Hoeg-Jensen, K. J. Jensen, *Langmuir* **2012**, *28*, 593-603.
449. M. Zieringer, A. Garcia-Bernabé, B. Costisella, H. Glatz, W. Bannwarth, R. Haag, *ChemPhysChem* **2010**, *11*, 2617-2622.
450. K. W. Laue, S. Kröger, E. Wegelius, G. Haufe, *Eur. J. Org. Chem.* **2000**, *2000*, 3737-3743.
451. S. Afonin, R. W. Glaser, M. Berdichevskaia, P. Wadhvani, K.-H. Gührs, U. Möllmann, A. Perner, A. S. Ulrich, *ChemBioChem* **2003**, *4*, 1151-1163.
452. Y. H. Zhao, M. H. Abraham, A. M. Zissimos, *J. Org. Chem.* **2003**, *68*, 7368-7373.
453. W. P. Aue, E. Bartholdi, R. R. Ernst, *J. Chem. Phys.* **1976**, *64*, 2229-2246.
454. M. Rance, *J. Magn. Reson. (1969)* **1987**, *74*, 557-564.
455. J. Jeener, B. H. Meier, P. Bachmann, R. R. Ernst, *J. Chem. Phys.* **1979**, *71*, 4546-4553.
456. A. Kumar, R. R. Ernst, K. Wüthrich, *Biochem. Biophys. Res. Commun.* **1980**, *95*, 1-6.
457. L. Braunschweiler, R. R. Ernst, *J. Magn. Reson. (1969)* **1983**, *53*, 521-528.
458. A. A. Bothner-By, R. L. Stephens, J. Lee, C. D. Warren, R. W. Jeanloz, *J. Am. Chem. Soc.* **1984**, *106*, 811-813.